University of Pavia

Department of Electrical, Computer and Biomedical Engineering

Ph.D. School in Electronics, Computer Science and Electrical Engineering

Local and Wide-Area Sliding Mode State Observation, Fault Reconstruction and Control with Application to Modern Power Systems

Ph.D. Candidate:

Gianmario Rinaldi

32nd Cycle

(2016-2019)

Tutor:

Prof. Antonella Ferrara

Those who are governed by reason,
desire nothing for themselves
which they do not also desire for the rest of humankind.

Baruch Spinoza

To the attentive eye, each moment of the year has its own beauty,
and in the same fields, it beholds, every hour,
a picture which was never seen before,
and which shall never be seen again.

Ralph Waldo Emerson

Perché la vita è un brivido che vola via,
è tutto un equilibrio sopra la follia.

Because the life is a thrill that flies away,
it's all a balance above the madness.

Vasco Rossi

Acknowledgements

First and foremost, an overwhelming thanks must go out to my PhD Supervisor Prof. Antonella Ferrara, for her constant support, inspiring ideas and enthusiasm in researching and teaching. I would like to thank Prof. Prathyush P. Menon and Prof. Christopher Edwards of the University of Exeter. It has been such a great pleasure and honour for me to visit and work together with them during my PhD. During these years of study at the University of Pavia, I had the great opportunity to live in Collegio Ghislieri. I would like to thank all the fantastic people and friends I met in this place during these years. I must express my acknowledgement to all the friends I met at the Faculty of Engineering at the University of Pavia and at the University of Exeter. Finally, I would like to thank my parents for providing me with support and encouragement.

Pavia, September 2019 Gianmario Rinaldi

Abstract

The present thesis summarises the research activity carried our by the PhD candidate Gianmario Rinaldi from October 2016 to September 2019 at the Department of Electrical, Computer and Biomedical Engineering at the University of Pavia, Italy.

In recent years, radical changes are taking place to power systems. A worldwide consensus has been reached for the reduction of greenhouse effects, by promoting the growth of renewable energy sources in power grids. Therefore, a special shared interest has been raised amongst researchers and practitioners to turn the existing power grids into smarter and more reliable ones, which are able to safely, efficiently, an reliably integrate the growing renewable energy sources.

Supervisory Control And Data Acquisition (SCADA) has been the conventional control and state estimation methodology practically used in the last few decades. Recent progress in computer science and electronic technologies has opened the door to the implementation of the so-called Wide Area Measurement Systems (WAMS). In particular, with a widespread deployment of Phasor Measurement Units (PMUs), a more accurate depiction of the state in power systems has become achievable in practice.

Latest advances in computer science and electronic technologies have laid the groundwork for the conception of the so-called cyber-attacks, which can be defined as computer-based algorithms capable of destabilising the power network by compromising the collected measurements to be sent to a control centre, attack the communication networks, or alter and delay the control variables.

In order to turn the existing power system into a smarter one capable of both harmoniously integrating renewable power sources and efficiently and safely dealing with faults and cyber-attacks, the attention is now focused on the following relevant research areas:

- The design and assessment of more accurate, robust and dynamic state estimators in power systems, which are able to obtain a near-real time depiction of all the state variables, instrumental in enhancing the monitoring of the networks.

- The implementation of timely fault detection, reconstruction and mitigation methodologies, devoted to preserve the stability of the entire power network, thus preventing wide-spread outages, blackouts, and degradations of the power quality.

- The design of identification schemes to determine key-properties of the components in power system context.

- The design and assessment of novel control approaches devoted to both regulate the frequency deviations and minimise the cost of the power generation. These control schemes are also

required to be robust to possible faults, disturbances, and uncertainties affecting the power systems.

The present thesis aims to fit into the aforementioned promising research areas in power systems. In particular, four challenges are addressed as follows:

- The first addressed challenge considers the design of robust state estimators which are able to depict in near real time the state of the overall power systems to globally enhance the monitoring of the power systems, thus reducing the number of the deployed sensors. The undertaken analysis started at the local level and then consider the power system as a large-scale system.
- The second addressed challenge focuses on the design of fault detection, reconstruction, and mitigation approaches devoted to enhance the resilience of the power network.
- The third addressed challenge considers the design and the assessment of robust sliding mode observer-based controllers which are capable of regulating the frequencies in power systems whilst minimising the cost associated with the generators.
- Finally, the fourth addressed challenges examines the identification of the relative degree properties with application to electrical and power systems frameworks.

Furthermore, the outline of the present thesis is coherent with the development of the contributions illustrated above. Specifically, four parts are introduced, which correspond to the four presented challenges.

Notation and Acronyms

Notation

The following standard notation is used in this thesis:

X^T	the transpose of the matrix (or the vector) X
X^{-1}	the inverse of the non-singular square matrix X
X_{ij}	the (i,j)-th entry of the matrix X
$\det(X)$	the determinant of the square matrix A
$\mathrm{rank}(X)$	the rank of the matrix X
$\lambda_{\max}(X)$	the largest eigenvalue of the square matrix X
$\lambda_{\min}(X)$	the smallest eigenvalue of the square matrix X
$X \succ 0$	the square matrix X is positive definite
I_n	the Identity Matrix of dimension $n \times n$
$\mathrm{Col}(x,y)$	the column vector composed of the two sub-vectors x and y
$\mathrm{Diag}(x,y)$	the diagonal matrix with elements x, y on its diagonal
$\mathrm{sign}(\cdot)$	the sign function
$\lvert x \rvert$	the absolute value of the real number x
$\lvert\lvert \cdot \rvert\rvert$	the euclidean norm
$\hat{x}$	the estimate of a continuous-time signal x
$x^{(r)}$	the r-th time derivative of a continuous-time signal x
$x[t_k]$	the value at the time instant t_k of a discrete-time signal x
$\Delta_{[t_c]}x(t_k) \triangleq x(t_k) - x(t_k - t_c)$	the forward difference with spacing t_c of a discrete-time signal x
$\mathbb{R}$	the set of real numbers
$\mathbb{R}^+$	the set of positive real numbers
$\mathbb{N}$	the set of natural numbers
$n!$	the factorial of the natural number n
$\triangleq$	equal to by definition
∇f	the gradient of the function f
$L_f\sigma(x) \triangleq \nabla\sigma(x)f(x)$	the Lie derivative of σ at the point x with respect to f
$\lceil x \rfloor^p \triangleq \lvert x \rvert^p \mathrm{sign}(x)$	where x is a scalar signal and p is a positive real exponent

Acronyms

The acronyms used throughout the present thesis are here listed in alphabetic order:

DAE	Differential Algebraic Equation
DC	Direct Current
DRNN	Dynamic Recurrent Neural Network
DSE	Dynamic State Estimation
ED	Economic Dispatch
EKF	Extended Kalman Filter
HOSM	Higher Order Sliding Mode
KF	Kalman Filter
LTI	Linear Time Invariant
MIMO	Multi Input-Single Output
MPC	Model Predictive Control
ODE	Ordinary Differential Equation
PI	Proportional Integral
PMUs	Phasor Measurement Units
RED	Reduced Economic Dispatch
RMSE	Root Means Square Error
SISO	Single Input-Single Output
SM	Sliding Mode
SMC	Sliding Mode Controller
SMO	Sliding Mode Observer
SOR	Successive Over Relaxation Method
ST	Super-Twisting
UI	Unknown Input
UIL	Unknown Input Luenberger Observer
WAMS	Wide Area Measurement Systems

Contents

Part I

Thesis Contributions, Sliding Mode Observation Theory, and Power System Description

Chapter 1

Thesis Contributions and Outlines

1.1 Introduction and Thesis Motivation

In recent years, radical changes are taking place to power systems. A worldwide consensus has been reached for the reduction of greenhouse effects, by promoting the growth of renewable energy sources in power grids [1]. As a consequence, the installed generation capacity of these kinds of sources is increasing worldwide, considerably led by wind power sources [2]. The renewable sources are characterised by an intrinsically intermittent and variable power generation profile, which can jeopardise the stability of the entire power grids [3], [4]. Therefore, a special shared interest has been raised amongst researchers and practitioners to turn the existing power grids into smarter and more reliable ones, which are able to safely, efficiently, an reliably integrate the growing renewable energy sources.

Supervisory Control And Data Acquisition (SCADA) has been the traditional power system control and state estimation technique practically used during the last few decades [5]. This method is based on a steady-state model of the power system and it is characterised by both a slow updating speed (in the order of seconds), and non-synchronous information about the network [6]. Recent progress in computer science and electronic technologies has opened the door to the implementation of the so-called Wide Area Measurement Systems (WAMS). In particular, the use of Phasor Measurement Units (PMUs) provide synchronised and faster measurements of real-time voltages, currents, phase angles, and frequencies in each area of a power network [4]. With a widespread deployment of PMUs, a more accurate depiction of the state in power systems has become achievable in practice. The measurement synchronisation is reached by means of timing signals from global positioning system satellites [4]. The interested reader is referred to [7] and [8], in which recent practical insights in PMUs context are illustrated.

Latest advances in computer science and electronic technologies have laid the groundwork for the conception of the so-called cyber-attacks [9]. In power systems context, this class of attacks can be defined as computer-based algorithms capable of destabilising the power network by compromising the collected measurements to be sent to a control centre, attack the communication networks, or alter and delay the control variables [10], [11].

In order to turn the existing power system into a smarter one capable of both harmoniously integrating renewable power sources and efficiently and safely dealing with faults and cyber-attacks,

the attention has been focused on the following relevant research areas:

- The design and assessment of more accurate, robust and dynamic state estimators in power systems, which are able to obtain a near-real time depiction of all the state variables, instrumental in enhancing the monitoring of the networks [12].
- The implementation of timely fault detection, reconstruction and mitigation architectures, devoted to preserve the stability of the entire power network, thus preventing wide-spread outages, blackouts, and degradations of the power quality [10], [13].
- The design of identification schemes to determine key-properties of the components in power system context [10], [14].
- The design and assessment of novel control approaches devoted to both regulate the frequency deviations and minimise the cost of the power generation [15]. These controllers are also required to be robust to possible faults, disturbances, and uncertainties affecting the power systems.

The present thesis aims to fit into the aforementioned promising research areas in power systems. In the rest of the present section, the contributions of the thesis, which are divided into four main challenges, will be presented.

- The first addressed challenge considers the design of robust state estimators which are able to depict in near real time the state of the overall power systems to globally enhance the monitoring of the power systems, thus reducing the number of the deployed sensors. The undertaken analysis starts at the local level and then it considers the power system as a large-scale system.
- The second addressed challenge focuses on the design of fault detection, reconstruction, and mitigation approaches devoted to enhance the resilience of the power network.
- The third addressed challenge considers the design and the assessment of robust sliding mode observer-based controllers which are capable of regulating the frequencies in power systems whilst minimising the cost associated with the generators.
- Finally, the fourth addressed challenge examines the identification of the relative degree properties with application to electrical and power systems frameworks.

For each of the four challenges, in the present chapter conventional and standard solutions previously adopted in the literature will be discussed. These are followed by the proposed solutions.

1.2 Challenge 1: Dynamic and Robust State Estimation in Power Systems

The Dynamic State Estimation (DSE) can be defined as the ability to reconstruct in real-time the unmeasurable states in power systems by means of limited and partial measurements (acquired by PMUs networks).

1.2.1 Conventional Solutions

Conventional estimators performing DSE in power systems can be divided into two three main categories: *i)* Linear Observers like Luenberger observers, Unknown Input (UI) observers, and Proportional Integral (PI) observers; *ii)* Kalman Filters (KF) and Extended Kalman Filters (EKF); *iii)* Sliding Mode Observers (SMO).

Linear observers conventionally rely on simplified and linearised dynamical models of power systems, and they are characterised by an asymptotic converge of the estimates to the actual values of the states [16], [17]. Furthermore, linear observers are capable of asymptotically reconstructing unknown time-constant disturbances[18].

Relevant works have proposed EKF-based dynamic state estimators in power systems, such as [19] and [12]. It is well-known that EKF techniques are able to perform good dynamic state estimation under nominal and unperturbed conditions, whereas most of them cannot tackle certain unmodelled dynamics, faults, unknown inputs, and cyber-attacks [20]. More recently, to perform correct state estimation under uncertain conditions, a network of derivative-free KF has been adopted interconnected in a decentralised fashion [21]. Furthermore, in [22], a H_∞ EKF has been proposed to tackle bounded model uncertainties such as changes to the generator reactances, noises and input disturbances. A common drawback of the aforementioned EKF-based methodologies is the fact that they usually require to increase the number of output measurements to deal with uncertainties and unknown inputs [12]. In practice, this results in higher cost associated with the deployment of sensors.

SMO has been revealed to be an efficient and alternative technique for robust dynamic state estimation with application to complex large-scale dynamical systems (such as power systems) affected by uncertainties [23]. The SM observers are totally insensitive to bounded uncertainties and perturbations appearing in the input channel of a dynamical system to be observed. In addition, the estimates generated by SMO can converge in a finite to the actual values of the unmeasured states. SMO have been employed to estimate both frequencies [24] and unknown input perturbations [25]. SM observers have also been adopted to estimate the uncertainties associated with the deployment of renewable sources, and to mitigate their impacts on the controllers performances [26].

1.2.2 Proposed Solutions

In the present thesis, theoretical, technological, and conceptual advances in SM state observers context are achieved. In particular:

Contribution 1 (**ST-like Observer Design and Assessment**)**.** An original Super Twisting(ST)-like sliding mode observer is designed to perform local robust estimation of the frequency deviation in synchronous generators. The effectiveness of the proposed observer is demonstrated both via simulation environment and via real data coming from the Nordic Power System. The undertaken real-data assessment is novel, since it is much more common in the existing literature to validate estimation schemes and control schemes by means of power networks model based on IEEE benchmarks.

Contribution 2 (**SM Observer Compared with EKF**)**.** A first order sliding mode observer is proposed to estimate at the local level both the generator voltage angle and the transient voltage of a

single synchronous generator. A comparison with the well-established EKF technique is undertaken. The proposed SM observer requires only one measurement output to perform robust state estimation, whilst the EKF requires three output measurements.

Contribution 3 (Distributed Observers in Power Systems). An interconnection of distributed heterogeneous observers is proposed for a structure-preserving dynamical model of power systems. Assuming only the voltage phase angles are measured, the observers scheme is composed of the aforementioned ST-like sliding mode observers to estimate the frequency deviation for each generator bus, and so-called algebraic observers, which are based on distributed iterative algorithms, to estimate the load voltage phase angle for each load bus. The proposed scheme is validated by considering the IEEE 39 bus SimPowerSystems benchmark. The proposal reveals higher accuracy when compared to the standard linear observers commonly adopted in the literature.

Contribution 4 (Observers for Hydrothermal Power Systems). A novel sliding mode observer-based scheme is developed to estimate and reconstruct the unmeasured state variables in power systems including hydroelectric and thermal power sources. In contrast to [27], [28], in which simplified mathematical models of the power networks have been used as a starting base to design the estimation schemes (neglecting both the hydrothermal turbine-governor dynamics and the nonlinearities in the synchronous generators dynamics), the power network dynamical model is significantly detailed in this thesis. Furthermore, the proposal reveals to be flexible to topological changes to power systems and it can be easily updated only where changes occur.

Contribution 5 (SM Observers for Hybrid Power Systems). The application of Higher Order Sliding Mode (HOSM) observers is exploited to robustly and dynamically estimate in finite time the unmeasured state variables in heterogeneous power systems, in which both traditional and renewable energy sources coexist. In particular, a power system composed of traditional, wind and inverter-based sources connected with dynamical loads is considered. In contrast to the SM observer schemes developed in the existing literature, in either traditional power grid models [24], [26], or renewable power sources [29], which are independently considered, a model where heterogeneous power sources and loads are simultaneously present is considered. As a consequence, the level of unknown, but bounded fluctuations and uncertainties is significantly higher in this case than in the conventional independent cases. Assuming that only the voltage phase angles are locally measured, a dedicated HOSM observer is designed for each component, which is able to estimate in finite time the unmeasured state variables. Numerical simulations, which are based on a prototype example [30], demonstrate the higher accuracy of the proposed scheme when compared to linear observers.

1.3 Challenge 2: Fault Detection, Reconstruction and Mitigation

The presence of faults and attacks can destabilise a power system, causing widespread outages and power-cut. The timely and accurate isolation and reconstruction of faults and disturbances can be exploited to mitigate their impact on the network. Specifically, the knowledge of the exact position of the fault along with its time evolution constitute useful information which are exploited to take remedial actions devoted to enhance the resilience of the power system.

1.3.1 Conventional Solutions

In the existing literature, different solutions have been proposed to isolate and reconstruct faults in power grids. Typically, Unknown Input (UI) linear observers have been adopted to asymptotically estimate the constant power in power systems modelled as interconnected areas [31], [32]. More recently, in [33] a linear unknown input observer has been used to detect and isolate faults in power systems comprising renewable energy sources and electrical vehicles dynamics. Sliding mode-based observers are becoming increasingly popular as a way of detecting and reconstructing faults in dynamical systems [34]. For example, in [24], a multi-variable SM observer has been created to detect and reconstruct a single load alteration in a power network. Several researchers have proposed different sliding mode based schemes to tackle faults and disturbances in power networks. For example, in [35] a distributed sliding mode control strategy has been proposed for optimal load frequency control. This approach was shown to be robust to bounded disturbances and faults, but no detection or reconstruction scheme has been implemented.

1.3.2 Proposed Solutions

Contribution 6 (**Adaptive ST Observers for Fault Detection**). A newly proposed adaptive super-twisting sliding mode observer is designed, exploiting ideas from [36]. In the standard super-twisting observers employing fixed gains, the tuning of the design constants is always conservative and therefore the upper-bounds of disturbances is overestimated. Differently, in this thesis, the formulated adaptation law acts by automatically adjusting the values of the observer gains as a function of the actual disturbances perturbing the system in a given time instant. This gives the proposed estimation architecture extreme flexibility from a practical perspective. In contrast to the the earlier work [24], in which a single fault at the load bus level was considered, the proposed scheme is capable of dealing with simultaneous faults affecting power systems. Furthermore, a fault mitigation strategy is proposed, and it is also shown that a standard pre-existing Proportional Integral (PI) controller can still be employed to stabilise the power systems, suitably coupled with a proposed disturbance compensation.

1.4 Challenge 3: Observers-Based Economic Dispatch in Power Systems

A hierarchical control architecture has been traditionally employed for the purpose of frequency control. This scheme is composed of three levels - from fast to slow in time-scale: a primary droop controller, a PI secondary controller, and a tertiary controller devoted to Economic Dispatch [37], [5]. While guaranteeing a balance between power generation and consumption, it is desirable to minimise the aggregated generation cost, thus satisfying the economic constraints. This problem is known as Economic Dispatch (ED) [37]. Recently, it has been argued that there is a need for breaking the conventional control hierarchy described above and for directly introducing ED in the secondary frequency control architecture.

1.4.1 Conventional Solutions

Different approaches have been formulated for ED in power grids. For example, in [38] both an incremental passivity technique and an internal model-based controller architecture have been employed to design distributed controllers for frequency regulation and ED in power networks. In [39] a linearised model of a power system has been employed as a starting point to design a distributed primary frequency controller, which also accounts for the cost associated with frequency-dependent loads. The approach was extended in [40], with the use of a distributed PI optimal controller stabilising power systems, and in [41], in which a plug and-play architecture was introduced. Recently, in [42] an optimisation architecture has been conceived for ED in smart power grids, where the optimisation problem was solved by only using local information available at the generator level. In [43], two second-order continuous algorithms for dynamically solving ED problem were developed, thus ensuring a fast speed of convergence.

1.4.2 Proposed Solutions

Contribution 7 (SMO-Based Controllers for Economic Dispatch-Strategy 1). Two original third order sliding mode observers capable of estimating, respectively, the frequency deviation and the governor output variation of each control area are designed. Then, the observers are suitably coupled with the control strategy proposed in [35], which relies on the Suboptimal Second Order Sliding Mode (SSOSM) control algorithm, and it guarantees to steer to zero frequency deviation, whilst minimising the generation costs (Economic Dispatch).

Contribution 8 (SMO-Based Controllers for Economic Dispatch-Strategy 2). A novel observer-based SM control scheme is proposed to achieve both frequency regulation and Economic Dispatch (ED) for structure-preserving power systems. The problem is addressed in an original two steps approach way. The first step involves the design of a distributed observer scheme, which is able to both estimate in finite time the frequency deviation, and the unknown power demand, both of which are essential for controllers design. The second step develops the design of the control scheme. A SM control scheme is employed to track in finite time the reference value of the optimal marginal cost, thus achieving in finite time the economic dispatch, and asymptotically steering to zero the frequency deviations. The underlying approach displays key-novelties when compared to existing methods in the literature. In particular, in contrast to [38], [15], and [35], in which the power demand is treated as an unknown input, in the present approach a strategy to estimate power demand in finite time is presented, thus reducing the complexity of the control scheme. Furthermore, the proposed approach is able to perform unknown input state estimation in finite time, and not asymptotically, as typically happens if UI Luenberger observers are employed [44]. Moreover, the use of observer considerably reduce the number of deployed sensors required for the practical implementation of the control schemes. In contrast to [15], [45], and [46], in which the optimal value of the marginal generation cost is asymptotically satisfied, the proposed scheme is able to reach the optimal marginal cost in finite time.

1.5 Challenge 4: Relative Degree Identification

The relative degree of the controlled output of a dynamical system with respect to the control input is a property of paramount importance in the controller synthesis. In general, the relative degree has to be known in advance, and it has to be time-invariant [47]. The relative degree has also a central role in the design of dynamic state observers for unknown input reconstruction and fault detection [48]. In this situation, it is required to know in advance the relative degree of the output observation error with respect to unknown inputs or faults [49], [50]. Some authors have tried to find innovative control approaches in which the relative degree is not known. For example, in [51] an active disturbance rejection controller has been formulated, which did not require the precise knowledge of the relative degree, but only its upper-bound. More recently, in [52], a method based on switching logic has been employed for global output-feedback stabilization for a class of nonlinear systems with unknown relative degree. In [53] the situation when discrepancies between the dynamical model adopted for the controllers designed and the actual systems can lead to changes to the relative degree during the system operation has been analysed. In such a scenario, it has been proven that the performance of the so-called homogeneous SM control do not degrade too much in presence of fluctuations of the relative degree [54]. More precisely, it has been proven that the norm of the sliding variable is kept bounded if a homogeneous higher order SM control strategy is applied, even in presence of a bounded disturbance making the relative degree of the system fluctuate. But apart from these few works, in the majority of approaches relevant to control or observers design the relative degree has to be assumed known.

1.5.1 Conventional Solutions

In spite of the importance of the knowledge of the relative degree for control design, a little attention has been paid in the literature to the identification of the relative degree, especially if this has to be performed online. i.e. during the system operations. In order to identify the relative degree, in [55], a set of rules relying on the physical properties of electronic devices and bond graph concepts have been provided. In [56], a Dynamic Recurrent Neural Network (DRNN) has been designed to identify the relative degree for nonlinear uncertain systems, and their effectiveness has been demonstrated considering a single-link manipulator. A similar proposal has been conceived in [57], with the application to chemical reactors. To the best of the author's knowledge, the only relevant work devoted to identify the relative degree via SM techniques is [58], which has been detailed in the book chapter in [59]. In these works the concept of "practical relative degree" has been formulated. In particular, it has been shown that if the system to be controlled is excited by a step input signal, then, via higher order SM differentiation, it was possible to estimate successive derivatives of the output, until the discontinuity caused by the step input signal visually appears. More recently, in [60] the practical relative degree architecture was employed to control a cam-plate driven ball and plate system via higher order sliding mode methodologies.

1.5.2 Proposed Solution

Contribution 9 (**Automatic Identification of the Relative Degree of Nonlinear Systems**)**.** In the method proposed in this thesis the identification of the relative degree is performed via a recursive algorithm which is based on analytical criteria. The test input signal is a triangular wave with prescribed maximum value and slope. This particular input signal is able to excite the system in such a way that the relative degree can be automatically identified. Through the recursive strategy proposed in the present thesis, any relative degree can be automatically identified since the method, by itself, is capable of selecting the order of the Levant's differentiator which is suitable to perform the identification. Furthermore, the experimental-based assessment of the method is illustrated relying on an set-up composed of a lab-scale overhead crane mechanically coupled with a DC motor.

1.6 Thesis Outline

The outline of the present thesis is coherent with the development of the contribution illustrated above. Specifically, four parts are introduced, which correspond to the four addressed challenges presented in this chapter.

Part I: Dynamic and Robust State Estimation in Power Systems

- **Chapter 2** presents to the reader basic theoretical concepts of SM observation and fault detections which are exploited later in the thesis.
- **Chapter 3** introduces the dynamical models of the components of power systems adopted in simulations and analysis.
- **Chapter 4** considers the application of sliding mode observation techniques to locally and robustly estimate the states of synchronous generators in power systems.
- **Chapter 5** presents a wide-area state estimation based on sliding mode observers. This includes both traditional and renewable sources interconnected with loads.

Part II: Fault Detection, Reconstruction and Mitigation

- **Chapter 6** proposes a distributed scheme based on an adaptive dual-layer super-twisting sliding mode architecture to perform robust fault and attack isolation, reconstruction, and mitigation in power systems.

Part III: Observers-Based Economic Dispatch in Power Systems

- **Chapter 7** considers a third order sliding mode observer scheme to be suitably coupled with a optimal load frequency control scheme in power systems.
- **Chapter 8** exploits a novel sliding mode observer-based control approach to both regulate the frequency and minimise the cost associated with the generations.

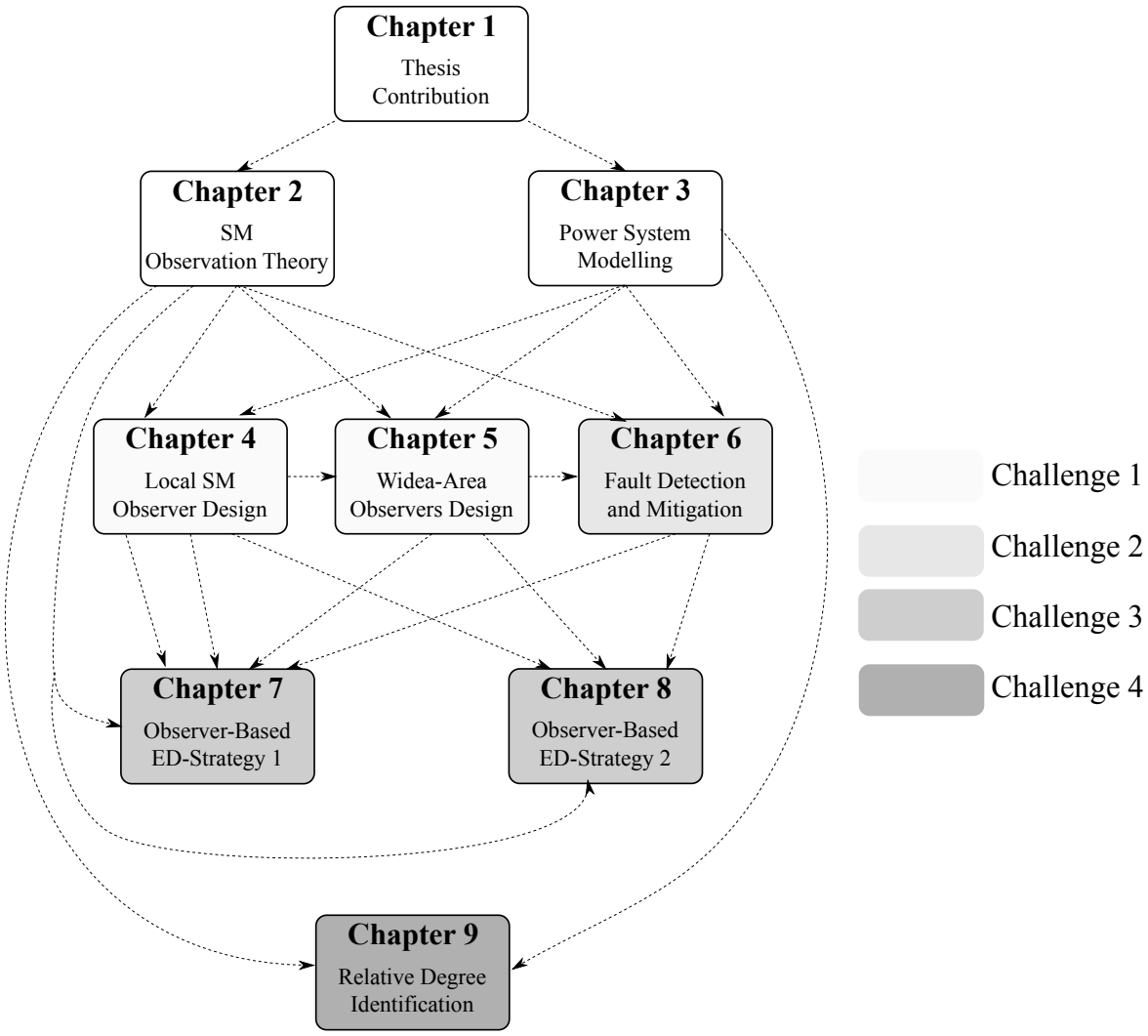

Figure 1.6.1: A schematic illustrating the dependences amongst the chapters of the thesis. The challenges to which the chapters belong are highlighted also.

Part IV: Relative Degree Identification

- **Chapter 9** proposes a novel approach to identify the relative degree of nonlinear uncertain single-input single-output systems.

Figure 1.6.1 shows the logical dependences amongst the chapters of the thesis.

1.7 List of Publications

The results obtained during the PhD are summarised in a peer-reviewed book chapter (Springer), and in a number of peer-reviewed papers published on both high impact journals (Automatica, IEEE Transactions on Control Systems Technologies, IEEE Control Systems Letters, Control Engineering Practice) and conference proceedings (American Control Conference, IEEE CDC Conference, European Control Conference, VSS Conference). The PhD candidate Gianmario Rinaldi has been first and corresponding author of all these publications, which are listed below:

1.7.1 Book Chapter

B1. **G. Rinaldi**, P. P. Menon, C. Edwards and A. Ferrara, "*Local and Wide-Area Sliding Mode Observers in Power Systems*", in Variable Structure Systems and Sliding Mode Control - Theory and Practice, Springer, 2019, accepted-to appear soon.

1.7.2 Journal Papers

J1. **G. Rinaldi**, M. Cucuzzella, and A. Ferrara, "*Third order sliding mod observer-based approach for distributed optimal load frequency control*", IEEE Control Systems Letters, vol. 1, no. 2, pp. 215–220, 2017.

J2. **G. Rinaldi**, P. P. Menon, C. Edwards and A. Ferrara, "*Sliding Mode Based Dynamic State Estimation for Synchronous Generators in Power Systems*", IEEE Control Systems Letters, vol. 2, no. 4, pp. 785-790, 2018.

J3. **G. Rinaldi**, M. Cucuzzella, and A. Ferrara, "*Sliding mode observers for a network of thermal and hydroelectric power plants*", Automatica, vol. 98, pp. 51–57, 2018.

J4. **G. Rinaldi**, P. P. Menon, C. Edwards and A. Ferrara, "*Design and Validation of a Distributed Observer- Based Estimation Scheme for Power Grids*", IEEE Transactions on Control System Technology, 2018.

J5. **G. Rinaldi**, P. P. Menon, C. Edwards and A. Ferrara, "*Higher Order Sliding Mode Observers in Power Grids with Traditional and Renewable Sources*", IEEE Control Systems Letters, vol. 4, no. 1, pp. 223-228, 2019.

J6. **G. Rinaldi** and A. Ferrara, "*Automatic Identification of the Relative Degree of Nonlinear Systems: Application to Sliding Mode Control Design and Experimental Assessment*", Control Engineering Practice, vol.94, 2020,

J7. **G. Rinaldi,** P. P. Menon, C. Edwards and A. Ferrara, "*Adaptive Dual-Layer Super-Twisting Sliding Mode Observers to Reconstruct and Mitigate Faults and Attacks in Power Network*", Automatica, 2019, under review, second round.

J8. **G. Rinaldi,** P. P. Menon, C. Edwards and A. Ferrara, "*Sliding Mode Observer-Based Finite Time Control Scheme for Frequency Regulation and Economic Dispatch in Power Grids*", IEEE Transactions on Control System Technology, 2020, under review, first round.

1.7.3 Conference Papers

C1. **G. Rinaldi,** P. P. Menon, C. Edwards, and A. Ferrara, "*Distributed observers for state estimation in power grids*," in Proc. American Control Conf., Seattle, WA, USA, May 2017, pp. 5824–5829.

C2. **G. Rinaldi** and A. Ferrara, "*Higher Order Sliding Mode Observers and Nonlinear Algebraic Estimators for State Tracking in Power Networks*," in Proc. 56-th IEEE Conference on Decision and Control, Melbourne, Australia, December 2017, pp. 6033–6038.

C3. **G. Rinaldi**, P. P. Menon, C. Edwards, and A. Ferrara, "*A Super-Twisting-Like Sliding Mode Observer for Frequency Reconstruction in Power Systems: Discussion and Real Data Based Assessment*," in Proc. 15-th International Workshop on Variable Structure Systems and Sliding Mode Control, Graz, Austria, July 2018, pp. 444–449.

C4. **G. Rinaldi** and A. Ferrara, "*Decentralized Integral Sliding Mode Approach for Frequency Control and Unknown Demand Reconstruction in Power Systems*," in Proc. 15-th International Workshop on Variable Structure Systems and Sliding Mode Control, Graz, Austria, July 2018, pp. 455–460.

C5. **G. Rinaldi** and A. Ferrara, "*Relative Degree Identification for Sliding Mode Controllers Design*", in Proc. 15-th International Workshop on Variable Structure Systems and Sliding Mode Control, July 2018, Graz, Austria, July 2018, pp. 55–60.

C6. **G. Rinaldi**, P.P. Menon, C. Edwards and A. Ferrara, "*Distributed Super-Twisting Sliding Mode Observers for Fault Reconstruction and Mitigation in Power Networks*", in Proc. 57-th IEEE Conference on Decision and Control, Miami Beach, FL, USA, December 2018, pp. 5550 - 5555.

C7. **G. Rinaldi**, P.P. Menon, C. Edwards and A. Ferrara, "*Variable Gains Decentralized Super-Twisting Sliding Mode Controllers for Large-Scale Modular Systems*", in Proc. European Control Conference, Naples, Italy, June 2019, pp. 3577-3582.

Chapter 2

Sliding Mode Observers: A Brief Presentation

Abstract This chapter aims to summarise well-established theoretical findings of sliding mode observers. The undertaken analysis considers two classes of dynamical system: a Linear Time Invariant (LT) system affected by unknown input, and a double integrator system with unknown nonlinearities. For the two systems, dedicated SM observers are introduced and sketch of their stability analysis is presented, which is based on a Lyapunov function approach. For a detailed and more comprehensive treatment of sliding mode observation theory, the interested reader can make reference to [61], [23], [62], and [63].

2.1 The Concept of Sliding Mode

Sliding mode control techniques have been successfully proposed in the last few decades for robust control and observation of nonlinear systems affected by uncertainties [64], [65]. The most relevant features of these techniques are their capability to enforce a finite time stability and to completely reject bounded matched uncertainties and disturbances (see, e.g., [65], [63], [61]). Sliding mode techniques have been also proposed for state estimation and observer-based control approaches in different application fields, such as robotics, electromechanical systems, and power systems, as illustrated in [65], [63], [66], and [67].

2.2 The Concept of State Observer

The knowledge of the actual values of the dynamical system states is of paramount importance in control theory and applications [47], [68]. This is required, for example, to solve control problems, to enhance the monitoring of the systems, and to perform near real-time fault detection, reconstruction and mitigation [65]. In practice, it is not always possible to measure all the state variables. For example, this limit can be imposed by physical reasons or economic constraints. A state observer can be defined as a dynamical architecture able to estimate the unmeasured state variables of a given system. The knowledge of the inputs and the outputs of the dynamical system along with expressions

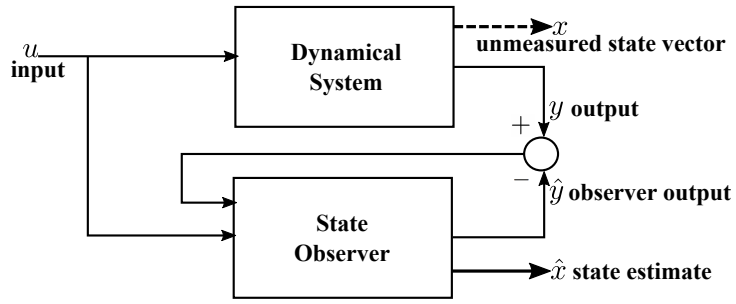

Figure 2.2.1: A schematic of a dynamical system together with the associated state observer. The meaning of the introduced variables is written along with their symbols.

of the dynamical model describing the system behaviours with acceptable accuracy are often required for the effective design of an observer [69]. The block diagram shown in Figure 2.2.1 summarises the underlying ideas of a state observer.

In the rest of the present chapter, relevant key-findings of sliding mode observers theory will be presented. Two relevant class of dynamical systems will be considered as a starting point for the observers design: the perturbed LTI SISO system, and the perturbed double integrator. For these two dynamical systems dedicated state observers will be presented.

2.3 SM Observers for LTI Perturbed Systems

2.3.1 Preliminaries and System Descriptions

Consider a Linear Time Invariant (LTI) Single Input Single Output (SISO) system governed by

$$\begin{aligned} \dot{x} &= Ax + B\left(u + d\right) \\ y &= Cx \end{aligned} \tag{2.3.1}$$

where $x \in \mathbb{R}^n$ is the state vector, $y \in \mathbb{R}$ is the output, $u \in \mathbb{R}$ is a known input, $d \in \mathbb{R}$ is an unknown input, whilst A, B, C are matrices and vectors of appropriate dimensions. It is assumed that the unknown input d is bounded, which means that

$$|d| \leq \Delta_d \tag{2.3.2}$$

where Δ_d is a known positive constant.

Definition 2.1 (Relative Degree)**.** Given the dynamical system in (2.3.1), if the input signal u explicitly appears for the first time on the r-th time derivative of the output y, then the positive integer number $r \in \mathbb{N}$ is called the relative degree of the output y, with respect to the input u [47].

Definition 2.2 (Strong Observability)**.** The LTI SISO perturbed linear system (2.3.1) is strongly observable if for any initial condition $x(0)$ and $d(0) = 0$, $y \equiv 0 \; \forall \; t \geq 0$ implies $x \equiv 0$.

The following criteria can be shown to ensure the strong observability property [70]:

- The Observability Matrix associated with the pair (A, C) is full rank.

- The system (2.3.1) is strongly observable if and only if output y of the system (2.3.1) has relative degree n with respect to the unknown input d.

Definition 2.3 (Strong Detectability)**.** The LTI SISO perturbed linear system (2.3.1) is said strongly detectable if for any d and initial condition $x(0)$, it follows from $y \equiv 0 \; \forall \; t \geq 0$ that $x \to 0$ for $t \to \infty$.

The following criteria can be shown to ensure the strong detectability property [70]:

- The Observability Matrix associated with the pair (A, C) is full rank.
- The system (2.3.1) is said strongly observable if and only if the relative degree of output y of the system (2.3.1) with respect to the unknown input d exists and the system is minimum phase.

2.3.2 Conventional First Order Sliding Mode Observer

Under the assumption that the dynamical system (2.3.1) is strongly observable or strongly detectable, the following observer

$$\dot{\hat{x}} \;\; = \;\; A\hat{x} + B\left(u - \rho\tfrac{FCe}{|FCe|}\right) - GCe, \tag{2.3.3}$$

is introduced, where the error variable $e \triangleq \hat{x} - x$, $F \in \mathbb{R}$, ρ is a positive design constant, $G \in \mathbb{R}^n$ is a design vector. By subtracting (2.3.1) from (2.3.3), the so-called error system dynamics can be obtained as follows

$$\dot{e} = \big(A - GC\big)e - B\left(d + \rho\frac{FCe}{|FCe|}\right). \tag{2.3.4}$$

Proposition 2.1. *Given error dynamics (2.3.4) and under the condition (2.3.2), suppose that for a positive definite symmetric matrix $P \succ 0$, one has*

$$PA_0 + A_0^T P < 0, \tag{2.3.5}$$

where $A_0 \triangleq A - GC$ and the structural constraint [62]

$$PB = C^T F^T \tag{2.3.6}$$

is satisfied. Then, the origin is an asymptotically stable equilibrium point for the error dynamics (2.3.4), provided that the constant ρ satisfies:

$$\rho > \Delta_d. \tag{2.3.7}$$

Proof. The reader is referred to [62] for the proof of Proposition 2.1. □

Note that the state variables vector $\hat{x}$ is estimated asymptotically, whereas the output observation error FCe is steered to zero in finite time [62].

2.3.3 Higher Order SM Observers

A variant of the observer (2.3.3) can be adopted to estimate in finite time the state variables of (2.3.1). Suppose that the vector C in (2.3.1) has the structure: $C = [1, 0, \ldots, 0]$. Following [70] the observer:

$$\begin{aligned} \dot{z} &= Az + Bu + L(y - Cz) \\ \hat{x} &= z + Kv \\ \dot{v} &= W(y - Cz, v) \end{aligned} \tag{2.3.8}$$

is created, where, with respect to (2.3.3), z is an additional estimate of x, K is a design matrix of appropriate dimensions, v is an additional observer variable, and $W(\cdot)$ is a nonlinear function depending on both the output observation error $y - Cz$ and v. The error dynamics, which is obtain by subtracting (2.3.1) from (2.3.8) yield:

$$\begin{aligned} \dot{e} &= (A - LC)\, e \\ \hat{x} &= z + Kv \\ \dot{v} &= W(y - Cz, v) \end{aligned} \tag{2.3.9}$$

Following [70], it is possible to show that the time evolution of e remains bounded and asymptotically converges to the origin, hence the matrix $(A - LC)$ is ensured Hurwitz via standard pole-placement technique. Furthermore, if the matrix $\tilde{O}$ is the Observability Matrix associated with the pair $(A - LC, C)$, the change of coordinates for the error dynamics (2.3.9) $\tilde{e} = \tilde{O}e$ is considered. In the new reference frame, one as

$$\dot{\tilde{e}} = \tilde{A}\tilde{e}$$

where the matrix $\tilde{A} \in \mathbb{R}^{n \times n}$ has the structure

$$\tilde{A} = \tilde{O}(A - LC)\tilde{O}^{-1} = \begin{bmatrix} 0 & 1 & \ldots & 0 & 0 \\ 0 & 0 & 1 & \ldots & 0 \\ \vdots & \vdots & \vdots & \ddots & 0 \\ \tilde{a}_1 & \tilde{a}_2 & \tilde{a}_3 & \ldots & a_n \end{bmatrix} \tag{2.3.10}$$

where $\tilde{a}_1, \ldots, \tilde{a}_n$ are known constants. It is easy to verify that only the first component $\tilde{e}_1$ of the vector $\tilde{e} = [\tilde{e_1}, \ldots, \tilde{e_n}]^T$ is known, thus coinciding with the output observation error. Since the matrix $\tilde{A}$ is Hurwitz, the time evolution of $\tilde{e}$ remains bounded [68]. By means of SM Levant's differentiator, the successive time derivatives of e_1, which are bounded [70], are accurately estimated in a finite time. This technique is governed by

$$\begin{aligned} \dot{v}_1 &= -k_1 \lceil y - Cz \rfloor^{\frac{n}{n+1}} + v_2 \\ \dot{v}_2 &= -k_2 \lceil y - Cz \rfloor^{\frac{n-1}{n+1}} + v_3 \\ \vdots \;&\vdots\; \vdots \\ \dot{v}_{n-1} &= -k_{n-1} \lceil y - Cz \rfloor^{\frac{1}{n+1}} + v_n \\ \dot{v}_n &= -k_n \lceil y - Cz \rfloor^{0} \end{aligned} \tag{2.3.11}$$

which is implemented in the so-called non-recursive form [71]. The underlying idea is to make use of the output observation error e_1 and create the n-th order dynamical estimator in (2.3.11). In [72] it has been shown that each estimate generated by the differentiator converges to the actual value in finite time. The tuning rules for the positive design constants $k_1, \ldots, k_n$ can be found, e.g., in [71] and [73]. It follows in finite time: $v_1 = \tilde{e}_1 = e_1$, $v_2 = \tilde{e}_2$, $\ldots$, $v_n = \tilde{e}_n$. After the linear change of coordinates $\hat{v} = \tilde{O}^{-1}\tilde{P}v$, it is possible to retrieve actual values of the error $\hat{v}$ in the original coordinates reference in finite time. These are used to compensate in real time the estimate z by introducing the following algebraic expression

$$\hat{x} = z - \hat{v}. \tag{2.3.12}$$

According to the algebraic relation in (2.3.12), the condition $\hat{x} = x$ holds in finite time.

2.4 SM Observers for Perturbed Double Integrator Systems

2.4.1 System Description and Preliminaries

Next consider the SISO [1]perturbed double integrator dynamical systems:

$$\begin{aligned} \dot{x}_1 &= x_2 \\ \dot{x}_2 &= f(x_1, x_2, t) + u \\ y &= x_1 \end{aligned} \tag{2.4.1}$$

where $x_1 \in \mathbb{R}$ and $x_2 \in \mathbb{R}$ are the two scalar state variables, $u \in \mathbb{R}$ is a known input, whilst $f(x_1, x_2, t) \in \mathbb{R}$ is an unknown but bounded nonlinear function which depends on both the states x_1 and x_2, and on the time t. Since $f(\cdot)$ is assumed bounded, it follows that

$$|f(x_1, x_2, t)| \leq \Delta_f \tag{2.4.2}$$

where Δ_f is a known positive constant.

2.4.2 Super-Twisting Sliding Mode Observers

To motivate the use of super-twisting sliding mode observer, a standard linear observer [68] can be employed as a tentative solution to estimate the state x_2 for the double integrator perturbed dynamical system (2.4.1):

$$\begin{aligned} \dot{\hat{x}}_1 &= \hat{x}_2 - L_1 (\hat{x}_1 - x_1) \\ \dot{\hat{x}}_2 &= u - L_2 (\hat{x}_1 - x_1) \\ \hat{y} &= \hat{x}_1 \end{aligned} \tag{2.4.3}$$

[1]Note that the developments in the present section can be easily extended to the multi-variable double integrator case, as suggested in [71] and [74].

where $\hat{x}_1$ is an estimate of x_1, $\hat{x}_2$ is an estimate of x_2, L_1 and L_2 are positive design constants. By subtracting (2.4.1) from (2.4.3), the so-called error dynamics yield

$$\begin{array}{rcl} \dot{e}_1 & = & e_2 - L_1 e_1 \\ \dot{e}_2 & = & -f(x_1, x_2, t) - L_2 e_1 \end{array} \tag{2.4.4}$$

where $e_1 \triangleq \hat{x}_1 - x_1$, and $e_2 \triangleq \hat{x}_2 - x_2$. The system in (2.4.4) can be compactly rewritten as:

$$\dot{e} = Ae + B\left(f(x_1, x_2, t)\right) \tag{2.4.5}$$

where $e \triangleq \mathrm{Col}(e_1, e_2)$ and the introduced matrices and vectors are

$$A = \begin{bmatrix} -L_1 & 1 \\ -L_2 & 0 \end{bmatrix}, \; B = \begin{bmatrix} 0 & -1 \end{bmatrix}^T \tag{2.4.6}$$

The design constants L_1 and L_2 can be chosen by using standard pole-placement techniques applied to the matrix A appearing in (2.4.6), in order to ensure that it is Hurwitz [69]. It is also easy to show that the time evolution of the error vector in e of (2.4.4) remains bounded, since the matrix A is Hurwitz and $f(\cdot)$ can be interpreted as a bounded unknown input. However, the condition $e = 0$ is not asymptotically satisfied, due to the presence of uncertainty function $B\left(f(x_1, x_2, t)\right)$.

An effective alternative solution is the design a robust state observer totally insensitive to unknown bounded disturbance. The so-called Super-Twisting (ST) sliding mode observer can be selected for this purpose. This observer was originally proposed in [75], and its stability analysis was undertaken via Lyapunov function technique in [76]. Given the double integrator dynamical system (2.4.1), the associated ST observer is governed by the following dynamics

$$\begin{array}{rcl} \dot{\hat{x}}_1 & = & -k_1 |e_1|^{1/2} \mathrm{sign}\left(e_1\right) + \hat{x}_2 \\ \dot{\hat{x}}_2 & = & -k_2 \mathrm{sign}\left(e_1\right) + u \\ \hat{y} & = & \hat{x}_1 \end{array} \tag{2.4.7}$$

where $\hat{x}_1$ is an estimate of x_1, $\hat{x}_2$ is an estimate of x_2, k_1 and k_2 are positive design constants. By subtracting (2.4.1) from (2.4.7), the error dynamics yield

$$\begin{array}{rcl} \dot{e}_1 & = & -k_1 |e_1|^{1/2} \mathrm{sign}\left(e_1\right) + e_2 \\ \dot{e}_2 & = & -k_2 \mathrm{sign}\left(e_1\right) - f(x_1, x_2, t) \end{array} \tag{2.4.8}$$

where, $e_1 \triangleq \hat{x}_1 - x_1$, and $e_2 \triangleq \hat{x}_2 - x_2$. It is necessary to prove that the point

$$\begin{bmatrix} e_1 & e_2 \end{bmatrix}^T = \begin{bmatrix} 0 & 0 \end{bmatrix}^T \tag{2.4.9}$$

is a finite-time stable equilibrium point for the system (2.4.8). This means that the trajectories of (2.4.8) converge to $\begin{bmatrix} 0 & 0 \end{bmatrix}^T$ in finite time. According to [76], a Lyapunov function candidate in the

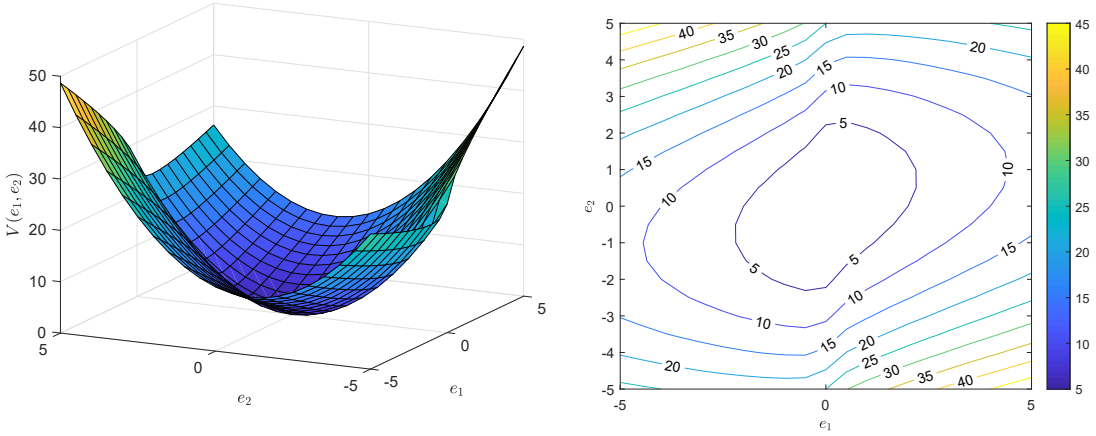

Figure 2.4.1: A 3-D plot of the Lyapunov function candidate (2.4.10), together with the associated contour plot.

form of

$$V\left(e_1, e_2\right) \triangleq 2k_2\left|e_1\right| + \frac{1}{2}e_2^2 + \frac{1}{2}\left(k_1\left|e_1\right|^{1/2}\operatorname{sign}\left(e_1\right) - e_2\right)^2, \tag{2.4.10}$$

can be selected. Equation (2.4.10) is rewritten in a more compact way:

$$V\left(e_1, e_2\right) = \zeta^T P \zeta, \tag{2.4.11}$$

where the vector $\zeta^T \in \mathbb{R}^2$ is given by

$$\zeta^T \triangleq \begin{bmatrix} \left|e_1\right|^{1/2}\operatorname{sign}\left(e_1\right) & e_2 \end{bmatrix}, \tag{2.4.12}$$

and the matrix $P \in \mathbb{R}^{2\times 2}$ can be shown to be:

$$P = \frac{1}{2}\begin{bmatrix} 4k_2 + k_1^2 & -k_1 \\ -k_1 & 2 \end{bmatrix}. \tag{2.4.13}$$

It is straightforward to verify that the matrix P is positive definite. It follows that $V(0,0) = 0$, and $V(e_1, e_2) > 0 \;\forall\; [e_1, e_2] \neq [0, 0]$. In Figure 2.4.1, a 3-D plot of the Lyapunov function candidate (2.4.10) is shown, in which the values $k_1 = k_2 = 1$ are chosen, and the domain $e_1, e_2 \in [-5\ 5]$. The contour plot of (2.4.10) is also illustrated in Figure 2.4.1.

Differentiating (2.4.10) with respect to time yields:

$$\dot{V}\left(e_1, e_2\right) = -\frac{1}{\left|e_1\right|^{1/2}}\zeta^T Q \zeta + f(x_1, x_2) q_2^T \zeta, \tag{2.4.14}$$

where the matrix $Q \in \mathbb{R}^{2\times 2}$ is defined as

$$Q \triangleq \frac{k_1}{2}\begin{bmatrix} 2k_2 + k_1^2 & -k_1 \\ -k_1 & 1 \end{bmatrix}, \tag{2.4.15}$$

and the auxiliary vector $q_2 \in \mathbb{R}^2$is given by

$$q_2^T = \begin{bmatrix} -k_1 & 2 \end{bmatrix}. \tag{2.4.16}$$

It can be shown that $\dot{V}(e_1, e_2)$ is bounded as:

$$\dot{V}(e_1, e_2) \leq -\frac{1}{|e_1|^{1/2}} \zeta^T \tilde{Q} \zeta, \tag{2.4.17}$$

where the auxiliary matrix $\tilde{Q} \in \mathbb{R}^{2\times 2}$ is in the form of

$$\tilde{Q} \triangleq \frac{k_1}{2} \begin{bmatrix} \tilde{Q}_{11} & \tilde{Q}_{12} \\ \tilde{Q}_{21} & \tilde{Q}_2 \end{bmatrix} = \frac{k_1}{2} \begin{bmatrix} 2k_2 + k_1^2 - 2\Delta_f & -\left(k_1 + \frac{2\Delta_f}{k_1}\right) \\ -\left(k_1 + \frac{2\Delta_f}{k_1}\right) & 1 \end{bmatrix}. \tag{2.4.18}$$

One can note that $\dot{V}(e_1, e_2) < 0$ outside the equilibrium point $[0, 0]$ if the matrix $\tilde{Q} \in \mathbb{R}^{2\times 2}$ in (2.4.18) is positive definite. The inequalities:

$$\begin{cases} \tilde{Q}_{11} & > 0, \\ \det\left(\tilde{Q}\right) & > 0, \end{cases} \tag{2.4.19}$$

ensure that $\tilde{Q}$ is positive definite [77]. Exploiting (2.4.19), it yields:

$$\begin{cases} \tilde{Q}_{11} = 2k_2 + k_1^2 - 2\Delta_f > 0, \\ \det\left(\tilde{Q}\right) = 2k_2 + k_1^2 - 2\Delta_f - \left(k_1 + \frac{2\Delta_f}{k_1}\right)^2 > 0, \end{cases} \tag{2.4.20}$$

Solving the system (2.4.20), the condition

$$2k_2 + k_1^2 - 2\Delta_f - \left(k_1 + \frac{2\Delta_f}{k_1}\right)^2 > 0 \tag{2.4.21}$$

verifies both the two inequalities in (2.4.20). Solving (2.4.21) for k_2 yields

$$k_2 > \Delta_f \left(3 + \frac{2\Delta_f}{k_1^2}\right). \tag{2.4.22}$$

Therefore, the tuning rules for the gains k_1 and k_2 are:

$$\begin{cases} k_1 & > 0, \\ k_2 & > \Delta_f \left(3 + \frac{2\Delta_f}{k_1^2}\right). \end{cases} \tag{2.4.23}$$

which ensure that $\dot{V}(e_1, e_2) < 0$. Furthermore, it is possible to show that:

$$\dot{V}(e_1, e_2) \leq -\frac{\lambda_{\min}^{1/2}\{P\}\lambda_{\min}\left\{\tilde{Q}\right\}}{\lambda_{\max}\{P\}} V^{1/2}(e_1, e_2). \tag{2.4.24}$$

Defining the auxiliary (positive) parameter γ as:

$$\gamma \triangleq \frac{\lambda_{\min}^{1/2}\{P\}\lambda_{\min}\left\{\tilde{Q}\right\}}{\lambda_{\max}\{P\}}, \tag{2.4.25}$$

one gets:

$$\dot{V}(e_1, e_2) \leq -\gamma V^{1/2}(e_1, e_2). \tag{2.4.26}$$

Given (2.4.26), the differential equation

$$\dot{v} = -\gamma\sqrt{v}, \;\; v(0) = v_0 \geq 0. \tag{2.4.27}$$

can be introduced. The analytical solution of (2.4.27) is [76]:

$$v = \left(\sqrt{v_0} - \frac{\gamma}{2}t\right)^2. \tag{2.4.28}$$

It is straightforward to verify that $V(e_1, e_2) \leq v$ if $V(e_1(0), e_2(0)) < v_0$, where $e_1(0)$ and $e_2(0)$ are the initial conditions for e_1, e_2, respectively. It follows that both $V(e_1, e_2)$, and the error components e_1, e_2 converge to zero in finite time. The value for the finite time can be computed as:

$$t^\star = 2\frac{\sqrt{V(e_1(0), e_2(0))}}{\gamma}. \tag{2.4.29}$$

From the development in this section, one can conclude that if the design constants of the ST observer satisfy (2.4.23), the conditions $e_1 = e_2 = 0$ are reached in a finite time $t^\star$. Once the sliding motion is enforced, the ST observer displays totally insensitivity to the bounded matched perturbation $f(x_1, x_2, t)$ appearing in the so-called matched channel of the perturbed double integrator dynamical system (2.4.1) [75].

2.4.2.1 Unknown Function Reconstruction via ST Observer

Super-Twisting SM observer can be profitably employed to asymptotically estimate the unknown function $f(x_1, x_2, t)$, which appears in the matched channel of the considered dynamical system (2.4.1). During the sliding motion of the error dynamics (2.4.8), the conditions $e_1 = e_2 = 0$ hold, which implies

$$-\left(k_2 \text{sign}(e_1)\right)_{eq} = f(x_1, x_2, t) \tag{2.4.30}$$

where $\left(k_2 \text{sign}(e_1)\right)_{eq}$ represents the average value of $k_2 \text{sign}(e_1)$. An approximation $\hat{f}$ of the unknown bounded function $f(x_1, x_2, t)$ can be obtained in real time by means of a low-pass filter with the associate time constant τ [64] [78]:

$$\hat{f} = \frac{1}{\tau}\left(-k_2 \text{sign}(e_1) - \hat{f}\right) \tag{2.4.31}$$

2.4.3 Sub-Optimal Sliding Mode Observer

The use of the so-called sub-optimal sliding mode methodology [79] can be effectively exploited to the design a robust SM observer. Given the double integrator dynamical system (2.4.1), the associated sub-optimal SM observer is governed by the following dynamics

$$\begin{array}{rcl} \dot{\hat{x}}_1 & = & \hat{x}_2 \\ \dot{\hat{x}}_2 & = & u_{\rm sub} \end{array} \tag{2.4.32}$$

where $\hat{x}_1$ is the estimate of x_1, $\hat{x}_2$ is the estimate of x_2, and $u_{\rm sub}$ is equal to [79]

$$u_{\rm sub} \triangleq -\mu V^{\max} \text{sign}\left(e_1 - \frac{1}{2}e_1^{\max}\right). \tag{2.4.33}$$

where $e_1 \triangleq x_1 - \hat{x}_1$. Moreover, the following relations are considered

$$\begin{cases} \mu^* & \in (0,1] \\ V^{\max} & > \max\left(\frac{\Delta_f}{\mu^*}, \frac{4\Delta_f}{3-\mu^*}\right). \end{cases} \tag{2.4.34}$$

The signal $e_1^{\max}$ is computed by using the peak detection algorithm. This algorithm was originally designed in [79] for control purpose, and it is extended in the present chapter to the observer purpose. Consider the following auxiliary signal.[2]

$$\Delta(t) \triangleq [e_1(t-\varepsilon) - e_1(t)]\, e_1(t), \tag{2.4.35}$$

where $\varepsilon > 0$ is a small constant (in practical cases, ε can represent a time delay either due to the switching or to the measuring devices). At the initial time instant t_0, the initial condition $e_1^{\max} = e_1(t_0)$ and $e_1(t_0 - \varepsilon) = 0,$ if $t < \varepsilon$, are adopted. $\forall t > t_0$, the following steps are executed:

1. if $(\Delta(t) < 0)$ $e_1^{\rm mem} = e_1(t)$;
2. if $(\Delta(t) \leq 0)$
   (a) if $(|e_1^{\rm mem}| \leq |e_1^{\max}|$ **and** $e_1^{\rm mem} e_1^{\max} > 0)$ $\quad e_1^{\max} = e_1^{\rm mem}$;
   (b) else $\quad e_1^{\max} = e_1^{\max}$;
3. if $(\Delta(t) > 0)$ $e_1^{\max} = e_1^{\rm mem}$

In addition, the variable μ is governed by

$$\mu = \begin{cases} \mu^* & \text{if } \left(e_1 - \frac{1}{2}e_1^{\max}\right)(e_1^{\max} - e_1) > 0 \\ 1 & \text{if } \left(e_1 - \frac{1}{2}e_1^{\max}\right)(e_1^{\max} - e_1) \leq 0. \end{cases} \tag{2.4.36}$$

[2] The explicit dependence on the time t is here introduced for the sake of clarity.

The error dynamics is obtained by subtracting the double integrator dynamical system (2.4.1) from the sub-optimal observer dynamics (2.4.32) and they are

$$\begin{array}{rcl} \dot{e}_1 & = & e_2, \\ \dot{e}_2 & = & -\phi_i - \mu V^{\max}\text{sign}\left(e_1 - \frac{1}{2}e_1^{\max}\right), \end{array} \tag{2.4.37}$$

where $e_2 = \hat{x}_2 - x_2$. The system in (2.4.37) is in the standard form for the sub-optimal sliding mode controlled system [79], [80]. More precisely, if the signal u_{sub} satisfies the inequalities in (2.4.34), it follows that (2.4.37) converges to the origin in finite time, guaranteeing a correct state estimation of the state variable x_2.

2.4.4 Third Order Sliding Mode Observer

It is now assumed that also the first time derivative of the nonlinearity appearing in (2.4.1) is bounded, which means that

$$|\dot{f}(x_1, x_2, t)| \leq \Delta_{\dot{f}} \tag{2.4.38}$$

where $\Delta_{\dot{f}}$ is a known positive constant. A third order SM observer in the form of

$$\begin{array}{rcl} \dot{\hat{x}}_1 & = & -k_1|e_1|^{2/3}\text{sign}\,(e_1) + \hat{x}_2 \\ \dot{\hat{x}}_2 & = & -k_2|e_1|^{1/3}\text{sign}\,(e_1) + \hat{z}_3 \\ \dot{\hat{z}}_3 & = & -k_3\text{sign}\,(e_1) \\ y & = & \hat{x}_1 \end{array} \tag{2.4.39}$$

can be introduced, where $\hat{x}_1$ is an estimate of x_1, $\hat{x}_2$ is an estimate of x_2, $\hat{z}_3$ is an auxiliary variable of the observer, $e_1 \triangleq \hat{x}_1 - x_1$, and k_1, k_2, and k_3 are positive constants to be designed. By subtracting (2.4.1) from (2.4.39), the error dynamics take the form

$$\begin{array}{rcl} \dot{e}_1 & = & -k_1|e_1|^{2/3}\text{sign}\,(e_1) + e_2 \\ \dot{e}_2 & = & -k_2|e_1|^{1/3}\text{sign}\,(e_1) + \hat{z}_3 - f(x_1, x_2, t) \\ \dot{\hat{z}}_3 & = & -k_3\text{sign}\,(e_1) \end{array} \tag{2.4.40}$$

where $e_2 \triangleq \hat{x}_2 - x_2$. The auxiliary error variable $e_3 \triangleq \hat{z}_3 - f(x_1, x_2)$ can be introduce, thus rewriting (2.4.40) as

$$\begin{array}{rcl} \dot{e}_1 & = & -k_1|e_1|^{2/3}\text{sign}\,(e_1) + e_2 \\ \dot{e}_2 & = & -k_2|e_1|^{1/3}\text{sign}\,(e_1) + e_3 \\ \dot{e}_3 & = & -k_3\text{sign}\,(e_1) - \dot{f}(x_1, x_2, t) \end{array} \tag{2.4.41}$$

The system in (2.4.41) is in the canonical form of the third order SM observer error dynamics in [81]. Following [82], a Lyapunov function candidate in the form of

$$V(e_1, e_2, e_3) = \beta_1|e_1|^{5/3} - \beta_2 e_1 e_2 + \beta_3|e_2|^{5/2} - \beta_4 e_2|e_3|^3\text{sign}(e_3) + \beta_5|e_3|^5 \tag{2.4.42}$$

can be employed to show that the origin is finite time stable for error dynamics (2.4.41), where $\beta_1, \ldots, \beta_5$ are arbitrary positive constants. In order to tune the design constants, let

$$\tilde{L} = \Delta_{\dot{f}}/\tilde{\Delta}_0 \tag{2.4.43}$$

where $\tilde{\Delta}_0$ is known constants. Then, if $[\overline{k}_1,\, \overline{k}_2,\, \overline{k}_3]^T$ are the triplet of the design constants tuned in [82] for the unperturbed case (i.e., for the case when $\dot{f}(x_1, x_2) = 0$), it is possible to prove that $[k_1,\, k_2,\, k_3]^T$ can be chosen according to [82] :

$$[k_1,\, k_2,\, k_3]^T = \mathrm{Diag}\left(\tilde{L}_i^{1/3},\, \tilde{L}_i^{2/3}, \tilde{L}_i\right) [\overline{k}_1,\, \overline{k}_2,\, \overline{k}_3]^T \tag{2.4.44}$$

The numerical representation of the tuning rules (2.4.44) is also developed in [73]:

$$k_3 > \Delta_{\dot{f}} \tag{2.4.45}$$

$$k_2 = 5.3k_3^{2/3} \tag{2.4.46}$$

$$k_1 = 3.34k_3^{1/3}. \tag{2.4.47}$$

Note that the gain k_3 is the first to be chosen in order to compensate the effect of $\dot{f}(x_1, x_2, t)$. Furthermore, if the vector of the initial conditions of (2.4.44) is $e_0 \triangleq \mathrm{Col}(e_1(0), e_2(0), e_3(0))$, then the error dynamics converge to the origin in a finite time T_{e_0}, which can upper-bounded as

$$T_{e_0} \leq \frac{V^{1/5}(e_0)}{c_i} \tag{2.4.48}$$

where c_i is a positive constant. Therefore, a sliding motion is characterised by the following conditions

$$e_1 = e_2 = e_3 = 0, \tag{2.4.49}$$

which are enforced in finite time and they guarantee a finite time state estimation.

2.4.4.1 Unknown Function Reconstruction

A scheme which is alternative to the one proposed in Section 2.4.2.1 can be adopted to estimate the unknown function $f(x_1, x_2, t)$. In contrast to the one proposed in 2.4.2.1, in the present framework the estimation is achieved in finite time and the low-pass filter is no longer required. These because during the sliding motion (2.4.49)

$$\hat{z}_3 - f(x_1, x_2, t) = 0 \tag{2.4.50}$$

From (2.4.50) it follows that an estimate $\hat{f}$ of $f(x_1, x_2)$ can be shown to be

$$\hat{z}_3 = \hat{f} \tag{2.4.51}$$

It is apparent that the continuous-time auxiliary variable $\hat{z}_3$, which is available in real time, constitutes an estimate of $f(x_1, x_2)$ in finite time.

Chapter 3

Power System Description

Abstract This chapter aims to present dynamical models of the components of power systems, including synchronous generators, hydroelectric and thermal turbine-governors, wind power sources, inverter power sources, static and dynamical loads. The introduced models represent the starting point to design schemes to monitor and control the systems developed in the rest of the present thesis. The second part of the chapter develops the so-called structure-preserving power system models, typically employed for simulations and stability analysis of large-scale power networks. For an extensive descriptions of the introduced dynamical models, the interested reader is also referred to dedicated books available in the literature. Amongst the others, it is worth remembering the relevant contributions [5], [4], [83], and [37].

3.1 Conventional Generators

Synchronous generators represent the most important power source component in power systems [5]. They are moved by different kinds of turbine (such as steam, hydraulic, gas or wind turbines), and they convert input mechanical power into electrical power to supply the demand. In power system analysis, several models have been employed for the synchronous generators, from the lower to the higher complexity and accuracy. In this section, the well-established swing equations will be explicitly derived, which model the unbalance between electromagnetic and mechanical torque [4], [5]. The transient voltage dynamics will be presented at the end of this section, which constitute, together with the aforementioned swing equations, the widely used flux-decay model [37]. Furthermore, the dynamics of the hydraulic and steam turbines-governors dynamics associated with conventional generators will be illustrated. Throughout the reading of this chapter and particularly whenever a dynamical model is introduced, the reader is encouraged to constantly refer to Section 3.6, where the list of all the symbols and variables introduced in the chapter is provided, together with the associated measurement units and physical meanings.

3.1.1 Synchronous Generators Dynamical Models

Angle Definitions Figure 3.1.1 shows a schematic of the cross-section of the i-th synchronous generator. Three reference frames are introduced: a fixed axis x, the reference frame dqO, which is

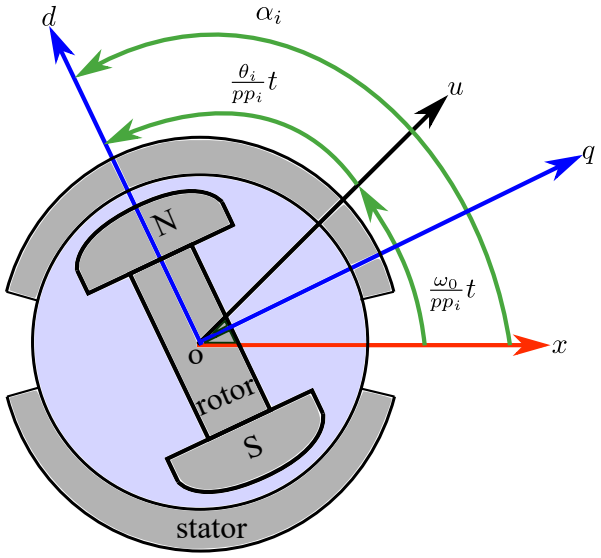

Figure 3.1.1: A simplified schematic of a synchronous generator along with the angles of interest in the swing equations.

in-built with the rotor, and the axis u, which rotates at the constant speed ω_0/pp_i, where $\omega_0 = 2\pi f_0$, f_0 is the rated value of the power grid electrical frequency, and pp_i is the number of the pole-pairs of the generator. Note that the rotor of a synchronous generator with pp_i pole-pairs has a rated mechanical angular speed equal to $\omega_{m_R} = \omega_0/pp_i$. The angular displacement between the axis x and the rotor is given by the variable α_i. It is also useful to introduce the angle $\omega_0 t/pp_i$ between the axis x and u. The auxiliary variable θ_i/pp_i denotes the angular displacement between the axis d and u. From the developments in the present section, it is apparent that the variable θ_i can be considered as the angular position of the rotor in electrical radians with respect to the synchronously rotating reference axis u. Justified by Figure 3.1.1, the basic algebraic relation follows:

$$\theta_i = pp_i\alpha_i - \omega_0 t. \tag{3.1.1}$$

Differentiating (3.1.1) with respect to time it yields

$$\dot{\theta}_i = pp_i\dot{\alpha}_i - \omega_0 = \Delta\omega_i, \tag{3.1.2}$$

where $\Delta\omega_i$ is the electrical angular speed deviation from the rated value ω_0. Differentiating (3.1.2) yields:

$$\ddot{\theta}_i = pp_i\ddot{\alpha}_i = \Delta\dot{\omega}_i. \tag{3.1.3}$$

Equations (3.1.1)-(3.1.3) become fundamental in deriving the Swing Equations.

Swing Equations The swing equations, which will be derived in the present section, are a set of two differential equations modelling the accelerations and the decelerations of synchronous generators due to possible mismatches between the power generation and consumption.

The kinetic energy E_i (expressed in (GJ)) stored in the rotating masses of a synchronous gener-

ator is defined by

$$E_i = S_i H_i, \tag{3.1.4}$$

where S_i is the apparent power base value (expressed in (GVA)), and H_i is the inertia constant of the generator (expressed in (s)). The basic equation of motion (Newton's equation) is [37]

$$J_i \dot{\omega}_{m_i} = J_i \ddot{\alpha}_i = T_{m_i} - T_{e_i}, \tag{3.1.5}$$

where J_i is the moment of inertia of the generator, ω_{m_i} is the mechanical angular speed, $\dot{\omega}_{m_i} = \ddot{\alpha}_i$ is the mechanical angular acceleration, T_{m_i} is the mechanical torque and T_{e_i} is the electromagnetic torque. Using (3.1.3), equation (3.1.5) can be rewritten as follows

$$J_i \frac{\ddot{\theta}_i}{pp_i} = T_{m_i} - T_{e_i}. \tag{3.1.6}$$

By making use of (3.1.4), one gets

$$H_i = \frac{E_i}{S_i} = \frac{\frac{1}{2} J_i \omega_{m_R}^2}{S_i}, \tag{3.1.7}$$

where ω_{m_R} is the rated value of the mechanical angular speed of the generator. Given (3.1.7), the moment of inertia J_i can be rewritten as function of the inertia constant as follow:

$$J_i = \frac{2H_i S_i}{\omega_{m_R}^2}. \tag{3.1.8}$$

Substituting for J_i from (3.1.8), equation (3.1.6) can be shown to become

$$\frac{2H_i S_i}{\omega_{m_R}^2} \frac{\ddot{\theta}_i}{pp_i} = T_{m_i} - T_{e_i}. \tag{3.1.9}$$

Since $\omega_{m_R} = \omega_0 / pp_i$, equation (3.1.9) becomes

$$\frac{2H_i S_i}{\frac{\omega_0{}^2}{(pp_i)^2}} \frac{\ddot{\theta}_i}{pp_i} = T_{m_i} - T_{e_i}. \tag{3.1.10}$$

Multiplying both the left and right side of (3.1.10) by $\dot{\alpha}_i$ and making use of (3.1.2), the balance of torque is transformed into the balance of power:

$$\frac{2H_i}{\frac{\omega_0{}^2}{(pp_i)^2}} \frac{\ddot{\theta}_i}{pp_i} \left(\frac{\dot{\theta}_i + \omega_0}{pp_i} \right) = \frac{T_{m_i} - T_{e_i}}{S_i} \dot{\alpha}_i \tag{3.1.11}$$

$$\frac{2H_i}{\omega_0^2} \ddot{\theta}_i \left(\dot{\theta}_i + \omega_0 \right) = P_{m_i} - P_{e_i}, \tag{3.1.12}$$

where P_{m_i} is the mechanical input power, and P_{e_i} is the total electrical active power injected into the power grid by the i-th synchronous generator. Note that both the two powers are normalised with respect to the base power S_i, and therefore expressed in (p.u.). By defining the parameter $M_i \triangleq 2H_i/\omega_0$, the system in equations (3.1.11)-(3.1.12) can be further compactly rewritten. In

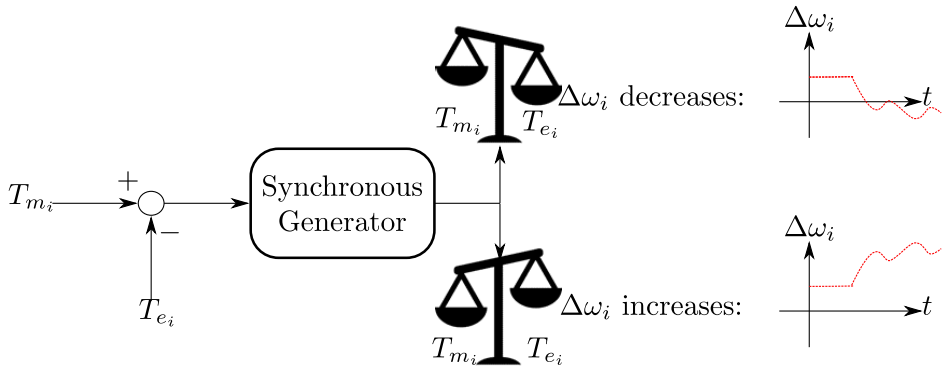

Figure 3.1.2: A visual representation of the unbalance between the mechanical torque T_{m_i} and the electrical torque T_{e_i}, which gives rise to changes to $\Delta\omega_i$ of opposite sign.

additions, two situations are introduced as follows:

$$M_i\ddot{\theta}_i = P_{m_i} - P_{e_i} \quad \text{if} \quad \dot{\theta}_i + \omega_0 \approx \omega_0, \tag{3.1.13}$$

$$\frac{M_i}{\omega_0}\ddot{\theta}_i = \frac{P_{m_i} - P_{e_i}}{\left(\dot{\theta}_i + \omega_0\right)} \quad \text{otherwise.} \tag{3.1.14}$$

Provided the mechanical angular speed remains sufficiently close to its rated value (which implies that $\dot{\theta}_i + \omega_0 \approx \omega_0$), equation (3.1.13) can represent the dynamics of the synchronous generator. If the previous condition is no longer satisfied, the equation to be considered is (3.1.14). A damping action described by the signal $-D_i\Delta\omega_i$ can be included in (3.1.14), which yields:

$$M_i\ddot{\theta}_i = P_{m_i} - P_{e_i} - D_i\Delta\omega_i. \tag{3.1.15}$$

Remark 3.1. Note that the signal $D_i\Delta\omega_i$ can represent the actions of both the damping and the droop control in (3.1.15) only when the turbine-governor dynamics are neglected in the simulation studies, as in [46]. The modification in the modelling due to the presence of the turbine-governor will be discussed in the rest of the present chapter.

A standard state-space representation can be introduced for the synchronous generator dynamics as follows:

$$\begin{aligned} \dot{\theta}_i &= \Delta\omega_i, \\ M_i\Delta\dot{\omega}_i &= P_{m_i} - P_{e_i} - D_i\Delta\omega_i \end{aligned} \tag{3.1.16}$$

It is important to highlight that in (3.1.16) the signal P_{m_i} denotes the input of the synchronous generator, whilst an expanded expression for P_{e_i}, depending on power grid topology, will be introduced in the remainder of the chapter. Figure 3.1.2 shows a visual representation of the qualitative behaviours of the synchronous generator in presence of unbalance of opposite sign between the mechanical and the electrical torques.

Figure 3.1.3: A picture of a thermal power plant. [Credits: free public domain images `Pixabay.com`]

3.1.2 Turbine-Governor Description

The turbine-governor systems aim to convert the kinetic energy of water and the thermal energy developed during the combustion of fossil fuels or nuclear reactions into mechanical energy moving the synchronous generators. Dedicated dynamical models have been developed for turbine-governor systems, and they are of paramount importance for simulations, dynamical stability, analysis and studies in power systems applications.

3.1.2.1 Steam Turbine-Governor

A simplified single steam-turbine dynamics are given by the following linear state-space representation [84]:

$$\begin{aligned} \dot{P}_{m_i} &= -\tfrac{1}{T_{t_i}} P_{m_i} + \tfrac{1}{T_{t_i}} P_{g_i} \\ \dot{P}_{g_i} &= -\tfrac{1}{R_i T_{g_i}} \Delta\omega_i - \tfrac{1}{T_{g_i}} P_{g_i} + \tfrac{1}{T_{g_i}} u_i \end{aligned} \tag{3.1.17}$$

$$\begin{aligned} \dot{\theta}_i &= \Delta\omega_i, \\ M_i \Delta\dot{\omega}_i &= P_{m_i} - P_{e_i} - D_i \Delta\omega_i \end{aligned} \tag{3.1.18}$$

In the system of equations (3.1.18), the synchronous generator dynamical model has been rewritten for the sake of clarity.

The so-called single tandem reheat arrangement constitutes the most common configuration practically used in large thermal power plants [84]. In such configuration, three steam turbines are attached to the same shaft. The steam coming from the boiler is expanded through three stages, thus producing three contributions for the mechanical power. The corresponding dynamical model can be shown to be:

$$\begin{aligned} \dot{P}_{m_{a_i}} &= -\tfrac{1}{T_{t_{a_i}}} P_{m_{a_i}} + \tfrac{1}{T_{t_{a_i}}} P_{g_i} \\ \dot{P}_{m_{b_i}} &= -\tfrac{1}{T_{t_{b_i}}} P_{m_{b_i}} + \tfrac{1}{T_{t_{b_i}}} P_{m_{a_i}} \\ \dot{P}_{m_{c_i}} &= -\tfrac{1}{T_{t_{c_i}}} P_{m_{c_i}} + \tfrac{1}{T_{t_{c_i}}} P_{m_{b_i}} \\ \dot{P}_{g_i} &= -\tfrac{1}{R_i T_{g_i}} \Delta\omega_i - \tfrac{1}{T_{g_i}} P_{g_i} + \tfrac{1}{T_{g_i}} u_i \\ P_{m_i} &= \alpha_{t_{a_i}} P_{m_{a_i}} + \beta_{t_{b_i}} P_{m_{b_i}} + \gamma_{t_{c_i}} P_{m_{c_i}} \end{aligned} \tag{3.1.19}$$

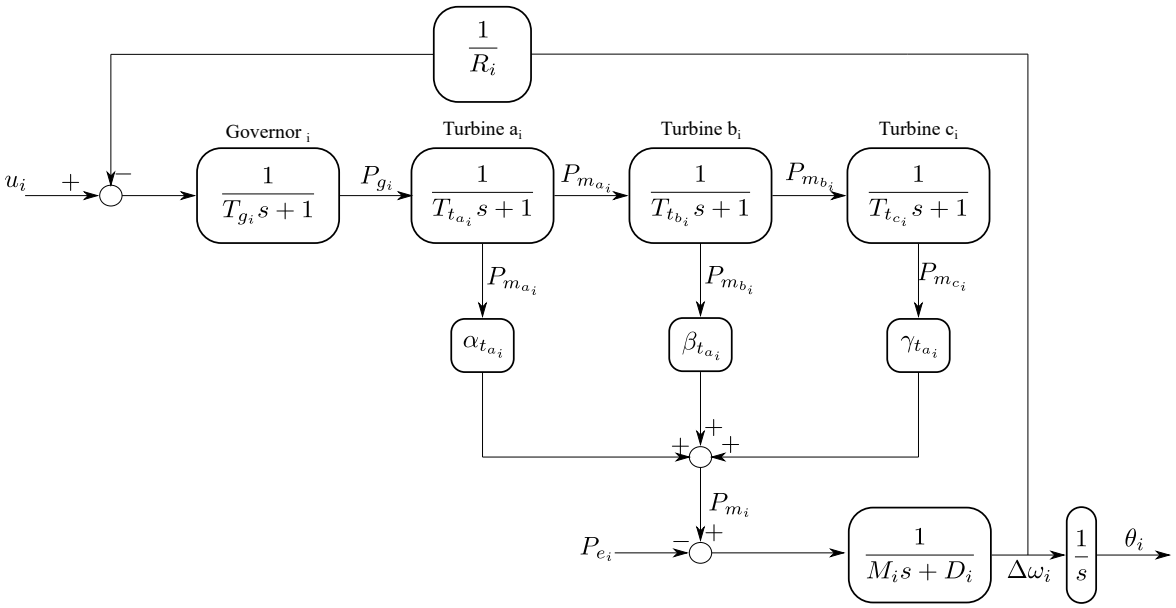

Figure 3.1.4: A schematic of a single tandem steam reheat steam turbines-governor dynamical model.

$$\begin{aligned} \dot{\theta}_i &= \Delta\omega_i, \\ M_i\Delta\dot{\omega}_i &= P_{m_i} - D_i\Delta\omega_i \end{aligned} \tag{3.1.20}$$

Figure 3.1.4 shows a block scheme of the system in equations (3.1.19)-(3.1.20). The standard transfer function representation [68] for linear time invariant system has been adopted in the schematic.

3.1.2.2 Hydraulic Turbine-Governor

The linearised hydraulic turbine and governor model comprises a governor (similar to the one just described for thermal power plants), a transient droop compensator, and the hydraulic turbine. Note that the transient droop compensator has to be included between the governor and the hydraulic turbine to ensure and to enhance the stability of the system [5]. Specifically, as discussed in [5], the transient compensator was conceived to deal with the peculiar dynamical response of water inertia. The resulting dynamical model for the hydroelectric power sources can be shown to be:

$$\begin{aligned} \dot{P}_{g_i} &= -\tfrac{D_{g_i}}{T_{g_i}}\Delta\omega_i - \tfrac{1}{T_{g_i}}P_{g_i} + \tfrac{1}{T_{g_i}}u_i \\ \dot{P}_{c_i} &= -\tfrac{1}{T_{c_{1_i}}}P_{c_i} + P_{g_i} \\ \dot{W}_i &= \tfrac{T_{c_{1_i}}}{T_{c_{2_i}}}P_{g_i} + \tfrac{T_{c_{2_i}}-T_{c_{1_i}}}{T^2_{c_{2_i}}}P_{c_i} - \tfrac{2}{T_{h_i}}W_i \\ P_{m_i} &= -2\tfrac{T_{c_{1_i}}}{T_{c_{2_i}}}P_{g_i} + 2\tfrac{T_{c_{1_i}}-T_{c_{2_i}}}{T^4_{c_{2_i}}}P_{c_i} + \tfrac{6}{T_{h_i}}W_i = P_{m_i}. \end{aligned} \tag{3.1.21}$$

$$\begin{aligned} \dot{\theta}_i &= \Delta\omega_i, \\ M_i\Delta\dot{\omega}_i &= P_{m_i} - P_{e_i} - D_i\Delta\omega_i \end{aligned} \tag{3.1.22}$$

Figure 3.1.4 shows a block scheme of the system in equations (3.1.21)-(3.1.22). The standard transfer function notation for linear time invariant system has been adopted also for the hydraulic turbine-governor dynamical model.

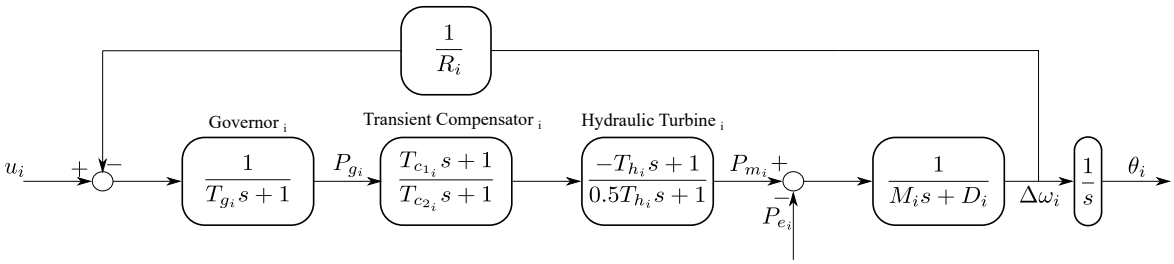

Figure 3.1.5: A schematic of hydraulic turbine-governor dynamical model.

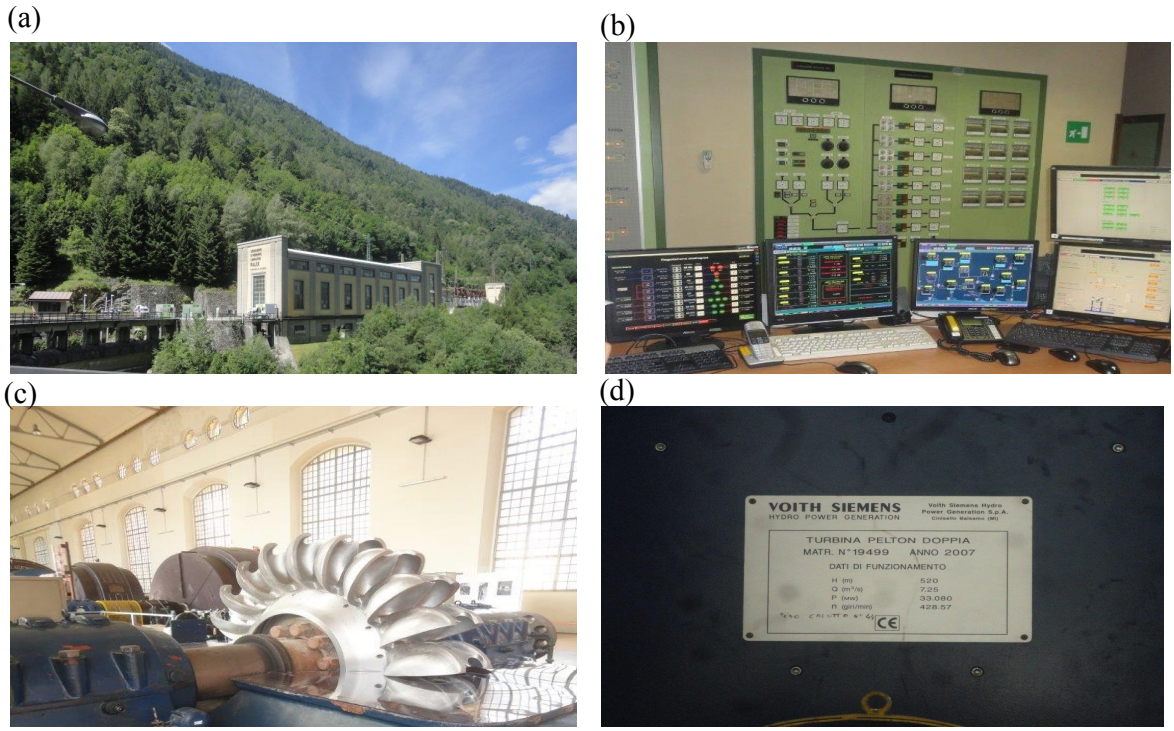

Figure 3.1.6: **(a):** The building of an hydroelectric power plant in the Alps, Italy. **(b):** A modern computer-based control and monitor scheme of hydroelectric power plant. **(c):** A Pelton wheel. **(d):** Numerical data of a Pelton wheel. [Credits: Gianmario Rinaldi].

Figure 3.2.1: A picture of a wind farm. [Credits: free public domain images `Pixabay.com`]

3.2 Renewable Sources Dynamical Models

In recent years, the installed capacity of renewable energy sources in power systems is increasing worldwide, especially led by wind power sources. In the present thesis, the dynamical models of both wind power sources and inverters with so-called capacitive inertia will be presented.

3.2.1 Wind Power Sources

The so-called two masses dynamical model for the wind power sources comprises two equivalent masses M_{w1_i} and M_{w2_i}, which are schematically represented in Figure 3.2.2. The mass M_{w1_i} accounts for the high speed shaft, the gearbox and the generator rotor, whilst the mass M_{w2_i} accounts for the low-speed turbine components. The corresponding dynamical model yields

$$\begin{aligned} \dot{\theta}_{w1_i} &= \Delta\omega_{w1_i} \\ M_{w1_i}\Delta\dot{\omega}_{w1_i} &= -D_{w_i}\left(\Delta\omega_{w1_i} - \Delta\omega_{w2_i}\right) - k_{w_i}\left(\theta_{w1_i} - \theta_{w2_i}\right) - P_{ew_i} \\ \dot{\theta}_{w2_i} &= \Delta\omega_{w2_i} \\ M_{w2_i}\Delta\dot{\omega}_{w2_i} &= D_{w_i}\left(\Delta\omega_{w1_i} - \Delta\omega_{w2_i}\right) + k_{w_i}\left(\theta_{w1_i} - \theta_{w2_i}\right) + T_{w_i} \end{aligned} \tag{3.2.1}$$

3.2.2 Inverter-Based Power Sources

Synchronous generators, which represent the conventional electrical power sources, are characterised by massive rotational parts, which therefore result in massive kinetic energy. The resulting mechanical energy reservoir exhibits a stabilising property when power unbalances or faults occur. The increasing interconnection of renewable energy-based sources, dominated by inverter-based configuration, partially compromises the intrinsic stabilising property of conventional synchronous generator-based power sources. To cope with this issue, it is possible to implement dedicated control architectures for the inverter-based renewable sources devoted to mimic and emulate the dynamical behaviours of synchronous generators has been pointed out. To this end, several promising control approaches of inverters have been conceived [85]. In the present section, the recently introduced

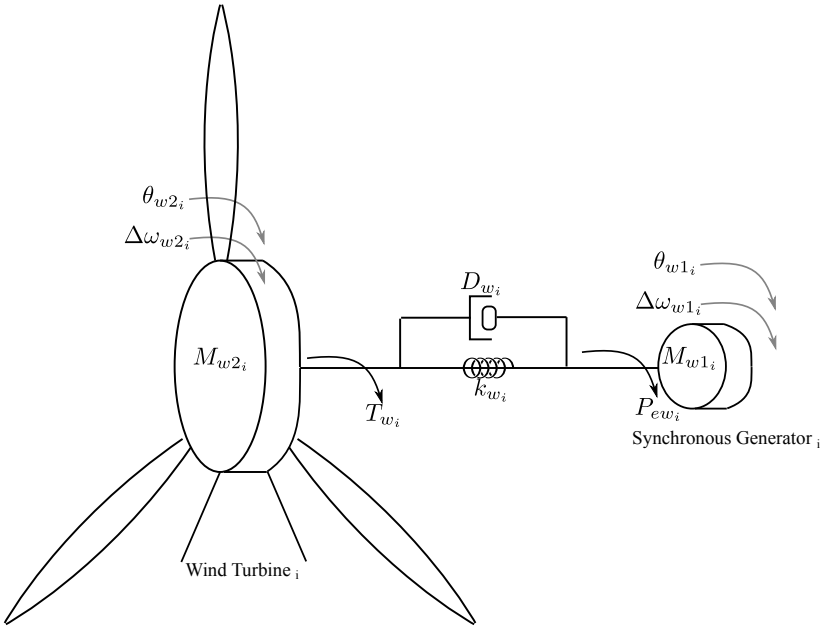

Figure 3.2.2: A schematic of the two masses wind power source.

Figure 3.2.3: A picture of a solar power plant. [Credits: free public domain images `Pixabay.com`]

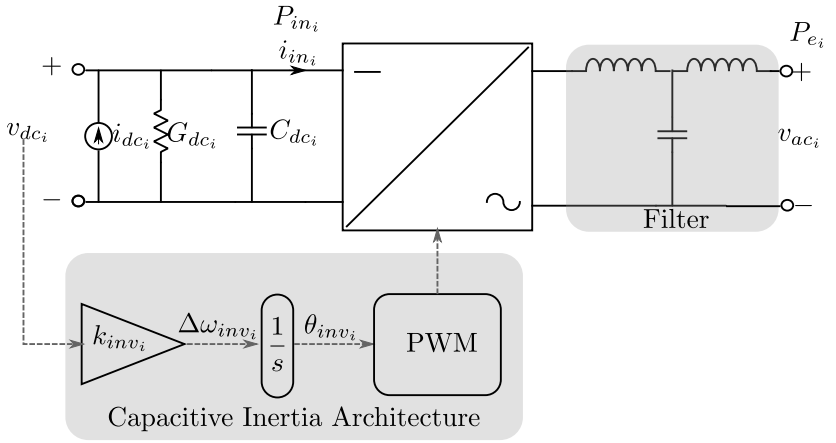

Figure 3.2.4: A schematic of the inverter with capacitive inertia architecture.

inverter with capacitive inertia methodology will be considered [86]. Exploiting Figure 3.2.4, the following differential equation can be obtained by applying standard circuit theory techniques:

$$C_{dc_i}\dot{v}_{dc_i} = -G_{dc_i}v_{dc_i} - i_{in_i} + i_{dc_i} \tag{3.2.2}$$

The underling idea of the inverter with capacitive inertia is to regulate the voltage v_{dc_i} of the dc-link capacitor C_{dc_i} according to the algebraic condition

$$v_{dc_i} = k_{inv_i}\Delta\omega_{inv_i} \tag{3.2.3}$$

where the positive known constant $k_{inv_i} = \omega_0/v^*_{dc_i}$, and $v^*_{dc_i}$ denotes the nominal value of the voltage of the dc capacitor. Given (3.2.3), the differential equation (3.2.2) is rewritten as:

$$\begin{aligned} \dot{\theta}_{inv_i} &= \Delta\omega_{inv_i}, \\ M_{inv_i}\Delta\dot{\omega}_{inv_i} &= -D_{inv_i}\Delta\omega_{inv_i} + \tfrac{P_{in_i}-P_{e_i}}{\Delta\omega_i+\omega_0} \end{aligned} \tag{3.2.4}$$

where the inverter inertia $M_{inv_i} \triangleq C_{dc_i}/k^2_{inv_i}$, and the inverter droop coefficient $D_{inv_i} \triangleq G_{dc_i}/k_{inv_i}$.

Remark 3.2. Note that the system in equation (3.2.4) is similar to the one in (3.1.14). Specifically, the system in (3.2.4) is the so-called improved swing equations [87].

3.3 Loads Dynamics

The term loads in power system context includes the components connected to the grid which consume electrical power for a large class of applications [37], [5]. In the present section, two types of models will be presented: the static load model, governed by algebraic equations, and the dynamical model, governed by ordinary differential equations.

3.3.1 Static Load Model

The static load model is described by

$$0 \quad = \quad P_{l_i} - P_{e_i} \tag{3.3.1}$$

where P_{l_i} denotes the specified electrical active power which is consumed by the i-th load, whilst P_{e_i} denotes the total electrical active power flowing from the i-th load to the neighbouring (generators or loads) components.

3.3.2 Dynamical Load Models

Frequency-dependent dynamical systems are often preferred for load modelling. This because they can also describe the so-called active loads, which are characterised by the presence of small locally distributed renewable energy sources. The following algebraic equation yields:

$$0 \quad = \quad -D_i \Delta\omega_i + P_{l_i} - P_{e_i} \tag{3.3.2}$$

Equation (3.3.2) can be easily transformed into a differential equation by introducing the voltage phase angle θ_i associated with the i-th load. Since $\dot{\theta}_i = \Delta\omega_i$, it follows that

$$D_i \dot{\theta}_i \quad = \quad P_{l_i} - P_{e_i} \tag{3.3.3}$$

For loads characterised by relevant value of inertia (such as utilities with high presence of induction and synchronous motors), th second order dynamical model

$$\begin{aligned} \dot{\theta}_i &= \Delta\omega_i, \\ M_i \Delta\dot{\omega}_i &= P_{l_i} - P_{e_i} - D_i \Delta\omega_i \end{aligned} \tag{3.3.4}$$

can be used.

3.4 Power Flow Description

Figure 3.4.1 shows a schematic of two components of a power system (which can be of any type, such as synchronous generators, loads, and inverters), connected via a lossless power transmission line with the associate line inductance x_{ij}. For practical perspective, Figure 3.4.2 shows a power transmission line under construction in Northern Italy. A voltage waveform in the form of $V_i \cos(\omega_0 t + \theta_i)$ is associate with each component. The positive variable V_i represents the voltage magnitude of the i-th component. The electrical active power flowing from the i-th to the j-th component can be described by a nonlinear or a linearised expressions.

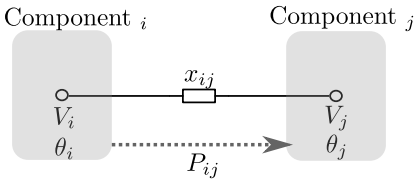

Figure 3.4.1: A schematic of two components i, j of a power system interconnected by a power transmission line x_{ij} allowing a power flow exchange P_{ij}.

Figure 3.4.2: A 380 kV voltage power transmission line under construction in Valtellina, Alps, Northern Italy [Credits: Gianmario Rinaldi].

3.4.1 Nonlinear Power Flow

The nonlinear expression for the electrical active power flowing from the i-th to the j-th component can be shown to be [37]

$$P_{ij} = \frac{V_i V_j}{x_{ij}} \sin\left(\theta_i - \theta_j\right) \tag{3.4.1}$$

In case the voltage magnitude is assumed constant, it is convenient to introduce the auxiliary (positive) constants

$$\gamma_{ij} \triangleq \frac{V_i V_j}{x_{ij}} \tag{3.4.2}$$

and to rewrite (3.4.1) as:

$$P_{ij} = \gamma_{ij} \sin\left(\theta_i - \theta_j\right) \tag{3.4.3}$$

Remark 3.3. According to the nonlinear power flow formulation in (3.4.1), one can conclude that also the signal P_{e_i}, which models the total electrical active power flowing from the i-th component to its neighbourhood $\mathcal{N}_i$, takes the same form. Therefore the expression

$$P_{e_i} = \sum_{j \in \mathcal{N}_i} \frac{V_i V_j}{x_{ij}} \sin\left(\theta_i - \theta_j\right) \tag{3.4.4}$$

can be substituted wherever used in the previous sections of this chapter.

Synchronous Generator Model with Transient Voltage Dynamics Given the nonlinear power flow approach, a more accurate dynamical model for the synchronous generator can be introduced. This accounts also for for the transient voltage dynamics and it is given by:

$$\begin{aligned} \dot{\theta}_i &= \Delta\omega_i, \\ \dot{e}_{q_i} &= \tfrac{1}{T_{d0_i}}\Big(E_{f_i} - e_{q_i} - \big(x_{d_i} - x'_{d_i}\big)\,\tfrac{e_{q_i} - V_i\cos(\theta_i)}{x'_{d_i}}\Big) \\ M_i\Delta\dot{\omega}_i &= \underbrace{P_{m_i} - \frac{V_i}{x'_{d_i}} e_{q_i}\sin(\theta_i) - \frac{V_i^2}{2}\Big(\frac{1}{x_{q_i}} - \frac{1}{x'_{d_i}}\Big)\sin\big(2\theta_i\big)}_{P_{e_i}} - D_i\Delta\omega_i \end{aligned} \tag{3.4.5}$$

Nonlinear Improved Swing Equations Under the nonlinear power flow formulation, a variant of the generator model (3.1.16) can be introduced in order to reflect better the dynamical behaviours of synchronous generators [88]:

$$\begin{aligned} \dot{\theta}_i &= \Delta\omega_i, \\ M_i\Delta\dot{\omega}_i &= \tfrac{P_{m_i} - P_{d_i}}{(\Delta\omega_i + \omega_0)} - \tfrac{\sum_{j\in\mathcal{N}_i} \frac{V_iV_j}{x_{ij}}\sin(\theta_i - \theta_j)}{(\Delta\omega_i + \omega_0)} - D_i\Delta\omega_i \end{aligned} \tag{3.4.6}$$

The system in (3.4.6) represents the so-called improved swing equations.

3.4.2 Linearised DC Power Flow

If the difference between the i-th and the j-th voltage phase angle is acceptably small, i.e. $\theta_i - \theta_j \ll 1$, the standard small angle approximation can be employed, which yields:

$$P_{ij} = \frac{V_iV_j}{x_{ij}}\left(\theta_i - \theta_j\right) \tag{3.4.7}$$

In case the voltage magnitudes remain constant and both equal to $1\ (p.u.)$ in the two components, the expression in (3.4.7) can be further simplified as

$$P_{ij} = b_{ij}\left(\theta_i - \theta_j\right) \tag{3.4.8}$$

where $b_{ij} = 1/x_{ij}$. Analogously, the signal P_{e_i} expanded in (3.4.4) can be rewritten by using in the DC Power flow method:

$$P_{e_i} = \sum_{j=1}^{N} b_{ij}\left(\theta_i - \theta_j\right) \tag{3.4.9}$$

3.5 Structure-Preserving Power System Models

The structure-preserving approach, originally presented in [89] and in [90] for power systems, aims to explicitly model each component of the network. In contrast to model-reduction techniques [91],

the structure-preserving approach reveals to be more accurate, thus considering the expression of electrical power flow in each edge (i.e., in each power transmission line). After some basic recalls of graph theory, four structure-preserving models will be introduced. These display both Differential Algebraic Equations (DAEs) and Ordinary Differential Equations (ODEs) structures.

3.5.1 Graph Theory Recalls

A structure-preserving power system can be considered as connected and undirected graph $G(\mathcal{B}, \mathcal{E})$, with the set of buses (commonly called also nodes) $\mathcal{B} = \{1, \ldots, |\mathcal{B}|\}$, and the set of edges $\mathcal{E} \subseteq \mathcal{B} \times \mathcal{B}$. The set of buses will be partitioned into the so-called generation buses $\mathcal{G} = \{1, \ldots, |\mathcal{G}|\}$ and load buses $\mathcal{L} = \{|\mathcal{G}| + 1, \ldots, |\mathcal{B}|\}$, such that $\mathcal{B} = \mathcal{G} \cup \mathcal{L}$. The set of generators $\mathcal{G}$ comprises all the components which are considered sources of electrical active power. Analogously, the set of loads $\mathcal{L}$ comprises all the components which demand a specific amount of electrical active power. Each edge corresponds to an unordered pair of distinct nodes (i, j) and it is also characterised by its weight, which is the reciprocal of the corresponding power transmission line reactance, denoted as b_{ij}. It follows that each edge can be represent according to the following expression: $\{(i, j),\ b_{ij}\} \in \mathcal{E}$.

Definition 3.1 (Adjacent Buses and Neighbourhood Set). The i-th and the j-th buses of a power systems are said to be directly adjacent if they are linked by a power transmission line, which means that:

$$\exists \{(i, j),\ b_{ij}\} \in \mathcal{E}. \tag{3.5.1}$$

The neighbourhood of the i-th bus corresponds to the set (denoted as $\mathcal{N}_i$) of the buses directly adjacent to the i-th bus, which means

$$\mathcal{N}_i \triangleq \{k \mid \{(i, k),\ b_{ik}\} \in \mathcal{E}\}. \tag{3.5.2}$$

The set $\mathcal{N}_i$ is the union of two subsets $\mathcal{N}_i = \mathcal{M}_i \cup \mathcal{O}_i$, which are the neighbouring generator buses set $\mathcal{M}_i$ and the neighbouring load buses set $\mathcal{O}_i$.

Incident Matrix The matrix $B \in \mathbb{R}^{|\mathcal{B}| \times |\mathcal{E}|}$ is the so-called incident matrix matrix. Then, by arbitrarily labelling with a '+' and a '-' the ends of an edge k, the elements of B are defined as:

$$B_{ik} = \begin{cases} +1 & \text{if } i \text{ is the positive end of } k \\ -1 & \text{if } i \text{ is the negative end of } k \\ 0 & \text{otherwise.} \end{cases} \tag{3.5.3}$$

Laplacian Matrix The Laplacian matrix $L \in \mathbb{R}^{|\mathcal{B}| \times |\mathcal{B}|}$ captures the topology of the interconnections amongst the buses for a given power system, and its elements are defined as follows:

$$L \ = \ \begin{cases} L_{ii} & = \sum_{k \in \mathcal{N}_i} b_{ik} \\ L_{ij} & = -b_{ij}. \end{cases} \tag{3.5.4}$$

The Laplacian matrix is partitioned into four sub-matrices, which can be show to be:

$$L = \begin{bmatrix} L^{gg} & L^{gl} \\ L^{lg} & L^{ll} \end{bmatrix}, \tag{3.5.5}$$

where the sub-matrices $L^{gg} \in \mathbb{R}^{|\mathcal{G}|\times|\mathcal{G}|}$, $L^{gl} \in \mathbb{R}^{|\mathcal{G}|\times|\mathcal{L}|}$, $L^{lg} \in \mathbb{R}^{|\mathcal{L}|\times|\mathcal{G}|}$, $L^{ll} \in \mathbb{R}^{|\mathcal{L}|\times|\mathcal{L}|}$. Furthermore, in (3.5.5), the matrix L^{ll} is invertible [91].

3.5.2 Structure-Preserving DAEs Models

This section considers a structure-preserving model for power systems which exhibits a Differential Algebraic Equations (DAEs).

Remark 3.4. Note that in all the structure-preserving models that will be introduced in the remaining of this section, the turbine-governor dynamics are not explicitly written, but they can be easily added to each generator bus dynamical model.

Nonlinear DAEs Model Given a power network comprising $|\mathcal{G}|$ generators an $|\mathcal{L}|$ loads, the generator dynamics (3.1.16), the load dynamics (3.3.1), and under the nonlinear power flow formulation (3.4.2)-(3.4.4), it follows:

$$\begin{array}{rcll} \dot{\theta}_i & = & \Delta\omega_i & i \in \mathcal{B} \\ M_i\Delta\dot{\omega}_i & = & -D_i\Delta\omega_i + P_{m_i} - \sum_{j\in\mathcal{N}_i}\gamma_{ij}\sin(\theta_i-\theta_j) & i \in \mathcal{G} \\ 0 & = & P_{l_i} - \sum_{j\in\mathcal{N}_i}\gamma_{ij}\sin(\theta_i-\theta_j) & i \in \mathcal{L} \end{array} \tag{3.5.6}$$

The system in (3.5.6) takes the form of a nonlinear DAEs model, in which the algebraic part comprises all the load buses. Furthermore, (3.5.6) can be rewritten in a vectorial form as follows:

$$\begin{array}{rcl} \dot{\theta} & = & \Delta\omega \\ M_{\mathcal{G}}\Delta\dot{\omega}_{\mathcal{G}} & = & -D_{\mathcal{G}}\Delta\omega_{\mathcal{G}} - \nabla_{\mathcal{G}}U(\theta) \\ 0 & = & -\nabla_{\mathcal{L}}U(\theta) \end{array} \tag{3.5.7}$$

where:

$$\theta \triangleq \mathrm{Col}(\theta_1,\ldots,\theta_{|\mathcal{B}|}) \in \mathbb{R}^{|\mathcal{B}|},\ \Delta\omega_{\mathcal{G}} \triangleq \mathrm{Col}(\Delta\omega_1,\ldots,\Delta\omega_{|\mathcal{G}|}) \in \mathbb{R}^{|\mathcal{G}|}$$
$$\Delta\omega_{\mathcal{L}} \triangleq \mathrm{Col}(\Delta\omega_{|\mathcal{G}|+1},\ldots,\Delta\omega_{|\mathcal{B}|}) \in \mathbb{R}^{|\mathcal{L}|},\ \Delta\omega \triangleq \mathrm{Col}(\Delta\omega_{\mathcal{G}},\Delta\omega_{\mathcal{L}}) \in \mathbb{R}^{|\mathcal{B}|}$$
$$M_{\mathcal{G}} \triangleq \mathrm{Diag}((M_i)_{i\in\mathcal{G}}),\ M_{\mathcal{G}} \succ 0,\ D_{\mathcal{G}} \triangleq \mathrm{Diag}((D_i)_{i\in\mathcal{G}}),\ D_{\mathcal{G}} \succ 0,\ D_{\mathcal{G}} \in \mathbb{R}^{|\mathcal{G}|\times|\mathcal{G}|}$$

Finally, $U(\theta)$ denotes the so-called open-loop potential energy of the aggregated generator and load buses, which is given by [40], [92]:

$$U(\theta) \triangleq \underline{1}^T\Gamma\cos\left(B^T\theta\right) - p^T\theta \tag{3.5.8}$$

where $\Gamma = \mathrm{Diag}\left(\gamma_{ij}\right)_{\gamma_{ij}\in\mathcal{E}}, \Gamma \in \mathbb{R}^{|\mathcal{E}|\times|\mathcal{E}|}$, $p = \mathrm{Col}\left(P_{m_1}, \ldots, P_{m_{|\mathcal{G}|}}, P_{l_1}, \ldots, P_{l_{|\mathcal{L}|}}\right),\ p \in \mathbb{R}^{|\mathcal{B}|}$.

$$\nabla U(\theta) = \begin{bmatrix} \nabla_{\mathcal{G}} U(\theta) \\ \nabla_{\mathcal{L}} U(\theta) \end{bmatrix},\ \nabla U(\theta) \in \mathbb{R}^{|\mathcal{B}|} \tag{3.5.9}$$

represents the gradient of the potential energy $U(\theta)$ in (3.5.8), and the sub-vectors $\nabla_{\mathcal{G}} U(\theta) \in \mathbb{R}^{|\mathcal{G}|}$ and $\nabla_{\mathcal{L}} U(\theta) \in \mathbb{R}^{|\mathcal{L}|}$ represent contributions composed only of the components from the the sets $\mathcal{G}$ and $\mathcal{L}$, respectively.

Linearised DAEs Model If the DC power flow method is adopted, the following linearised system yields:

$$\begin{array}{rcll} \dot{\theta}_i & = & \Delta\omega_i & i \in \mathcal{B} \\ M_i \Delta\dot{\omega}_i & = & -D_i\Delta\omega_i + P_{m_i} - L^{gg}_{ii}\theta_i - \sum_{j\in\mathcal{N}_i} L^{gl}_{ij}\theta_j & i \in \mathcal{G} \\ 0 & = & P_{l_i} - L^{ll}_{ii}\theta_i - \sum_{j\in\mathcal{M}_i} L^{lg}_{ij}\theta_j - \sum_{k\in\mathcal{O}_i} L^{ll}_{ij}\theta_j & i \in \mathcal{L} \end{array} \tag{3.5.10}$$

The system in equation takes the form of a linear DAEs model. In analogy with (3.5.7), the vectorial form of (3.5.10) yields:

$$\begin{array}{rcl} \dot{\theta} & = & \Delta\omega \\ M_{\mathcal{G}}\Delta\dot{\omega}_{\mathcal{G}} & = & -D_{\mathcal{G}}\Delta\omega_{\mathcal{G}} + P_m - L^{gg}\theta_{\mathcal{G}} - L^{gl}\theta_{\mathcal{L}} \\ 0 & = & P_l - L^{lg}\theta_{\mathcal{G}} - L^{ll}\theta_{\mathcal{L}} \end{array} \tag{3.5.11}$$

where, with respect to (3.5.7), the following additional vectors are introduced: $\theta_{\mathcal{G}} \triangleq \mathrm{Col}(\theta_1, \ldots, \theta_{|\mathcal{G}|}) \in \mathbb{R}^{|\mathcal{G}|}$, and $\theta_{\mathcal{L}} \triangleq \mathrm{Col}(\theta_{|\mathcal{G}|+1}, \ldots, \theta_{|\mathcal{B}|}) \in \mathbb{R}^{|\mathcal{L}|}$.

3.5.3 Structure-Preserving ODE Models

If the frequency-dependent load dynamics (3.3.2) are considered, it is possible to show that the structure-preserving power system model exhibits a Ordinary Differential Equations (ODEs) architecture.

Nonlinear ODEs Model Given the generator dynamics (3.3.4) and the load dynamics (3.3.2), it follows:

$$\begin{array}{rcll} \dot{\theta}_i & = & \Delta\omega_i & i \in \mathcal{B} \\ M_i\Delta\dot{\omega}_i & = & -D_i\Delta\omega_i + P_{m_i} - \sum_{j\in\mathcal{N}_i}\gamma_{ij}\sin\left(\theta_i - \theta_j\right) & i \in \mathcal{G} \\ 0 & = & -D_i\Delta\omega_i + P_{l_i} - \sum_{j\in\mathcal{N}_i}\gamma_{ij}\sin\left(\theta_i - \theta_j\right) & i \in \mathcal{L} \end{array} \tag{3.5.12}$$

Note that the load algebraic relation appearing in (3.5.12) can be transformed into a differential equation as:

$$D_i\dot{\theta}_i = P_{l_i} - \sum_{j\in\mathcal{N}_i}\gamma_{ij}\sin\left(\theta_i - \theta_j\right) \quad i \in \mathcal{L} \tag{3.5.13}$$

The vectorial form of (3.5.12) can be shown to be:

$$\begin{aligned} \dot{\theta} &= \Delta\omega \\ M_{\mathcal{G}}\Delta\dot{\omega}_{\mathcal{G}} &= -D_{\mathcal{G}}\Delta\omega_{\mathcal{G}} - \nabla_{\mathcal{G}}U(\theta) \\ 0 &= -D_{\mathcal{L}}\Delta\omega_{\mathcal{L}} - \nabla_{\mathcal{L}}U(\theta) \end{aligned} \tag{3.5.14}$$

where: $D_{\mathcal{L}} \triangleq \mathrm{Diag}((D_i)_{i\in\mathcal{L}}),\ D_{\mathcal{L}} \succ 0,\ D_{\mathcal{L}} \in \mathbb{R}^{|\mathcal{L}|\times|\mathcal{L}|}$

Linearised ODEs Model Using again the linearised DC power flow approach along with the Laplacian matrix structure, the following linear ODE model yields:

$$\begin{aligned} \dot{\theta}_i &= \Delta\omega_i && i \in \mathcal{B} \\ M_i\Delta\dot{\omega}_i &= -D_i\Delta\omega_i + P_{m_i} - L^{gg}_{ii}\theta_i - \textstyle\sum_{j\in\mathcal{N}_i} L^{gl}_{ij}\theta_j && i \in \mathcal{G} \\ 0 &= -D_i\Delta\omega_i + P_{l_i} - L^{ll}_{ii}\theta_i - \textstyle\sum_{j\in\mathcal{M}_i} L^{lg}_{ij}\theta_j - \sum_{k\in\mathcal{O}_i} L^{ll}_{ij}\theta_j && i \in \mathcal{L} \end{aligned} \tag{3.5.15}$$

Also in this situation, the algebraic equation for the loads can be transformed into a linear differential equation:

$$D_i\dot{\theta}_i = P_{l_i} - L^{ll}_{ii}\theta_i - \textstyle\sum_{j\in\mathcal{M}_i} L^{lg}_{ij}\theta_j - \sum_{k\in\mathcal{O}_i} L^{ll}_{ij}\theta_j \quad i \in \mathcal{L} \tag{3.5.16}$$

Furthermore, the vectorial structure of (3.5.12) follows:

$$\begin{aligned} \dot{\theta} &= \Delta\omega \\ M_{\mathcal{G}}\Delta\dot{\omega}_{\mathcal{G}} &= -D_{\mathcal{G}}\Delta\omega_{\mathcal{G}} + P_m - L^{gg}\theta_{\mathcal{G}} - L^{gl}\theta_{\mathcal{L}} \\ 0 &= -D_{\mathcal{L}}\Delta\omega_{\mathcal{L}} - P_l - L^{lg}\theta_{\mathcal{G}} - L^{ll}\theta_{\mathcal{L}} \end{aligned} \tag{3.5.17}$$

Remark 3.5. Note that the only mutual interaction among the components constituting the power system takes place at the level of electrical active power exchange, which can be modelled according to the power flow methods. This is valid for all the introduced structure-preserving dynamical models.

3.6 List of Symbols and Variables

Synchronous Generator		
Symbol	Units	Physical Meaning
α_i	(rad)	angular position of the rotor
θ_i	(rad)	generator voltage phase angle
ω_{m_i}	(rad/s)	mechanical angular speed
T_{m_i},T_{e_i}	(N m)	mechanical, electrical torques
P_{m_i},P_{e_i}	(N m)	mechanical, electrical powers
e_{q_i}	(p.u.)	transient voltage
E_{f_i}	(p.u.)	excitation voltage
pp_i	(–)	number of pole-pairs of the generator
ω_0	(rad/s) or (Hz)	rated value of the electrical angular speed
ω_{m_R}	(rad/s)	rated value of the mechanical angular speed
E_i	(GJ)	generator base energy
S_i	(GVA)	generator base power
H_i	(s)	inertia constant
J_i	(kg m^2)	rotational mass
M_i	(p.u.)	inertia
T_{d0_i}	(s)	d-circuit time constant
x_{d_i}, x'_{d_i}	(p.u.)	d-axis reactance, d-axis transient reactance
x_{q_i}	(p.u.)	q-axis reactance
Steam Turbine-Governor		
$P_{m_{a_i}}$, $P_{m_{b_i}}$, $P_{m_{c_i}}$	(p.u.)	a, b, c steam turbine power variation
$\alpha_{t_{a_i}}$,$\beta_{t_{b_i}}$, $\gamma_{t_{c_i}}$	(–)	a, b, c steam turbine power conversion constants
$T_{t_{a_i}}$,$T_{t_{b_i}}$, $T_{t_{c_i}}$	(s)	a, b, c steam turbine time constants
Hydraulic Turbine-Governor		
P_{c_i}	(p.u.)	hydro transient compensator power variation
W_i	(p.u.)	hydro turbine water speed variation
$T_{c_{1_i}}$, $T_{c_{2_i}}$	(s)	compensator time constants
T_{h_i}	(s)	hydro turbine time constant
Wind Power Sources		
θ_{w1_i}	(rad)	wind source voltage phase angle
θ_{w2_i}	(rad)	wind turbine rotor angle
$\Delta\omega_{w1_i}$	(p.u) or (Hz)	wind generator frequency deviation
$\Delta\omega_{w2_i}$	(p.u) or (Hz)	wind turbine frequency deviation
T_{w_i}	(p.u)	wind input torque
M_{w1_i}	(p.u.)	wind generator inertia
M_{w2_i}	(p.u.)	wind turbine inertia
D_{w_i}	(p.u.)	wind turbine-generator damping

k_{w_i}	(p.u.)	wind source stiffness coefficient
Inverter Power Sources		
v_{dc_i}	(p.u.) or (V)	dc-link voltage
i_{dc_i}	(p.u.) or (A)	dc generated current
θ_{inv_i}	(rad)	inverter voltage phase angle
$\Delta\omega_{inv_i}$	(p.u) or (Hz)	inverter frequency deviation
G_{dc_i}	(p.u.) or (Ω^{-1})	dc side conductance
C_{dc_i}	(p.u) or (S)	dc-link capacitor
Loads		
P_{l_i}	(p.u.)	load power consumption
Variables and Symbols used for Different Components		
$\Delta\omega_i$	(p.u) or (Hz)	frequency deviation
P_{g_i}	(p.u.)	governor output power variation
V_i	(p.u) or (V)	voltage magnitude
D_i	(p.u)	droop control coefficient/damping factor
T_{g_i}	(s)	turbine time constant
T_{t_i}	(s)	governor time constant
$1/R_i$	(p.u.)	droop control coefficient

Part II

Local and Wide-Area Sliding Mode Observers in Power Systems: State Estimation and Fault Reconstruction

Chapter 4

Design and Validation of Local Sliding Mode Observers for Synchronous Generators

Abstract This chapter considers the application of sliding mode observation techniques to locally and robustly estimate the states of synchronous generators in power systems. Specifically, two original sliding mode observers will be proposed. The first one, which relies on a novel super-twisting-like sliding mode architecture, is able to locally estimate in finite time the frequency deviation for a synchronous generator governed by the dynamical model (3.1.16). A real-data based scenario demonstrates the accuracy of the proposed scheme. The second one relies on the more accurate dynamical model (3.4.5). A stability analysis of the error dynamics is undertaken, which is based on the Grownwall-Bellman Inequality approach. The present chapter is mainly based on the following authored publications:

- **G. Rinaldi**, P. P. Menon, C. Edwards, and A. Ferrara, "*Sliding mode based dynamic state estimation for synchronous generators in power systems*," IEEE Control Systems Letters, vol. 2, no. 4, pp. 785–790, 2018.
- **G. Rinaldi**, P. P. Menon, A. Ferrara, and C. Edwards, "*A super-twisting-like sliding mode observer for frequency reconstruction in power systems: Discussion and real data based assessment*," in Proc. of 15-th International Workshop on Variable Structure Systems (VSS), Graz, Austria, pp. 444–449, July 2018.

4.1 The Concept of Local State Estimation

The term local state estimation refers to a dynamic state estimation implemented at the level of a single component of the power network (synchronous generators, turbine-governor systems, loads, wind power sources, etc.) [12]. It reveals to be a completely decentralised technique, thus requiring only the local information and local knowledge of the model parameters. Furthermore, it is not affected by the complexity of the power systems, i.e. by the number and the typology of the buses and the topology of the interconnections amongst the buses.

4.2 Design and Real Data-Based Assessment of a Super-Twisting-Like Sliding Mode Observer for Frequency Reconstruction in Synchronous Generators

In this section, a super-twisting-like sliding mode observer is presented, which has the ability to estimate in finite time the frequency deviation $\Delta\omega_i$ for a single generator bus governed by the dynamical model (3.1.16).

4.2.1 Facts and Assumptions

The dynamics in (3.1.16) can be rewritten to include the output measurement as follows:

$$\begin{aligned} \dot{\theta}_i &= \Delta\omega_i, \\ M_i\Delta\dot{\omega}_i &= P_{m_i} - P_{e_i} - D_i\Delta\omega_i \\ y_{g_i} &= \theta_i \end{aligned} \tag{4.2.1}$$

Assumption 4.1. *Only the generator voltage phase angle θ_i is locally measured.*

This can be easily implemented in practical situations by equipping a generator with a PMUs [4].

The objective is:

Objective 4.1. *Given the (local) dynamical model for the synchronous generator (4.2.1), estimate in finite time the frequency deviation $\Delta\omega_i$, ensuring robustness with respect to the unknown power imbalance $P_{m_i} - P_{e_i}$*

The following assumption is now introduced:

Assumption 4.2. *The signal*

$$\nu_i \triangleq \frac{P_{m_i} - P_{e_i}}{M_i} \tag{4.2.2}$$

is bounded so that

$$|\nu_i| \leq \Delta_{\nu_i} \tag{4.2.3}$$

here Δ_{ν_i} is a positive known constant, which is determined from an understanding of the system.

Note that Assumption 4.2 is always satisfied in practical cases, since the imbalance between mechanical power delivered by the turbine P_{m_i} and the electrical active power P_{e_i} injected into the power network remains bounded [37].

4.2.2 Super-Twisting-Like Sliding Mode Observer Design

The following super-twisting-like sliding mode observer is proposed to estimate in finite time the frequency deviation of the synchronous generator [93]:

$$\begin{aligned} \dot{\hat{\theta}}_i &= \Delta\hat{\omega}_i - a_i e_{\theta_i} - k_{g1_i} |e_{\theta_i}|^{1/2} \operatorname{sign}(e_{\theta_i}) \\ \Delta\dot{\hat{\omega}}_i &= -k_{g2_i} \operatorname{sign}(e_{\theta_i}) - a_i^2 e_{\theta_i} + a_i \Delta\hat{\omega}_i - k_{g1_i} a_i |e_{\theta_i}|^{1/2} \operatorname{sign}(e_{\theta_i}) \\ \hat{\omega}_i &= (\Delta\hat{\omega}_i + 1)\,\omega_0, \end{aligned} \tag{4.2.4}$$

where k_{g1_i} and k_{g2_i} are positive constants to be designed, $e_{\theta_i} \triangleq \hat{\theta}_i - \theta_i$ is the so-called output observation error, and the auxiliary parameter a_i is defined as $a_i \triangleq -D_i/M_i$. The estimate of the frequency in (Hz) or in (rad/s) can be obtained from its deviation measured in (p.u.) according to the algebraic equation appearing in (4.2.4).

Remark 4.1. Note that the proposed observer differs from the standard super-twisting sliding mode architecture as formulated in [75] for the presence of original terms included in the dynamics. Specifically, these are $-a_i e_{\theta_i}$ in the first line of (4.2.4), and $-a_i^2 e_{\theta_i}$, $-k_{g1_i} a_i |e_{\theta_i}|^{1/2} \operatorname{sign}(e_{\theta_i})$ in the second differential equation of (4.2.4). These terms represent a theoretical novelty and they are instrumental both in deriving a simplified error dynamics in the form of the super-twisting architecture, and in having only the signal ν_i (defined in (4.2.2)) as matched disturbance.

By subtracting the system of equations in (4.2.1) to (4.2.4), the so-called error system dynamics are obtained as

$$\begin{aligned} \dot{e}_{\theta_i} &= e_{\omega_i} - a_i e_{\theta_i} - k_{g1_i} |e_{\theta_i}|^{1/2} \operatorname{sign}(e_{\theta_i}) \\ \dot{e}_{\omega_i} &= -k_{g2_i} \operatorname{sign}(e_{\theta_i}) - a_i^2 e_{\theta_i} - k_{g1_i} a_i |e_{\theta_i}|^{1/2} \operatorname{sign}(e_{\theta_i}) - \nu_i + a_i e_{\omega_i}, \end{aligned} \tag{4.2.5}$$

where $e_{\omega_i} \triangleq \Delta\hat{\omega}_i - \Delta\omega_i$. By defining the auxiliary error variable as

$$\tilde{e}_{\omega_i} \triangleq e_{\omega_i} - a_i e_{\theta_i}, \tag{4.2.6}$$

the following error dynamics are obtained

$$\begin{aligned} \dot{e}_{\theta_i} &= \tilde{e}_{\omega_i} - k_{g1_i} |e_{\theta_i}|^{1/2} \operatorname{sign}(e_{\theta_i}) \\ \dot{\tilde{e}}_{\omega_i} &= -k_{g2_i} \operatorname{sign}(e_{\theta_i}) - a_i^2 e_{\theta_i} - k_{g1_i} a_i |e_{\theta_i}|^{1/2} \operatorname{sign}(e_{\theta_i}) - \nu_i + a_i e_{\omega_i} \\ &\quad -a_i \left(\tilde{e}_{\omega_i} - k_{g1_i} |e_{\theta_i}|^{1/2} \operatorname{sign}(e_{\theta_i}) \right) \end{aligned} \tag{4.2.7}$$

After straightforward algebraic simplifications, one gets:

$$\begin{aligned} \dot{e}_{\theta_i} &= -k_{g1_i} |e_{\theta_i}|^{1/2} \operatorname{sign}(e_{\theta_i}) + \tilde{e}_{\omega_i} \\ \dot{\tilde{e}}_{\omega_i} &= -k_{g2_i} \operatorname{sign}(e_{\theta_i}) - \nu_i. \end{aligned} \tag{4.2.8}$$

The system in (4.2.8) is in the form of the super-twisting sliding mode architecture [71]. Specifically, note that the disturbance ν_i appears in the matched channel of the system in (4.2.8), for which the origin represents a finite time stable equilibrium point, as shown in Section 2.4.2 on page 19. Furthermore, under Assumption 4.2 and given equation (4.2.3), the design constants k_{g1_i} and k_{g2_i} can

be tuned according to the following rules:

$$\begin{aligned} k_{g1_i} &= 1.5\sqrt{\Delta_{\nu_i}} \\ k_{g2_i} &= 1.1\Delta_{\nu_i} \end{aligned} \tag{4.2.9}$$

Remark 4.2. Note that the observer in the form of (4.2.4) depends on the auxiliary parameter $a_i = -D_i/M_i$, which is a ratio between the droop coefficient D_i and the inertia M_i of the generator model. In case constant a_i is uncertain or not known, it is possible to define an auxiliary signal

$$\tilde{\nu}_i = \nu_i - \frac{D_i}{M_i}\Delta\omega_i, \tag{4.2.10}$$

and by assuming that

$$|\tilde{\nu}_i| \leq \Delta_{\tilde{\nu}_i} \tag{4.2.11}$$

where $\Delta_{\tilde{\nu}_i}$ is an auxiliary known positive constant, the following (standard) super-twisting sliding mode observer can be introduced:

$$\begin{aligned} \dot{\hat{\theta}}_i &= \Delta\hat{\omega}_i - k_{g1_i}\left|e_{\theta_i}\right|^{1/2}\mathrm{sign}\left(e_{\theta_i}\right) \\ \Delta\dot{\hat{\omega}}_i &= -k_{g2_i}\mathrm{sign}\left(e_{\theta_i}\right) \\ \hat{\omega}_i &= \left(\Delta\hat{\omega}_i + 1\right)\omega_0. \end{aligned} \tag{4.2.12}$$

The finite time convergence of the super-twisting observer in the form of (4.2.12) can be easily proven as above, since its error dynamics are in the form of (4.2.8) (the reader is referred to [75] for further details).

4.2.3 Real Data Based ST-Like Observer Validation

Preliminaries In this section, the super-twisting-like sliding mode observer proposed in (4.2.4) is assessed by real data. This assessment approach is innovative, since it is much more common to employ IEEE power network benchmarks to validate estimation and control architectures (see, e.g, [24], [94], [95], [96]). Differently, the idea developed in this framework provides to compare the measurement data of the frequency available for the Nordic Power System in [97] with the estimates generated by the designed observer in (4.2.4). More precisely, the lumped Nordic Power System model data presented in [98] is employed as a starting point to design the observer (4.2.4). This model exhibits the same structure as in (4.2.1). Then, the measurement data displaying the time evolution of the frequency is recovered during two major faults which took place in 2015. Technical data about these two faults are reported in [99]. The frequency measurements in [97] have been captured in a discrete-time fashion, with the use of a sampling time of 0.1 seconds, by means of a network of PMUs deployed in different locations in Nordic Power System. Following [99], it is assumed that this measurement data represents the frequency of the whole Nordic Power System. The comparison between the real frequency measurements and the estimates reveals a high level of accuracy of the observer (4.2.4) during the first seconds after the faults.

Remark 4.3. Note that the real Nordic Power System has complex (and unknown) dynamics, which have not been modelled for the design of observer in (4.2.4). The unknown nonlinearities are treated

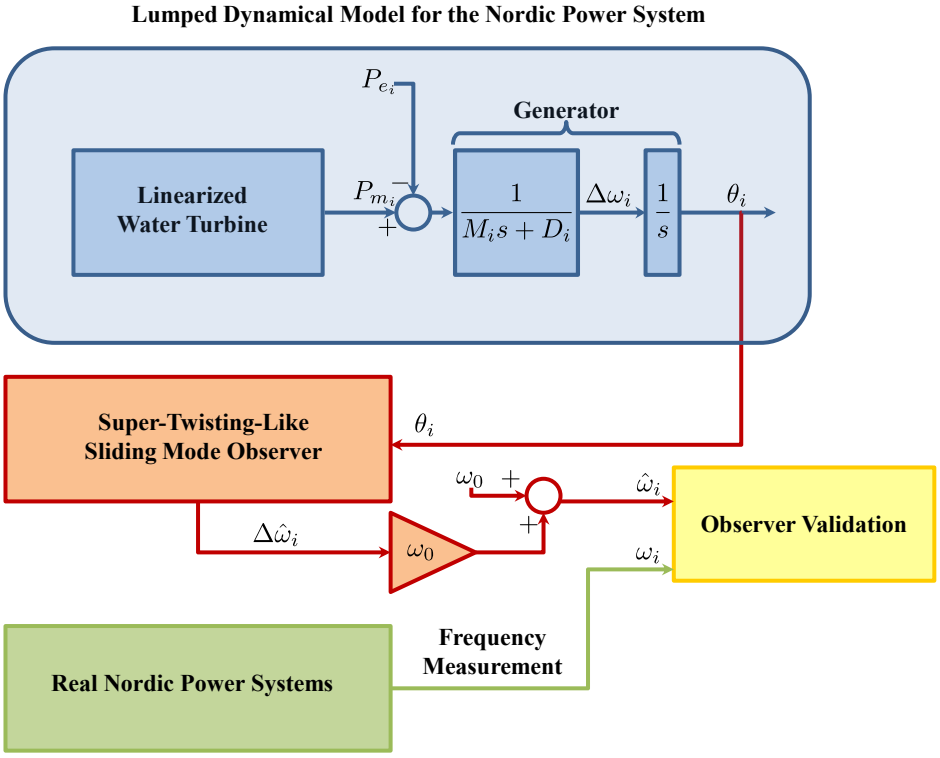

Figure 4.2.1: A schematic of the lumped Nordic Power System dynamical model, coupled with the designed super-twisting-like observer for the frequency estimation.

Table 4.2.1: Relevant Data of the Disturbance on the 5-th June 2015 (left) and on the 8-th August 2015 (right).

Starting Time	11:54:00 PM	Starting Time	2:21:00 PM
Fault Time	11:54:50 PM	Fault Time	2:22:08 PM
Ending Time	11:57:00 PM	Ending Time	2:24:00 PM
Disturbance Magnitude	878 MW	Disturbance Magnitude	600 MW
Kinetic Energy	160 GJ	Kinetic Energy	160 GJ
Cause	Nuclear Power Plant	Cause	Loss of an HVDC

as disturbances, and their impact on the performance of the observer in (4.2.4) will be evaluated.

Figure 4.2.1 shows a schematic of the underlying idea of the proposed assessment. The dynamical model in [98] comprises an equivalent linearised water turbine (due to the presence of hydro-power generators participating in frequency regulation), and an equivalent synchronous generator. The two major faults, which took place in 2015 in the Nordic Power System, are:

1. On 5-th June 2015, at 11:54:50 PM, a nuclear power plant with a generation capacity of 878 MW was suddenly disconnected. Relevant data for this fault is reported in Table;

2. On 8-th August 2015, at 2:22:08 PM, an outage affected an High Voltage Direct Current (HVDC) power transmission line, causing a sudden loss of consumption of 600 MW.

Relevant data for this fault is reported in Table 4.2.1.

Numerical Representation of Variables and Parameters By using the data in [98], the kinetic energy of the equivalent synchronous generator is equal to $E_i = 160$ (GJ). Since the total apparent power $S_i = 29.28$ (GVA) for the Nordic Power System, the nominal inertia constant, defined in (3.1.7), can be shown to be equal to

$$H_i = \frac{E_i}{S_i} = 5.46\ (s). \tag{4.2.13}$$

The nominal value of the droop coefficient is $D_i = 0.9$ (p.u.) [98]. The linearised model in Figure 4.2.1 coupled with the proposed observer in (4.2.4) are used for the two considered faults. The observer parameter $a_i = -D_i/M_i$ is set equal to $a_i = -4.12$ (p.u.). Defining $\Delta_{\nu_i} = 0.5$, the design constants of the super-twisting-like sliding mode observer are tuned according to the rules (4.2.9),

$$\begin{array}{rcl} k_{g1_i} & = & 1.06 \\ k_{g2_i} & = & 0.55. \end{array} \tag{4.2.14}$$

By exploiting (4.2.2) and (4.2), one gets

$$|M_i \nu_i| \ = \ |P_{m_i} - P_{e_i}| \leq M_i \Delta_{\nu_i}. \tag{4.2.15}$$

If the actual values of the variables are substituted, the numerical representation

$$|P_{m_i} - P_{e_i}| \leq 0.11\ (p.u) \approx 3.20\ (GW), \tag{4.2.16}$$

follows. This implies that a maximum value for the power unbalance $P_{m_i} - P_{e_i}$ is equal to 3.20 (GW), which is satisfied in practice for all the past faults described in [99]. The system as depicted in Figure 4.2.1 with the proposed sliding mode observer was implemented in Matlab-Simulink R2017a. The fixed-step method *Ode1(Euler)* was employed with an integration step size of 0.1 milliseconds.

Fault on the 5-th of June 2015 Later during the night, on the 5-th June 2015, a nuclear power plant was suddenly disconnected from the rest of Nordic Power System. Figure 4.2.2-(a) shows both the estimates of the frequency generated by the proposed super-twisting-like sliding mode observer as a solid (red) line, and the real measured values as a dotted (blue) line coming from the data. A transient can be identified during the first seconds, due to the reaching of the sliding motion of the observer, which took place in finite time. During the pre-fault scenario, the estimated and the real values of the frequency are slightly different. Specifically, small oscillations can be noted, which are due to unmodelled dynamics. During the first seconds after the fault, the estimated and the real values are practically the same. During the post-fault scenario, the estimated and the real values of the frequency are again slightly different. These differences can be justified by the presence of unmodelled components, such as voltage-dependent and frequency-dependent loads, the action of electrical protection devices, and voltage oscillations which are present in practice in the power system [5]. These have not been considered in the current model (4.2.1). However, the impact of these simplified assumptions for the observer design can be considered to be minimal by exploiting the difference between the real measured values and the estimated ones in Figure 4.2.2-(a).

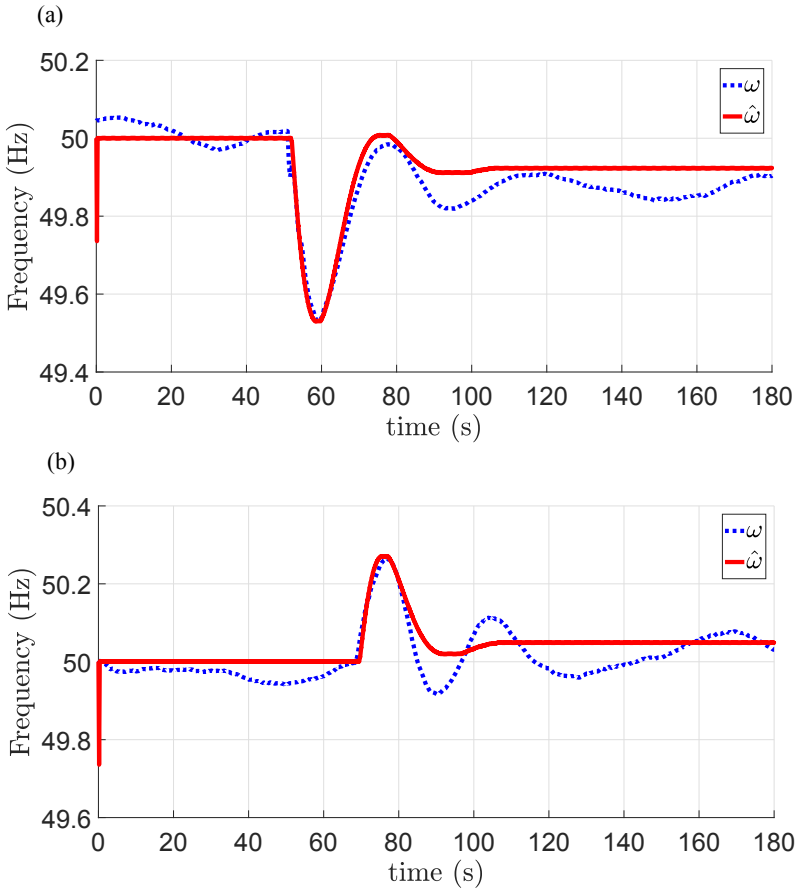

Figure 4.2.2: Time evolution of both the frequency measured in the Nordic Power Systems (dotted line) and the estimate value (solid line) from the proposed observer. **(a)** Fault on the 5-th June 2015. The starting point $t = 0$ (s) in the plot corresponds to the time instant $11 : 54 : 00$ PM. **(b)** Fault on the 8-th August 2015. The starting point $t = 0$ (s) in the plot corresponds to the time instant $02 : 21 : 00$ PM.

Fault on the 8-th of August 2015 Exploiting the same idea, the observer-assessment will now be performed considering the fault which took place during the afternoon of 8-th August 2015, when a High Voltage Direct Current (HVDC) power transmission line was disconnected from the rest of the Nordic Power System. Figure 4.2.2-(b) shows the results following the notation adopted as above. The same considerations discussed above still hold. Note that in this case the frequency increases because there was a loss of power demand. This is in accordance with the swing equation approach (see, e.g, the schematic in Figure 3.1.2 on page 30).

4.3 Design and Simulation-Based Assessment of a Sliding Mode Observer for a Single Synchronous Generator with Transient Voltage Dynamics

In this section, a first order sliding mode observer is proposed to estimate at the local level both the generator voltage angle and the transient voltage of a single generator bus. It is assumed to locally measure only the frequency deviation. With respect to Section 4.2, the detailed dynamics description in (3.4.5) is employed for a single synchronous generator, which makes the approach adopted in this section more general. Differently from Section 4.2, in which the estimation scheme was demonstrated via real data, in the current framework a simulation-based assessment will be provided, with a comparison with the well-established Extended Kalman Filter (EKF) technique.

4.3.1 Assumptions and Facts

In the rest of the present chapter, the following assumption is imposed:

Assumption 4.3. *It is assumed to locally measure only the frequency deviation of the generator.*

The synchronous generator is also assumed to have nonlinear dynamics around its nominal (stable) working point, as expressed by the following assumption:

Assumption 4.4. *There exists an asymptotically stable equilibrium point for the nonlinear system (3.4.5), given the constant input signals $\overline{P}_{m_i}$, $\overline{E}_{f_i}$, $\overline{V}_i$. In practice, this equilibrium corresponds to the nominal working point of the synchronous generator. The resulting constant (nominal) state variables are $\big(\overline{\theta}_i, \overline{e}_{q_i}, \Delta\overline{\omega}_i = 0\big)$.*

Following Assumption 4.4, it is possible to introduce time-varying perturbations ΔV_i, ΔE_{f_i}, ΔP_{m_i} of the external inputs around their nominal values as follows: $V_i = \overline{V}_i + \Delta V_i$, $E_{f_i} = \overline{E}_{f_i} + \Delta E_{f_i}$, $P_{m_i} = \overline{P}_{m_i} + \Delta P_{m_i}$. Only the perturbation ΔV_i is assumed to be known. For fixed inputs $\overline{P}_{m_i}$, $\overline{E}_{f_i}$, $\overline{V}_i$, the system in (3.4.5) can be represented as a combination of linear and nonlinear terms:

$$\begin{aligned} \dot{X}_{1_i} &= A_{1_i}X_{1_i} + A_{2_i}X_{2_i} + G_{1_i}(X_{1_i}, \Delta V_i) + g_{1_i}(E_{f_i}) \\ \dot{X}_{2_i} &= A_{3_i}X_{1_i} + A_{4_i}X_{2_i} + G_{2_i}(X_{1_i}, \Delta V_i) + g_{2_i}(U_i) \\ y_i &= X_{2_i} = C_iX_i, \end{aligned} \tag{4.3.1}$$

where $X_i = \mathrm{Col}\,(X_{1_i},\ X_{2_i})$, and the components $X_{1_i} = \mathrm{Col}\,(\theta_i,\ e_{q_i})$, $X_{2_i} = \Delta\omega_i$; the vector $C_i = \begin{bmatrix} 0 & 0 & 1 \end{bmatrix}$; $G_{1_i}(\cdot)$, $G_{2_i}(\cdot)$, $g_{1_i}(\cdot)$, and $g_{2_i}(\cdot)$ are properly defined functions, and the input

$U_i = \mathrm{col}(\Delta P_{m_i}, \Delta E_{f_i}, \Delta V_i)$. Only $\Delta\omega_i$ is measured by employing the PMUs [4]. The states θ_i and e_{q_i} have to be estimated for the purpose of enhancing the monitoring of the synchronous generator. Matrix A_i, is the Jacobian matrix of the nonlinear system (3.4.5) about an equilibrium point $\left(\overline{\theta}_i, \overline{e}_{q_i}, \Delta\overline{\omega}_i = 0\right)$, and it can be shown to be and it is given by

$$A_i = \left[\begin{array}{c|c} A_{1_i} & A_{2_i} \\ \hline A_{3_i} & A_{4_i} \end{array}\right] = \left[\begin{array}{cc|c} 0 & 0 & 1 \\ \frac{-\overline{V}_i \sin(\overline{\theta}_i)(x_{d_i} - x'_{d_i})}{T_{d0_i} x'_{d_i}} & \frac{-x_d}{T_{d0} x'_d} & 0 \\ \hline -\frac{\overline{V}_i}{M_i x'_{d_i}} \left(\frac{\overline{V}_i (x'_{d_i} - x_{q_i})}{x_{q_i}} \cos(2\overline{\theta}_i) + \overline{e}_{q_i} \cos(\overline{\theta}_i) \right) & \frac{-\overline{V}_i \sin(\overline{\theta}_i)}{M_i x'_{d_i}} & -\frac{D_i}{M_i} \end{array}\right] \tag{4.3.2}$$

where $A_{1_i} \in \mathbb{R}^{2\times 2}$, $A_{2_i} \in \mathbb{R}^{2\times 1}$, $A_{3_i} \in \mathbb{R}^{1\times 2}$, and $A_{4_i} \in \mathbb{R}^{1\times 1}$. Matrix A_i is Hurwitz, since the equilibrium point $\left(\overline{\theta}_i, \overline{e}_{q_i}, \Delta\overline{\omega}_i = 0\right)$ is assumed asymptotically stable.

Proposition 4.1. *Given the dynamical system (4.3.1), and Assumption 4.4, the pair (A_i, C_i) is detectable.*

Proof. It is possible to determine the Observability Matrix M_{O_i} associated with the pair (A_i, C_i) in (4.3.1). For the conditions $\overline{V}_i = 0$, $\overline{\theta}_i = 0$, and $\overline{e}_{q_i} = \overline{V}_i \left(x_{q_i} - x'_{d_i}\right)/x_{d_i}$, $\det\left(M_{O_i}\right) = 0$, i.e. M_O is not full rank and hence the system is not observable. However, $\overline{V}_i = 0$ and $\overline{\theta}_i = 0$ are unacceptable (voltage magnitude and rotor angle cannot be equal to zero at steady state [4]), whereas $\overline{e}_{q_i} = \overline{V}_i \left(x_{q_i} - x'_{d_i}\right)/x_{d_i}$ can be acceptable. Since the equilibrium point $\left(\overline{\theta}_i, \overline{e}_{q_i}, \Delta\overline{\omega}_i = 0\right)$ is locally asymptotically stable, although $\det\left(M_{O_i}\right) = 0$, the pair (A_i, C_i) will be detectable. This proves the proposition.

The following assumption holds: □

Assumption 4.5. *It is assumed that:*

(A1) The nonlinear functions $G_{1_i}(\cdot)$, $G_{2_i}(\cdot)$, and therefore the function $G_i(\cdot) = \mathrm{Col}(G_{1_i}(\cdot), G_{2_i}(\cdot))$ are Lipschitz with respect to the state variable X_{1_i}. Let $L_{G_{1_i}}$, $L_{G_{2_i}}$, L_{G_i} be the known Lipschitz constants associated with $G_1(\cdot)$, $G_2(\cdot)$, and $G(\cdot)$, respectively.

(A2) The functions $g_{1_i}(\cdot)$, $g_{2_i}(\cdot)$, and $g_i(\cdot) = \mathrm{Col}(g_{1_i}(\cdot), g_{2_i}(\cdot))$ are unknown bounded external inputs, with the associated known positive upper bounds on their norms $\Delta_{g_{1_i}}$, $\Delta_{g_{2_i}}$, and Δ_{g_i}, respectively.

The state estimation problem can be summarised as follows:

Objective 4.2. *Given the (local) dynamical model for the synchronous generator (4.3.1), estimate the generator voltage phase angle θ_i and the transient voltage magnitude e_{q_i}.*

4.3.2 Sliding Mode Observer Design

A robust sliding mode observer is proposed to dynamically estimate the generator voltage phase angle and the transient voltage. Since (A_i, C_i) is proven to be detectable, there exists a matrix R_i

such that $(A_i - R_i C_i)$ is Hurwitz . (Note that A_i is assumed stable, so the trivial choice $R_i = 0$ can be made.) For any $Q_i > 0$ the Lyapunov Equation [47]

$$(A_i - R_i C_i)^T P_i + P_i (A_i - R_i C_i) = -Q_i, \tag{4.3.3}$$

has a unique symmetric positive definite solution denoted as $P_i \succ 0,\ P_i \in \mathbb{R}^{4\times 4}$. Analogously to (4.3.2), the matrix P_i is partitioned as

$$P_i = \begin{bmatrix} P_{1_i} & P_{2_i} \\ P_{2_i}^T & P_{3_i} \end{bmatrix} \tag{4.3.4}$$

where $P_{1_i} \in \mathbb{R}^{2\times 2}$, $P_{2_i} \in \mathbb{R}^{2\times 1}$ and $P_{3_i} \in \mathbb{R}^{1\times 1}$. A linear change of coordinates

$$Z_i = \mathrm{col}\,(Z_{1_i},\ Z_{2_i}) \triangleq T_i X_i \tag{4.3.5}$$

is now introduced for the dynamical system (4.3.1) where the matrix T_i is defined as

$$T_i \triangleq \begin{bmatrix} I_2 & P_{1_i}^{-1} P_{2_i} \\ 0_{12} & I_1 \end{bmatrix} \tag{4.3.6}$$

Note that the change of coordinate is required to obtain a canonical form of the generator dynamics instrumental for designing the observer, in which $(A_{1_i} + P_{1_i}^{-1} P_{2_i} A_{3_i})$ is Hurwitz [78]. The matrix $\tilde{A}_i = T_i A_i T_i^{-1}$ can be shown to be

$$\tilde{A}_i = \begin{bmatrix} \tilde{A}_{1_i} & \tilde{A}_{2_i} \\ \tilde{A}_{3_i} & \tilde{A}_{4_i} \end{bmatrix} = \left[\begin{array}{c|c} A_{1_i} + P_{1_i}^{-1} P_{2_i} A_{3_i} & \begin{array}{c} A_{2_i} - A_{1_i} P_{1_i}^{-1} P_{2_i} \\ +P_{1_i}^{-1} P_{2_i} \left(A_{4_i} - A_{3_i} P_{1_i}^{-1} P_{2_i}\right) \end{array} \\ \hline A_{3_i} & A_{4_i} - A_{3_i} P_{1_i}^{-1} P_{2_i} \end{array}\right] \tag{4.3.7}$$

Given (4.3.7), in the new coordinate reference, the system in equations in (4.3.1) can be written as

$$\left.\begin{array}{rcl} \dot{Z}_{1_i} &=& \tilde{A}_{1_i} Z_{1_i} + \tilde{A}_{2_i} Z_{2_i} + G_{1_i}(Z_i, \Delta V_i) + g_{1_i}(E_{f_i}) \\ & & +P_{1_i}^{-1} P_{2_i} \left(G_{2_i}(Z_i, \Delta V_i) + g_{2_i}\left(U_i\right)\right) \\ \dot{Z}_{2_i} &=& \tilde{A}_{3_i} Z_{1_i} + \tilde{A}_{4_i} Z_{2_i} + G_{2_i}(Z_i, \Delta V_i) + g_{2_i}\left(U_i\right) \\ y_i &=& Z_{2_i}. \end{array}\right\} \tag{4.3.8}$$

Let the sliding mode observer for (4.3.8) be:

$$\left.\begin{array}{rcl} \dot{\hat{Z}}_{1_i} &=& \tilde{A}_{1_i} \hat{Z}_{1_i} + \tilde{A}_{2_i} Z_{2_i} + G_{1_i}(\hat{Z}_i, \Delta V_i) + P_{1_i}^{-1} P_{2_i} \left(G_{2_i}(\hat{Z}_i, \Delta V_i)\right) \\ \dot{\hat{Z}}_{2_i} &=& \tilde{A}_{3_i} \hat{Z}_{1_i} + \tilde{A}_{4_i} \hat{Z}_{2_i} + G_{2_i}(\hat{Z}_i, \Delta V_i) + \psi_i \\ \hat{y}_i &=& \hat{Z}_{2_i} \\ \psi_i &=& \left(\left\|\tilde{A}_{4_i}\right\| \|e_{y_i}\| + \rho_i\right) \mathrm{sign}\,(e_{y_i}) \end{array}\right\} \tag{4.3.9}$$

where $\hat{Z}_{1_i}$ represents the estimate of Z_{1_i}, $\hat{Z}_{2_i}$ represents the estimate of Z_{2_i}, ρ_i is a positive constant to be designed, and ψ_i is a discontinuous term depending on the observation error $e_{y_i} \triangleq Z_{2_i} - \hat{Z}_{2_i}$.

The error system dynamics is obtained by subtracting (4.3.8) from (4.3.9):

$$\dot{e}_{1_i} = \tilde{A}_{1_i} e_{1_i} + [I_2 \; P_{1_i}^{-1} P_{2_i}] \Big(G_i(Z_i, \Delta V_i) - G_i(\hat{Z}_i, \Delta V_i) + g_i(U_i) \Big) \tag{4.3.10a}$$

$$\dot{e}_{y_i} = \tilde{A}_{3_i} e_{1_i} + \tilde{A}_{4_i} e_{y_i} + G_{2_i}(Z_i, \Delta V_i) - G_{2_i}(\hat{Z}_i, \Delta V_i) + g_{2_i}(U_i) - \psi_i. \tag{4.3.10b}$$

where $e_{1_i} \triangleq Z_{1_i} - \hat{Z}_{1_i}$. The sliding surface associated with (4.3.10a)- (4.3.10b) is chosen as:

$$\mathcal{S}_i = \{ (e_{1_i}, e_{y_i}) \, | e_{y_i} = 0 \} . \tag{4.3.11}$$

The following proposition is introduced

Proposition 4.2. *Under Assumptions 4.4-4.5, the error dynamics (4.3.10a)-(4.3.10b) satisfy the following:*

i) *The Euclidean norm $\|e_{1_i}\|$ remains bounded $\forall t \geq 0$, i.e. $\|e_{1_i}\| \leq \gamma_i$, where γ_i is a positive constant.*

ii) *If the external inputs $g_i(U_i) = 0$ and*

$$\lambda_{\min}(Q_{1_i}) > 2 \, \| [P_{1_i} \;\; P_{2_i}] \| \, L_{G_i}, \tag{4.3.12}$$

then the point $e_{1_i} = 0$ is an asymptotically stable equilibrium point for the system (4.3.10a).

iii) *System (4.3.10a)-(4.3.10b) is driven to the sliding surface (4.3.11) in a finite time t_{r_i} if the design constant ρ_i appearing in ψ_i is tuned according to the following inequality*

$$\rho_i > \Big(\Big\| \tilde{A}_{3_i} \Big\| + L_{G_{2_i}} \Big) \gamma_i + \Delta_{g_{2_i}} + \eta_i, \tag{4.3.13}$$

where η_i is a positive constant.

Proof. ***i)*** The symbolic solution of the differential equation (4.3.10a) can be shown to be

$$\begin{aligned} e_{1_i} = \; & \exp\Big\{ \tilde{A}_{1_i} t \Big\} e_{1_i}(0) + \int_0^t \Big(\exp\Big\{ \tilde{A}_{1_i} (t - \tau) \Big\} \\ & \cdot \Big([I_2 \; P_{1_i}^{-1} P_{2_i}] \Big(G_i \left(Z_i(\tau), \Delta V_i(\tau) \right) - G \left(\hat{Z}_i(\tau), \Delta V_i(\tau) \right) + g_i(U_i(\tau)) \Big) d\tau, \end{aligned} \tag{4.3.14}$$

in which the matrix $\tilde{A}_{1_i}$ is Hurwitz. Given the linear change of coordinates (4.3.5), it is obvious that $G_i(\cdot)$ is a Lipschitz function with respect to the state variable Z_i, and there exist positive constants a_{0_i} and c_{0_i} such that [78].

$$\begin{aligned} \|e_{1_i}\| \leq \; & c_{0_i} \exp\{-a_{0_i} t\} \, \|e_{1_i}(0)\| \\ & + \int_0^t c_{0_i} \exp\{-a_{0_i}(t - \tau)\} \, \| [I_2 \;\; P_{1_i}^{-1} P_{2_i}] \| \Big(L_{G_i} \|e_{1_i}(\tau)\| + \Delta_{g_i} \Big) d\tau. \end{aligned} \tag{4.3.15}$$

Multiplying both sides of (4.3.15) by $\exp\{a_{0_i}t\}$,

$$\begin{aligned}\exp\{a_{0_i}t\}\,\|e_{1_i}\| &\leq c_{0_i}\Big(\|e_{1_i}(0)\| + L_{G_i}\|[I_2 \;\; P_{1_i}^{-1}P_{2_i}]\| \\ &\quad \cdot\int_0^t \exp\{a_{0_i}\tau)\}\,\|e_{1_i}(\tau)\|d\tau\Big) \\ &\quad +\frac{c_{0_i}}{a_{0_i}}\Delta_{g_i}\|[I_2 \;\; P_{1_i}^{-1}P_{2_i}]\|\left(\exp\{a_{0_i}t\}-1\right).\end{aligned} \tag{4.3.16}$$

By making use of the Grownwall-Bellman Inequality [78], if

$$y_i(t) \leq \lambda_i(t) + \int_0^t \mu_i(\tau)y_i(\tau)d\tau \tag{4.3.17}$$

then

$$y_i(t) \leq \lambda_i(t) + \int_0^t \lambda_i(\tau)\mu_i(\tau)\Big\{\exp\int_\tau^t \mu(s)ds\Big\}d\tau. \tag{4.3.18}$$

where y_i, λ_i, and μ_i denote given time signals. Exploiting the structure of equation (4.3.16), if

$$y_i(t) \triangleq \exp\big\{a_{0_i}t\big\}\,\|e_{1_i}(t)\| \tag{4.3.19}$$

$$\mu_i \triangleq c_{0_i}L_{G_i}\|[I_2 \;\; P_{1_i}^{-1}P_{2_i}]\| \tag{4.3.20}$$

$$\lambda_i(t) \triangleq c_{0_i}\,\|e_{1_i}(0)\| + \frac{c_{0_i}}{a_{0_i}}\Delta_{g_i}\|[I_2 \;\; P_{1_i}^{-1}P_{2_i}]\|\left(\exp\big\{a_{0_i}t\big\}-1\right), \tag{4.3.21}$$

then (4.3.16) has the form of (4.3.17). The key idea here is to make us of (4.3.18) to obtain a simpler expression for the inequality (4.3.16). The starting point provides to determine the expression of $F_{e_{1_i}}(t) \triangleq \int_0^t \lambda_i(\tau)\mu_i(\tau)\exp\left\{\int_\tau^t \mu_i(s)ds\right\}d\tau$, where $F_{e_{1_i}}(t)$ is an auxiliary signal to simplify the notation.

$$\begin{aligned}F_{e_{1_i}}(t) &= \int_0^t\Big(\big(c_{0_i}\,\|e_{1_i}(0)\| + \tfrac{c_{0_i}}{a_{0_i}}\Delta_{g_i}\|[I_2 \;\; P_{1_i}^{-1}P_{2_i}]\|(\exp\big\{a_{0_i}t\big\}-1)\big) \\ &\quad c_{0_i}L_{G_i}\|[I_2 \;\; P_{1_i}^{-1}P_{2_i}]\| \\ &\quad \exp\big\{\textstyle\int_\tau^t c_{0_i}\mathcal{L}_G\|[I_2 \;\; P_{1_i}^{-1}P_{2_i}]\|ds\big\}d\tau\Big)\end{aligned} \tag{4.3.22}$$

The solution of inner integral $\big\{\int_\tau^t c_{0_i}L_{G_i}\|[I_2 \;\; P_{1_i}^{-1}P_{2_i}]\|ds\big\}$ is trivial, thus getting

$$\begin{aligned}F_{e_{1_i}}(t) &= \int_0^t\Big(\big(c_{0_i}\,\|e_{1_i}(0)\| + \tfrac{c_{0_i}}{a_{0_i}}\Delta_{g_i}\|[I_2 \;\; P_{1_i}^{-1}P_{2_i}]\|(\exp\big\{a_{0_i}t\big\}-1)\big) \\ &\quad c_{0_i}L_{G_i}\|[I_2 \;\; P_{1_i}^{-1}P_{2_i}]\| \\ &\quad \exp\big\{c_{0_i}\mathcal{L}_G\|[I_2 \;\; P_{1_i}^{-1}P_{2_i}]\|(t-\tau)\big\}\,d\tau\Big)\end{aligned} \tag{4.3.23}$$

After straightforward algebraic manipulations, by solving the integrals in (4.3.23) using standard techniques of calculus for the exponential functions, the expression

$$F_{e_{1_i}}(t) = \frac{c_{0_i}^2}{a_{0i}}\Delta_{g_i}\mu_i\Big(\frac{1}{\mu_i} + \frac{\exp\{a_{0_i}t\}}{(a_{0_i}-\mu_i)} - \frac{a_{0_i}}{\mu_i\cdot(a_{0_i}-\mu_i)}\exp\{\mu_i t\}\Big) \tag{4.3.24}$$

is obtained. Given both (4.3.18) and (4.3.24), one gets:

$$\begin{aligned}\exp\{a_{0_i}t\}\,\|e_{1_i}\| \;\leq\; & c_{0_i}\,\|e_{1_i}(0)\| + \tfrac{c_0}{a_0}\Delta_{g_i}\|[I_2 \;\; P_{1_i}^{-1}P_{2_i}]\|\cdot(\exp\{a_{0_i}t\}-1)\\ & +\tfrac{c_{0_i}^2}{a_{0i}}\Delta_{g_i}\mu_i\Big(\tfrac{1}{\mu_i}+\tfrac{\exp\{a_{0_i}t\}}{(a_0-\mu_i)}-\tfrac{a_{0_i}}{\mu_i\cdot(a_{0_i}-\mu_i)}\exp\{\mu_i t\}\Big)\end{aligned} \tag{4.3.25}$$

Dividing (4.3.25) by $\exp\{a_{0_i}t\}$, the inequality

$$\begin{aligned}\|e_1\| \;\leq\; & c_{0_i}\,\|e_{1_i}(0)\|\exp\{-a_{0_i}t\} + \tfrac{c_{0_i}^2}{a_{0_i}}\Delta_{g_i}\|[I_2 \;\; P_{1_i}^{-1}P_{2_i}]\|\cdot(1-\exp\{-a_{0_i}t\})\\ & +\tfrac{c_{0_i}^2}{a_{0i}}\Delta_{g_i}\exp\{-a_{0_i}t\} + \tfrac{c_{0_i}^2}{a_{0_i}(a_{0_i}-\mu_i)}\Delta_{g_i} - \Delta_{g_i}\tfrac{c_{0_i}^2}{\mu_i\cdot(a_{0_i}-\mu_i)}\exp\{\mu_i - a_{0_i}t\}\end{aligned} \tag{4.3.26}$$

is obtained. It follows that (4.3.26) remains bounded if

$$\mu_i = c_{0_i}L_{G_i}\|[I_2 \;\; P_{1_i}^{-1}P_{2_i}]\| < a_{0_i} \tag{4.3.27}$$

If the condition (4.3.27) is satisfied, then

$$\|e_{1_i}\| \leq \beta_i, \tag{4.3.28}$$

where β_i is a positive constants.

ii) To prove the asymptotic stability of the point $e_{1_i} = 0$, following [78], the Lyapunov function $V_{e_{1_i}} = e_{1_i}P_{1_i}e_{1_i}$ is chosen. The time derivative of $V_{e_{1_i}}$ along the trajectory of (4.3.10a) can be shown to be

$$\dot{V}_{e_1} = e_{1_i}^T\Big(P_{1_i}\tilde{A}_{1_i} + \tilde{A}_{1_i}^T P_{1_i}\Big)e_1 + 2e_1^T\,[P_{1_i}\;P_{2_i}]\Big(G(Z_i,\Delta V_i) - G(\hat{Z}_i,\Delta V_i)\Big). \tag{4.3.29}$$

In [78] it has been proven that the relation

$$P_{1_i}\tilde{A}_{1_i} + \tilde{A}_{1_i}^T P_{1_i} = -Q_{1_i} \tag{4.3.30}$$

holds. It follows that

$$\dot{V}_{e_1} = -e_{1_i}^T Q_{1_i}e_{1_i} + 2e_1^T\,[P_{1_i}\;P_{2_i}]\Big(G_i(Z_i,\Delta V_i) - G(\hat{Z}_i,\Delta V_i)\Big). \tag{4.3.31}$$

Then, according to Assumption 4.5, the inequality

$$\dot{V}_{e_{1_i}} \;\leq\; -\left(\lambda_{\min}(Q_{1_i}) + 2\,\|[P_{1_i}\;P_{2_i}]\|\,L_{G_i}\right)\|e_{1_i}\|^2. \tag{4.3.32}$$

is verified. It follows $\dot{V}_{e_{1_i}}$ is strictly negative if the inequality

$$\lambda_{\min}(Q_{1_i}) > 2\,\|[P_{1_i}\;P_{2_i}]\|\,L_{G_i}, \tag{4.3.33}$$

is satisfied. This proves ***ii).***

iii) Given (4.3.10b), it follows

$$e_{y_i}^T \dot{e}_{y_i} = e_{y_i}^T \Big(\tilde{A}_{3_i} e_{1_i} + \tilde{A}_{4_i} e_{y_i} + G_{2_i}(Z_i, \Delta V_i) - G_{2_i}(\hat{Z}_i, \Delta V_i) + g_{2_i}(U_i) - \nu_i \Big). \quad (4.3.34)$$

Under Assumption 4.5, the following inequalities can be obtained

$$\begin{aligned} e_y(t)^T \dot{e}_y(t) &\leq \Big(\big(||\tilde{A}_{3_i}|| + L_{G_2} \big) ||e_{1_i}| + \Delta_{g_{2i}} - \rho_i \Big) ||e_{y_i}|| \\ &\leq \Big(\big(||\tilde{A}_{3_i}|| + L_{G_2} \big) \beta_i + \Delta_{g_{2i}} - \rho_i \Big) ||e_{y_i}|| \end{aligned} \quad (4.3.35)$$

The reachability condition [61] is satisfied if

$$\rho_i > \big(\left\| \tilde{A}_{3_i} \right\| + L_{G_{2_i}} \big) \beta + \Delta_{g_{2_i}} + \eta_i, \quad (4.3.36)$$

which guarantees reaching of the sliding surface and proves ***iii)***. □

Note that condition e_{y_i} is reached in a finite time t_{r_i} which is upper-bounded as follows [61] :

$$t_{r_i} < \frac{2 \left\| e_{y_i}(0) \right\|}{\eta_i}. \quad (4.3.37)$$

Remark 4.4. Note that [78] considers the special case when Δ_{g_i}. A theoretical contribution of the proposed observer, compared to [78], is that the term $||e_{1_i}||$ remains bounded even in the presence of time varying bounded unknown inputs. Furthermore, one can not that equation (4.3.26) exhibits the same structure obtained in [78] if $\Delta_{g_i} = 0$, which is

$$\|e_1\| \leq c_{0_i} \left\| e_{1_i}(0) \right\| \exp\{-a_{0_i} t\} \quad (4.3.38)$$

The performance metric $\mathcal{P}_i$ can be introduced to evaluate the performances of the proposed observer

$$\mathcal{P}_i \triangleq \int_{t_{r_i}}^{t} \left\| e_{y_i}(\tau) \right\| d\tau, \quad (4.3.39)$$

It is expected that $\mathcal{P}_i$ is almost zero. This will also be demonstrated in a simulation environment.

Noise Effect Remarks Suppose that a differentiable band-limited measurement noise ψ_i affects the output of the system (4.3.8) as

$$y_i = Z_{2_i} + \psi_i \quad (4.3.40)$$

Then, the output estimation error becomes

$$e_{y_i} \triangleq Z_{2_i} + \psi_i - \hat{Z}_{2_i} \quad (4.3.41)$$

Given (4.3.10a)-(4.3.10b), the effect of the noise can be included as part of the unknown bounded input $g_i(U_i)$, by updating the value for Δ_{g_i} accordingly (see Assumption 4.5). It follows that part ***i)*** of Proposition 4.2 still holds in this case, thus maintaining the bounded properties of $\|e_{1_i}\|$ again. As for part ***iii)***, the sliding motion $e_{y_i} = 0$ still takes place in a finite time. However, by defining the

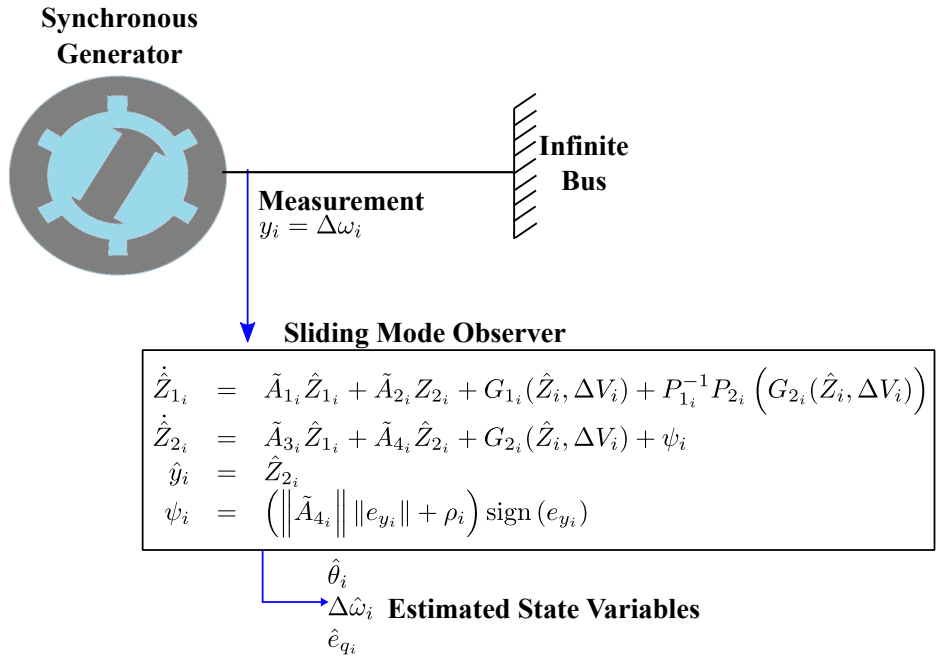

Figure 4.3.1: A schematic of a synchronous generator along with the SM observer architecture in (4.3.9).

noise-free output error as follows

$$\check{e}_{y_i} \triangleq Z_{2_i} - \hat{Z}_{2_i} \tag{4.3.42}$$

the condition

$$\hat{Z}_2 = Z_2 + \psi_i \tag{4.3.43}$$

holds in a finite time, as proven in[100].

Figure 4.3.1 shows a schematic of a synchronous generator. The dynamics of the observer in (4.3.9) is also reported.

4.3.3 Simulation-Based Observer Assessment

Simulation results are now presented to assess the proposed sliding mode observer in (4.3.9). A single synchronous generator connected to the grid is considered. The numerical representation of the model parameters, together with the values for both the state variables and input signals evaluated for the nominal equilibrium point are taken from [19] and from [101], and they are shown on Table 4.3.1. The reader is referred to Section 3.6 on page 44 for their description.

The simulation time horizon was set equal to 10 seconds, and the synchronous generator was modelled in the *Matlab-Simulink R2017b* environment by using the *Ode1-Euler* solver with an integration step size $\tau = 1 \times 10^{-4}$ seconds. The (Hurwitz) Jacobian Matrix A in (4.3.2) evaluated for the equilibrium data together with its eigenvalues λ are:

$$A = \begin{bmatrix} 0 & 0 & 377.000 \\ -20.100 & -42.830 & 0 \\ -0.180 & -0.160 & -0.005 \end{bmatrix}, \quad \lambda = \begin{bmatrix} -42.173 \\ -0.331 + 6.329j \\ -0.331 - 6.329j \end{bmatrix} \tag{4.3.44}$$

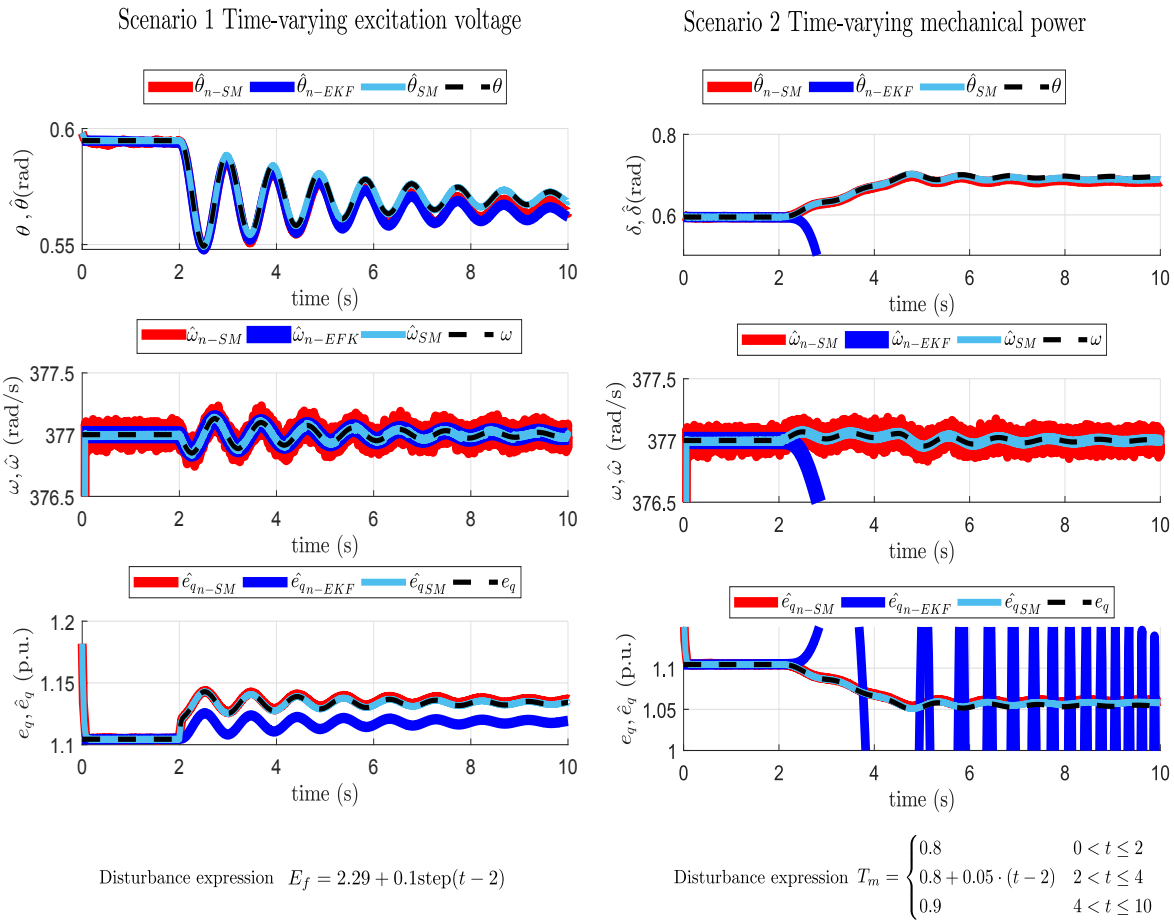

Figure 4.3.2: From the top: time evolution of the voltage phase angle and its estimate; time evolution of the frequency deviation and its estimates; time evolution of the transient voltage together with its estimates for the two considered scenarios. The mathematical expression for the two disturbances is also shown.

Table 4.3.1: Initial conditions for the state variables and numerical representations of the model parameters.

$\theta_i(0)$ (rad)	0.59
$\Delta\omega_i(0)$ (p.u.)	0.00
$e_{q_i}(0)$ (p.u.)	0.84
$E_{f_i}(0)$ (p.u.)	2.29
$P_{m_i}(0)$ (p.u.)	0.80
$V_i(0)$ (p.u.)	1.02
T_{d0_i}	0.13
x_{d_i}	2.06
x'_{d_i}	1.21
x_{q_i}	0.37
M_i	10.00
D_i	0.05

In order to solve the Lyapunov Equation (4.3.3), matrix $Q = I_3$, and the gain matrix R is chosen equal to $R = \begin{bmatrix} 376.0877 & -173.7180 & -0.0124 \end{bmatrix}^T$. Then, the unique symmetric positive definite solution P of (4.3.3) results in being

$$P = \begin{bmatrix} 10.8153 & -7.2107 & -0.5481 \\ -7.2107 & 19.2845 & 3.9179 \\ -0.5481 & 3.9179 & 0.9121 \end{bmatrix} \tag{4.3.45}$$

The design constant of the observer is set as $\rho = 0.5$. Matrix $\tilde{A}$ is required for the computer-based implementation of the observer (4.3.9), and it is obtained as follows:

$$\tilde{A} = TAT^{-1} = \begin{bmatrix} -0.020 & -0.017 & 377.000 \\ -20.125 & -42.866 & -0.001 \\ -0.180 & -0.160 & -0.005 \end{bmatrix} \tag{4.3.46}$$

Two scenarios are introduced:

Description of Scenario 1 During Scenario 1 the armature voltage is affected by a step variation of 0.1 (p.u.), which can be shown to be

$$E_f = 2.29 + 0.1\text{step}(t-2). \tag{4.3.47}$$

Note that the same scenario was also considered in [19].

Description of Scenario 2 During Scenario 2, the mechanical input power obeys to the following time-varying law

$$P_m = \begin{cases} 0.8 & 0 < t \leq 2 \\ 0.8 + 0.05 \cdot (t-2) & 2 < t \leq 4 \\ 0.9 & 4 < t \leq 10 \end{cases} \tag{4.3.48}$$

Note that the input disturbances E_f and P_m are unknown by the observer in the two scenario.

Three different schemes are considered for the two scenarios, in order to make a comparison with existing and well-established estimation methods. More precisely, if x represents a state variables, $\hat{x}_{SM}$ denotes its estimated via the sliding mode observer (4.3.9) in a measurement noise-free condition, $\hat{x}_{n-SM}$ represents the estimate obtained again via (4.3.9) with measurement noise, whilst $\hat{x}_{n-EFK}$ is used for the estimate from an EFK with measurement noise. The interested reader is encouraged to refer to [19] for the details about the implementation of EKF. The same variance of the measurement noise as in [19] is chosen, which is set equal to $\sigma^2 = 0.1$. As shown in Figure 4.3.2, the proposed sliding mode estimation scheme can acceptably estimate the unmeasured state variables in the noise-free condition, but also in presence of measurement disturbances. It is apparent that the EKF displays a better attenuation of the measurement noise than sliding mode observer, as revealed in Figure 4.3.2. However, the EKF performance can deteriorate in the presence of unknown inputs affecting the system. The evolution of the performance metric $\mathcal{P}(t_{sim})$ in (4.3.39) as function of the

Table 4.3.2: Performance metric $\mathcal{P}(t_{sim})$ defined in (58) as a functions of the noise variance σ^2 simulation time $t_{sim} = 10$ seconds. The expression (μp.u) represents (1e-6 p.u.), Scenario 1

σ^2	0.00	0.02	0.04	0.06	0.08	0.10	(p.u)^2
$\mathcal{P}(t_{sim})$	225	509	883	1259	1637	2026	(μp.u)

variance of the measurement noise 2 is almost linear, as shown in in Table 4.3.2. Only Scenario 1 is considered in Table 4.3.2, since Scenario 2 displays analogous features.

4.4 Conclusions

In this chapter, two different sliding mode state observers have been proposed to locally estimate the unmeasured state variables for synchronous generators. Furthermore, two different strategies have been employed to demonstrate the effectiveness of the designed state observers. The first observer, which relies on the novel super-twisting-like sliding mode architecture (4.2.4), is able to locally estimate in finite time the frequency deviation for a synchronous generator described by the dynamical model (3.1.16). The undertaken novel data-based assessment, which has made use of the Nordic Power System real faults, has demonstrated that the observer can estimate the frequency deviation with acceptably accuracy. The second observer, which relies on the more accurate dynamical model (3.4.5) for a local synchronous generator, was compared with the well-established EKF technique. In such a context, the proposed observer revealed to be robust and totally insensitive to unknown bounded matched uncertainties and requires only one measurement output when compared with EKF.

Chapter 5

Wide-Area Sliding Mode Observer for Dynamic State Estimation in Power Systems

Abstract In this chapter, the sliding mode observer-based state estimation moves from the local to the wide-area level with application to modern power systems. In such a context, power system is interpreted as complex large-scale network composed of an interconnection of different components which dynamically interact to each others. The diversified structure-preserving dynamical models introduced in Chapter 3 will be exploited as starting point for the design of SM observer. The present chapter is structured as follows:

1. In Section 5.1, an interconnection of distributed observers is proposed for the structure-preserving dynamical model in (3.5.10). Assuming only the voltage phase angles are measured, the observers scheme is composed of super-twisting-like sliding mode observers to estimate the frequency deviation for each generator bus, and so-called algebraic observers to estimate the load voltage phase angle for each load bus based on distributed iterative algorithms. The observer-based estimation scheme is validated by considering the IEEE 39 bus SimPowerSystems model.

2. In Section 5.2, a novel sliding mode observer-based scheme is developed to estimate and reconstruct the unmeasured state variables in power networks including hydroelectric power sources (3.1.19), (3.4.6) and thermal power sources (3.1.21), (3.4.6). The proposed approach reveals also to be flexible to topological changes to power networks and can be easily updated only where changes occur. The discussed numerical simulations validate the effectiveness of the proposed estimation scheme.

3. Section 5.3 considers the application of HOSM observers to robustly and dynamically estimate the unmeasured state variables in hybrid power systems, in which both traditional and renewable energy sources coexist. In particular, a power system composed of traditional, wind and inverter-based sources connected with dynamical loads is considered. Assuming that only the voltage phase angles are locally measured, a dedicated higher order SM observer is designed

for each component, which is able to estimate in finite time the unmeasured state variables. Numerical simulations demonstrate the accuracy of the proposed scheme.

The present chapter is mainly based on the following authored publications:

- **G. Rinaldi**, P. P. Menon, C. Edwards, and A. Ferrara, "*Distributed observers for state estimation in power grids*," in Proc. of American Control Conference, (Seattle,WA, USA), pp. 5824–5829, May 2017

- **G. Rinaldi,** P. P. Menon, C. Edwards, and A. Ferrara, "*Design and validation of a distributed observer-based estimation scheme for power grids*," IEEE Transactions on Control Systems Technology, 2018.

- **G. Rinaldi,** M. Cucuzzella, and A. Ferrara, "*Sliding mode observers for a network of thermal and hydroelectric power plants*," Automatica, vol. 98, pp. 51–57, 2018.

- **G. Rinaldi**, P. P. Menon, C. Edwards and A. Ferrara, "*Higher Order Sliding Mode Observers in Power Grids with Traditional and Renewable Sources*", IEEE Control Systems Letters, vol. 4, no. 1, pp. 223-228, 2019.

5.1 Design and Validation of Distributed Observers for Linearised DAEs Power System Model

In this section, a wide-area network is considered and a distributed observer scheme is formulated to estimate both the frequency deviation in each generator bus and the voltage phase angle of each load bus. The super-twisting-like sliding mode observer in (4.2.4) previously adopted in the present thesis for local state estimation at the single generator bus, will now be employed to perform distributed state estimation in all the generator buses of a given power system [102]. Moreover, distributed iterative algorithms (Jacobi and SOR methods) are used to estimate the voltage phase angle in each load node, relying on an exchange of local information and local knowledge of the system [66]. Finally, a simulation-based assessment is presented, which makes use of the well-established IEEE 39 bus benchmark [96] [95]. Figure 5.1.1 summarises the key-ideas of the conception of a distributed observer for wide-area monitoring in power networks.

5.1.1 Preliminaries

The starting point of the proposed distributed observer is the dynamical model in (3.5.11). The following assumption is imposed

Assumption 5.1. *Only the voltage phase angle associated with each generator bus* $\theta_i,\ i \in \mathcal{G}$ *is measured. Furthermore, the electrical active power demand of each load node* $P_{l_i},\ i \in \mathcal{L}$ *is specified.*

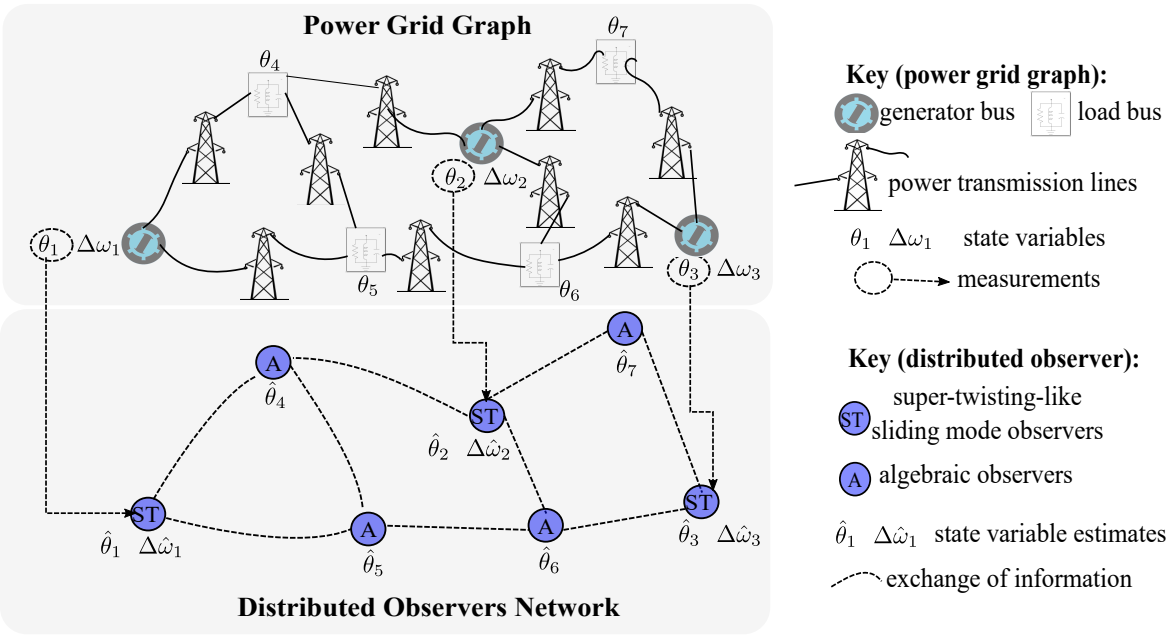

Figure 5.1.1: **(Top):** A schematic of a power system comprising generator buses and load buses connected via power transmission lines. **(Bottom):** A schematic of a distributed observer comprising ST-like observers for the generator buses, and algebraic observer for load buses.

Given Assumption 5.1, the system in (3.5.11) can be rewritten as:

$$\begin{aligned} \dot{\theta} &= \Delta\omega \\ M_{\mathcal{G}}\Delta\dot{\omega}_{\mathcal{G}} &= -D_{\mathcal{G}}\Delta\omega_{\mathcal{G}} + P_m - L^{gg}\theta_{\mathcal{G}} - L^{gl}\theta_{\mathcal{L}} \\ 0 &= P_l - L^{lg}\theta_{\mathcal{G}} - L^{ll}\theta_{\mathcal{L}} \\ y &= \theta_{\mathcal{G}} \end{aligned} \tag{5.1.1}$$

The following estimation objective is formulated:

Objective 5.1. *Estimate in a distributed fashion the generator frequency deviations $\Delta\omega_{\mathcal{G}}$ and the voltage phase angles of the loads $\theta_{\mathcal{L}}$.*

Objective 5.1 will now be achieved in two steps:

1. Two iterative algorithm are proposed to estimate the voltage phase angles of the loads.
2. The super-twisting-like observer in (4.2.4) will be employed in each generator bus to estimate in finite time the frequency deviation.

5.1.2 Algebraic Observer for the Loads Design

Under Assumption 5.1, the voltage phase angle of each generator $\theta_i,\ i \in \mathcal{G}$ is measured, and the electrical active power demand of each load node $P_{l_i},\ i \in \mathcal{L}$ is specified, using a ample period of τ seconds. Note that reasonable values for τ can be chosen according to [103]. By making use of the load (algebraic) equations in (5.1.1), at the k-th sampling instant, the following algebraic relation yields

$$0 = P_l[k] - L^{ll}\theta_{\mathcal{L}}[k] - L^{lg}\theta_{\mathcal{G}}[k], \tag{5.1.2}$$

where $\theta_{\mathcal{G}}[k]$, $\theta_{\mathcal{L}}[k]$, and $P_l[k]$ are the sampled versions of $\theta_{\mathcal{G}}$, $\theta_{\mathcal{L}}$, and P_l, respectively. By defining $b[k] \triangleq P_l[k] - L^{ll}\theta_{\mathcal{L}}[k]$, equation (5.1.2) takes the form

$$L^{ll}\theta_{\mathcal{L}}[k] = b[k]. \tag{5.1.3}$$

The signal $b[k]$ is fixed within the time interval $[k\tau,\ k\tau+\tau]$ and it is possible to estimate $\theta_{\mathcal{L}}[k]$ by solving, in a distributed fashion, the linear system of $|\mathcal{L}|$ equations

$$L^{ll}\hat{\theta}_{\mathcal{L}}[k] = b[k], \tag{5.1.4}$$

in order to obtain an estimate $\hat{\theta}_{\mathcal{L}}[k]$. This will be achieved by using an iterative scheme operating within each sampling period. Two methods are discussed for this purpose: the Jacobi Method and the Successive Over Relaxation (SOR) Method [104].

$$\hat{\theta}_{\mathcal{L}_{\mathrm{Jac}}}[k,h+1] = \left(I_{n_a} - \mathcal{D}^{-1}L^{ll}\right)\hat{\theta}_{\mathcal{L}_{\mathrm{Jac}}}[k,h] + \mathcal{D}^{-1}b[k], \tag{5.1.5}$$

$$\hat{\theta}_{\mathcal{L}_{\mathrm{Sor}}}[k,h+1] = \overbrace{\left(I_{n_a} - \kappa\left(\mathcal{D}-\kappa\mathcal{E}\right)^{-1}L^{ll}\right)}^{M_\kappa}\hat{\theta}_{\mathcal{L}_{\mathrm{Sor}}}[k,h] + \kappa\left(\mathcal{D}-\kappa\mathcal{E}\right)^{-1}b[k], \tag{5.1.6}$$

Equation (5.1.5) governs the Jacobi method, whilst equation (5.1.6) governs the SOR method. The vector $\hat{\theta}_{\mathcal{L}_{\mathrm{Jac}}}[k,h] \in \mathbb{R}^{|\mathcal{L}|}$ represents the h-th estimate of $\theta_{\mathcal{L}}[k]$ using the Jacobi method during the iteration cycle occurring in the time interval $[k\tau,\ k\tau+\tau]$, $\hat{\theta}_{\mathcal{L}_{\mathrm{Sor}}}[k,h] \in \mathbb{R}^{|\mathcal{L}|}$ represents the h-th estimate of $\theta_{\mathcal{L}}[k]$ using the SOR method during the iteration cycle occurring in the time interval $[k\tau,\ k\tau+\tau]$, the matrix $\mathcal{D}$ is defined according to:

$$\mathcal{D}_{ij} = \begin{cases} L^{ll}_{ij} & \text{if } i=j, \\ 0. & \end{cases} \tag{5.1.7}$$

The matrix $M_\kappa \triangleq \left(I_{n_a} - \kappa\left(\mathcal{D}-\kappa\mathcal{E}\right)^{-1}L^{ll}\right)$ in (5.1.6) is a function of the design weight $\kappa \in \mathbb{R}^+$, and $\mathcal{E}$ is defined according to:

$$\mathcal{E}_{ij} \begin{cases} -L^{ll}_{ij} & \text{if } i<j, \\ 0 & \text{otherwise.} \end{cases} \tag{5.1.8}$$

If the discrete-time linear systems in the form of (5.1.5)-(5.1.6) are asymptotically stable (a detailed stability analysis will be provided in the rest of section), the steady-state relations

$$\hat{\theta}_{\mathcal{L}_{\mathrm{Jac}}}[k,\cdot] = \left(I_{n_a} - \mathcal{D}^{-1}L^{ll}\right)\hat{\theta}_{\mathcal{L}_{\mathrm{Jac}}}[k,\cdot] + \mathcal{D}^{-1}b[k] \tag{5.1.9}$$

$$\hat{\theta}_{\mathcal{L}_{\mathrm{Sor}}}[k,\cdot] = \left(I_{n_a} - \kappa\left(\mathcal{D}-\kappa\mathcal{E}\right)^{-1}L^{ll}\right)\hat{\theta}_{\mathcal{L}_{\mathrm{Sor}}}[k,\cdot] + \kappa\left(\mathcal{D}-\kappa\mathcal{E}\right)^{-1}b[k], \tag{5.1.10}$$

are satisfied, where $\hat{\theta}_{\mathrm{Jac}}[k,\cdot]$ and $\hat{\theta}_{\mathrm{Sor}}[k,\cdot]$ are the Jacobi and SOR steady-state solutions, respectively. The relations (5.1.9)-(5.1.10) imply

$$L^{ll}\hat{\theta}_{\mathcal{L}_{\mathrm{Jac}}}[k,\cdot] = b[k] \tag{5.1.11}$$

$$L^{ll}\hat{\theta}_{\mathcal{L}_{\mathrm{Sor}}}[k,\cdot] = b[k]. \tag{5.1.12}$$

5.1.2.1 Stability Analysis of Jacobi and SOR Methods

The matrix L^{ll} is (weakly) diagonally dominant according to the Laplacian matrix definition. Then, by making use of Gershgorin's Theorem [104], each eigenvalue λ_i of $\left(I_{n_a} - \mathcal{D}^{-1}L^{ll}\right)$ satisfies $|\lambda_i| \leq 1$. Furthermore, if all the eigenvalues of $\left(I_{n_a} - \mathcal{D}^{-1}\mathcal{L}^{ll}\right)$ lie (strictly) inside the unit disk in the complex plane, it follows (5.1.5) converges and $\hat{\theta}_{\mathcal{L}_{\mathrm{Jac}}}[k,h+1] \to \hat{\theta}_{\mathcal{L}_{\mathrm{Jac}}}[k,h]$ as $h \to \infty$. On the other hand, if there are eigenvalues of absolute value close to 1 or equal to 1, the Jacobi Method may converge too slowly or not converge at all, respectively. Therefore, the use of SOR method represents a valid alternative solution. In (5.1.6), the design constant κ has to be selected according to the convergence criteria presented in [105]. These criteria ensure that the eigenvalues of M_κ lie inside the unit disk. In particular, κ has to satisfy the condition [105]:

$$\kappa\left(\mathcal{D} + k\mathcal{E}L^{llT}\right) + \kappa L^{ll}\left(\mathcal{D} + \kappa L^{llT}\right) - \kappa^2 L^{ll}L^{llT} > 0, \tag{5.1.13}$$

where L^{llT} denotes the transpose of the matrix L^{ll}. Moreover, the optimal value κ^* of κ satisfying equation (5.1.13), is given by:

$$\kappa^* = \arg\min_{\kappa}\left(\rho(M_\kappa)\right), \tag{5.1.14}$$

where $\rho(M_\kappa)$ denotes the spectral radius of the matrix M_κ.

Remark 5.1. Note that the number of iterations in the algebraic schemes (5.1.5)-(5.1.6) affects the accuracy of the estimations. More precisely, the greater the number of iterations, the greater the estimation accuracy at the expense of a prolonged sampling time and an higher computational cost. Furthermore, the position of the eigenvalues of the matrix M_κ in the complex plane influences the accuracy of the estimation. Specifically, if these eigenvalues are placed close to the origin (by selecting the optimal value of the weight κ according to (5.1.14)), a better accuracy can be achieved by using the same number of iterations. In practice, the optimisation as in (5.1.14) can be performed off-line and only once, given a set of values for the weight $\kappa \in (0,2)$ and the matrix $M_\kappa = \left(I_{n_a} - \kappa\left(\mathcal{D} - \kappa\mathcal{E}\right)^{-1}\mathcal{L}^{ll}\right)$ is computed accordingly [105].

5.1.3 Initial Conditions

For both the Jacobi and the SOR method, the initial conditions

$$\hat{\theta}_{\mathcal{L}_{(\mathrm{Jac,Sor})}}[k,h=0] = \begin{cases} \hat{\theta}_{\mathcal{L}_{(\mathrm{Jac,Sor})}}[0] & \text{if } k=1, \\ \hat{\theta}_{\mathcal{L}_{(\mathrm{Jac,Sor})}}[k-1,\cdot] & \text{if } k>1, \end{cases} \tag{5.1.15}$$

are selected, where $\hat{\theta}_{\mathcal{L}_{(\mathrm{Jac,Sor})}}[0]$ is an arbitrarily chosen initial condition for the two considered methods, while $\hat{\theta}_{\mathcal{L}_{(\mathrm{Jac,Sor})}}[k-1,\cdot]$ is the steady-state estimate associated with the $(k-1)$-th sample period.

Note that according to (5.1.15), for $k > 1$ the steady state estimates $\hat{\theta}_{\mathcal{L}_{(\mathrm{Jac,Sor})}}[k,\cdot]$ are assumed close to the previous ones $\hat{\theta}_{\mathcal{L}_{(\mathrm{Jac,Sor})}}[k-1,\cdot]$.

5.1.3.1 Root-Mean-Square Error Metric

The Root-Mean-Square Error (RMSE) metric is adopted to determine the global performance of the algebraic observer schemes (5.1.5)-(5.1.6). This metric is defined as

$$\mathrm{RMSE}_{(\mathrm{Jac,Sor})}[k,h] = \sqrt{\frac{\sum_{i=1}^{|\mathcal{L}|}\left(\theta_i[k] - \hat{\theta}_{i_{(\mathrm{Jac,Sor})}}[k,h]\right)^2}{|\mathcal{L}|}},\ \forall k,\ \forall i \in \mathcal{L}. \tag{5.1.16}$$

where $\hat{\theta}_{i_{(\mathrm{Jac,Sor})}}$ denotes the estimate of the i-th voltage phase angle $\theta_i \in \mathcal{L}$. According to the development in this section, the RMSE is expected to converge to zero within each time interval $[k\tau, k\tau+\tau]$.

5.1.4 Super-Twisting-Like Sliding Mode Observer for the Generators

In order to estimate the frequency deviation in each generator bus, it will be shown in this section that the super-twisting-like sliding mode observer structure in (4.2.4) can still be employed. The novelty here is an exchange of local information of the estimates coming from the neighbouring (load) observers. These estimates will appear in the matched channel of the error dynamics of the SM observer. The structure of the ST-like observer for each i-th generator bus is

$$\left.\begin{array}{rcl} \dot{\hat{\theta}}_i & = & \Delta\hat{\omega}_i - a_i e_{\theta_i} - k_{g1_i}\left|e_{\theta_i}\right|^{1/2}\mathrm{sign}\left(e_{\theta_i}\right) \\ \Delta\dot{\hat{\omega}}_i & = & -k_{g2_i}\mathrm{sign}\left(e_{\theta_i}\right) - a_i^2 e_{\theta_i} + a_i\Delta\hat{\omega}_i \\ & & -k_{g1_i}a_i\left|e_{\theta_i}\right|^{1/2}\mathrm{sign}\left(e_{\theta_i}\right) + \varphi_i^{ZOH} + \frac{P_{m_i}}{M_i} \end{array}\right\} i \in \mathcal{G} \tag{5.1.17}$$

Note that in (5.1.17), the i-th generator super-twisting-like sliding mode observer receives estimates from its neighbouring algebraic observers. In particular:

$$\varphi_i^{ZOH} \triangleq -\frac{1}{M_i}\Big(\sum_{j\in\mathcal{N}_i, j\in\mathcal{L}} L_{ij}^{gl}\hat{\theta}_j^{ZOH}\Big),\ i \in \mathcal{G},\ j \in \mathcal{L} \tag{5.1.18}$$

where $\hat{\theta}_j^{ZOH},\ j \in \mathcal{L}$ is the Zero Order Hold (ZOH) version (piecewise constant) [106] of the j-th load bus voltage phase angle estimate communicated by the j-th neighbouring algebraic observer. Note that in the rest of the present section the symbol $\hat{\theta}_j^{ZOH},\ j \in \mathcal{L}$ denote the estimate of $\theta_j,\ j \in \mathcal{L}$, without specifying if computed via Jacobi or SOR method. This exchange of local information gives the proposed observers a distributed architecture.

Remark 5.2. Note that the algebraic observers are discrete-time systems, whilst the super-twisting-like ones are continuous-time systems. It follows that the ZOH implementation is required to include signals coming from discrete-time systems into the input channel of continuous-time systems [66].

The error dynamics of the super-twisting-like sliding mode observer have the same structure of

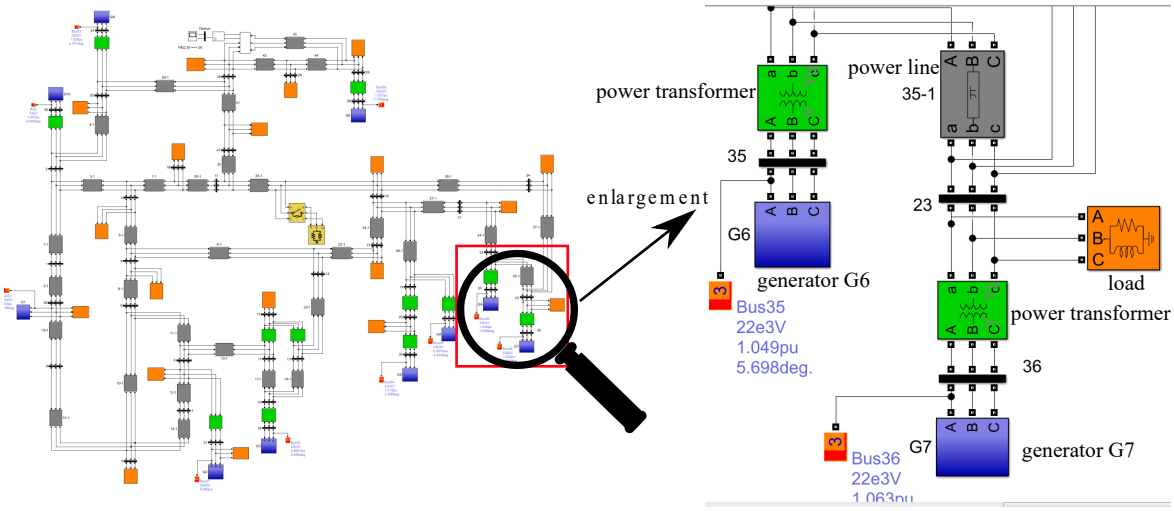

Figure 5.1.2: A scheme of the IEEE 39 bus implemented in the SimPowerSystems interface. The enlargement on the left shows the standard symbols adopted to model generator buses, load buses, power transformers, and power transmission lines.

(4.2.5), and they are given by

$$\left.\begin{array}{rcl} \dot{e}_{\theta_i} & = & e_{\omega_i} - a_i e_{\theta_i} - k_{g1_i} |e_{\theta_i}|^{1/2} \operatorname{sign}(e_{\theta_i}) \\ \dot{e}_{\omega_i} & = & -k_{g2_i} \operatorname{sign}(e_{\theta_i}) - a_i^2 e_{\theta_i} - k_{g1_i} a_i |e_{\theta_i}|^{1/2} \operatorname{sign}(e_{\theta_i}) - \Phi_i + a_i e_{\omega_i}, \end{array}\right\} i \in \mathcal{G} \quad (5.1.19)$$

where the matched perturbation Φ_i can be shown to be

$$\Phi_i \triangleq \varphi_i^{ZOH} + \frac{1}{M_i}\Big(\sum_{j \in \mathcal{N}_i} L_{ij}^{gl}\theta_j\Big),\ i \in \mathcal{G},\ j \in \mathcal{L} \quad (5.1.20)$$

Note that φ_i^{ZOH} converges to $\frac{1}{M_i}\big(\sum_{j\in\mathcal{N}_i} L_{ij}^{gl}\vartheta_j\big)$ according to the convergences of the schemes. It follows that Φ_i is a bounded disturbance appearing in the matched channel of (5.1.19). Therefore, following the same arguments presented in Section 4.2.2, the system in equation (5.1.19) converges to the origin in finite time.

5.1.5 Simulation Results

5.1.5.1 Preliminaries

The IEEE 39 node (also called the 10-machine New-England) power system is chosen as a benchmark for the assessment and it has been implemented in a *Matlab-SimPowerSystems* environment. The basic data for this power system is available in the literature in [96]. Figure 5.1.2 shows the implementation of the IEEE 39 bus benchmark in the *SimPowerSystems* environment. In the enlarged view it is possible to distinguish the generators, the power transformers, the loads and the power transmission lines.

If t is the simulation time, for $0 \leq t < 5$ (s) the overall system is at steady state. This condition is characterised by a perfect balance between power generation and consumption [84]. A step variation

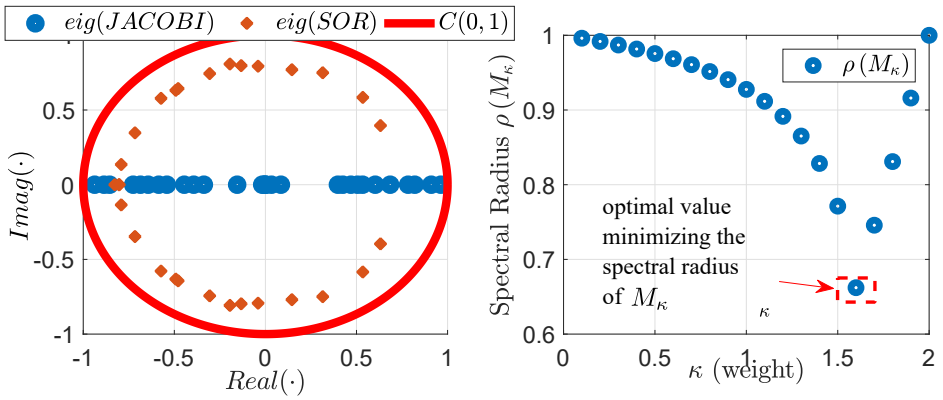

Figure 5.1.3: **(Left):** The eigenvalues in the complex plane for the matrices of the Jacobi and SOR method (5.1.5)-(5.1.6). **(Right):** The spectral radius of the matrix M_κ and the optimal choice of the weight κ, selected according to (5.1.14) and to Remark 5.1.

in the electrical active power demand at the 16-th load bus takes place, which can be described by

$$P_{l_{16}} = 329 + 300\,\text{step}(t-5) - 300\,\text{step}(t-10)\ \ (\text{MW}) \tag{5.1.21}$$

The time-varying power demand (5.1.21) makes the electrical frequency of each generator deviate from its rated value as shown in Figure 5.1.5. Furthermore, when the load alteration ends (for $t = 10$ (s)), the frequency of each generator asymptotically tends again to the rated value of 60 Hz.

5.1.5.2 Algebraic Observer Performances

Two values of the sampling time τ are considered: 0.1 and 0.5 seconds, and within each sampling interval a maximum of 1000 iterations can be executed. Figure 5.1.3 shows that the matrix $\left(I_{n_a} - \mathcal{D}^{-1}\mathcal{L}^{ll}\right)$ in (5.1.5) has a spectral radius too close to one and the convergence speed is expected to be slow. Figure 5.1.3 shows also the optimal choice of the weight κ, which is governed by (5.1.14). The eigenvalues of the matrix M_{κ^*} are drawn in the complex plane together with the eigenvalues of $\left(I_{n_a} - \mathcal{D}^{-1}\mathcal{L}^{ll}\right)$ for the Jacobi method, and the unit disk. For $t > 5$ (s), the transient behaviours of the algebraic observers are shown in the enlargement in Figure 5.1.4. This transient behaviour is due to the update of the term $b[k]$ every 0.1 seconds, and the subsequent iterations within each time interval $[k\tau; k\tau + \tau]$ governed by . The SOR method displays a faster speed of convergence compared to the Jacobi method, for both the two considered values of the sampling time.

5.1.5.3 Super-Twisting-Like Observer Performances

The design constants for the super-twisting-like sliding mode observer are set as follows: $k_{g1_i} = 5$, and $k_{g2_i} = 50$. As clarified in this chapter, the ST observers have continuous-time dynamics, then, the solver *Ode1 (Euler)* is select in the *Matlab-Simulink* environment, with a fixed integration step size set equal to 0.1 milliseconds. The well-established Luenberger observers are compared with the proposed sliding mode estimator, in order to demonstrate the superiority of the proposed ST-like observers. Note that Figure 5.1.5 shows both the actual values and the estimate of the frequencies, which can be obtained starting from the frequency deviation according to the standard expressions

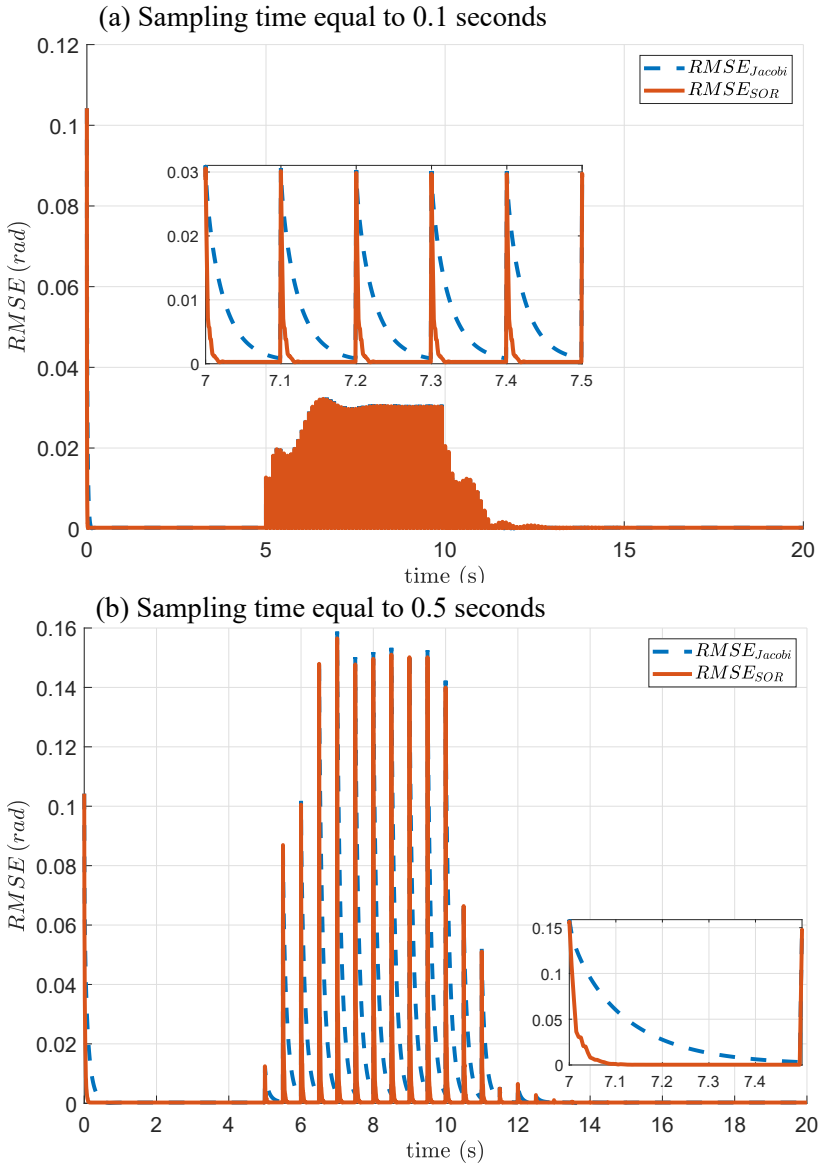

Figure 5.1.4: **(a):** Load node voltage phase angles RMSE metric for the Jacobi and SOR method, for the value $\tau = 0.1$ (s), **(b):** Load node voltage phase angles RMSE metric for the Jacobi and SOR method, for the value $\tau = 0.5$ (s).

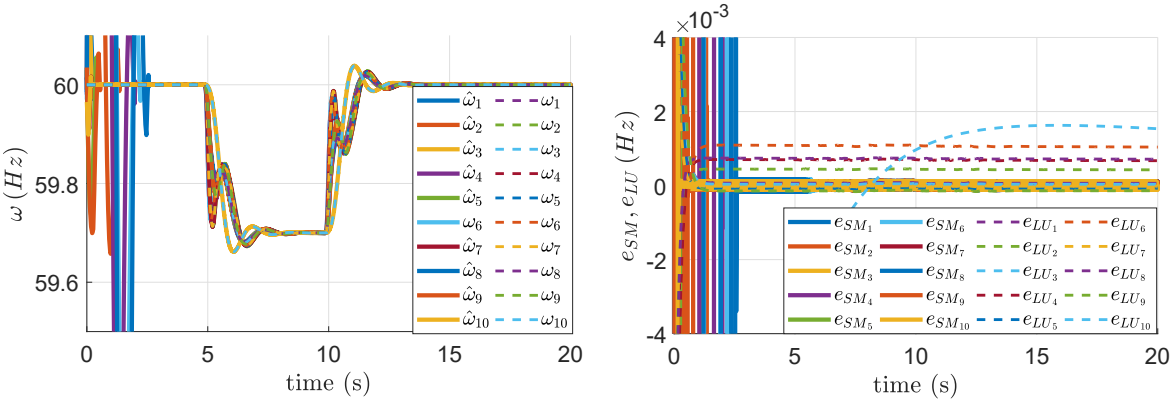

Figure 5.1.5: **(Left):** Time evolution of the frequency of each generator together with its estimate via super-twisting-like sliding mode observer. **(Right):** Frequency estimation error for each super-twisting-like sliding mode observer, denoted as e_{SM_i}, and for the well-established Luenberger observer, denoted as e_{LU_i}.

$\omega_i = (\Delta\omega_i + 1)\,\omega_0$, and $\hat{\omega}_i = (\Delta\hat{\omega}_i + 1)\,\omega_0$, respectively. Figure 5.1.5 shows that the accuracy of the sliding mode observers is clearly higher than the Luenberger ones, as shown in Figure. This is also in accordance with the developments in [107].

5.1.6 Conclusions

In this section, a distributed observer formulation involving the interconnection of super-twisting-like sliding mode observers for each generator, and distributed algebraic observers schemes, is proposed for state estimation and monitoring in power systems. The scheme exploits the underlying topology of the power systems and requires only local information available at the bus level of the graph. The numerical simulations based on the IEEE 39 bus benchmark validate the effectiveness of the proposed method. In particular, it has been possible to ensure robustness for the super-twisting-like sliding mode observer with respect to matched disturbances arising from modelling the nonlinear dynamics of the networks.

5.2 SM Observers for a Network of Hydro-Thermal Power Sources

In this section, a network of SM observers is designed to robustly estimate the unmeasured state variables in power systems composed of interconnections of thermal power sources and hydroelectric power sources. Two SM state observers are created for each sources, with a local communication at the bus level [50].

5.2.1 Preliminaries

Thermal and Hydraulic Turbine-Governor The dynamics of the steam turbine-governor in (3.1.19) on page 31 can be compactly rewritten as

$$\begin{aligned} \dot{x}_{p_{t_i}} &= A_{t_i} x_{p_{t_i}} + B_{t_i}\left(u_i - \tfrac{\Delta\omega_i}{R_i}\right) \\ y_{t_{i_1}} &= C_{t_i} x_{p_{t_i}}, \end{aligned} \tag{5.2.1}$$

where

$$\begin{aligned} x_{p_{t_i}} &\triangleq \begin{bmatrix} P_{m_{a_i}} & P_{m_{b_i}} & P_{m_{c_i}} & P_{g_i} \end{bmatrix} \\ A_{t_i} &\triangleq \begin{bmatrix} -\frac{1}{T_{t_{a_i}}} & 0 & 0 & \frac{1}{T_{t_{a_i}}} \\ 0 & -\frac{1}{T_{t_{b_i}}} & \frac{1}{T_{t_{b_i}}} & 0 \\ 0 & 0 & -\frac{1}{T_{t_{c_i}}} & \frac{1}{T_{t_{c_i}}} \\ 0 & 0 & 0 & -\frac{1}{T_{g_i}} \end{bmatrix} \\ B_{t_i} &\triangleq \begin{bmatrix} 0 & 0 & 0 & \frac{1}{T_{g_i}} \end{bmatrix}^T \\ C_{t_i} &\triangleq \begin{bmatrix} \alpha_{t_{a_i}} & \beta_{t_{b_i}} & \gamma_{t_{c_i}} & 0 \end{bmatrix} \end{aligned}$$

Analogously, the dynamics of the hydraulic turbine-governor in (3.1.21) on page 32 can be compactly rewritten as

$$\begin{aligned} \dot{x}_{p_{h_i}} &= A_{h_i} x_{p_{h_i}} + B_{h_i}\left(u_i - \tfrac{\Delta\omega_i}{R_i}\right) \\ y_{h_{i_1}} &= C_{h_i} x_{p_{h_i}}, \end{aligned} \tag{5.2.2}$$

$$\begin{aligned} x_{p_{h_i}} &\triangleq \begin{bmatrix} P_{g_i} & P_{c_i} & W_i \end{bmatrix}^T \\ A_{h_i} &\triangleq \begin{bmatrix} -\frac{1}{T_{g_i}} & 0 & 0 \\ 1 & -\frac{1}{T_{c_{2_i}}} & 0 \\ \frac{T_{c_{1_i}}}{T_{c_{2_i}}} & \frac{T_{c_{2_i}} - T_{c_{1_i}}}{T_{c_{2_i}}^2} & -\frac{2}{T_{h_i}} \end{bmatrix} \\ B_{t_i} &\triangleq \begin{bmatrix} \frac{1}{T_{g_i}} & 0 & 0 \end{bmatrix}^T \\ C_{h_i} &\triangleq \begin{bmatrix} -2\frac{T_{c_{1_i}}}{T_{c_{2_i}}} & 2\frac{T_{c_{1_i}} - T_{c_{2_i}}}{T_{c_{2_i}}^4} & \frac{6}{T_{h_i}} \end{bmatrix} \end{aligned}$$

For the purpose of designing the observers, it is possible to rewrite both (5.2.1) and (5.2.2), which display a similar structure, in the following general form

$$\begin{aligned} \dot{x}_i &= A_i x_i + B_i\left(u_i + d_i\right) \\ y_{1i} &= C_i x_i \end{aligned} \tag{5.2.3}$$

where $x_i,\ A_i,\ B_i,\ u_i,\ d_i,\ C_i,\ y_i$ are suitably defined vectors and matrices of appropriate dimensions.

Synchronous Generator The generator dynamics in (3.4.6) can be compactly rewritten in the following form

$$\begin{aligned} \dot{\theta}_i &= \Delta\omega_i, \\ \Delta\dot{\omega}_i &= \phi_i \\ y_{2i} &= \theta_i \end{aligned} \tag{5.2.4}$$

where the auxiliary signal ϕ_i is defined as

$$\phi_i \triangleq \frac{P_{m_i}}{M_i\left(\Delta\omega_i + \omega^*\right)} - \frac{\sum_{j\in\mathcal{N}_i} \frac{V_i V_j}{x_{ij}} \sin\left(\theta_i - \theta_j\right)}{M_i\left(\Delta\omega_i + \omega^*\right)} - \frac{D_i \Delta\omega_i}{M_i} - P_{d_i}, \tag{5.2.5}$$

where P_{d_i} is an additional bounded disturbance.

5.2.2 Assumptions and Facts

Important properties of (5.2.1), (5.2.2), and (5.2.4) will now be discussed, together with key-assumptions, which are instrumental for the observers design.

Proposition 5.1. *The matrix A_{t_i} in (5.2.1) and A_{h_i} in (5.2.2) are Hurwitz*

Proof. By direct calculations, the eigenvalues of A_{t_i} can be shown to be: $-\frac{1}{T_{t_{a_i}}}$,$-\frac{1}{T_{t_{a_i}}}$, $-\frac{1}{T_{t_{a_i}}}$, and$-\frac{1}{T_{t_{a_i}}}$. Analogously, the eigenvalues of A_{h_i} can be shown to be $-\frac{1}{T_{g_i}}$, $-\frac{1}{T_{c_{2_i}}}$ and $-\frac{2}{T_{h_i}}$. It straightforwardly follows that all the eigenvalues of A_{t_i} and A_{h_i} are real and strictly negative, which proves the proposition. □

Remark 5.3. Each thermal power source is governed by (5.2.1) together with (5.2.4), whilst each hydroelectric power source is governed by (5.2.2) together with (5.2.4). It is assumed to measure at the local level only the mechanical power delivered by the turbine P_{m_i} and the generator angle θ_i both in the thermal and hydroelectric power sources. All the other state variables have to be estimated via observers. Moreover, the matrices and vectors in (5.2.1) and (5.2.2) are assumed to be known at each power source node level.

Proposition 5.2. *The pair (A_{t_i}, C_{t_i}) in (5.2.1) and (A_{h_i}, C_{h_i}) in (5.2.2) are observable.*

Proof. The determinant of the Observability Matrix $\mathcal{O}_{t_i}$ associated with the pair (A_{t_i}, C_{t_i}) is given by:

$$\begin{aligned} \det\left(\mathcal{O}_{t_i}\right) &= -\frac{\gamma_{t_{c_i}}}{T_{t_{a_i}}^3 T_{t_{b_i}}^3 T_{t_{c_i}}^3 T_{g_i}^2}\left(T_{t_{b_i}} - T_{t_{c_i}} - \alpha_{t_{a_i}} T_{t_{b_i}} + \alpha_{t_{a_i}} T_{t_{c_i}} + \gamma_{t_{c_i}} T_{t_{c_i}}\right) \\ &\quad \left(T_{g_i}^2 - T_{g_i} T_{t_{c_i}} + \alpha_{t_{a_i}} T_{t_{b_i}} T_{t_{c_i}} - \alpha_{t_{a_i}} T_{t_{b_i}} T_{g_i} + \gamma_{t_{c_i}} T_{g_i} T_{t_{c_i}}\right) \\ &\quad \left(T_{t_{a_i}}^2 - T_{t_{a_i}} T_{t_{c_i}} + \alpha_{t_{a_i}} T_{t_{b_i}} T_{t_{c_i}} - \alpha_{t_{a_i}} T_{t_{b_i}} T_{t_{a_i}} + \gamma_{t_{c_i}} T_{t_{a_i}} T_{t_{c_i}}\right). \end{aligned} \tag{5.2.6}$$

Given the value ranges for the parameters reported in [37], the expression of the determinant (5.2.6) can be shown to be always different from zero, by separately considering the four terms constituting its expression. This ensures that the matrix $\mathcal{O}_{t_i}$ is always full rank, thus implying the pair (A_{t_i}, C_{t_i}) is observable [69]. The first term of (5.2.6) satisfies

$$-\frac{\gamma_{t_{c_i}}}{T_{t_{a_i}}^3 T_{t_{b_i}}^3 T_{t_{c_i}}^3 T_{g_i}^2} < 0. \tag{5.2.7}$$

Considering now the second term, it is possible to show that it is always strictly positive:

$$\begin{aligned} T_{t_{b_i}} - T_{t_{c_i}} - \alpha_{t_{a_i}} T_{t_{b_i}} + \alpha_{t_{a_i}} T_{t_{c_i}} + \gamma_{t_{c_i}} T_{t_{c_i}} &= \left(1 - \alpha_{t_{a_i}}\right) T_{t_{b_i}} + \left(\alpha_{t_{a_i}} + \gamma_{t_{c_i}} - 1\right) T_{t_{c_i}} \\ & \left(\beta_{t_{b_i}} + \gamma_{t_{c_i}}\right) T_{t_{b_i}} + \beta_{t_{b_i}} T_{t_{c_i}} > 0 \end{aligned} \tag{5.2.8}$$

As for the term

$$\left(T_{g_i}^2 - T_{g_i} T_{t_{c_i}} + \alpha_{t_{a_i}} T_{t_{b_i}} T_{t_{c_i}} - \alpha_{t_{a_i}} T_{t_{b_i}} T_{g_i} + \gamma_{t_{c_i}} T_{g_i} T_{t_{c_i}}\right), \tag{5.2.9}$$

two case are considered:

i) If $T_{g_i} = T_{t_{c_i}}$, then the term (5.2.9) can be simplified as:

$$T_{g_i}^2 - T_{g_i}^2 + \alpha_{t_{a_i}} T_{t_{b_i}} T_{g_i} - \alpha_{t_{a_i}} T_{t_{b_i}} T_{g_i} + \gamma_i T_{g_i}^2 = \gamma_{t_{c_i}} T_{g_i}^2 > 0, \tag{5.2.10}$$

which is strictly positive.

ii) If $T_{g_i} < T_{t_{c_i}}$, then (5.2.9) can be rewritten as:

$$\left(T_{g_i} - \alpha_{t_{a_i}} T_{t_{b_i}}\right)\left(T_{g_i} - T_{t_{c_i}}\right) + \gamma_{t_{c_i}} T_{g_i} T_{t_{c_i}}. \tag{5.2.11}$$

It is straightforward to show that $\gamma_{t_{c_i}} T_{g_i} T_{t_{c_i}} > 0$ and

$$\left(T_{g_i} - \alpha_{t_{a_i}} T_{t_{b_i}}\right)\left(T_{g_i} - T_{t_{c_i}}\right) > 0$$

since $T_{g_i} - T_{t_{c_i}} < 0$, and $T_{g_i} - \alpha_i T_{t_{b_i}} < 0$ relying on the data [37]. Therefore, one can conclude that (5.2.11) is always strictly greater then zero.

Consider now the term

$$\left(T_{t_{a_i}}^2 - T_{t_{a_i}} T_{t_{c_i}} + \alpha_{t_{a_i}} T_{t_{b_i}} T_{t_{c_i}} - \alpha_{t_{a_i}} T_{t_{b_i}} T_{t_{a_i}} + \gamma_{t_{c_i}} T_{t_{a_i}} T_{t_{c_i}}\right). \tag{5.2.12}$$

Note that (5.2.12) and (5.2.9) displays the same structure. Two possible cases can take place

i) If $T_{t_{a_i}} = T_{t_{c_i}}$, then (5.2.12) becomes

$$T_{t_{a_i}}^2 - T_{t_{a_i}}^2 + \alpha_{t_{a_i}} T_{t_{b_i}} T_{t_{a_i}} - \alpha_{t_{a_i}} T_{t_{b_i}} T_{t_{a_i}} + \gamma_{t_{c_i}} T_{t_{a_i}}^2 = \gamma_{t_{c_i}} T_{a_i}^2 > 0. \tag{5.2.13}$$

ii) If $T_{t_{a_i}} < T_{t_{c_i}}$, then (5.2.12) can be shown to be equal to

$$T_{t_{a_i}}\left(T_{t_{a_i}} - T_{t_{c_i}}\right) - \alpha_{t_{a_i}} T_{t_{b_i}}\left(T_{t_{a_i}} - T_{t_{c_i}}\right) + \gamma_{t_{c_i}} T_{t_{a_i}} T_{t_{c_i}} \tag{5.2.14}$$

One can note that $\gamma_{t_{c_i}} T_{a_i} T_{c_i} > 0$ and

$$\left(T_{t_{a_i}} - \alpha_{t_{a_i}} T_{t_{b_i}}\right)\left(T_{t_{a_i}} - T_{t_{c_i}}\right) > 0 \tag{5.2.15}$$

since in the considered case $T_{t_{a_i}} - T_{t_{c_i}} < 0$, and the inequality $T_{t_{a_i}} - \alpha_{t_{a_i}} T_{t_{b_i}} < 0$ is satisfied according to the numerical data available in [37]. Therefore, all the terms in (5.2.6) are always

different from zero, which ensures that $\mathcal{O}_{t_i}$ is full rank.

The determinant of the Observability Matrix $\mathcal{O}_{h_i}$ associated with the pair (A_{h_i}, C_{h_i}) is given by

$$\det\left(\mathcal{O}_{h_i}\right) = 24\frac{\left(T_{g_i}+T_{t_i}\right)\left(T_{c_{2_i}}+T_{h_i}\right)\left(T_{g_i}-T_{h_{1_i}}\right)\left(T_{c_{1_i}}-T_{c_{2_i}}\right)}{T_{g_i}^2 T_{c_{2_i}} T_{h_i}^3}. \tag{5.2.16}$$

which becomes equal to zero if $T_{g_i} = T_{h_{1_i}}$ or $T_{c_{1_i}} = T_{c_{2_i}}$. Again according to the data [37], the two conditions are not acceptable. □

Assumption 5.2. *The signal ϕ_i in (5.2.5) is bounded with positive known upper-bound as follows:*

$$|\phi_i| \leq \Delta_{\phi_i} \tag{5.2.17}$$

Remark 5.4. It is reasonable to assume that the interconnections amongst the sources change with respect to time. This can be due, for example, to scheduled electricity trade among the sources. For the observers design purposes, the most conservative situation will be adopted, in which all the possible interconnections amongst the sources are considered. Note that the signal ϕ_i include all the voltage phase angles of the neighbouring sources in the most conservative situation here specified. It follows that the condition (5.2.17) is satisfied also in case the network is not operating in the most conservative situation. Moreover, in such approach, the interactions amongst the sources detailed in Remark 3.5 on page 43 are treated as bounded disturbances. It follows that the sliding mode observers reveals to be completely decentralised features.

5.2.3 Observers Design

5.2.3.1 Synchronous Generator Observers

For the sake of clarity, the sub-optimal sliding mode observer to robustly estimate the frequency deviation of each generator will be designed first. The stability analysis of the sub-optimal observer will be exploited to design the sliding mode observers for the turbine-governor dynamics.

Consider the following sub-optimal sliding mode observer

$$\begin{aligned} \dot{\hat{\theta}}_i &= \Delta\hat{\omega}_i, \\ \Delta\dot{\hat{\omega}}_i &= u_{\mathrm{sub}_i} \end{aligned} \tag{5.2.18}$$

where $\hat{\theta}_i$ is the estimate of θ_i, $\Delta\hat{\omega}_i$ is the estimate of $\Delta\omega_i$, and u_{sub_i} is equal to [79]

$$u_{\mathrm{sub}_i} \triangleq -\mu_i V_i^{\max}\mathrm{sign}\left(e_{\theta_i} - \frac{1}{2}e_{\theta_i}^{\max}\right). \tag{5.2.19}$$

where $e_{\theta_i} \triangleq \theta_i - \hat{\theta}_i$. Moreover, the following relations are considered

$$\begin{cases} \mu_i^* & \in (0,1] \\ V_i^{\max} & > \max\left(\frac{\Lambda_i}{\mu_i^*}, \frac{4\Lambda_i}{3-\mu_i^*}\right). \end{cases} \tag{5.2.20}$$

The signal $e_{\theta_i}^{\max}$ is computed by using the peak detection algorithm. This algorithm was originally designed in [79] for control purpose, and it is extended in the present chapter to the observer purpose. Consider the following auxiliary signal.[1]

$$\Delta_i(t) \triangleq [e_{\theta_i}(t-\varepsilon) - e_{\theta_i}(t)]\, e_{\theta_i}(t), \tag{5.2.21}$$

where $\varepsilon > 0$ is a small constant (in practical cases, ε can represent a time delay either due to the switching or to the measuring devices). At the initial time instant t_0, the initial condition $e_{\theta_i}^{\max} = e_{\theta_i}(t_0)$ and $e_{\theta_i}(t_0 - \varepsilon) = 0,$ if $t < \varepsilon$, are adopted. $\forall t > t_0$, the following steps are executed:

1. if $(\Delta_i(t) < 0)$ $e_{\theta_i}^{\mathrm{mem}} = e_{\theta_i}(t)$;
2. if $(\Delta_i(t) \leq 0)$
   (a) if $\left(\left|e_{\theta_i}^{\mathrm{mem}}\right| \leq \left|e_{\theta_i}^{\max}\right|$ **and** $e_{\theta_i}^{\mathrm{mem}} e_{\theta_i}^{\max} > 0\right)$ $\quad e_{\theta_i}^{\max} = e_{\theta_i}^{\mathrm{mem}}$;
   (b) else $\quad e_{\theta_i}^{\max} = e_{\theta_i}^{\max}$;
3. if $(\Delta_i(t) > 0)$ $e_{\theta_i}^{\max} = e_{\theta_i}^{\mathrm{mem}}$

In addition, the variable μ_i is governed by

$$\mu_i = \begin{cases} \mu_i^* & \text{if } \left(e_{\theta_i} - \frac{1}{2} e_{\theta_i}^{\max}\right)\left(e_{\theta_i}^{\max} - e_{\theta_i}\right) > 0 \\ 1 & \text{if } \left(e_{\theta_i} - \frac{1}{2} e_{\theta_i}^{\max}\right)\left(e_{\theta_i}^{\max} - e_{\theta_i}\right) \leq 0. \end{cases} \tag{5.2.22}$$

The error dynamics is obtained by subtracting the generator dynamics (5.2.4) from the sub-optimal observer dynamics (5.2.18) and they are

$$\begin{array}{rcl} \dot{e}_{\theta_i} & = & e_{\omega_i}, \\ \dot{e}_{\omega_i} & = & -\phi_i - \mu_i V_i^{\max} \mathrm{sign}\left(e_{\theta_i} - \frac{1}{2} e_{\theta_i}^{\max}\right), \end{array} \tag{5.2.23}$$

where $e_{\omega_i} = \Delta\hat{\omega}_i - \Delta\hat{\omega}_i$. The following proposition will now be proven.

Proposition 5.3. *Under Assumption 5.2, and given the signal u_{sub_i} governed by (5.2.19), the origin is a finite-time stable equilibrium point for the error dynamics (5.2.23).*

Proof. The system in (5.2.23) is in the standard form for the sub-optimal sliding mode controlled system [79], [80]. More precisely, if the signal u_{sub_i} satisfies the inequalities in (5.2.20), it follows that (5.2.23) converge to the origin in finite time, guaranteeing a correct state estimation of the frequency deviation of each generator. □

Remark 5.5. Note that in [67] a linear combination of the two state errors has been selected as a sliding surface for the sub-optimal SM observers to be nullified

$$\sigma_i = e_{\theta_i} + c_i e_{\omega_i} \tag{5.2.24}$$

[1] The explicit dependence on the time t is here introduced for the sake of clarity.

where c_i is a positive known constant. Differently, in the present approach, the sliding surface to be nullified reveals to be equal to

$$\sigma_i = e_{\theta_i} \tag{5.2.25}$$

Remark 5.6. Note that Proposition 5.3 is still valid if additional bounded uncertainties, appearing in the matched channel of the system (5.2.4), are included in the definition of the term ϕ_i in (5.2.5). These additional uncertainties can be due to unmodelled dynamics, parameters variation and external disturbances. This confirms that the proposed observer (5.2.18) guarantees the robustness property typical of sliding mode observers.

5.2.3.2 Turbine-Governors Observers

Consider now the following sliding mode observer for the dynamical system (5.2.3)

$$\dot{\hat{x}}_i \;=\; A_i\hat{x}_i + B_i\left(u_i + \hat{d}_i - \rho_i\tfrac{F_iC_ie_i}{|F_iC_ie_i|}\right) - G_iC_ie_i \tag{5.2.26}$$

where $e_i \triangleq \hat{x}_i - x_i$, $F_i \in \mathbb{R}$, ρ_i is a positive design constant, G_i is a design matrix, and $\hat{d}_i \triangleq \Delta\hat{\omega}_i/R_i$ is the estimated value of the frequency deviation $\Delta\omega_i$, communicated by the sub-optimal observer for the generator of the same source. From the development in Section 5.2.3.1, it is reasonable to assume that

$$\psi_i \triangleq \frac{(\Delta\hat{\omega}_i - \Delta\omega_i)}{R_i} = \frac{e_{\omega_i}}{R_i} \tag{5.2.27}$$

is a bounded disturbance, which means that its modulus is upper-bounded. Moreover, ψ_i converges to zero in finite by virtue of Proposition 5.3. By subtracting (5.2.3) from (5.2.26), the so-called error system dynamics can be obtained as follows

$$\dot{e}_i = \big(A_i - G_iC_i\big)e_i - B_i\left(\psi_i + \rho_i\frac{F_iC_ie_i}{|F_iC_ie_i|}\right). \tag{5.2.28}$$

The following proposition holds.

Proposition 5.4. *Given error dynamics (5.2.28), suppose that for a positive definite symmetric matrix $P_i \succ 0$, one has*

$$P_iA_{0_i} + A_{0_i}^T < 0, \tag{5.2.29}$$

where $A_{0_i} \triangleq A_i - G_iC_i$ and the following structural constraint [62] is satisfied

$$P_iB_i = C_i^TF_i^T. \tag{5.2.30}$$

Then, the origin is an asymptotically stable equilibrium point for the error dynamics (5.2.28), provided that the constant ρ_i is chosen such that

$$\rho_i > |\psi_i|\,. \tag{5.2.31}$$

Proof. The system in (5.2.28) is in the standard form of the perturbed sliding mode observer error dynamics [71], with the associated sliding surface $\sigma_i = F_iC_{t_i}e_{p_{t_i}} = 0$ to be reached in a finite

time. The proposition can be proven in perfect analogy to Proposition 2.1 on page 17 of the present thesis. □

Remark 5.7. Note that, in analogy with Proposition 5.3, Proposition 5.4 is still valid if additional bounded uncertainties, appearing in the matched channel of the system (5.2.3), are included in the term ψ_i in (5.2.27). These uncertainties can be due to unmodelled dynamics, parameters variation and external disturbances as mentioned before. The robustness property typical of sliding mode observer is guaranteed also for the observer (5.2.28).

5.2.4 Scalability And Resilience of the Observers

The proposed estimation scheme can be easily modified whenever changes alter the topology of the power system. In the present section, the analysis will be focused on the opening/closing of power transmission lines and on the plug-in of a novel source. It is assumed currently that the changes occur independently, and for each situation specific modification rules are provided. However, it is possible that all these changes take place simultaneously. In such a scenario, one has to simultaneously consider the rules and apply them sequentially.

Opening or Closing of a Power Transmission Line According to Remark 5.4, the interconnection between the generator buses can change with respect to time. However, as stated in Assumption 5.2, the sub-optimal sliding mode observer for the generators is designed taking into account the maximum amount of uncertainty, which is upper-bounded. In case of an opening or closing of the power transmission line connecting the i-th and the j-th source, the resulting variation of the magnitude of uncertainty in the disturbances ϕ_i and ϕ_j does not affect the sliding motion of (5.2.19).

Plugging-in of a Source Suppose now that a new j-th source is interconnected with to a given number of existing sources via power transmission lines. Let $\mathcal{N}_j$ be the set of the existing sources directly connected to the new j-th source. The proposed estimation scheme can be updated as follows:

1. For the given j-th new source, design a sliding mode observer in the form of (5.2.26).

2. Re-tune the gains of the pre-existing sub-optimal observers for the generators of all the neighbours sources $k \in \mathcal{N}_j$, by updating the terms Δ_{ϕ_k} (see (5.2.17)), and satisfying the tuning rules for the sub-optimal architecture (5.2.20). Note that this re-tuning is required since the amount of uncertainty increases in the sources directly connected to the new one.

3. Design a new sub-optimal sliding mode observer to estimate the frequency deviation of the new j-th plant.

Remark 5.8. The proposed observer-based estimation scheme has to be updated only where topological changes occur, i.e., at the level of the new bus and of its neighbourhood. All the other observers do not need to be updated. Therefore, one can conclude that the estimation scheme is scalable in case of adding new sources and it is resilient in case of changing in the operation of the power transmission lines.

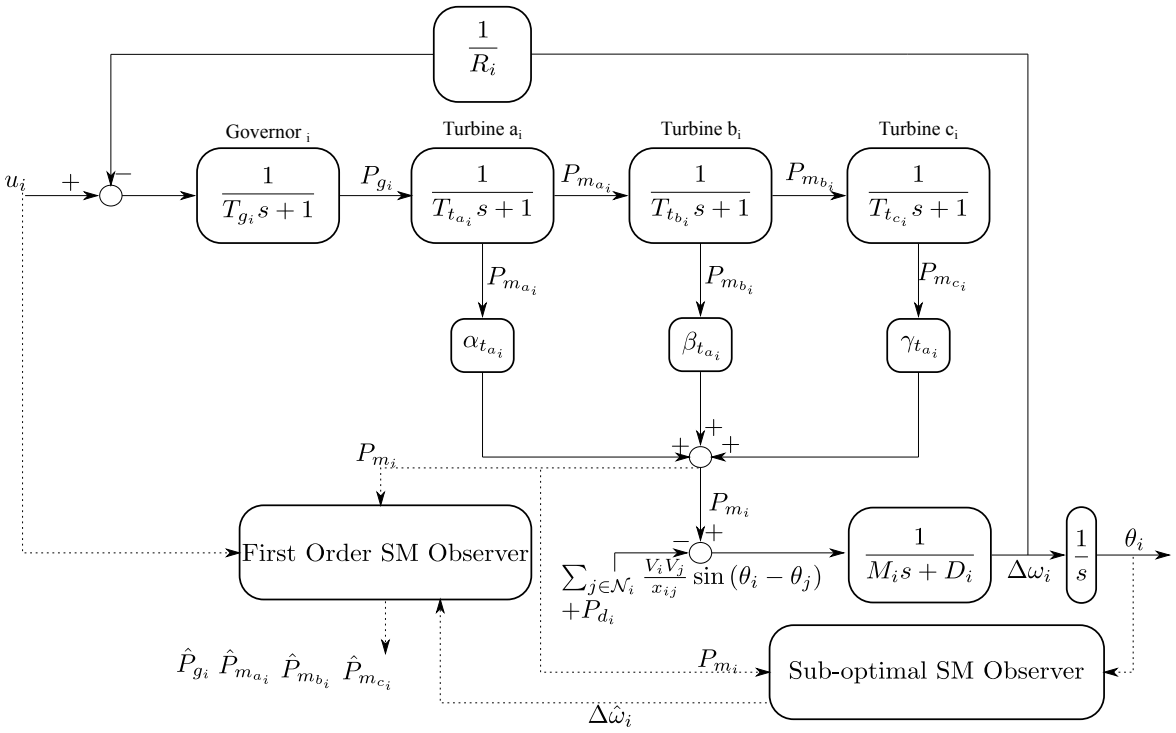

Figure 5.2.1: The block diagram of the i-th thermal power source dynamical model together with the proposed observers. The local communication between the two observers is also underlined.

Figure 5.2.1 and Figure 5.2.2 show a schematic of the thermal and hydroelectric power sources illustrated on page 32 and on page 33, together with the proposed observers.

5.2.5 Simulations Results

In this section, the effectiveness of observer-based scheme is demonstrated in simulations. The proposed estimation scheme is compared with the well-established linear state observers, originally proposed in [108] and applied to a large class of dynamical systems. In this framework, symbol $\tilde{x}$ denotes the estimate of the state variable x via Unknown Input (UI) Luenberger observer. A power system composed of two thermal power sources and two hydroelectric power sources interconnected via power transmission lines is considered (see Figure 5.2.3 and the numerical representations of the parameter in Table 5.2.1). In this simulation case it is assumed that each source is controlled only via primary frequency controller [5]. It follows that the control input u_i is set equal to zero in each source. The simulation time interval is $T = 200$ seconds, whilst the integration step size is set equal to 1 millisecond. The selected sub-optimal sliding mode observer parameters are $V^{\max} = 10$, $\rho_i = 10$, for all the observers. The values of the reactances of the edges are: $x_{12} = 0.19$ (p.u.), $x_{23} = 0.20$ (p.u.), $x_{34} = 0.22$ (p.u.), $x_{14} = 0.19$ (p.u.). Power system dynamics have been numerically simulated in a Matlab-Simulink R2017b environment. Table 5.2.1 shows the numerical representation of the model parameters. Note that the same network has been employed in relevant works in the literature, such as [35], [94]. The following three scenarios are considered:

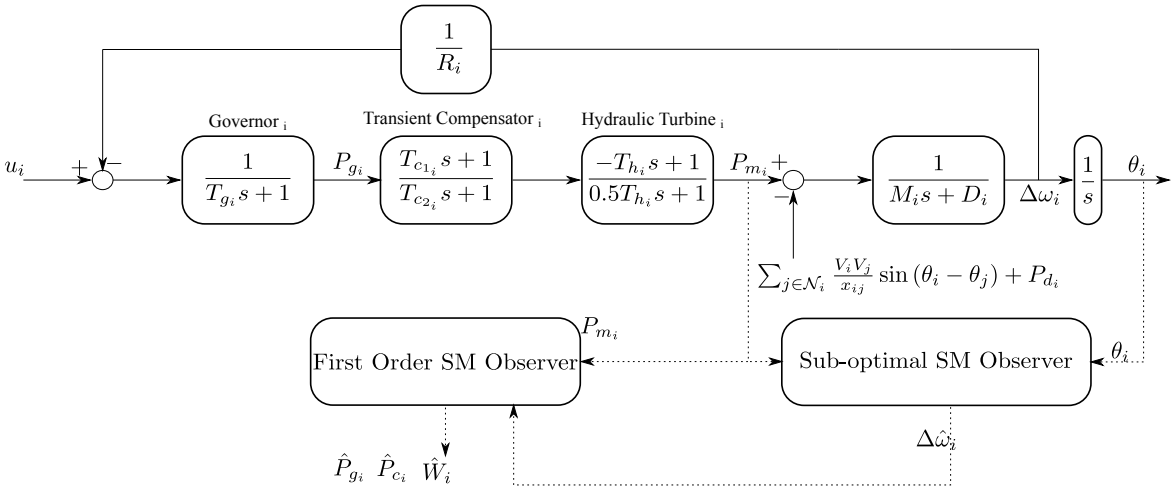

Figure 5.2.2: The block diagram of the i-th hydroelectric power source dynamical model together with the proposed observers. The local communication between the two observers is also underlined.

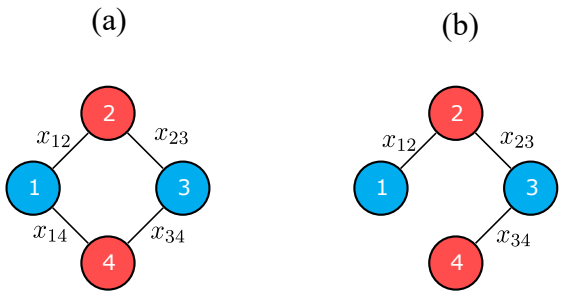

Figure 5.2.3: A schematic of the considered power system composed of two thermal power sources (red circles) and two hydroelectric power sources (blue circles) in the most conservative operation (a), and with the power transmission line x_{14} open (b).

Table 5.2.1: Numerical Representation of the Parameters of the power system test case (base power of 1000 MVA)

	Source 1	Source 2	Source 3	Source 4
T_{t_a}	–	0.30	–	0.35
T_{t_b}	–	7.00	–	10.00
T_{t_c}	–	0.50	–	0.45
T_{c_1}	5.00	–	4.50	–
T_{c_2}	50.00	–	40.00	–
T_h	2.00	–	2.20	–
T_g	0.50	0.25	0.45	0.27
D	1.4×10^{-4}	1.5×10^{-4}	1.3×10^{-4}	1.7×10^{-4}
R	2.50	2.60	2.70	2.80
M	28×10^{-4}	38×10^{-4}	38×10^{-4}	42×10^{-4}
P_d	0.10	0.50	0.20	0.70

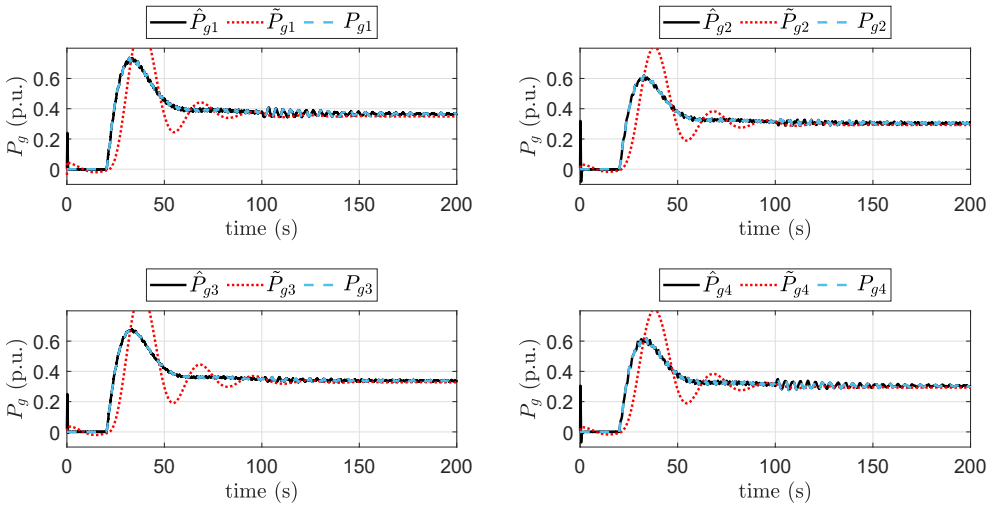

Figure 5.2.4: Time histories of the governor power variation P_{g_i} in each source, its estimated values $\hat{P}_{g_i}$ via proposed sliding mode observer and $\tilde{P}_{g_i}$ via UI Luenberger observer.

1. **Scenario 1**, $0 \leq t < 20$ (s), during which the power network is at steady state, which means that there is a perfect balance between electrical active power generation and consumption;

2. **Scenario 2**, $20 \leq t < 100$ (s), during which, after a step variation of the active power demand in each node according to Table , the frequency decreases;

3. **Scenario 3**, $100 \leq t \leq 200$ (s), during which the power transmission line x_{14} in Figure 5.2.3 is disconnected.

Scenario 1 Performances During Scenario 1, the power system is at steady-state. In such situation each sliding mode observer for turbine-governor dynamics and each sub-optimal sliding mode observer for the frequency deviation are able to asymptotically estimate all the unmeasured states (see Figures 5.2.4, 5.2.5, 5.2.6, and 5.2.8). Note that there are fast transients during the first seconds, which are due to the initial conditions of the observers which are set different from the actual states to be estimated (see again Figures 5.2.4, 5.2.5, 5.2.6, and 5.2.8).

Scenario 2 Performances During Scenario 2, the sudden variation of electrical active power demand P_{d_i} in each source causes a transient during which the frequency of each generator decreases (see both (3.4.6) on page 39 and the schematic shown in Figure 3.1.2 on page 30 for a formal mathematical justification). All the sources, assumed controllable via the primary frequency controllers, response by increasing the electrical active power generation. All the observers are capable of tracking the time evolution of all the unmeasured state variables (see again Figures 5.2.4, 5.2.5, 5.2.6, and 5.2.8).

Scenario 3 Performances During Scenario 3, the power transmission line interconnecting the 1-st and the 4-th source is open. This causes relevant oscillations of the frequencies, mainly in the 1-st

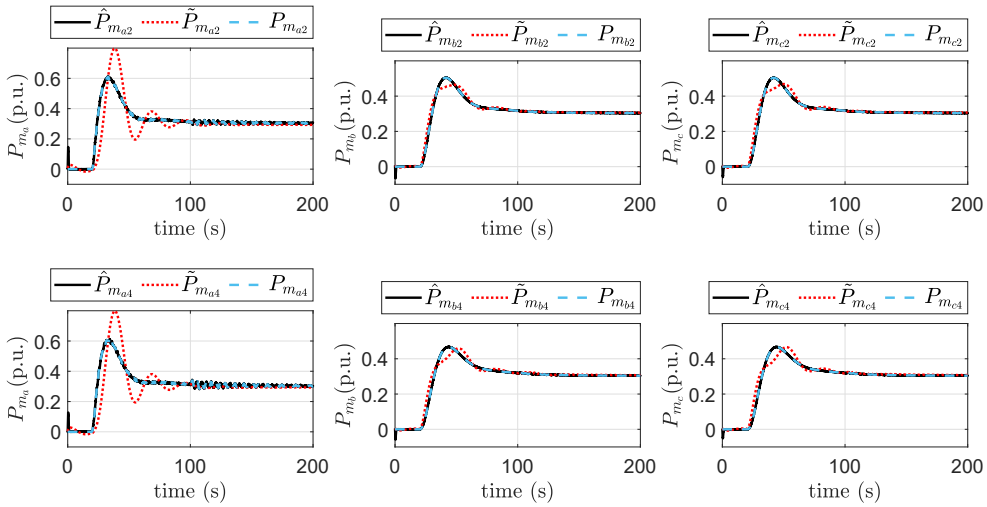

Figure 5.2.5: Time histories of the turbine power variation $P_{m_{a_i}}$, $P_{m_{b_i}}$, and P_{mc_i} in each thermal power plant and their estimated values $\hat{P}_{m_{a_i}}$, $\hat{P}_{m_{b_i}}$, and $\tilde{P}_{mc_i}$ via proposed sliding mode observer and their estimate values $\tilde{P}_{m_{a_i}}$, $\tilde{P}_{m_{b_i}}$, and $\tilde{P}_{mc_i}$ via UI Luenberger observer.

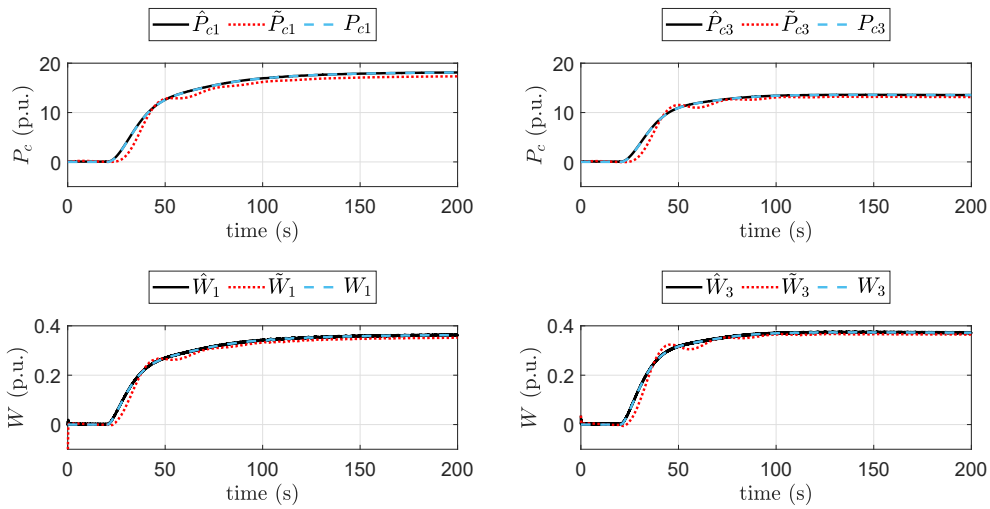

Figure 5.2.6: Time histories of transient compensator power variation P_{c_i}, the water speed variation W_i in each hydroelectric power plant and their estimated value $\hat{P}_{c_i}$ and $\hat{W}_i$ via proposed sliding mode observer and $\tilde{P}_{c_i}$ and $\tilde{W}_i$ via UI Luenberger observer, respectively.

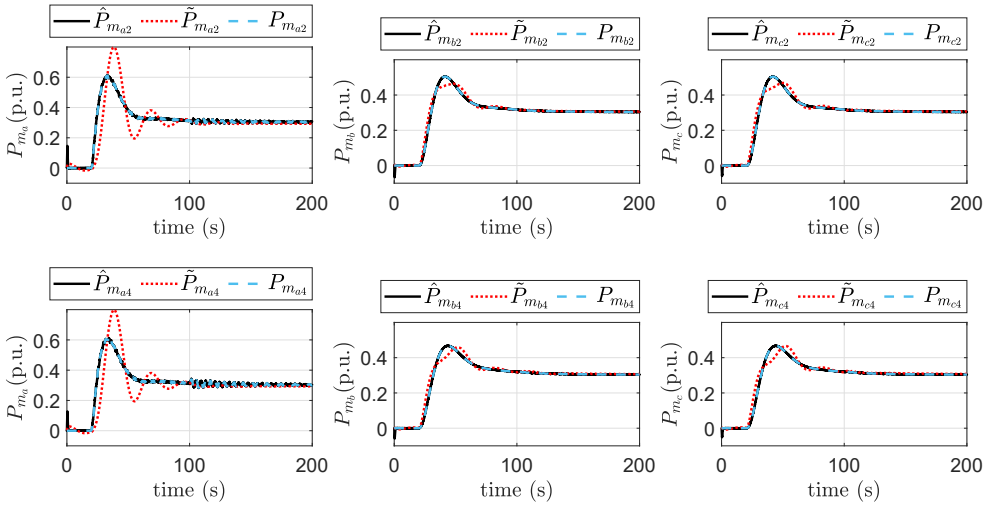

Figure 5.2.7: Time histories of the turbine power variation $P_{m_{a_i}}$,$P_{m_{b_i}}$, and P_{mc_i} in each thermal power source and their estimated values $\hat{P}_{m_{a_i}}$, $\hat{P}_{m_{b_i}}$, and $\tilde{P}_{mc_i}$ via proposed sliding mode observer and their estimate values $\tilde{P}_{m_{a_i}}$, $\tilde{P}_{m_{b_i}}$, and $\tilde{P}_{mc_i}$ via UI Luenberger observer

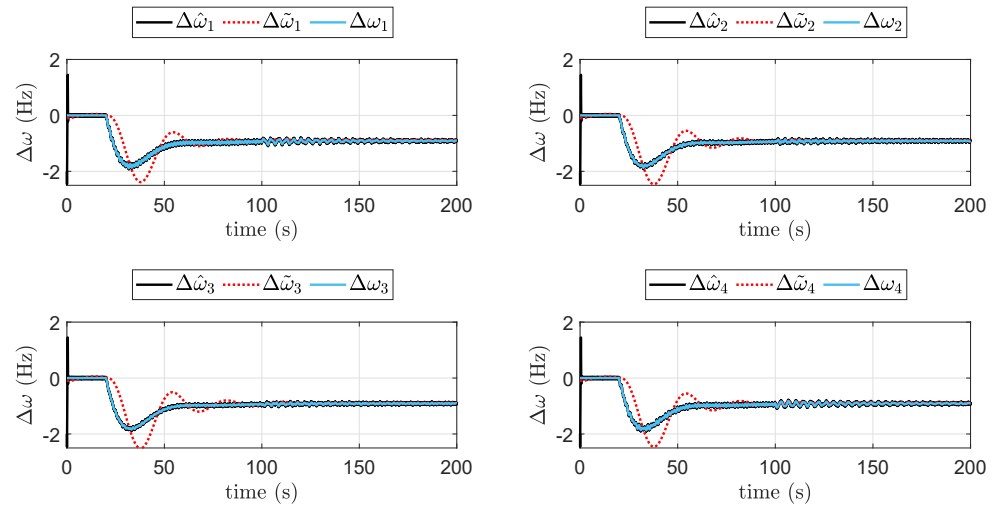

Figure 5.2.8: Time histories of the frequency deviation $\Delta\omega_i$ in each synchronous generator, its estimated value via the proposed sliding mode observer $\Delta\hat{\omega}_i$ and via UI Luenberger observer $\Delta\tilde{\omega}_i$.

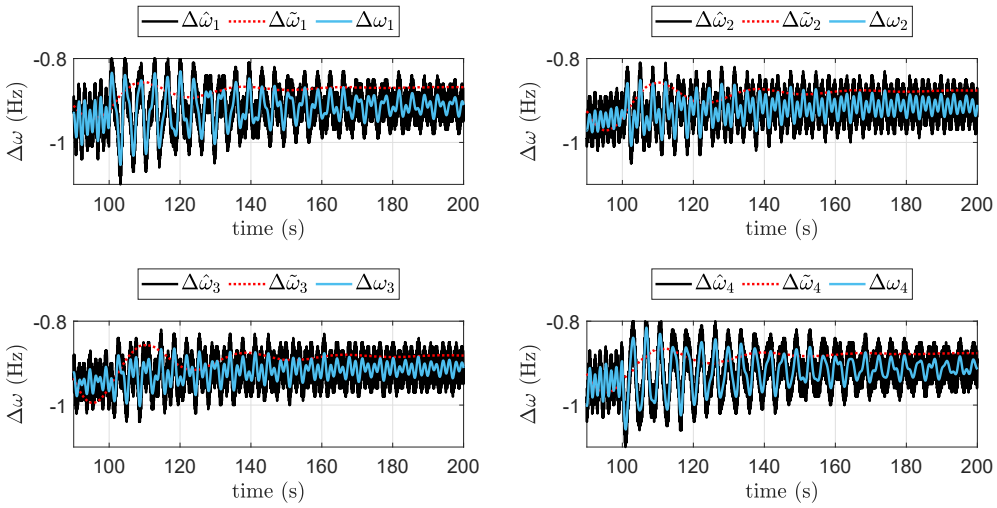

Figure 5.2.9: An enlarged view of the time histories of the frequency deviation $\Delta\omega_i$ in each synchronous generator, its estimated value via the proposed sliding mode observer $\Delta\hat{\omega}_i$ and via UI Luenberger observer $\Delta\tilde{\omega}_i$.

and the 4-th source, as shown in Figure 5.2.9. Also in such transient, all the observers track the unmeasured state without losing the induced sliding motion (see again Figures 5.2.4, 5.2.5, 5.2.6, and 5.2.8).

Remark 5.9. Note that in all the three Scenarios, the proposed sliding mode observers are capable of tracking the unmeasured state variables with higher accuracy with respect to the well-established UIL observers, particularly during transients. This is also in accordance to [107].

5.2.6 Conclusions

In this section, a novel sliding mode observers scheme has been designed to estimate and track the unmeasured states of power systems composed of an interconnections of thermal and hydroelectric sources. The proposed scheme has also revealed to be flexible to topological changes affecting the power systems. Moreover, the simulation performances in the discussed scenarios have validated the effectiveness of the proposal.

5.3 Higher Order Sliding Mode Observers in Hybrid Power Systems

In the present section, the analysis focuses on the so-called hybrid power systems, in which traditional power sources (treated in the previous section) coexist together with renewable sources and dynamical loads. In contrast to the SM observer schemes reported in the existing literature, the present section focuses on a model where heterogeneous power sources and loads are simultaneously present and are coupled through the power flow exchanges. As a consequence, the level of unknown, but bounded fluctuations and uncertainties that an observer would have to cope with, is significantly higher in this case than in the conventional independent cases.

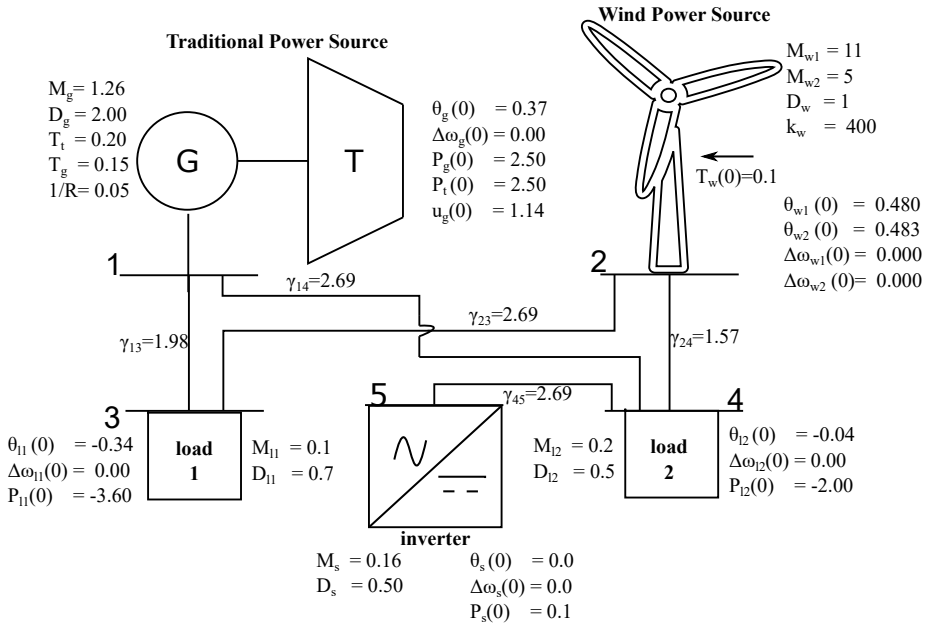

Figure 5.3.1: A schematic of the considered hybrid power system composed of a traditional source, a wind source, an inverter source and two loads. The numerical representations of the model parameters and the initial conditions of the state variables will be used in the simulation assessment.

5.3.1 Preliminaries

Important properties of the models described in Chapter 3 will now be illustrated. The power system considered here consists of an interconnection of four types of components: traditional power sources, wind power sources, inverter power sources, and loads. Figure 5.3.1 shows a typical power system in which the the four considered components are depicted.

Notation Clarification The notation for the parameters and state variables previously adopted in Chapter 3 still holds in the current section. However, in order to distinguish the heterogeneous 5 components of the network, in Figure 5.3.1 the following additional subscripts are introduced: for a given state variables or model parameter x, the subscript x_g represents conventional generator source, the subscript x_w wind power sources, the subscript x_w inverter power source, whilst x_l denotes the load components.

5.3.2 Traditional Power Source Dynamical Model

The traditional generation dynamical model (3.1.17)-(3.1.18) on page 31 can be compactly rewritten as

$$\begin{aligned} \dot{x}_{g_i} &= A_{g_i} x_{g_i} + B_{g1_i} u_{g_i} + B_{g2_i} \Big(P_{eg_i}(y_{g_i}, y_{j|_{j\in\mathcal{N}_{g_i}}}) + d_{eg_i} \Big) \\ y_{g_i} &= C_{g_i} x_{g_i} \end{aligned} \tag{5.3.1}$$

where

$$x_{g_i} \triangleq \begin{bmatrix} \theta_{g_i} & \Delta\omega_{g_i} & P_{t_i} & P_{m_i} \end{bmatrix}^T \tag{5.3.2}$$

$$A_{g_i} \triangleq \begin{bmatrix} 0 & 1 & 0 & 0 \\ 0 & \frac{-D_{g_i}}{M_{g_i}} & \frac{1}{M_{g_i}} & 0 \\ 0 & 0 & -\frac{1}{T_{t_i}} & \frac{1}{T_{t_i}} \\ 0 & -\frac{1}{T_{g_i}} & 0 & -\frac{1}{R_i T_{g_i}} \end{bmatrix} \tag{5.3.3}$$

$$B_{g1_i} \triangleq \begin{bmatrix} 0 & 0 & 0 & \frac{1}{T_{g_i}} \end{bmatrix}^T,\ B_{g2} \triangleq \begin{bmatrix} 0 & -\frac{1}{M_{g_i}} & 0 & 0 \end{bmatrix}^T \tag{5.3.4}$$

$$C_{g_i} \triangleq \begin{bmatrix} 1 & 0 & 0 & 0 \end{bmatrix} \tag{5.3.5}$$

In (5.3.1) the signal $P_{eg_i}\left(y_{g_i}, y_{j|_{j\in\mathcal{N}_{g_i}}}\right) + d_{eg_i}$ denotes the total electrical active power flowing from the traditional power source i to its neighbourhood $\mathcal{N}_{g_i}$, and it is defined as

$$P_{eg_i}\left(y_{g_i}, y_{j|_{j\in\mathcal{N}_{g_i}}}\right) + d_{eg_i} \triangleq \sum_{j\in\mathcal{N}_{g_i}} \gamma_{g_{ij}} \sin\left(y_{g_i} - y_j\right) + d_{eg_i} \tag{5.3.6}$$

The term y_j brings further interactions from its neighbourhood $\mathcal{N}_{g_i}$, which could be any type from the heterogeneous components set.

5.3.3 Wind Power Source Dynamical Model

The two-mass system for dynamics of wind turbines, described in (3.2.1) on page 34, can be more compactly rewritten as:

$$\begin{aligned} \dot{x}_{w_i} &= A_{w_i} x_{w_i} + B_{w1_i} T_{w_i} + B_{w2_i}\left(P_{ew_i}\left(y_{w_i}, y_{j|_{j\in\mathcal{N}_{w_i}}}\right) + d_{ew_i}\right) \\ y_{w_i} &= C_{w_i} x_{w_i} \end{aligned} \tag{5.3.7}$$

where:

$$x_{w_i} \triangleq \begin{bmatrix} \theta_{w1_i} & \Delta\omega_{w1_i} & \theta_{w2_i} & \Delta\omega_{w2_i} \end{bmatrix}^T \tag{5.3.8}$$

$$A_{w_i} \triangleq \begin{bmatrix} 0 & 1 & 0 & 0 \\ \frac{-k_{w_i}}{M_{w1_i}} & -\frac{D_{w_i}}{M_{w1_i}} & \frac{k_{w_i}}{M_{w1_i}} & \frac{D_{w_i}}{M_{w1}} \\ 0 & 0 & 0 & 1 \\ \frac{k_{w_i}}{M_{w2_i}} & \frac{D_{w_i}}{M_{w2_i}} & -\frac{k_{w_i}}{M_{w2_i}} & -\frac{D_{w_i}}{M_{w2_i}} \end{bmatrix} \tag{5.3.9}$$

$$B_{w1_i} \triangleq \begin{bmatrix} 0 & -\frac{1}{M_{w1_i}} & 0 & 0 \end{bmatrix}^T,\ B_{w2_i} \triangleq \begin{bmatrix} 0 & 0 & 0 & \frac{1}{M_{w2_i}} \end{bmatrix}^T \tag{5.3.10}$$

$$C_{w_i} \triangleq \begin{bmatrix} 1 & 0 & 0 & 0 \end{bmatrix} \tag{5.3.11}$$

In (5.3.7) the signal $P_{ew_i}\big(y_{w_i}, y_{j|_{j\in\mathcal{N}_{w_i}}}\big)+d_{ew_i}$ denotes the total electrical active power flowing from the wind power source to its neighbourhood $\mathcal{N}_w$, and it is defined as

$$P_{ew_i}\big(y_{w_i}, y_{j|_{j\in\mathcal{N}_{w_i}}}\big)+d_{ew_i} \triangleq \sum_{j\in\mathcal{N}_{w_i}} \gamma_{w_{ij}} \sin\left(y_{w_i} - y_j\right) + d_{ew_i}. \tag{5.3.12}$$

5.3.4 Inverter-Based Power Source Dynamical Model

The dynamical model of the so-called inverters with capacitive inertia (3.2.4) on page 36 can be rewritten in the form of

$$\begin{aligned} \dot{x}_{s_i} &= A_{s_i}x_{s_i} + B_{s_i}\phi_{s_i}\big(x_{s_i}, y_{j|_{j\in\mathcal{N}_{s_i}}}, P_{s_i}, d_{es_i}\big) \\ y_{s_i} &= C_{s_i}x_{s_i} \end{aligned} \tag{5.3.13}$$

where the vectors and matrices are:

$$x_s \triangleq \begin{bmatrix} \theta_{s_i} \\ \Delta\omega_{s_i} \end{bmatrix},\ A_{s_i} \triangleq \begin{bmatrix} 0 & 1 \\ 0 & -\frac{D_{s_i}}{M_{s_i}} \end{bmatrix},\ B_{s_i} \triangleq \begin{bmatrix} 0 \\ 1 \end{bmatrix},\ C_{s_i} \triangleq \begin{bmatrix} 1 & 0 \end{bmatrix} \tag{5.3.14}$$

In (5.3.13) the signal $\phi_{s_i}\big(x_{s_i}, y_{j|_{j\in\mathcal{N}_{s_i}}}, P_{s_i}, d_{es_i}\big)$ is given by

$$\phi_{s_i}\big(x_{s_i}, y_{j|_{j\in\mathcal{N}_{s_i}}}, P_{s_i}, d_{es_i}\big) \triangleq \frac{P_{s_i} - \sum_{j\in\mathcal{N}_{s_i}} \gamma_{s_{ij}} \sin\left(y_{s_i} - y_j\right) + d_{es_i}}{\Delta\omega_{s_i} + \omega_0} \tag{5.3.15}$$

where $\mathcal{N}_{s_i}$ is the neighbourhood of the inverter source.

5.3.5 Load Dynamical Model

The dynamical model of the load considered in (3.3.4) on page 37 can be rewritten as:

$$\begin{aligned} \dot{x}_{l_i} &= A_{l_i}x_{l_i} + B_{l_i}\phi_{l_i}\big(y_{l_i}, y_{j|_{j\in\mathcal{N}_{l_i}}}, P_{l_i}, d_{el_i}\big) \\ y_{l_i} &= C_{l_i}x_{l_i} \end{aligned} \tag{5.3.16}$$

$$x_{l_i} \triangleq \begin{bmatrix} \theta_{l_i} \\ \Delta\omega_{l_i} \end{bmatrix},\ A_{l_i} \triangleq \begin{bmatrix} 0 & 1 \\ 0 & -\frac{D_{l_i}}{M_{l_i}} \end{bmatrix}\ B_{l_i} \triangleq \begin{bmatrix} 0 \\ 1 \end{bmatrix},\ C_{l_i} \triangleq \begin{bmatrix} 1 & 0 \end{bmatrix} \tag{5.3.17}$$

In (5.3.16) the signal $\phi_{l_i}\big(y_{l_i}, y_{j|_{j\in\mathcal{N}_{l_i}}}, P_{l_i}, d_{el_i}\big)$ is given by

$$\phi_{l_i}\big(y_{l_i}, y_{j|_{j\in\mathcal{N}_{l_i}}}, P_{l_i}, d_{el_i}\big) \triangleq P_{l_i} - \sum_{j\in\mathcal{N}_{l_i}} \gamma_{l_{ij}} \sin\left(y_{l_i} - y_j\right) + d_{el_i} \tag{5.3.18}$$

5.3.6 Assumptions and Facts

In this section, important properties of the power system dynamical models previously described will be discussed, together with key-assumptions, which are instrumental for the observers design.

Proposition 5.5. *Given the dynamics in (5.3.1), (5.3.7), (5.3.13), and (5.3.16), the associated pairs* (A_{g_i}, C_{g_i}), (A_{w_i}, C_{w_i}), (A_{s_i}, C_{s_i}), *and* (A_{l_i}, C_{l_i}) *are all observable.*

Proof. Given the pair (A_{g_i}, C_{g_i}), Observability Matrix $O_{g_i} \triangleq [C_{g_i},\ C_{g_i}A_{g_i},\ \ldots, C_{g_i}A_{g_i}A_{g_i}A_{g_i}]^T$ can be shown to be

$$O_{g_i} = \begin{bmatrix} 1 & 0 & 0 & 0 \\ 0 & 1 & 0 & 0 \\ 0 & \frac{-D_{g_i}}{M_{g_i^2}} & \frac{1}{M_{g_i}} & 0 \\ 0 & \left(\frac{-D_{g_i}}{M_{g_i}}\right)^2 & \frac{-D_g}{M_{g_i^2}} - \frac{1}{M_{g_i}T_{t_i}} & \frac{1}{M_{g_i}T_{t_i}} \end{bmatrix} \tag{5.3.19}$$

and

$$\det\left(O_{g_i}\right) = \frac{1}{M_{g_i}^2 T_{t_i}} \tag{5.3.20}$$

It is apparent that the two singularities of the determinant, which are $M_{g_i} = 0$ and $T_{t_i} = 0$, are not acceptable from engineering perspective. It follows that O_{g_i} is always full rank.

Given the pair (A_{w_i}, C_{w_i}), Observability Matrix

$$O_{w_i} = \begin{bmatrix} 1 & 0 & 0 & 0 \\ 0 & 1 & 0 & 0 \\ \frac{-k_{w_i}}{M_{w1_i}} & \frac{-D_{w_i}}{M_{w1_i}} & \frac{k_{w_i}}{M_{w1_i}} & \frac{D_{w_i}}{M_{w1_i}} \\ \frac{D_{w_i}k_{w_i}M_{wT_i}}{\overline{M}_{w_i}} & \frac{D_{w_i}^2 M_{wT_i} - M_{wp_i}k_{w_i}}{\overline{M}_{w_i}} & \frac{-D_{w_i}k_{w_i}M_{wT_i}}{\overline{M}_{w_i}} & \frac{-D_{w_i}^2 M_{wT_i} + M_{wp_i}k_{w_i}}{\overline{M}_{w_i}} \end{bmatrix} \tag{5.3.21}$$

where the auxiliary (positive) parameters are defined as $M_{wT_i} \triangleq M_{w1_i} + M_{w2_i}$, $M_{wp_i} \triangleq M_{w1_i}M_{w2_i}$, $\overline{M}_{w_i} \triangleq M_{w1_i}^2 M_{w2_i}$. The determinant of O_{w_i} can be shown to be

$$\det\left(O_{w_i}\right) = \frac{k_{w_i}^2}{M_{w1_i}^2} \tag{5.3.22}$$

The determinant is equal to zero when $k_{w_i} = 0$, which is not an acceptable solution from a physical understanding of the system [109]. For the same reason, the singularity $M_{w1_i} = 0$ is not acceptable. It follows that O_{w_i} is always full rank.

The observability matrices associated with the pairs (A_{s_i}, C_{s_i}), and (A_{l_i}, C_{l_i}) are full rank, since they coincide with the Identity matrix $I_2 \in \mathbb{R}^{2\times 2}$ in both cases for all parameter values. □

In what follows, these assumptions are imposed:

Assumption 5.3. *It is assumed that:*

(A1) The voltage phase angle is locally measured for each component. Furthermore, each component receive instantaneously the measurements collected from its neighbourhood. In practice, this can be achieved by a deployment a network of of PMUs [8].

(A2) The signals P_{eg} in (5.3.1) and P_{ew} in (5.3.7) are considered to be known, since they can be practically reconstructed by a local exchange of information about the measurements.

(A3) The signals d_{eg} in (5.3.1), d_{ew} in (5.3.7), d_{es} in (5.3.13), and d_{el} in (5.3.16) are bounded, which means that $|d_{eg}| \leq \Delta_{d_{eg}}$, $|d_{ew}| \leq \Delta_{d_{ew}}$, $|d_{es}| \leq \Delta_{d_{es}}$, $|d_{el}| \leq \Delta_{d_{el}}$, where $\Delta_{d_{eg}}$, $\Delta_{d_{ew}}$, $\Delta_{d_{es}}$, and $\Delta_{d_{el}}$ are known positive constants.

(A4) The signal ϕ_s in (5.3.13) and ϕ_l in (5.3.16) are unknown but bounded, which means that $|\phi_s| < \Delta_{\phi_s}$, $|\phi_l| < \Delta_{\phi_l}$ where Δ_{ϕ_s} and Δ_{ϕ_l} are known positive constants.

Remark 5.10. Note that the value of the power flowing from a component to its neighbourhood is always bounded by the maximum power capacity of the power transmission lines [4], which is equal to the line susceptance γ_{ij} (this is true in the most conservative situation, which occurs when $\sin(\theta_i - \theta_j) = 1$). In practice, reasonable values for the bounds of the uncertain signals d_{eg}, d_{ew}, d_{es}, and d_{el} in Assumption 5.3 can be obtained according to:

$$\begin{array}{l} \Delta_{d_{eg}} \geq \sum_{j\in\mathcal{N}_g} \gamma_{gj},\ \Delta_{d_{ew}} \geq \sum_{j\in\mathcal{N}_w} \gamma_{wj} \\ \Delta_{d_{es}} \geq \sum_{j\in\mathcal{N}_s} \gamma_{sj},\ \Delta_{d_{el}} \geq \sum_{j\in\mathcal{N}_l} \gamma_{lj} \end{array} \tag{5.3.23}$$

Let Δ_{P_s} and Δ_{P_l} be the maximum value of the modulus of the signals P_s in (5.3.13) and P_l in (5.3.16), and let Δ_{ω_s} represent the minimum value of $\omega_s + \omega_0 > 0$ in (5.3.15). Then, given (5.3.23), reasonable values of the bounds for Δ_{ϕ_s} and Δ_{ϕ_l} can be obtained as:

$$\begin{array}{rcl} \Delta_{\phi_s} & \geq & \frac{\Delta_{P_s}+\Delta_{d_{es}}}{\Delta_{\omega_s}} \\ \Delta_{\phi_l} & \geq & \Delta_{P_l} + \Delta_{d_{el}} \end{array} \tag{5.3.24}$$

Remark 5.11. Note that the degree of the unknown inputs d_{eg} in (5.3.1) and d_{e_w} in (5.3.7) with respect to the measured output y_g and y_w are equal to 2 in both the two systems. Given Proposition 5.5, and following the theoretical developments in [70], the dynamical systems in (5.3.1) and in (5.3.7) are strongly detectable.

5.3.7 Observers Design

In this section, dedicated SM-based observers are introduced to dynamically track the unmeasured state variable in the three types of generation nodes and in the load nodes. The goal of the present section can be summarised as:

Objective 5.2. *Given the dynamical models (5.3.1), (5.3.7), (5.3.13), (5.3.16) of the components of an hybrid power system, design dedicated SM observers able to estimate in finite time all the unmeasured state variables, thus ensuring robustness to the perturbations (5.3.6), (5.3.12), (5.3.15), (5.3.18) introduced in the power flow exchanges.*

5.3.7.1 Traditional and Wind Power Sources Observers

For the purpose of designing the observers, it is possible to rewrite both (5.3.1) and (5.3.7), which display a similar structure, in the following general form:

$$\begin{array}{rcl} \dot{x} & = & Ax + B_1 u_1 + B_2\Big(G\big(y, y_{j|_{j\in\mathcal{N}}}\big)+d\Big) \\ y & = & Cx \end{array} \tag{5.3.25}$$

where x represents the state vector, A, B_1, B_2, and C are vectors and matrices of appropriate dimensions, $G\big(y, y_{j|_{j\in\mathcal{N}}}\big)$ is a scalar known nonlinearity which models the power flow exchanges, u_1

is the known control input, and d is a bounded unknown signal (i.e. $|d| \leq \Delta_d$, where Δ_d is a known constant) representing disturbances and unmodelled dynamics in the power flow channel. The following is a special case of the theoretical developments in [70] (in which higher order SM observers were designed for both stable and unstable, observable and detectable linear systems with unknown inputs):

Proposition 5.6. *Given the dynamics in (5.3.25), Proposition 5.5, and Remark 5.11, consider the following SM observer for both the traditional and wind power sources:*

$$\begin{aligned} \dot{z} &= Az + B_1 u_1 + B_2 G\big(y, y_{j|_{j\in\mathcal{N}}}\big) - L(Cz - y) \\ \hat{x} &= z - \hat{e} \\ \hat{e} &= P\overline{e} \\ \hat{y} &= Cz \end{aligned} \tag{5.3.26}$$

where z and $\hat{x}$ represent two estimates of x, $L \in \mathbb{R}^{4\times 1}$ is a design vector, $P \in \mathbb{R}^{4\times 4}$ is a matrix to be designed. The auxiliary signal $\overline{e} = \mathrm{Col}(\overline{e}_1, \ldots, \overline{e}_4)$ is governed by the following fourth order SM architecture:

$$\begin{aligned} \dot{\overline{e}}_1 &= -k_1 \left|\overline{e}_1 - e_1\right|^{3/4} \mathrm{sign}\left(\overline{e}_1 - e_1\right) + \overline{e}_2 \\ \dot{\overline{e}}_2 &= -k_2 \left|\overline{e}_1 - e_1\right|^{2/4} \mathrm{sign}\left(\overline{e}_1 - e_1\right) + \overline{e}_3 \\ \dot{\overline{e}}_3 &= -k_3 \left|\overline{e}_1 - e_1\right|^{1/4} \mathrm{sign}\left(\overline{e}_1 - e_1\right) + \overline{e}_4 \\ \dot{\overline{e}}_4 &= -k_4 \mathrm{sign}\left(\overline{e}_1 - e_1\right) \end{aligned} \tag{5.3.27}$$

where $e_1 \triangleq \hat{y} - y$ is the output observation error, $\overline{e}_1$ denotes an estimate of e_1, whilst the auxiliaries signals $\overline{e}_2, \ldots, \overline{e}_4$, represent successive time derivatives of $\overline{e}_1$. If the design constants $k_1,\ k_2,\ k_3,\ k_4$ are tuned according to the standard rules for the Levant's differentiator [72], and the design vector L is chosen such that $(A - LC)$ is Hurwitz, then it will be shown that the estimate $\hat{x}$ satisfies in finite time $\hat{x} = x$.

Proof. By subtracting (5.3.25) from (5.3.26), the error dynamics yield

$$\dot{e} = (A - LC)e - B_2 d \tag{5.3.28}$$

where $e \triangleq z - x$. The vector L is designed to ensure that the matrix $(A - LC)$ is Hurwitz, thus assigning arbitrarily chosen eigenvalues. Since the pair (A, C) is observable as proven in Proposition 5.5, the pair $(A - LC, C)$ is also observable, with the associated Observability Matrix $\tilde{O}$. By making use of the matrix $\tilde{O}$, the following change of coordinates is considered:

$$\tilde{e} = \tilde{O}e \tag{5.3.29}$$

with the associated error dynamics in the new coordinates:

$$\dot{\tilde{e}} = \tilde{A}\tilde{e} - \tilde{B}_2 d \tag{5.3.30}$$

Note that following the change of coordinates $\tilde{C} = C$, and the matrix $\tilde{A}$ has the following structure

[69] [70]:

$$\tilde{A} = \tilde{O}(A - LC)\tilde{O}^{-1} = \begin{bmatrix} 0 & 1 & 0 & 0 \\ 0 & 0 & 1 & 0 \\ 0 & 0 & 0 & 1 \\ \tilde{a}_1 & \tilde{a}_2 & \tilde{a}_3 & \tilde{a}_4 \end{bmatrix} \tag{5.3.31}$$

where $\tilde{a}_1, \ldots, \tilde{a}_4$ are known constants. It is easy to verify that only the first component $\tilde{e}_1$ of the vector $\tilde{e} = [\tilde{e_1}, \ldots, \tilde{e_4}]^T$ is known, thus coinciding with the output observation error. Since the matrix $\tilde{A}$ is Hurwitz, and the unknown input d is assumed bounded, the time evolution of $\tilde{e}$ remains bounded [69]. The problem of finding in finite time the successive time derivative of e_1, which are bounded, can be solved by means of SM Levant's differentiator [72], as argued in [70]. This technique is governed by (5.3.27), which corresponds to a third order SM Levant's differentiator implemented in the so-called non-recursive form. The underlying idea is to make use of the output observation error e_1 and create the fourth order dynamical system in (5.3.27). In [72] it has been shown that each estimate generated by the differentiator converge to the actual value in finite time. The tuning rules for the positive design constants $k_1, \ldots, k_4$ can be found, e.g., in [73] and [71]. It follows in finite time: $\overline{e}_1 = \tilde{e}_1 = e_1$, $\overline{e}_2 = \tilde{e}_2$, $\overline{e}_3 = \tilde{e}_3$, $\overline{e}_4 = \tilde{e}_4$. After the linear change of coordinates $\hat{e} = P\overline{e}$, where $P = \tilde{O}^{-1}$, it is possible to retrieve actual values of the error $\hat{e}$ in the original coordinates reference in finite time. These are used to compensate in real time the estimate z by introducing the following algebraic expression

$$\hat{x} = z - \hat{e}. \tag{5.3.32}$$

According to the algebraic relation in (5.3.32), the condition $\hat{x} = x$ holds in finite time. □

5.3.7.2 Observer for the Inverter Sources and Loads

In this section a super-twisting-like SM observer is employed to estimate in finite time the frequency deviation both in inverter with capacitive inertia and in loads. Note that the dynamics in (5.3.13) and (5.3.16) share the same structure, which can be rewritten as

$$\begin{aligned} \dot{\theta} &= \omega \\ \Delta\dot{\omega} &= a\Delta\omega + \phi \\ y &= \theta \end{aligned} \tag{5.3.33}$$

where θ denotes the (inverter and load) voltage phase angle and the $\Delta\omega$ the (inverter and load) frequency deviation, respectively, and in (5.3.33) the model parameter $a = -D/M$ is the ratio between the droop control and the inertia. The bounded unknown signal ϕ represents either ϕ_s and ϕ_l. It follows that $|\phi| \leq \Delta_\phi$, where Δ_ϕ is a known constant.

Proposition 5.7. *Given the dynamics (5.3.33), and Assumption 5.3, consider the following super-twisting-like SM observer [93]:*

$$\begin{aligned} \dot{\hat{\theta}} &= \Delta\hat{\omega} - \alpha_1 |e_\theta|^{1/2} \operatorname{sign}(e_\theta) - ae_\theta \\ \Delta\dot{\hat{\omega}} &= -\alpha_2 \operatorname{sign}(e_\theta) - a^2 e_\theta + a\Delta\hat{\omega} - a\alpha_1 |e_\theta|^{1/2} \operatorname{sign}(e_\theta) \end{aligned} \tag{5.3.34}$$

Table 5.3.1: Performance Metrics $\mathcal{E}$ for the SM and PI Observers (SMO, PIO). Values Expressed in $(mp.u.) = 1e-3(p.u.)$. Sensitivity Analysis is Provided in the Right Column, in which $\Delta A = 30\%A$.

			Sensitivity analysis	
node	SMO	PIO	SMO	PIO
1	2.29	4.06	136.90	159.60
2	0.12	156.67	64.18	9489.00
3	9.64	51.83	9.67	51.83
4	9.78	27.26	9.78	27.26
5	0.56	9.73	0.57	9.73

where $\hat{\theta}$ is the estimate of θ, $\Delta\hat{\omega}$ is the estimate of $\Delta\omega$, the output observation error $e_\theta \triangleq \hat{\theta} - \theta$, and α_1, α_2 are positive design constants. The error dynamics, which is determined by subtracting (5.3.33) from (5.3.34), can be shown to be

$$\begin{aligned} \dot{e}_\theta &= e_\omega - \alpha_1 |e_\theta|^{1/2} \operatorname{sign}(e_\theta) - a e_\theta \\ \dot{e}_\omega &= -\alpha_2 \operatorname{sign}(e_\theta) - a^2 e_\theta + a e_\omega - a\alpha_1 |e_\theta|^{1/2} \operatorname{sign}(e_\theta) - \phi \end{aligned} \tag{5.3.35}$$

where $e_\omega \triangleq \hat{\omega} - \omega$. The system in (5.3.35) is finite-time stable if the design constants satisfy

$$\alpha_1 = 1.5\sqrt{\Delta_\phi},\ \alpha_2 = 1.1\Delta_\phi \tag{5.3.36}$$

Therefore, the conditions $\hat{\theta} = \theta$ and $\hat{\omega} = \omega$ hold in finite time.

Proof. Proposition can be proven in perfect analogy to the developments in Section 4.2.2 on page 51. □

Remark 5.12. Consider the matrix A in (5.3.25) with unknown bounded uncertainty on the model parameters as follows $A \pm \Delta A$, where ΔA represents the maximum parameter deviations. The model uncertainty affects the observer error dynamics (5.3.28) as $\dot{e} = Ae \mp (\Delta A)x - B_2 d$. However, the time evolution of e remains ultimate bounded as long as x remains bounded. The compensation strategy in (5.3.32) is also affected. In particular, it can be shown that $\hat{x} = x \pm \Delta\hat{x}$, where the deviation $\Delta\hat{x}$ remains bounded. Furthermore, in case the model parameter a in (5.3.33) is uncertain, the super-twisting-like observer in (5.3.34) can be replaced via a standard super-twisting one [66]. It follows that in such a situation the impact of the model uncertainties can be totally circumvented.

5.3.8 Simulation Results

In this section, the effectiveness of the proposed SM observer scheme will be demonstrated by numerical simulations implemented in the Matlab-Simulink. The solver Ode1 (Euler Method) is employed also in this case for the numerical implementation of the observers, with a fixed integration step size equal to 10 microseconds. The adopted value of the sampling time is acceptable in practice, according to the technical data about the PMUs which are available in [8]. A power system composed of a conventional power source, a wind power source, an inverter-based source, and two loads is considered. The base power for the network is chosen equal to 10 (MVA). The schematic in Figure 5.3.1

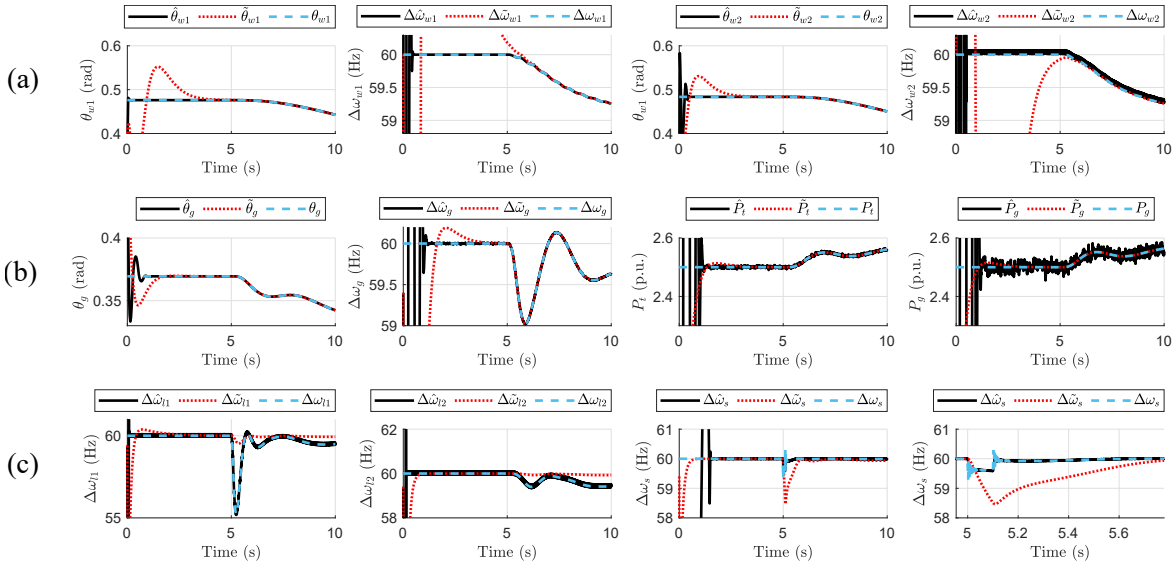

Figure 5.3.2: Time evolution of: **(a)** $\theta_{w1},\ \Delta\omega_{w1},\ \theta_{w2}, \Delta\omega_{w2}$, together with their estimates $\hat{\theta}_{w1},\ \Delta\hat{\omega}_{w1},\ \hat{\theta}_{w2},\ \Delta\hat{\omega}_{w2}$, via proposed SM observer, and the estimates $\tilde{\theta}_{w1},\ \Delta\tilde{\omega}_{w1},\ \tilde{\theta}_{w2},\ \Delta\tilde{\omega}_{w2}$ via PI observer. **(b)** $\theta_g,\ \Delta\omega_g,\ P_t,\ P_g$, together with their estimates $\hat{\theta}_g,\ \Delta\hat{\omega}_g,\ \hat{P}_t,\ \hat{P}_g$, via proposed SM observer, and the estimates $\tilde{\theta}_g,\ \Delta\tilde{\omega}_g,\ \tilde{P}_t,\ \tilde{P}_g$ via PI observer. **(c)** $\Delta\omega_{l1},\ \Delta\omega_{l2}$ and of inverter state variable $\Delta\omega_s$, together with their estimates $\Delta\hat{\omega}_{l1},\ \Delta\hat{\omega}_{l2},\ \Delta\hat{\omega}_s$, via proposed SM observer, and the estimates $\Delta\tilde{\omega}_{l1},\ \Delta\tilde{\omega}_{l2},\ \Delta\tilde{\omega}_s$ via PI observer. An enlarged view is provided for the inverter state variable and estimates.

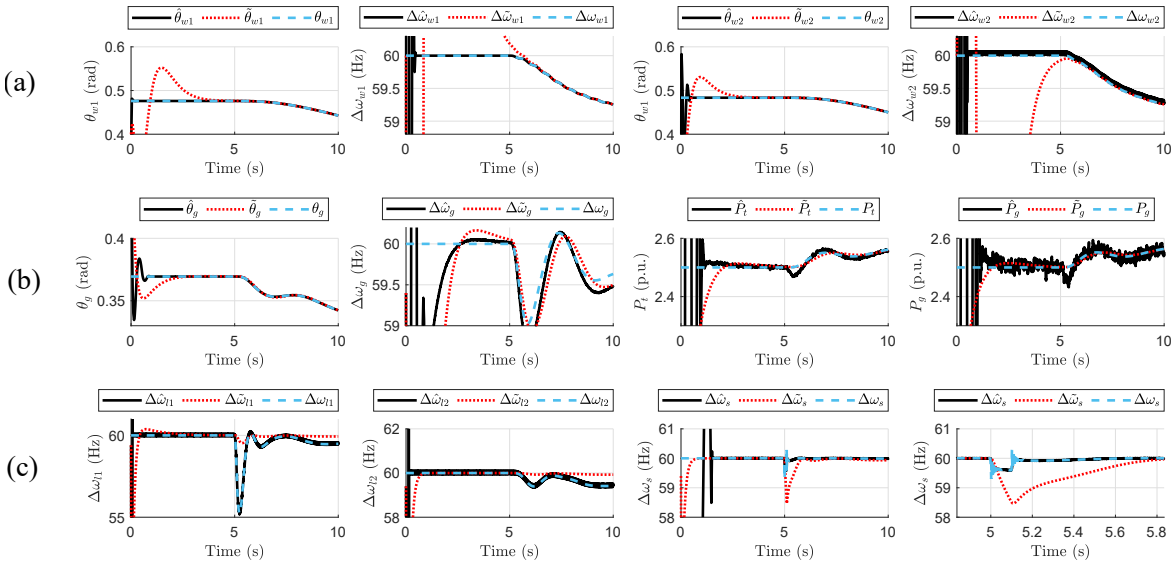

Figure 5.3.3: Sensitivity analysis. Time evolution of: **(a)** $\theta_{w1},\ \Delta\omega_{w1},\ \theta_{w2}, \Delta\omega_{w2}$, together with their estimates $\hat{\theta}_{w1},\ \Delta\hat{\omega}_{w1},\ \hat{\theta}_{w2},\ \Delta\hat{\omega}_{w2}$, via proposed SM observer, and the estimates $\tilde{\theta}_{w1},\ \Delta\tilde{\omega}_{w1},\ \tilde{\theta}_{w2},\ \Delta\tilde{\omega}_{w2}$ via PI observer. **(b)** $\theta_g,\ \Delta\omega_g,\ P_t,\ P_g$, together with their estimates $\hat{\theta}_g,\ \Delta\hat{\omega}_g,\ \hat{P}_t,\ \hat{P}_g$, via proposed SM observer, and the estimates $\tilde{\theta}_g,\ \Delta\tilde{\omega}_g,\ \tilde{P}_t,\ \tilde{P}_g$ via PI observer. **(c)** $\Delta\omega_{l1},\ \Delta\omega_{l2}$ and of inverter state variable $\Delta\omega_s$, together with their estimates $\Delta\hat{\omega}_{l1},\ \Delta\hat{\omega}_{l2},\ \Delta\hat{\omega}_s$, via proposed SM observer, and the estimates $\Delta\tilde{\omega}_{l1},\ \Delta\tilde{\omega}_{l2},\ \Delta\tilde{\omega}_s$ via PI observer. An enlarged view is provided for the inverter state variable and estimates.

shows the system topology, together with the numerical representation of the model parameters and the initial conditions for the state variables and inputs. The data was take from [30] and [4]. The grid is considered to be at steady state during the time interval $0 \leq t \leq 5$ seconds. At the time instant $t = 5$ seconds, the power generated by the inverter power source goes to zero, causing a loss of generation of 0.1 (p.u.). It follows that a disturbance in the form of $d_{es} = -0.1\text{step}(t-5)$ appears in (5.3.15). Furthermore, a differentiable band-limited noise affects the measurements of all the voltage phase angles. These are simulated in Simulink choosing standard deviation equal to 3.00 (mrad).

The design constants for the observers in (5.3.26) for both the traditional and wind power sources are chosen equal to $k_1 = 25.5$, $k_2 = 72$, $k_3 = 220$, $k_4 = 330$, exploiting the tuning rules in [71]. By setting $\Delta_\phi = 300$, the design constants of the observers in (5.3.36) are $\alpha_1 = 26$, $\alpha_2 = 330$. The proposed schemes in (5.3.26) and in (5.3.34) does not satisfy the rank conditions needed to use UIL [107], and hence are compared with PI observers, originally proposed in [110].

Using standard pole-placement techniques, the vector $L = \underline{100},\ L \in \mathbb{R}^4$, is chosen for conventional and wind sources, whilst $L = \underline{100},\ L \in \mathbb{R}^2$ is chosen for inverter sources and loads. According to Figure 5.3.2, it is possible to demonstrate that the proposed SM scheme is able to faithfully estimate the unmeasured state variables, both when the grid is at steady-state and during the transient caused by the loss of generation from the inverter. In addition, the proposed observer is revealed to be totally insensitive to disturbances appearing in the matched channels of the systems (5.3.35). All the PI observers display less accuracy. Moreover, small oscillations can be noted in the estimates produced by the SM observers. These are due to the effect of the introduced measurement noise.

The following performance metric can be introduced for all the observers in the noise-free scenario:

$$\mathcal{E} = \frac{\int_{T_1=1}^{T_f=10} ||e(\tau)||d\tau}{T_f - T_1} \tag{5.3.37}$$

where the state estimation error vector e differs for each considered observer. The interval of integration starts at the time instant $T_1 = 1$ seconds, when all the proposed observers have reached the sliding motion, and it stops at the time instant $T_f = 10$ seconds, when the simulation ends. Table 5.3.1 demonstrates that the SM observers display smaller values of the proposed metric.

A sensitivity analysis is shown in Table 5.3.1 and in Figure 5.3.3, where the matrix A in (5.3.25) and the constant a in (5.3.33) are affect by uncertainty of 30%. In accordance with Remark 5.12, the observer (5.3.34) is totally insensitive to the model uncertainty, whilst the observer (5.3.26) is affected by this uncertainty, without compromising its stability. However, the SM observers always display a smaller value of the performance metric when compared to PI observers.

5.3.9 Conclusions

In this section, a comprehensive SM-based scheme has been developed for dynamic state estimation in power systems comprising both traditional and renewable power sources. This section distinguished from the earlier works in the literature, in which SM state observer was separately developed for traditional and renewable components in power grids. By means of higher order SM architecture it has been possible to enforce a finite time convergence of the observer error dynamics, thus ensuring better performances when compared to well-established linear observers.

Chapter 6

Sliding Mode-Based Fault Reconstruction and Mitigation in Structure-Preserving Power Systems

Abstract In this chapter, a distributed scheme based on an adaptive dual-layer super-twisting sliding mode architecture is proposed to perform robust fault and attack isolation, reconstruction, and mitigation in power systems. Simultaneous attacks and faults affecting generators and loads are considered. An adaptation law for the super-twisting observer gains is formulated. This is a key-novelty, since it is no longer required to know a priori the value for the upper-bounds of the disturbances. Furthermore, the adaptation scheme does not generate conservative overestimation of uncertainty. This helps mitigating chattering and the amplification of noise. Furthermore, a class of communication attacks amongst the observers is tackled.

6.1 Preliminaries, Assumptions and Facts

The nonlinear structure-preserving power system dynamical model (3.5.13) on page 42 is used a starting point to design the adaptive observers. The adopted model is rewritten in order to include possible faults in its dynamics as:

$$\begin{array}{rcll} \dot{\theta}_i & = & \Delta\omega_i & \in \mathcal{B} \\ M_i\Delta\dot{\omega}_i & = & -D_i\Delta\omega_i + P_{m_i} - \sum_{j\in\mathcal{N}_i}\gamma_{ij}\sin\left(\theta_i-\theta_j\right) + f_{g_i} & i \in \mathcal{G} \\ 0 & = & -D_i\Delta\omega_i + P_{l_i} - \sum_{j\in\mathcal{N}_i}\gamma_{ij}\sin\left(\theta_i-\theta_j\right) + f_{l_i} & i \in \mathcal{L} \\ y_i & = & \theta_i & i \in \mathcal{B} \end{array} \tag{6.1.1}$$

The reader is referred to Chapter 3 for the understanding of the state variables and model parameters introduced in (6.1.1). Furthermore, note that f_{g_i} and f_{l_i} are faults that can act on the i-th generator or on the i-th load bus, respectively. It is assumed that:

Assumption 6.1. *Signal f_{g_i} in (6.1.1) is a bounded disturbance. The bound for the disturbance is assumed unknown but finite. The signal f_{l_i} in (6.1.1) is also a bounded differentiable disturbance.*

The bounds for the disturbance itself and for its time derivative are assumed to be finite but unknown.

Assumption 6.2. *Each bus instantaneously receives the measurements acquired from its neighbourhood.*

6.2 Adaptive Observers Design

In this section, two adaptive dual-layer super-twisting sliding mode observers are created to estimate simultaneous faults acting on generator and load buses.

6.2.1 Generator Adaptive Super-Twisting Observer

The following adaptive super-twisting-like sliding mode observer is proposed to estimate the frequency deviation in each generator bus, exploiting ideas from [66] and from [36][1]:

$$\left.\begin{array}{rcl} \dot{\hat{\theta}}_i & = & -\alpha_i(t)\left|e_{\theta_i}\right|^{1/2}\text{sign}\left(e_{\theta_i}\right) - a_i e_{\theta_i} + \Delta\hat{\omega}_i + \Phi_i\left(L_i, e_{\theta_i}\right) \\ \Delta\dot{\hat{\omega}}_i & = & \frac{1}{M_i}\Big(P_{m_i} - D_i\Delta\hat{\omega}_i - \sum_{j\in\mathcal{N}_i}\gamma_{ij}\sin\left(y_i - y_j\right)\Big) - \beta_i(t)\text{sign}\left(e_{\theta_i}\right) \\ & & -a_i^2 e_{\theta_i} + a_i\Phi_i\left(L_i, e_{\theta_i}\right) - a_i\alpha_i(t)\left|e_{\theta_i}\right|^{1/2}\text{sign}\left(e_{\theta_i}\right) \end{array}\right\} i \in \mathcal{G} \quad (6.2.1)$$

where $\hat{\theta}_i$ is the estimate of θ_i, $\Delta\hat{\omega}_i$ is the estimate of $\Delta\omega_i$, $e_{\theta_i} \triangleq \hat{\theta}_i - \theta_i$, $a_i \triangleq -D_i/M_i$, whilst $\alpha_i(t)$ and $\beta_i(t)$ are time-varying gains. The term $\Phi_i(\cdot)$ is an auxiliary term driven by e_{θ_i} and will be described in detail in the rest of the present section.

Remark 6.1. In the first differential equation of (6.2.1), an additional term $-a_i e_{\theta_i}$ is included when compared to the adaptive ST approach in [36], whilst in the second differential equation of (6.2.1) the original terms are $-a_i^2 e_{\theta_i} + a_i\Phi_i\left(L_i, e_{\theta_i}\right) - a_i\alpha_i(t)\left|e_{\theta_i}\right|^{1/2}\text{sign}\left(e_{\theta_i}\right)$. The motivation for these choices will be explained in the rest of this section. In addition, in contrast to [66], the proposed observer in (6.2.1) exploits measurements of the voltage phase angles y_j from the neighbouring load buses, gathered by PMUs.

The error dynamics for the observer (6.2.1) are:

$$\left.\begin{array}{rcl} \dot{e}_{\theta_i} & = & -\alpha_i(t)\left|e_{\theta_i}\right|^{1/2}\text{sign}\left(e_{\theta_i}\right) - a_i e_{\theta_i} + e_{\omega_i} + \Phi_i\left(L_i, e_{\theta_i}\right) \\ \dot{e}_{\omega_i} & = & a_i\Phi_i\left(L_i, e_{\theta_i}\right) - a_i\alpha_i(t)\left|e_{\theta_i}\right|^{1/2}\text{sign}\left(e_{\theta_i}\right) \\ & & +a_i e_{\omega_i} - \beta_i(t)\text{sign}\left(e_{\theta_i}\right) - a_i^2 e_{\theta_i} - \frac{f_{g_i}}{M_i} \end{array}\right\} i \in \mathcal{G} \quad (6.2.2)$$

where $e_{\omega_i} = \Delta\hat{\omega}_i - \Delta\omega_i$. Following [36], the time-varying gains are chosen

$$\alpha_i(t) = \sqrt{L_i(t)}\alpha_{0_i} \quad (6.2.3)$$

$$\beta_i(t) = L_i(t)\beta_{0_i}, \quad (6.2.4)$$

[1]The time dependence is explicitly written only for the two time-varying gain, respectively $\alpha_i(t)$ and $\beta_i(t)$ for the sake of readability.

where α_{0_i} and β_{0_i} are positive constants. The time varying positive gain $L_i(t)$ is selected as

$$L_i(t) = l_{0_i} + l_i(t),\ i \in \mathcal{G} \tag{6.2.5}$$

where l_{0_i} is a positive constant and $l_i(t)$ satisfies the adaptation law

$$\dot{l}_i(t) = -\rho_i(t)\text{sign}\left(\varphi_i(t)\right)\ i \in \mathcal{G}. \tag{6.2.6}$$

The additional nonlinear term $\Phi_i(\cdot)$ is selected as

$$\Phi_i\left(L_i(t), e_{\theta_i}(t)\right) = -\frac{\dot{L}_i(t)}{L_i(t)} e_{\theta_i}(t),\ i \in \mathcal{G}. \tag{6.2.7}$$

In (6.2.6), the time-varying scalar $\rho_{g_i}(t)$ is given by

$$\rho_i(t) = r_{0_i} + r_i(t),\ i \in \mathcal{G} \tag{6.2.8}$$

where r_{0_i} is a positive design constant and $r_i(t)$ satisfies

$$\dot{r}_i(t) = \gamma_i \left|\varphi_i(t)\right|,\ i \in \mathcal{G} \tag{6.2.9}$$

where γ_i is a positive design constant. The signal $\varphi_i(t)$ in (6.2.6) and (6.2.9) is defined as

$$\varphi_i(t) = L_i(t) - \frac{1}{\eta_i \beta_{0_i}} \left|v_i(t)\right|,\ i \in \mathcal{G} \tag{6.2.10}$$

where the constant η_i is chosen such that $0 < \eta_i < 1/\beta_{0_i} < 1$. Finally, signal $v_i(t)$ represents an approximation of the equivalent injection associated with the discontinuous signal $-\beta_i(t)\text{sign}\left(e_{\theta_i}\right)$ in (6.2.1), and it is generated from the low pass filter:

$$\dot{v}_i(t) = \frac{1}{\tau_i}\left(-\beta_i(t)\text{sign}\left(e_{\theta_i}\right) - v_i(t)\right),\ i \in \mathcal{G} \tag{6.2.11}$$

where τ_i is a small positive constant. The following proposition is now proven.

Proposition 6.1. *Given the relations (6.2.3)-(6.2.11) and under Assumptions 6.1 and 6.2, the error dynamics in (6.2.2) are driven to the origin in a finite time.*

Proof. By defining the auxiliary error variable $\overline{e}_{\omega_i} = e_{\omega_i} - a_i e_{\theta_i}$, the system in (6.2.2) can be rewritten as

$$\left.\begin{array}{rcl} \dot{e}_{\theta_i} & = & -\alpha_i(t)\left|e_{\theta_i}\right|^{1/2}\text{sign}\left(e_{\theta_i}\right) + \overline{e}_{\omega_i} + \Phi_i\left(L_i, e_{\theta_i}\right) \\ \dot{\overline{e}}_{\omega_i} & = & a_i\Phi_i\left(L_i, e_{\theta_i}\right) - a_i\alpha_i(t)\left|e_{\theta_i}\right|^{1/2}\text{sign}\left(e_{\theta_i}\right) \\ & & +a_i e_{\omega_i} - \beta_i(t)\text{sign}\left(e_{\theta_i}\right) - a_i^2 e_{\theta_i} - \frac{f_{g_i}}{M_i} \\ & & +a_i\alpha_i(t)\left|e_{\theta_i}\right|^{1/2}\text{sign}\left(e_{\theta_i}\right) - a_i e_{\omega_i} + a_i^2 e_{\theta_i} - a_i\Phi_i\left(L_i, e_{\theta_i}\right) \end{array}\right\} i \in \mathcal{G} \tag{6.2.12}$$

After straightforward algebraic manipulations, one gets

$$\left.\begin{array}{rcl} \dot{e}_{\theta_i} & = & -\alpha_i(t)\left|e_{\theta_i}\right|^{1/2}\text{sign}\left(e_{\theta_i}\right)+\overline{e}_{\omega_i}+\Phi_i\left(L_i,e_{\theta_i}\right) \\ \dot{\overline{e}}_{\omega_i} & = & -\beta_i(t)\text{sign}\left(e_{\theta_i}\right)-\frac{f_{g_i}}{M_i} \end{array}\right\} i\in\mathcal{G} \tag{6.2.13}$$

The system in equation (6.2.13) is in the standard form of the adaptive dual-layer ST algorithm in [36], and it converges to the origin in a finite time if the relations (6.2.3)-(6.2.11) hold [36].

□

6.2.1.1 Fault Reconstruction Scheme

The sliding motion in system (6.2.13) is characterised by the conditions $e_{\theta_i}=\overline{e}_{\omega_i}=0$, which are satisfied in a finite time. The average value v_i of the discontinuous signal $-\beta_i(t)\text{sign}\left(e_{\theta_i}\right)$ compensates for the signal $-f_{g_i}/M_i$ and therefore during the sliding motion

$$v_i=\frac{f_{g_i}}{M_i},\ i\in\mathcal{G}. \tag{6.2.14}$$

Exploiting (6.2.14), an estimation $\hat{f}_{g_i}$ for the fault f_{g_i} is given by

$$\hat{f}_{g_i}=M_i v_{g_i},\ i\in\mathcal{G}. \tag{6.2.15}$$

Remark 6.2. A low-pass filter [61] (governed by (6.2.11)) can be used to obtain the signal v_i from the discontinuous signal $-\beta_i(t)\text{sign}\left(e_{\theta_i}\right)$. The choice of bandwidth of the filter used to estimate the equivalent injection is of paramount importance. In particular, the bandwidth must be set sufficiently large so the key-frequency components of the disturbances are captured but not too large so that noise becomes part of the injection signal.

6.2.1.2 Fault Detection Scheme

During the tuning process the signal v_i can be examined to determine whether it represents a meaningful disturbance based on existing statistics of the faults and an engineering understanding of the dynamics and bandwidths of any uncertainty. A fault isolation procedure can be easily implemented whenever the modulus of $\hat{f}_{g_i}$ passes an appropriate positive small threshold ε_{g_i}. The threshold can also be chosen relying on the statistical hypothesis testing technique [111]. It yields:

$$\begin{cases} |\hat{f}_{g_i}|\geq\varepsilon_{g_i} & \text{i-th generator node is faulty} \\ |\hat{f}_{g_i}|<\varepsilon_{g_i} & \text{no fault.} \end{cases} \tag{6.2.16}$$

Remark 6.3. The proposed distributed estimator for a fault in one generator bus is totally insensitive to other simultaneous faults in other (generator or load) buses. This can be understood by considering the dynamical coupling between the buses in the power network (6.1.1). This takes place at the voltage phase angle level (see (6.1.1)), which are measured by neighbouring PMUs and communicated as stated above.

6.2.2 Load Adaptive Super-Twisting Observer

Next consider the following adaptive super-twisting sliding mode observer to estimate faults in each load bus

$$\left.\begin{array}{rcl} \dot{\hat{\theta}}_i & = & -\lambda_i(t)\left|e_{\theta_i}\right|^{1/2}\text{sign}\left(e_{\theta_i}\right)+\frac{1}{D_i}\left(P_{l_i}-\sum_{j\in\mathcal{N}_i}\gamma_{ij}\sin\left(y_i-y_j\right)\right)+\Phi_i\left(L_i,e_{\theta_i}\right) \\ \dot{\hat{\psi}}_i & = & -\mu_i(t)\text{sign}\left(e_{\theta_i}\right) \end{array}\right\} i\in\mathcal{L} \tag{6.2.17}$$

where $\hat{\theta}_i$ represents the estimate of $\hat{\theta}_i$, $\hat{\psi}_i$ is an auxiliary state variable, $e_{\theta_i}\triangleq\hat{\theta}_i-\theta_i$, $\lambda_i(t)$ and $\mu_i(t)$ are time-varying gains, and the additional term $\Phi_i(\cdot)$ is selected analogously to (6.2.7). The observer in (6.2.17) receives both the measurements of the voltage phase angles y_j of the neighbouring buses. By defining the new variable

$$e_{\psi_i}\triangleq\hat{\psi}_i-\frac{f_{l_i}}{D_i},\ i\in\mathcal{L} \tag{6.2.18}$$

the error dynamics for the adaptive super-twisting load observer are obtained by subtracting the load dynamics in (6.1.1) (divided by D_i) from (6.2.17):

$$\left.\begin{array}{rcl} \dot{e}_{\theta_i} & = & -\lambda_i(t)\left|e_{\theta_i}\right|^{1/2}\text{sign}\left(e_{\theta_i}\right)+e_{\psi_i} \\ \dot{e}_{\psi_i} & = & -\mu_i(t)\text{sign}\left(e_{\theta_i}\right)-\frac{\dot{f}_{l_i}}{D_i} \end{array}\right\} i\in\mathcal{L} \tag{6.2.19}$$

Analogously to (6.2.13), under Assumption 6.1, the system in equation (6.2.19) is driven to the origin in a finite time.

6.2.2.1 Fault Reconstruction Scheme

The sliding motion of the system in (6.2.19) is characterised by the conditions $e_{\theta_i}=e_{\psi_i}=0$. Since e_{ψ_i} is steered to zero in a finite time, exploiting its definition in (6.2.18), which holds for any time instant, it is apparent that the condition

$$\hat{f}_{l_i}=D_i\hat{\psi}_i,\ i\in\mathcal{L} \tag{6.2.20}$$

holds in a finite time. From (6.2.20) it is apparent that an estimate $\hat{f}_{l_i}$ of the load fault f_{l_i} can be obtained.

Remark 6.4. Note that, in contrast to Remark 6.2, the low-pass filter is not required to reconstruct the load fault, since the signal $\hat{\psi}_i$ is continuous.

6.2.2.2 Fault Detection Scheme

Analogously to (6.2.16), the following (practical) criteria for local load fault isolation can be adopted

$$\begin{cases} |\hat{f}_{l_i}|\geq\varepsilon_{l_i} & i\text{-th load node is faulty} \\ |\hat{f}_{l_i}|<\varepsilon_{l_i} & \text{no fault,} \end{cases} \tag{6.2.21}$$

where ε_{l_i} is an appropriate positive small threshold.

6.2.3 Communication Attacks Mitigation Reconstruction

In this section, a class of attacks is considered to potentially affect the proposed adaptive super-twisting observers. Specifically, it is assumed that each observer receives corrupted measurements gathered from the neighbouring buses and the effect of the fault is cancelled throughout an injection of an attack signal. It will be shown that these kinds of attacks can be isolated and reconstructed by introducing an additional decentralised adaptive super-twisting observer for each bus of the power system.

6.2.3.1 Generator Observer Communication Attacks Reconstruction

Suppose that each adaptive super-twisting-like sliding mode (6.2.1) receives the corrupted measurements gathered by the neighbouring buses and an attack cancelling the effect of the fault in its matched channel. This means that the attack signal m_{g_i}, defined as

$$m_{g_i} \triangleq \frac{f_{g_i} + \sum_{j\in\mathcal{N}_i} \gamma_{ij} \sin\left(y_i - y_j\right)}{M_i},\ i \in \mathcal{G}, \tag{6.2.22}$$

will be included in equation (6.2.1).

By using (6.2.22), the corrupted observer error dynamics (6.2.2) become

$$\left.\begin{array}{rcl} \dot{e}_{\theta_i} & = & -\alpha_i(t)\left|e_{\theta_i}\right|^{1/2}\text{sign}\left(e_{\theta_i}\right) + \overline{e}_{\omega_i} + \Phi_i\left(L_i, e_{\theta_i}\right) \\ \dot{\overline{e}}_{\omega_i} & = & -\beta_i(t)\text{sign}\left(e_{\theta_i}\right) + \frac{\sum_{j\in\mathcal{N}_i}\gamma_{ij}\sin(y_i-y_j)}{M_i} \end{array}\right\} i \in \mathcal{G} \tag{6.2.23}$$

The effect of the bounded disturbance m_{g_i} appears in the matched channel of the system (6.2.23), which converges to the origin in a finite time as proved in Section 6.2.1. Moreover, equation (6.2.14) is modified as

$$v_i = -\frac{\sum_{j\in\mathcal{N}_i} \gamma_{ij} \sin\left(y_i - y_j\right)}{M_i},\ i \in \mathcal{G}. \tag{6.2.24}$$

From (6.2.24) one can conclude that the generator fault f_{g_i} is no longer reconstructed, since its effect has been cancelled by (6.2.22). In order to solve this issue, an additional decentralised adaptive-super-twisting-like sliding mode observer for each generator bus is introduced:

$$\left.\begin{array}{rcl} \dot{\tilde{\theta}}_i & = & -\tilde{\alpha}_i(t)\left|\tilde{e}_{\theta_i}\right|^{1/2}\text{sign}\left(\tilde{e}_{\theta_i}\right) - a_i\tilde{e}_{\theta_i} + \Delta\tilde{\omega}_i + \tilde{\Phi}_i\left(\tilde{L}_i, \tilde{e}_{\theta_i}\right) \\ \Delta\dot{\tilde{\omega}}_i & = & \frac{1}{M_i}\left(P_{m_i} - D_i\Delta\tilde{\omega}_i\right) - \tilde{\beta}_i(t)\text{sign}\left(\tilde{e}_{\theta_i}\right) \\ & & -a_i^2\tilde{e}_{\theta_i} + a_i\tilde{\Phi}_i\left(\tilde{L}_i, \tilde{e}_{\theta_i}\right) - a_i\tilde{\alpha}_i(t)\left|\tilde{e}_{\theta_i}\right|^{1/2}\text{sign}\left(\tilde{e}_{\theta_i}\right) \end{array}\right\} i \in \mathcal{G} \tag{6.2.25}$$

where $\tilde{\theta}_i$ denotes now an additional estimate of θ_i, $\Delta\tilde{\omega}_i$ denotes an additional estimate of $\Delta\omega_i$, $\tilde{e}_{\theta_i} \triangleq \tilde{\theta}_i - \theta_i$, while $\tilde{\alpha}_i(t)$, $\tilde{\beta}_i(t)$, and $\tilde{\Phi}_i(\cdot)$ are selected as in Section 6.2.1. Following the developments in Section 6.2.1, the error dynamics for the i-th decentralised observer are given by

$$\left.\begin{array}{rcl} \dot{e}_{\theta_i} & = & -\tilde{\alpha}_i(t)\left|\tilde{e}_{\theta_i}\right|^{1/2}\text{sign}\left(\tilde{e}_{\theta_i}\right) + \tilde{e}_{\omega_i} + \Phi_i\left(L_i, \tilde{e}_{\theta_i}\right) \\ \dot{\tilde{e}}_{\omega_i} & = & -\tilde{\beta}_i(t)\text{sign}\left(\tilde{e}_{\theta_i}\right) - \frac{f_{g_i}}{M_i} + \frac{\sum_{j\in\mathcal{N}_i}\gamma_{ij}\sin(\theta_i-\theta_j)}{M_i} \end{array}\right\} i \in \mathcal{G} \tag{6.2.26}$$

which converge to the origin in a finite time as previously shown. Now the average value $\tilde{v}_{g_i}$ of the

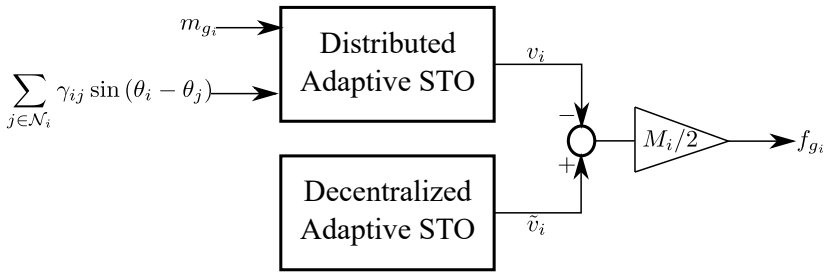

Figure 6.2.1: A schematic of the distributed adaptive Super Twisting Observer (STO) in equations (6.2.1), suitably coupled with the additional decentralized STO in (6.2.25), for the purpose of fault reconstruction in presence of the communication attack m_{g_i}.

discontinuous signal $-\tilde{\beta}_i(t)\text{sign}\,(\tilde{e}_{\theta_i})$ satisfies

$$\tilde{v}_{g_i} = \frac{f_{g_i} - \sum_{j\in\mathcal{N}_i}\gamma_{ij}\sin(\theta_i-\theta_j)}{M_i}. \tag{6.2.27}$$

By making use of both (6.2.24) and (6.2.27) and exploiting basic algebraic relations, an estimate $\hat{f}_{g_i}$ for f_{g_i} an be obtained as follows.

$$\hat{f}_{g_i} \;=\; \tfrac{M_i}{2}\big(\tilde{v}_{g_i} - v_{g_i}\big). \tag{6.2.28}$$

Figure 6.2.1 shows a schematic of the proposed solution to tackle communication attacks for the generator observers.

6.2.3.2 Load Observer Communication Attacks Reconstruction

The same ideas applied in Section 6.2.3.1 will be now adopted to reconstruct communication attacks at the level of each load observer. Since the procedure displays similarities to Section 6.2.1, only a sketch will be provided. Suppose that each super-twisting-like sliding mode observer for the load in the form of (6.2.17) receives the corrupted measurements gathered by the neighbouring (generator and load) buses and the effect of the load fault is cancelled by an attack signal. This means that

$$\left.\begin{array}{rcl}\Omega_i &\triangleq& \sum_{j\in\mathcal{N}_i}\gamma_{ij}\sin\Big(y_i - y_j\Big)\\ m_{l_i} &=& \frac{f_{l_i}+\Omega_i}{D_{l_i}}\end{array}\right\} i\in\mathcal{L} \tag{6.2.29}$$

The signal in (6.2.29) is added to (6.2.17) and to the definition of e_{ψ_i} in (6.2.18). The error dynamics (6.2.19) take the form:

$$\left.\begin{array}{rcl}\dot{e}_{\theta_i} &=& -\lambda_i(t)\,|e_{\theta_i}|^{\,1/2}\text{sign}\,(e_{\theta_i}) + e_{\psi_i}\\ \dot{e}_{\psi_i} &=& -\mu_i(t)\text{sign}\,(e_{\theta_i}) + \frac{\dot{\Omega}_i}{D_i}\end{array}\right\} i\in\mathcal{L} \tag{6.2.30}$$

and the expression for $\hat{\psi}_i$

$$\hat{\psi}_i = -\frac{\Omega_i}{D_i},\; i\in\mathcal{L} \tag{6.2.31}$$

holds in a finite time. Again it is not possible to isolate and reconstruct the load fault. However, exploiting the same idea as in Section 6.2.3.1, a decentralised adaptive super-twisting sliding mode observer is created for each load bus:

$$\left.\begin{array}{rcl} \dot{\tilde{\theta}}_i &=& -\tilde{\lambda}_i(t)\left|\tilde{e}_{\theta_i}\right|^{1/2}\text{sign}\left(\tilde{e}_{\theta_i}\right)+\frac{P_{l_i}}{D_i}+\tilde{\Phi}_i\left(\tilde{L}_i,\tilde{e}_{\theta_i}\right) \\ \dot{\tilde{\psi}}_i &=& -\tilde{\mu}_i(t)\text{sign}\left(\tilde{e}_{\theta_i}\right) \end{array}\right\} i\in\mathcal{L} \tag{6.2.32}$$

where $\tilde{\theta}_i$ represents additional estimate of θ_i, $\tilde{\psi}_i$ is an auxiliary state variable, $\tilde{e}_{\theta_i}\triangleq\tilde{\theta}_i-\theta_i$, $\tilde{\lambda}_i(t)$, $\tilde{\mu}_i(t)$, and the $\tilde{\Phi}_i(\cdot)$ are selected analogously to Section 6.2.1. Then the error dynamics for the i-th decentralised observer (6.2.32) are

$$\left.\begin{array}{rcl} \dot{e}_{\theta_i} &=& -\tilde{\lambda}_i(t)\left|\tilde{e}_{\theta_i}\right|^{1/2}\text{sign}\left(\tilde{e}_{\theta_i}\right)+\tilde{e}_{\psi_i} \\ \dot{\tilde{e}}_{\psi_i} &=& -\tilde{\mu}_i(t)\text{sign}\left(\tilde{e}_{\theta_i}\right)+\frac{\dot{\Omega}_i-\dot{f}_{l_i}}{D_i} \end{array}\right\} i\in\mathcal{L} \tag{6.2.33}$$

Analogously to (6.2.31), one gets

$$\tilde{\psi}_i=\frac{f_{l_i}-\Omega_i}{D_i},\ i\in\mathcal{L} \tag{6.2.34}$$

By using both (6.2.31) and (6.2.34), it is possible to obtain an estimate for $\hat{f}_{l_i}$ as

$$\hat{f}_{l_i} \;=\; \frac{D_i}{2}\left(\tilde{\psi}_i-\hat{\psi}_i\right),\ i\in\mathcal{L}. \tag{6.2.35}$$

6.2.4 Fault Mitigation for Generator Buses

In this section, the proposed fault isolation and reconstruction will be applied to mitigate the effect of the faults at the level of the generator buses. The key-assumption is that there exists a PI controller which stabilises the i-th fault-free generator bus. The aim of the proposed approach is to mitigate the impact of generator faults by making use of both the pre-existing PI controller and the estimate of the generator fault. Specifically, consider that the generator input power P_{m_i} (the control input) is the output of a standard PI controller as follows:

$$P_{m_i}=K_{P_i}\Delta\hat{\omega}_i+K_{I_i}\int_0^t\Delta\hat{\omega}_i(\tau)d\tau,\ i\in\mathcal{G} \tag{6.2.36}$$

where K_{P_i} and K_{I_i} are respectively the proportional and the integral gain, which have been tuned (by following standard rules, for example as in [5]), to stabilise the i-th fault-free generator bus. The control input in (6.2.36) is modified as follows:

$$\overline{P}_{m_i}=P_{m_i}-\hat{f}_{g_i},\ i\in\mathcal{G} \tag{6.2.37}$$

in which the disturbance estimate $\hat{f}_{g_i}$ is added. It is assumed in the present approach that the expression for $\overline{P}_{m_i}$ in (6.2.37) holds only after the attainment of the sliding motion in the system in equations (6.2.13), which takes place in a finite time. The resulting controlled generator dynamics are given by

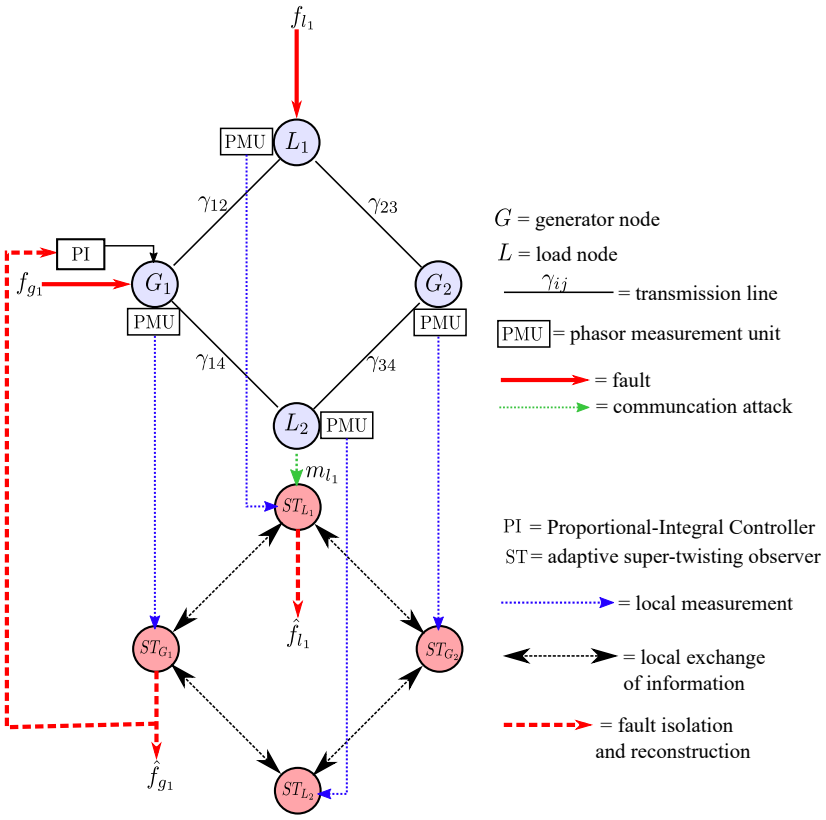

Figure 6.3.1: From the top: A schematic of a power system composed of two generator buses and two load buses; The proposed adaptive distributed super-twisting sliding mode observers. A fault mitigation schematic is represented for the 1-st generator bus.

$$M_i\Delta\dot{\omega}_i = -D_i\Delta\omega_i + K_{P_i}\Delta\hat{\omega}_i + K_{I_i}\int_0^t \Delta\hat{\omega}_i(\tau)d\tau - \hat{f}_{g_i} - \sum_{j\in\mathcal{N}_i}\gamma_{ij}\sin(\theta_i-\theta_j) + f_{g_i},\ i\in\mathcal{G} \tag{6.2.38}$$

According to the developments in Section 6.2.1, it is apparent that the effect of the generator faults is compensated, since $\hat{f}_{g_i}$ asymptotically tends to f_{g_i}. Therefore, in the presence of the fault mitigation strategy in (6.2.37), the pre-existing PI controller gains can still be employed. As a result, $\Delta\omega_i$ asymptotically tends to zero.

6.3 Simulation Results

In this section, simulation results are undertaken to demonstrate the effectiveness of the proposed adaptive super-twisting sliding mode based scheme. The power system is composed of an interconnection of two generator buses and two load buses, as depicted in Figure 6.3.1. Table 6.3.1 shows the numerical values of both the model parameters and the initial conditions for the load and the generator nodes. Note that Table 6.3.1 shows the initial values of the state variables and inputs at the time instant $t = 0$ seconds. The parameters of the power transmission lines are: $\gamma_{12} = 5.4\ (p.u.)$, $\gamma_{23} = 5.00\ (p.u.)$, $\gamma_{34} = 4.50\ (p.u.)$, $\gamma_{14} = 5.20\ (p.u.)$. The proportional and integral gains are

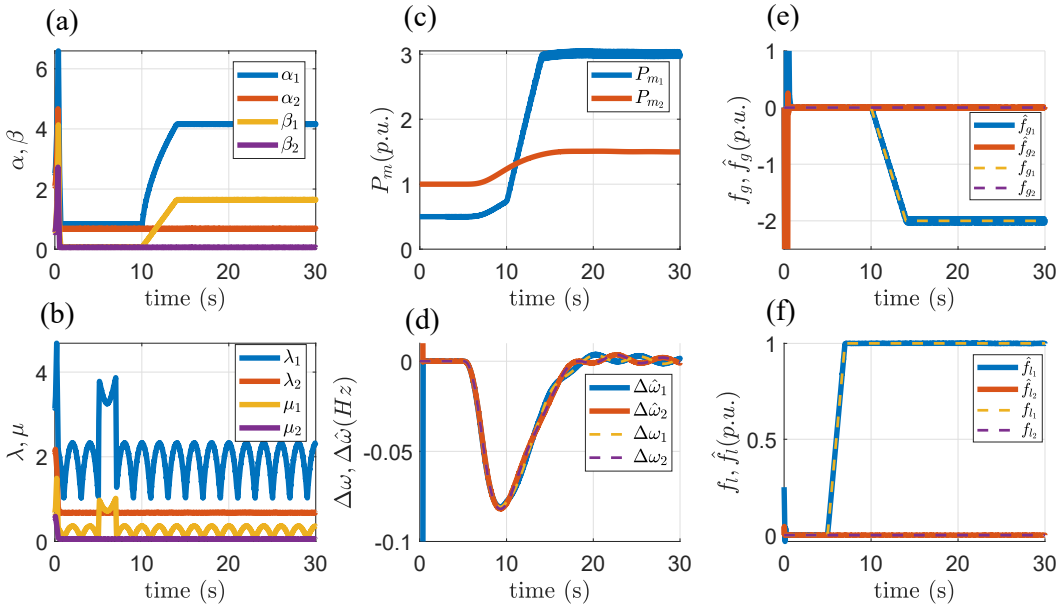

Figure 6.3.2: Time evolution of: **(a):** the adaptive gains in each generator adaptive super-twisting observer; **(b):** the adaptive gains in each load adaptive super-twisting observer; **(c):** the control inputs; **(d):** the frequency deviations and their estimates; **(e):** the faults in the generator buses; **(f):** and load buses together with their estimates.

Table 6.3.1: Numerical Representation of the Parameters of the Power Network Test Case (Base Power of 1000 MVA)

	Generator 1	Generator 2	Load 1	Load 2
$\theta_i(0)$ (rad)	0.076	0.137	0.056	0
$\Delta\omega_i(0)$ (Hz)	0	0	0	0
$P_{m_i}(0)$ (p.u.)	0.5	1	-	-
$P_{l_i}(0)$ (p.u.)	-	-	0.5	1
D_i (p.u.)	0.4	0.38	0.04	0.04
M_i (p.u.)	8.00	7.69	-	-

set equal to $K_{P_i} = 3$ and $K_{I_i} = 1$ in each generator bus. The design constants for all the adaptive super-twisting sliding mode observers (see equations (6.2.3)-(6.2.11)), are set equal to: $\alpha_{0_i} = 6.6$, $\beta_{0_i} = 5.5$, $l_{0_i} = 0.1$ $\tau_i = 0.01$ seconds, $\gamma_i = 8$, $r_{0_i} = 0.1$, and $\eta_i = 0.15$. The power system together with the estimation scheme is implemented in a *Matlab-Simulink R2018a* environment, using the integration method *Ode1* (Euler method) with a fixed integration step size equal to 1×10^{-4} seconds.

The power system is at steady state for $0 < t < 5$ seconds, which means that the power generation is equal to the consumption amongst the buses (see Table 6.3.1). As shown in Figure 6.3.2-(c), at the time instant $t = 5$ seconds, a fault acts on the 1-st load bus, whilst at the time instant $t = 10$ seconds, a fault affects the 1-st generator bus. Note that these kinds of faults can be considered in practice as unregulated generations and consumptions in power systems. The proposed distributed estimation scheme displays the following features:

- As shown in Figure 6.3.2-(d), it is possible to dynamically track the evolution of the frequency deviation of each generator node, both at steady state and during the transient due to the faults.
- The estimates of the faults and the frequency deviations are characterised by a fast transient during the first seconds, which is due to the reaching of the sliding motion, (see Figure 6.3.2-(d) again and Figure 6.3.2-(e)).
- The proposed scheme is able to accurately track both the generator fault and load fault, (Figure 6.3.2-(e) and -(f)).
- The input power at each generator node is regulated according to (6.2.37) in a decentralized fashion, by using the local estimate of the frequency deviation and the local generator fault reconstruction. From Figure 6.3.2-(c) it is possible to note that that the two generator input powers increase, thus asymptotically bringing the frequency deviation back to zero in each generator.
- The gains for all the observer are time-varying, and automatically increase and decrease to deal with the magnitude of the disturbances, as shown in Figure 6.3.2-(a) and -(b).

6.4 Conclusions

In the chapter, an adaptive distributed estimation scheme has been formulated to isolate and reconstruct simultaneous faults and attacks affecting power systems. Relying on a local exchange of information about the system, it has been possible to design a network of adaptive super-twisting sliding mode observers connected in a distributed fashion. Moreover, it has been shown that traditional PI controller, which constitute the most common control architecture in practice, can still be used suitably coupled with the proposed sliding mode-based fault compensation scheme.

Part III

Sliding Mode Observer-Based Control in Power Systems: Design and Applications

Chapter 7

Third Order Sliding Mode Observer-Based Distributed Optimal Load Frequency Control in Power Systems

Abstract In this chapter, a third order sliding mode observer scheme is designed and suitably coupled with an optimal load frequency control scheme in power systems. Each bus is modelled via an equivalent generator including second-order turbine-governor dynamics (3.1.17)-(3.1.18) on page 31. Assuming only the generator voltage phase angle and the turbine output power variations are locally measured in each bus, two original third order sliding mode observers are designed. The proposed observers are able to estimate the unmeasured state variables (which are the frequency deviation and the governor output power variation) in finite time. A distributed second order sliding mode control strategy is also introduced, which makes use of the estimates coming from the observers and achieves both frequency regulation and minimisation of generation costs. The simulation results demonstrate the validity of the proposed approach. The present chapter is mainly based on the following publications:

- G. Rinaldi, M. Cucuzzella, and A. Ferrara, "*Third order sliding mode observer-based approach for distributed optimal load frequency control*," IEEE Control Systems Letters, vol. 1, no. 2, pp. 215–220, 2017.

7.1 Preliminaries and Assumptions

Each bus of the power system is modelled as follows:

$$\begin{aligned} \dot{P}_{m_i} &= -\tfrac{1}{T_{t_i}} P_{m_i} + \tfrac{1}{T_{t_i}} P_{g_i} \\ \dot{P}_{g_i} &= -\tfrac{1}{R_i T_{g_i}} \Delta\omega_i - \tfrac{1}{T_{g_i}} P_{g_i} + \tfrac{1}{T_{g_i}} u_i \\ y_{1i} &= P_{m_i} \end{aligned} \tag{7.1.1}$$

$$\begin{aligned} \dot{\theta}_i &= \Delta\omega_i, \\ M_i\Delta\dot{\omega}_i &= P_{m_i} - P_{d_i} - \textstyle\sum_{j\in\mathcal{N}_i} \frac{V_i V_j}{x_{ij}} \sin(\theta_i - \theta_j) - D_i\Delta\omega_i \\ y_{2i} &= \theta_i \end{aligned} \tag{7.1.2}$$

Note that (7.1.2) differs from (3.1.18) for the presence of the signal P_{d_i}. This additional signal accounts for uncertainties and disturbances appearing in the power flow exchanges. The convenient vectorial compact form of (7.1.1)-(7.1.2) can be obtained as

$$\begin{aligned} \dot{\theta} &= \Delta\omega \\ \Delta\dot{\omega} &= M^{-1}\left(P_m - P_d - D\Delta\omega - B\Gamma\,\sin\left(B^T\theta\right)\right) \\ y_1 &= \theta \\ \dot{P}_m &= -T_t^{-1}P_m + T_t^{-1}P_g \\ \dot{P}_g &= R^{-1}T_g^{-1}f - T_g^{-1}P_g + T_g^{-1}u \\ y_2 &= P_m \end{aligned} \tag{7.1.3}$$

where $\theta \in \mathbb{R}^{|\mathcal{B}|}$, $\Delta\omega \in \mathbb{R}^{|\mathcal{B}|}$, $P_m \in \mathbb{R}^{|\mathcal{B}|}$, $P_g \in \mathbb{R}^{|\mathcal{B}|}$, $\Gamma = \mathrm{Diag}(\gamma_1, \ldots, \gamma_{|\mathcal{E}|})$, with $\gamma_k = V_i\,V_j/x_{ij}$, $P_d \in \mathbb{R}^{|\mathcal{B}|}$, $u \in \mathbb{R}^{|\mathcal{B}|}$, $y_1 \in \mathbb{R}^{|\mathcal{B}|}$, and $y_2 \in \mathbb{R}^{|\mathcal{B}|}$. Matrices $T_t,\ T_g,\ K_p,\ D$ are suitable $|\mathcal{B}| \times |\mathcal{B}|$ diagonal matrices, whilst B is the incident matrix, which is defined in (3.5.3) on page 40.

The two observation and control objectives can be summarised as:

Objective 7.1. *Given the (local) dynamical model for the generator bus (7.1.1)-(7.1.2), estimate in finite time both the frequency deviation $\Delta\omega_i$ and P_{g_i}, ensuring robustness to matched disturbances and unmodelled dynamics.*

Objective 7.2. *Design an observer-based distributed SM controller, which is able to both regulate the frequency deviation and minimise the costs of the generation (ED problem).*

The dynamics in (7.1.1) can be rewritten in a more compact form as:

$$\begin{aligned} \dot{P}_{m_i} &= -b_i P_{m_i} + b_i P_{g_i} \\ \dot{P}_{g_i} &= d_i\Delta\omega_i + c_i P_{g_i} - c_i u_i \\ y_{1i} &= P_{m_i} \end{aligned} \tag{7.1.4}$$

where the auxiliary model parameters are: $b_i \triangleq 1/T_{t_i}$, $c_i \triangleq -1/T_{g_i}$, and $d_i \triangleq -1/(R_i T_{g_i})$. Furthermore, the linear change of coordinates

$$\begin{bmatrix} \widetilde{P}_{m_i} \\ \widetilde{P}_{g_i} \end{bmatrix} = \overbrace{\begin{bmatrix} 1 & 0 \\ 0 & b_i \end{bmatrix}}^{E_{2_i}} \begin{bmatrix} P_{m_i} \\ P_{g_i} \end{bmatrix}. \tag{7.1.5}$$

is introduced for (7.1.4). In new coordinate system, equation (7.1.4) becomes

$$\begin{aligned} \dot{\widetilde{P}}_{m_i} &= -b_i \widetilde{P}_{m_i} + \widetilde{P}_{g_i} \\ \dot{\widetilde{P}}_{g_i} &= c_i \widetilde{P}_{g_i} + b_i d_i \Delta\omega_i - b_i c_i u_i \\ y_{1i} &= P_{m_i} \end{aligned} \tag{7.1.6}$$

Analogously, the system in (3.1.18) can be rewritten as

$$\begin{aligned} \dot{\theta}_i &= \Delta\omega_i, \\ \Delta\dot{\omega}_i &= \tfrac{P_{m_i}}{M_i} + \phi_i - a_i \Delta\omega_i \\ y_{2i} &= \theta_i \end{aligned} \tag{7.1.7}$$

where $a_i = D_i/M_i$, and the auxiliary signal ϕ_i is

$$\phi_i \triangleq \frac{-P_{d_i} - \sum_{j\in\mathcal{N}_i} \frac{V_i V_j}{x_{ij}} \sin(\theta_i - \theta_j)}{M_i} \tag{7.1.8}$$

Assumption 7.1. *It is assumed that:*

(A1) Variables P_{m_i} and θ_i are locally measured at the i-th generator bus.

(A2) The disturbance P_{d_i} is unknown, and both the disturbance itself and its first time derivative are bounded as follows

$$|P_{d_i}| \le \Delta_{P_{d_i}}, \quad |\dot{P}_{d_i}| \le \Delta_{\dot{P}_{d_i}}, \tag{7.1.9}$$

where $\Delta_{P_{d_i}}$ and $\Delta_{\dot{P}_{d_i}}$ are positive constants that can be determined relying on data analysis and engineering understanding.

(A3) The voltage magnitude V_i and V_j are unknown but bounded.

(A4) The model parameters $T_{g_i},\ T_{t_i},\ D_i$ and M_i are assumed to be known at the i-th bus.

Remark 7.1. Note that, under Assumption 7.1, it follows that the auxiliary signal ϕ_i is bounded as follows

$$|\phi_i| \le \Delta_{\phi_i} \tag{7.1.10}$$

7.2 Observers Design

In this section, the procedure for the design of the observers to estimate the unmeasured state variables of each bus is presented. Specifically, two original third order sliding mode observers are proposed for each bus, which are capable of estimating respectively the frequency deviation and the governor output power variation. The introduced observation architecture reveals to be completely decentralised, since no communication is introduced among observers belonging to different buses [15].

7.2.1 Observer for Frequency Deviation Estimation

Next consider the following original third order sliding mode observer

$$\begin{aligned}\dot{\hat{\theta}}_i &= -k_{1_i}\lceil e_{\theta_i}\rfloor^{2/3} - \boldsymbol{a_i e_{\theta_i}} + \Delta\hat{\omega}_i \\ \Delta\dot{\hat{\omega}}_i &= -k_{2_i}\lceil e_{\theta_i}\rfloor^{1/3} + \tfrac{P_{m_i}}{M_i} - a_i\hat{f}_i - \boldsymbol{a_i^2 e_{\theta_i}} \boldsymbol{-k_{1_i}\lceil e_{\theta_i}\rfloor^{2/3}} + \hat{z}_i \\ \dot{\hat{z}}_i &= -k_{3_i}\lceil e_{\theta_i}\rfloor^{0}\end{aligned} \tag{7.2.1}$$

where $\hat{\theta}_i$ is the estimate of θ_i, $e_{\theta_i} \triangleq \hat{\theta}_i - \theta_i$, $\Delta\hat{\omega}_i$ is the estimate of $\Delta\omega_i$, $\hat{z}_i$ is an auxiliary variable, and k_{1_i}, k_{2_i}, k_{3_i} are positive scalar design. Note that the observer in (7.2.1) differs from the one proposed in [81] because of the presence of additional terms. These terms are highlighted in bold. Furthermore, the compact representation $\lceil e_{\theta_i}\rfloor^p \triangleq |e_{\theta_i}|^p \mathrm{sign}(e_{\theta_i})$ is employed in (7.2.1), as clearly indicated in the Notation section on page ix. By subtracting (7.1.7) from (7.2.1), the error dynamics yield

$$\begin{aligned}\dot{e}_{\theta_i} &= -k_{1_i}\lceil e_{\theta_i}\rfloor^{2/3} - a_i e_{\theta_i} + e_{\omega_i} \\ \dot{e}_{\omega_i} &= -k_{2_i}\lceil e_{\theta_i}\rfloor^{1/3} + a_i e_{\omega_i} - a_i^2 e_{\theta_i} - k_{1_i}\lceil e_{\theta_i}\rfloor^{2/3} - \hat{z}_i + \phi_i \\ \dot{\hat{z}}_i &= k_{3_i}\lceil e_{\theta_i}\rfloor^{0}\end{aligned} \tag{7.2.2}$$

where $e_{\omega_i} \triangleq \Delta\hat{\omega}_i - \Delta\omega_i$. The following proposition will now be proven:

Proposition 7.1. *Given Assumption 7.1, Remark 7.1, the origin is a finite-time stable equilibrium point for the error dynamics (7.2.2), if the design constants satisfies the following:* $k_{3_i} > \tilde{\Delta}_{\phi_i}$, $k_{2_{g_i}} = 5.3k_{3_{g_i}}^{2/3}$, $k_{1_{g_i}} = 3.34k_{3_{g_i}}^{1/3}$, *where* $\tilde{\Delta}_{\phi_i}$ *is a known positive constant.*

Proof. It is now possible to define two auxiliary error variables $\overline{e}_{\omega_i} \triangleq e_{\omega_i} - a_i e_{\theta_i}$, and $e_{z_i} \triangleq -\hat{z}_i + \phi_i$, then rewrite (7.2.2) as

$$\begin{aligned}\dot{e}_{\theta_i} &= -k_{1_i}\lceil e_{\theta_i}\rfloor^{2/3} + \overline{e}_{\omega_i} \\ \dot{\overline{e}}_{\omega_i} &= -k_{2_i}\lceil e_{\theta_i}\rfloor^{1/3} + a_i e_{\omega_i} - a_i^2 e_{\theta_i} - k_{1_i}\lceil e_{\theta_i}\rfloor^{2/3} + e_{z_i} \\ &\quad -a_i\left(-k_{1_i}\lceil e_{\theta_i}\rfloor^{2/3} - a_i e_{\theta_i} + e_{\omega_i}\right) \\ \dot{e}_{z_i} &= -k_{3_i}\lceil e_{\theta_i}\rfloor^{0} + \dot{\phi}_i\end{aligned} \tag{7.2.3}$$

After straightforward algebraic manipulations, one gets:

$$\begin{aligned}\dot{e}_{\theta_i} &= -k_{1_i}\lceil e_{\theta_i}\rfloor^{2/3} + \overline{e}_{\omega_i} \\ \dot{\overline{e}}_{\omega_i} &= -k_{2_i}\lceil e_{\theta_i}\rfloor^{1/3} + e_{z_i} \\ \dot{e}_{z_i} &= -k_{3_i}\lceil e_{\theta_i}\rfloor^{0} + \dot{\phi}_i\end{aligned} \tag{7.2.4}$$

The system in (7.2.4) is in the canonical form of the third order SM observer error dynamics in [81] or, analogously, of the second order SM differentiator error dynamics [54]. Following [82], a Lyapunov function candidate in the form of

$$V_{g_i}(e_{\theta_i}, \overline{e}_{\omega_i}, e_{z_i}) = \beta_{1i}|e_{\theta_i}|^{5/3} - \beta_{2i}e_{\theta_i}\overline{e}_{\omega_i} + \beta_{3i}|\overline{e}_{\omega_i}|^{5/2} - \beta_{4i}\overline{e}_{\omega_i}|e_{z_i}|^3\mathrm{sign}(e_{z_i}) + \beta_{5i}|e_{z_i}|^5 \tag{7.2.5}$$

can be employed to prove that the origin is finite time stable for error dynamics in , where $\beta_{1i}, \ldots, \beta_{5i}$ are arbitrary positive constants. The tuning rule for the gains relies on a recursive architecture. Let

$\tilde{L}_i = \Delta_{\phi_i}/\tilde{\Delta}_{i0}$, where $\tilde{L}_i$ and $\tilde{\Delta}_{i0}$ are known constants. Then, if $[\overline{k}_{1_i}, \overline{k}_{2_i}, \overline{k}_{3_i}]^T$ are the triplet of the gains suggested in [82] for the unperturbed case (i.e., for the case when $\phi_i = 0$), using a scaled parameters technique, the tuning rules

$$[k_{1_i}, k_{2_i}, k_{3_i}]^T = \text{Diag}\left(\tilde{L}_i^{1/3}, \tilde{L}_i^{2/3}, \tilde{L}_i\right)[[\overline{k}_{1_i}, \overline{k}_{2_i}, \overline{k}_{3_i}]^T \tag{7.2.6}$$

are proposed [82]. The numerical representation of the tuning rules introduced in [73] can be shown to be:

$$\begin{array}{rcl} k_{3_i} & > & \Delta_{\phi_i} \\ k_{2_i} & = & 5.3k_{3_i}^{2/3} \\ k_{1_i} & = & 3.34k_{3_i}^{1/3} \end{array} \tag{7.2.7}$$

Note that the gain k_{3_i} is chosen first to compensate the effect of $\dot{\phi}_i$. Furthermore, if the vector of the initial conditions of (7.2.4) is $e_{0_{g_i}} \triangleq \text{Col}(e_{\theta_i}(0), \overline{e}_{\omega_i}(0), e_{z_i}(0))$, then the dynamics converge to the origin in a finite time $T_{e_{0_{g_i}}}$, which is upper-bounded according to:

$$T_{e_{0_{g_i}}} \leq \frac{V_{g_i}^{1/5}(e_{0_{g_i}})}{c_{g_i}} \tag{7.2.8}$$

where c_{g_i} is a positive constant. Therefore, a sliding motion is characterized by the following conditions

$$e_{\theta_i} = \overline{e}_{\omega_i} = e_{\omega_i} = e_{z_i} = 0, \tag{7.2.9}$$

which are enforced in finite time. It follows that it is possible to correctly estimate the frequency deviation $\Delta\omega_i$, since $e_{\omega_i} = \omega_i - \hat{\omega}_i = 0$. This proves the proposition. □

7.2.2 Observer for Governor Power Estimation

To locally estimate the governor output power P_{g_i} of each bus, it is possible to exploit again a third order sliding mode observer architecture. Since the design procedure is similar to Section 7.2.1, only the key-differences will be underlined.

Next consider the following original third order SM observer:

$$\begin{array}{rcl} \dot{\hat{P}}_{m_i} & = & -k_{4_i}\left\lceil e_{P_{m_i}}\right\rfloor^{2/3} - \boldsymbol{(c_i - b_i)e_{P_{m_i}}} + \hat{P}_{g_i} - b_i\hat{P}_{m_i} \\ \dot{\hat{P}}_{g_i} & = & -k_{5_i}\left\lceil e_{P_{m_i}}\right\rfloor^{1/3} + c_i\hat{P}_{g_i} - \boldsymbol{c_i^2 e_{P_{m_i}}} \\ & & -b_i c_i u_i - \boldsymbol{k_{4_i} c_i}\left\lceil \boldsymbol{e_{P_{m_i}}}\right\rfloor^{\boldsymbol{2/3}} + b_i d_i \Delta\hat{\omega}_i + \hat{w}_i \\ \dot{\hat{w}}_i & = & -k_{6_i}\left\lceil e_{P_{m_i}}\right\rfloor^{0} \end{array} \tag{7.2.10}$$

where $\hat{P}_{m_i}$ is the estimate of $\widetilde{P}_{m_i}$,$e_{P_{m_i}} \triangleq \hat{P}_{m_i} - \widetilde{P}_{m_i}$, $\hat{P}_{g_i}$ is the estimate of $\widetilde{P}_{g_i}$, $\hat{w}_i$ is an auxiliary variable, and k_{4_i}, k_{5_i}, and k_{6_i} are positive design constants.

Remark 7.2. Note that also the observer (7.2.10) distinguishes from the ones in [81] for the presence of additional terms highlighted in bold. There are useful to obtain a canonical form for the stability

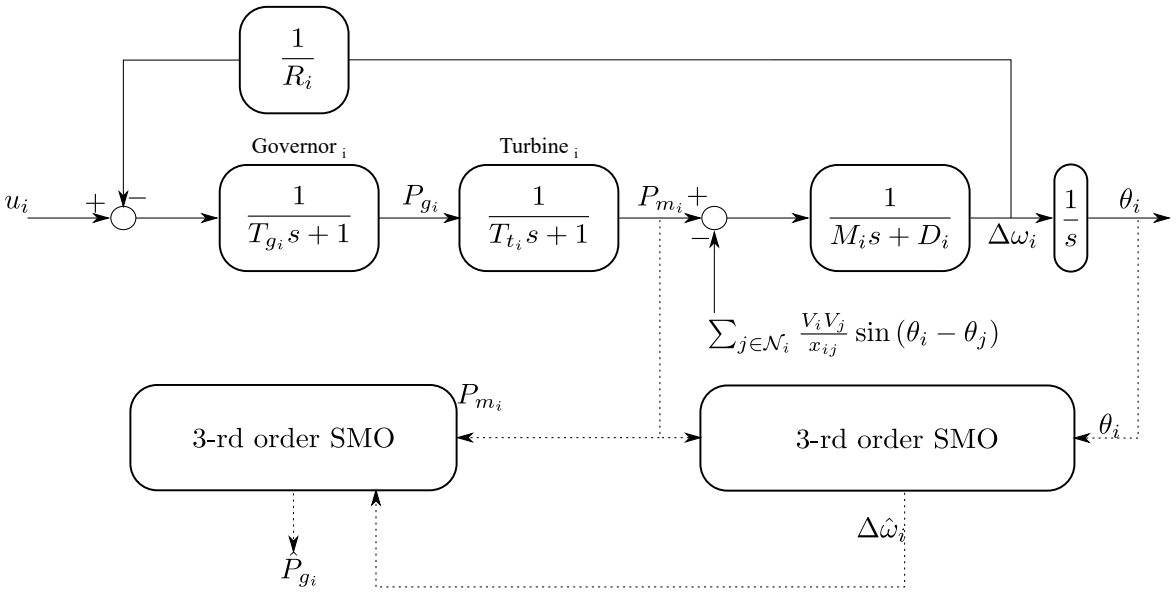

Figure 7.2.1: The block diagram of the i-th generator bus together with the designed 3-rd order sliding mode observers.

analysis of the error dynamics. In addition, (7.2.10) receives the estimate of the frequency coming from (7.2.1). This gives rise to a local exchange of information between the observer (7.2.1) and (7.2.10) , both of which belong to the same i-th bus.

By subtracting (7.1.6) from (7.2.10), the error dynamics yield

$$\begin{aligned}
\dot{e}_{P_{m_i}} &= -k_{4_i}\left\lceil e_{P_{m_i}}\right\rfloor^{2/3} + e_{P_{g_i}} - c_i e_{P_{m_i}} \\
\dot{e}_{P_{g_i}} &= -k_{5_i}\left\lceil e_{P_{m_i}}\right\rfloor^{1/3} + c_i e_{P_{g_i}} - c_i^2 e_{P_{m_i}} - k_{4_i}c_i\left\lceil e_{P_{m_i}}\right\rfloor^{2/3} + b_i d_i e_{\omega_i} + \hat{w}_i \\
\dot{\hat{w}}_i &= -k_{6_i}\left\lceil e_{P_{m_i}}\right\rfloor^{0}
\end{aligned} \tag{7.2.11}$$

If the auxiliary error variables $\overline{e}_{P_{g_i}} \triangleq -c_i e_{P_{t_i}} + e_{P_{g_i}}$, and $e_{w_i} \triangleq b_i d_i e_{\omega_i} + \hat{w}_i$ are introduced, one gets

$$\begin{aligned}
\dot{e}_{P_{m_i}} &= -k_{4_i}\left\lceil e_{P_{m_i}}\right\rfloor^{2/3} + \overline{e}_{P_{g_i}} \\
\dot{\overline{e}}_{P_{g_i}} &= -k_{5_i}\left\lceil e_{P_{m_i}}\right\rfloor^{1/3} + e_{w_i} \\
\dot{e}_{w_i} &= -k_{6_i}\left\lceil e_{P_{m_i}}\right\rfloor^{0} + b_i d_i \dot{e}_{\omega_i}
\end{aligned} \tag{7.2.12}$$

Also the system in 7.2.12 is in the standard form for the of the third order observer error dynamics, which is finite-time stable according to the developments in Section 7.2.1.

Remark 7.3. Note that the matched disturbance $b_i d_i \dot{e}_{\omega_i}$ appearing in (7.2.12) reveals to be bounded, since the trajectories of (7.2.1) are bounded and they converge to the origin in finite time, as proven in Section 7.2.1.

The schematic in Figure 7.2.1 shows the dynamical model of the i-th bus together with the proposed third order SM observer. The local communication between the two observers for the i-th bus, which has been highlighted in the developments of this section, is also graphically illustrated.

7.3 Observer-Based SM Controller Design

In this section, the controller proposed in [35] is briefly recalled for the sake of completeness. Before introducing the control problem, consider the following optimisation problem, which is the ED problem [40]:

$$\min_{P_m} C(P_m) = \min_{P_{m_i}} \sum_{i\in\mathcal{B}} C_i(P_{m_i}) \tag{7.3.1}$$

$$\text{s.t.}0 = \sum_{i\in\mathcal{B}} P_{m_i} - \sum_{i\in\mathcal{B}} P_{d_i} \tag{7.3.2}$$

where $C(P_m)$ represents the total costs of the power generation required to regulate the frequency. The expression for $C(P_m)$ adopted in the present chapter is:

$$C(P_m) = \frac{1}{2} P_m^T Q\, P_m + R^T P_m + 1_n^T S, \tag{7.3.3}$$

where $Q \in \mathbb{R}^{|\mathcal{B}|\times|\mathcal{B}|}$, $Q \succ 0$ is a positive definite diagonal matrix and $R, S \in \mathbb{R}^{|\mathcal{B}|}$. In order to both design a sliding manifold on which a useful passivity property of the turbine-governor can be exploited, and to satisfy ED at steady state, an auxiliary variable is introduced $\xi = \text{Col}(\xi_i), \xi \in \mathbb{R}^{|\mathcal{B}|}$, which governed by the following dynamics:

$$T_\xi \dot{\xi} = P_m - \xi - \Lambda L_c(Q\xi + R), \tag{7.3.4}$$

where $\Lambda \in \mathbb{R}^{|\mathcal{B}|\times|\mathcal{B}|}$ is a positive definite diagonal matrix suitably selected, while L_c denote the Laplacian matrix associated with the communication graph. Note that the induced communication is required to achieve optimality. According to [35], the sliding function is selected as

$$\hat{\sigma} = M_1 \Delta\hat{\omega} + M_2 P_m + M_3 \hat{P}_g + M_4 \xi, \tag{7.3.5}$$

with $M_1 > 0, M_2 \geq 0, M_3 > 0$, $M_4 = -(M_2 + M_3)$, and $\Lambda = (M_2 + M_3)^{-1} M_1 Q$ in (7.3.4). Then, in order to enforce a Second Order Sliding Mode (i.e., to nullify $\hat{\sigma}$ and $\dot{\hat{\sigma}}$ to zero in a finite time), the well-established Suboptimal SOSM control algorithm is used [80].

Remark 7.4. Note that the proposed distributed sliding mode controller acts on each bus only after the finite time convergence to the origin of the error dynamics of the observers in (7.2.1) and in (7.2.10). During this fast transient, the so-called primary load-frequency control (whose control signal is equal to $-\Delta\omega_i/R_i$) guarantees that, given a constant power demand, the state variables of asymptotically converge to an equilibrium point characterized by a frequency deviation generally different from zero [37]. Furthermore, the adopted distributed sliding mode control architectures establishes a second order sliding mode, i.e., $\hat{\sigma} = \dot{\hat{\sigma}} = 0$ and only $\ddot{\hat{\sigma}}$ is affected by the discontinuous control input [112]. As proven in [81], all the states in the sliding variable must have continuous first time derivative. Then, by measuring θ_i and using a third order sliding mode observer, the discontinuity appears in the time derivative of $\hat{z}_i$, so that $\Delta\dot{\hat{\omega}}_i$ is continuous. Analogously, by measuring P_{m_i}, the discontinuity appears in the time derivative of $\hat{w}_i$, so that $\dot{\hat{P}}_{g_i}$ is continuous. Otherwise, if a second order sliding mode observer was used, both $\Delta\dot{\hat{\omega}}_i$ and $\dot{\hat{P}}_{g_i}$ would be discontinuous, which is in contrast to second

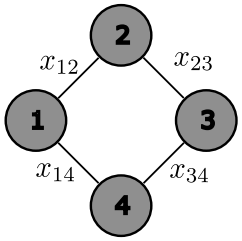

Figure 7.4.1: Scheme of the considered power system composed of 4 generator buses.

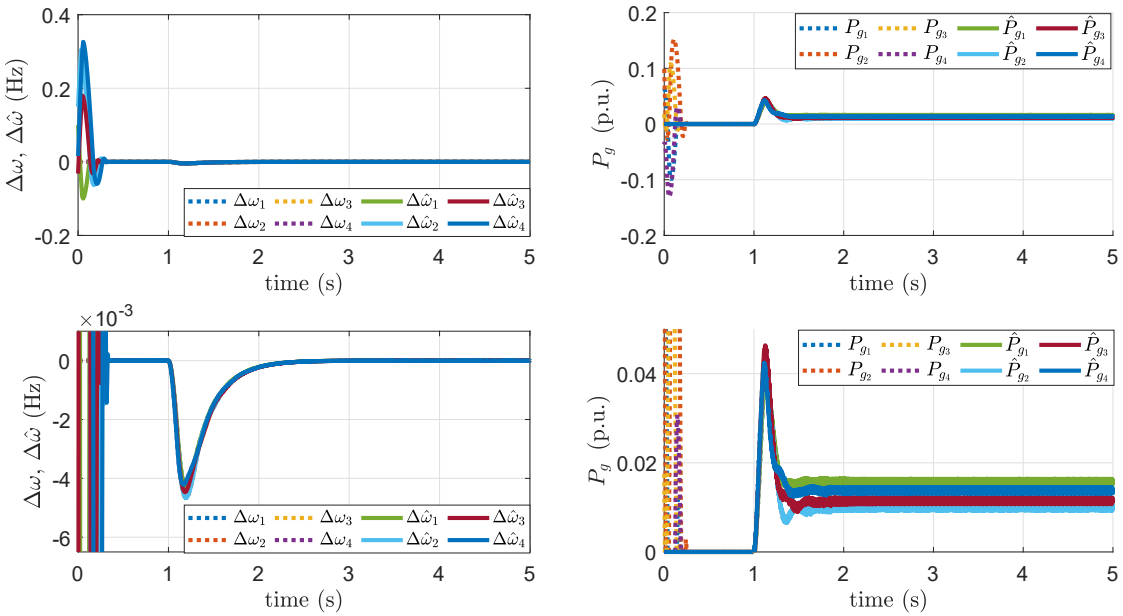

Figure 7.4.2: **(Left):** Time evolution of the frequency deviation in each bus together with an enlarged view. **(Right):** Time evolution of the governor output power variation in each bus together with an enlarged view.

order sliding modes [81].

The relevant contribution of this chapter is the design of dedicated third order SMO observer to estimate the unmeasured state variables to reduce the number of the required sensor for the implementation of the SM control scheme [35]. Therefore, the interested reader is referred to the aforementioned paper for furthers details about the stability analysis of the controller.

7.4 Simulation Test Cases

In this section, the proposed observers-based distributed control approach is demonstrated in simulation environment. The considered network is composed of four buses as illustrated in Figure 7.4.1. The numerical representations for the parameters of the power system and the disturbance variations P_{d_i} of each bus are shown in Table 7.4.1. The line parameters are $\gamma_1 = 5.4$ (p.u.), $\gamma_2 = 5.0$

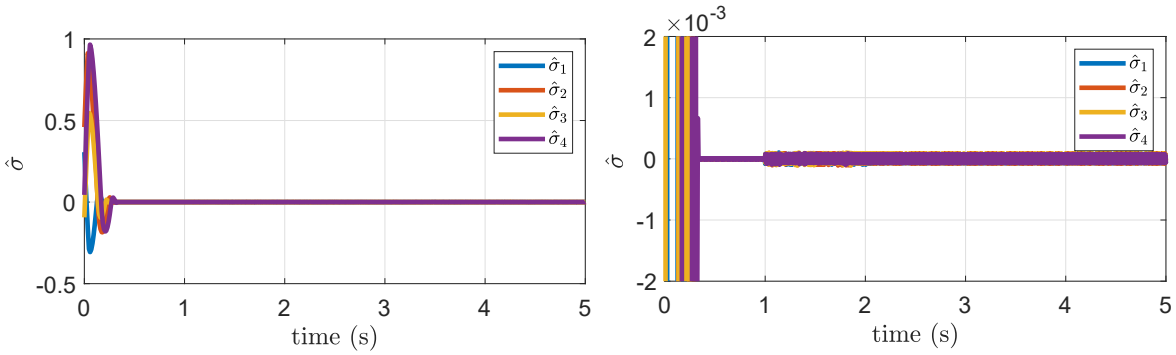

Figure 7.4.3: **(Left):** Time evolution of the sliding surface **(Right):** An enlarged view.

Table 7.4.1: Numerical Representation of the Parameters of the power network test case (base power of 1000 MVA).

	Bus 1	Bus 2	Bus 3	Bus 4
T_t	0.30	0.33	0.35	0.28
T_g	0.080	0.072	0.070	0.081
D	1.4×10^{-4}	1.5×10^{-4}	1.3×10^{-4}	1.7×10^{-4}
R	2.50	2.60	2.70	2.80
M	28×10^{-4}	38×10^{-4}	38×10^{-4}	42×10^{-4}
P_d	0.010	0.015	0.012	0.014

(p.u.), $\gamma_3 = 4.5$ (p.u). and $\gamma_4 = 5.2$ (p.u.). The gains of the observers are selected as follows: $k_{1_i} = k_{4_i} = 20$; $k_{2_i} = k_{5_i} = 67$;$k_{3_i} = k_{6_i} = 250$, $\forall i = 1, \ldots, 4$. The matrices in (7.3.5) are chosen as $M_1 = 3I_4$, $M_2 = I_4$, $M_3 = 0.1I_4$ and $M_4 = -(M_2 + M_3)$, $I_4 \in \mathbb{R}^{4\times4}$, while in the cost function (7.3.3) $Q = \text{Diag}([2.41,\ 3.78,3.31,\ 2.75])$, and $R = S = 0$. In simulation, the system is initially at the steady state. At the instant $t = 1$ seconds, disturbances affect each bus. The values for the disturbances are shown in the last column of Table 7.4.1. Figure 7.4.2 show that the unmeasured state variables, i.e. $\Delta\omega_i$ and P_{g_i} can be profitably tracked, ensuring also total insensitivity to matched perturbation, which appears in (7.2.2) and (7.2.11). Figure 7.4.3 shows that the estimated sliding variables are steered to the sliding manifold after a transient due to the observers convergence. From Figure 7.4.2-(left) one can note a transient during which the frequency drops because of the disturbances perturbing the power system. Then, in order to bring the frequency deviation back to zero, the proposed controllers increase the power generation, as shown in Figure 7.4.2-(right).

7.5 Conclusions

In this chapter, two novel third order sliding mode observers have been designed to estimate the frequency deviation and the governor output power variation in each generator bus of power systems. The proposed observers revealed to be robust to a class of matched uncertainties and disturbances, and are able to perform state estimation in finite time, generating also differentiable estimates. To assess in simulation the performance of the proposed state estimation technique, the designed ob-

servers have been coupled with a distributed second order sliding mode control strategy proposed by some of the authors in [35] and [15]. Simulation evidence shows the effectiveness of the proposed method.

Chapter 8

Sliding Mode Observer-Based Finite Time Control for Economic Dispatch and Frequency Regulation

Abstract In this chapter a novel observer-based SM control scheme is proposed to achieve both frequency regulation and ED for structure-preserving power systems. A distributed heterogeneous SM observer scheme is formulated to estimate in finite time the frequency deviation in generator buses and the unknown power associated with all the buses. Then, a reference maker node is introduced, which has the task to collect the estimates coming from the observers and generate the optimal value for the marginal cost. A SM control scheme is introduced to drive the control input to its optimal value in finite time.

8.1 Preliminaries, Assumptions and Facts

The structure-preserving dynamical model for the power system (3.5.12) on page 42 can be rewritten to include unknown power injections and demand associated with each bus as follows:

$$\begin{array}{rcll} \dot{\theta}_i & = & \Delta\omega_i & i \in \mathcal{B} \\ M_i\Delta\dot{\omega}_i & = & -D_i\Delta\omega_i + P_{m_i} - \sum_{j\in\mathcal{N}_i}\gamma_{ij}\sin\left(\theta_i-\theta_j\right) + p_i & i \in \mathcal{G} \\ 0 & = & -D_i\Delta\omega_i + P_{l_i} - \sum_{j\in\mathcal{N}_i}\gamma_{ij}\sin\left(\theta_i-\theta_j\right) + p_i & i \in \mathcal{L} \\ y_i & = & \theta_i & i \in \mathcal{B} \end{array} \tag{8.1.1}$$

Following (3.5.14) on page 43 vectorial compact form can be shown to be:

$$\begin{array}{rcl} \dot{\theta} & = & \Delta\omega \\ M_{\mathcal{G}}\Delta\dot{\omega}_{\mathcal{G}} & = & -D_{\mathcal{G}}\Delta\omega_{\mathcal{G}} + P_m - \nabla_{\mathcal{G}}U(\theta) \\ 0 & = & -D_{\mathcal{L}}\Delta\omega_{\mathcal{L}} - \nabla_{\mathcal{L}}U(\theta) \\ y & = & \theta \end{array} \tag{8.1.2}$$

Assumption 8.1. *The unknown power injection or demand vector $p \triangleq \mathrm{Col}(p_1,\ldots,p_{|\mathcal{B}|}) \in \mathbb{R}^{|\mathcal{B}|}$ is bounded, with a bounded first time derivative. Furthermore, it is assumed the bounds are known and*

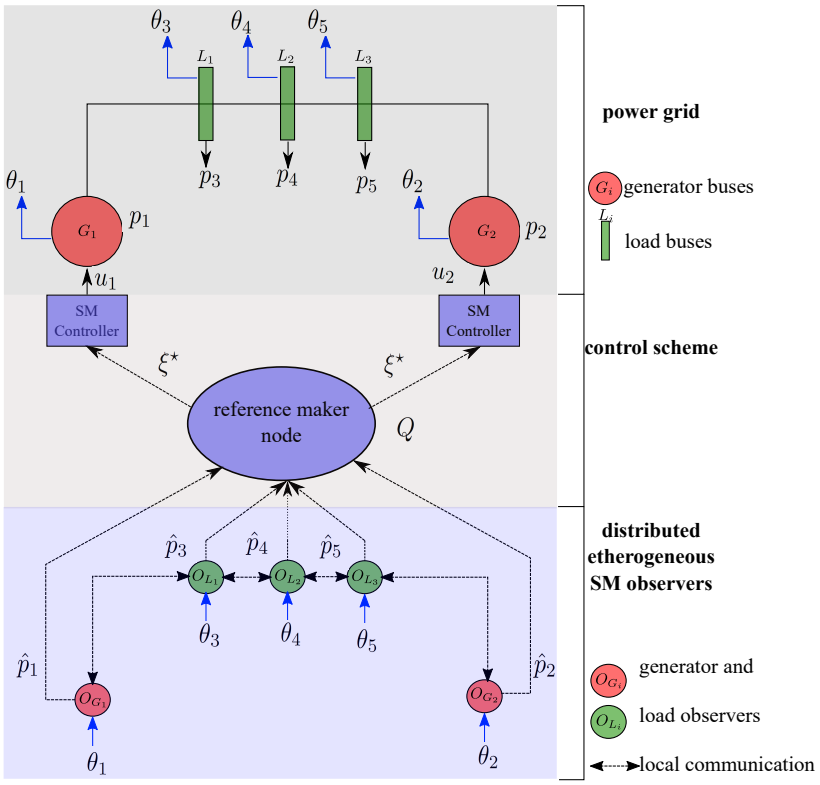

Figure 8.1.1: A schematic of the proposed SM observer-based control approach.

the scalars Λ_p *and* $\Lambda_{\dot{p}}$ *as such that:*

$$||p|| \leq \Lambda_p \tag{8.1.3}$$

$$||\dot{p}|| \leq \Lambda_{\dot{p}} \tag{8.1.4}$$

Assumption 8.2. *Each bus instantaneously receives the measurements acquired from its neighbourhood.*

The rest of the chapter will be devoted to the description of the proposed observer-based SM control architecture, which is able to achieve two objectives:

Objective 8.1. *Design SM observers capable of estimating in finite time the unknown power demand associated with each bus of the power system and the frequency deviation in each generator bus.*

Objective 8.2. *Design SM control schemes capable of achieving both frequency regulation and economic dispatch.*

The problem will be addressed in a two steps approach way when compared to earlier works [35], [38] [15], and [45].

Figure 8.1.1 shows a schematic of the proposed SM observer-based control scheme. The first step involves the design of a distributed heterogeneous SM observer scheme. The network of observers is composed of third order SM observers for the generator buses, and super-twisting SM observers for the load buses. The estimation scheme is able to both estimate in finite time the frequency deviation

in each generator bus, and the unknown power demand associated with each bus, both of which are essential for controllers design.

The second step develops the synthesis of the controller. A so-called reference-maker node creates the optimal values for the generation cost, by using the unknown power demands, which are estimate in finite time in the first step. A SM control scheme is employed to track in finite time the reference value of the optimal marginal cost, thus achieving in finite time the economic dispatch, and asymptotically steering to zero the frequency deviations.

8.2 Observers Design and Unknown Demand Reconstruction

In Chapter 7, the third order SM observer (7.2.1) was proposed for optimal load frequency control in power networks. In this chapter, the aforementioned observer scheme is further developed with both the aim of estimating in finite time the frequency deviation, and the unknown power p_i associated with each generator. The use of third order SM observer to estimate in finite time unknown inputs in power system context is novel and it has never been proposed before.

8.2.1 Third Order SM Observer for Generator Buses

Given the generator dynamics in (8.1.1) and under Assumption 8.1, it is possible to adopt the observer in (7.2.1) to estimate in a finite time $\Delta\omega_i,\ \forall i \in \mathcal{G}$. The observer structure in (7.2.1) is here recalled for the sake of clarity:

$$\left.\begin{array}{rcl} \dot{\hat{\theta}}_i &=& -k_{1_i} \lceil e_{\theta_i} \rfloor^{2/3} - a_i e_{\theta_i} + \Delta\hat{\omega}_i \\ \Delta\dot{\hat{\omega}}_i &=& -k_{2_i} \lceil e_{\theta_i} \rfloor^{1/3} + \frac{P_{m_i}}{M_i} - a_i \hat{f}_i - a_i^2 e_{\theta_i} - k_{1_i} \lceil e_{\theta_i} \rfloor^{2/3} + \hat{z}_i \ - \sum_{i \in \mathcal{N}_i} \gamma_{ij} \sin\left(y_i - y_j\right) \\ \dot{\hat{z}}_i &=& -k_{3_i} \lceil e_{\theta_i} \rfloor^{0} \end{array}\right\} \forall i \in \mathcal{G} \tag{8.2.1}$$

Furthermore, the error dynamics associated with the observer can be shown to be

$$\left.\begin{array}{rcl} \dot{e}_{\theta_i} &=& -k_{1_i} \lceil e_{\theta_i} \rfloor^{2/3} + \overline{e}_{\omega_i} \\ \dot{\overline{e}}_{\omega_i} &=& -k_{2_i} \lceil e_{\theta_i} \rfloor^{1/3} + e_{z_i} \\ \dot{e}_{z_i} &=& -k_{3_i} \lceil e_{\theta_i} \rfloor^{0} - \dot{p}_i \end{array}\right\} \forall i \in \mathcal{G} \tag{8.2.2}$$

The reader is referred to Chapter 7 for the physical interpretation of the introduced variables, model parameters a and the undertaken stability analysis of (8.2.2). Note that in (8.2.2) the auxiliary error variable is defined

$$e_{z_i} \triangleq \hat{z}_i - \frac{p_i}{M_i},\ \forall i \in \mathcal{G} \tag{8.2.3}$$

During the sliding motion of (8.2.2), the condition

$$e_{\theta_i} = \overline{e}_{\omega_i} = e_{\omega_i} = e_{z_i} = 0,\ \forall i \in \mathcal{G} \tag{8.2.4}$$

are enforced in finite time. Two objectives are achieved once the sliding motion (8.2.4) occurs: i) it is possible to correctly estimate the frequency deviation $\Delta\omega_i$, since $e_{\omega_i} = \Delta\omega_i - \Delta\hat{\omega}_i = 0$, ii) since

$e_{z_i} = 0$, according to (8.2.3), it results that condition

$$\hat{p}_i = M_i \hat{z}_i, \ \forall i \in \mathcal{G} \tag{8.2.5}$$

is satisfied in finite time, which allows to estimate p_i in finite time.

8.2.2 Super-Twisting SM Observers for Load Buses

Inspired by [66], the following proposition holds for each load bus $i \in \mathcal{L}$.

Proposition 8.1. *Given the load algebraic relation in (8.1.1), and under Assumptions 8.1 and 8.2, the following super-twisting SM observer is able to estimate in finite time the unknown power demand p_i:*

$$\left.\begin{array}{rcl} \dot{\hat{\theta}}_i & = & k_{1_{l_i}} |e_{\theta_i}|^{1/2} \text{sign}(e_{\theta_i}) - \frac{1}{D_i} \sum_{j \in \mathcal{N}_i} \gamma_{ij} \sin(y_i - y_j) + \hat{\psi}_i \\ \dot{\hat{\psi}}_i & = & k_{2_{l_i}} \text{sign}(e_{\theta_i}) \end{array}\right\} \forall i \in \mathcal{L} \tag{8.2.6}$$

where $\hat{\psi}_i$ is an auxiliary variable, $e_{\theta_i} \triangleq \theta_i - \hat{\theta}_i$, and $k_{1_{l_i}}$, $k_{2_{l_i}}$ are positive design constants. An estimate $\hat{p}_i$ of the unknown power p_i can be obtained by using the following relation:

$$\hat{p}_i = D_i \hat{\psi}_i, \ \forall i \in \mathcal{L} \tag{8.2.7}$$

Proof. The error dynamics for each load bus are computed by subtracting (8.2.6) from (8.1.1), and they are given by:

$$\left.\begin{array}{rcl} \dot{e}_{\theta_i} & = & -k_{1_{l_i}} |e_{\theta_i}|^{1/2} \text{sign}(e_{\theta_i}) + \frac{p_i}{D_i} - \hat{\psi}_i \\ \dot{\hat{\psi}}_i & = & k_{2_{l_i}} \text{sign}(e_{\theta_i}) \end{array}\right\} \forall i \in \mathcal{L} \tag{8.2.8}$$

It is possible to introduce an auxiliary error variable

$$e_{\psi_i} \triangleq -\hat{\psi}_i + \frac{p_i}{D_i}, \ \forall i \in \mathcal{L} \tag{8.2.9}$$

thus obtaining the following error dynamics

$$\left.\begin{array}{rcl} \dot{e}_{\theta_i} & = & -k_{1_{l_i}} |e_{\theta_i}|^{1/2} \text{sign}(e_{\theta_i}) + e_{\psi_i} \\ \dot{e}_{\psi_i} & = & -k_{2_{l_i}} \text{sign}(e_{\theta_i}) + \frac{\dot{p}_i}{D_i}. \end{array}\right\} \forall i \in \mathcal{L} \tag{8.2.10}$$

The system in equation (8.2.10) is in the canonical form of a super-twisting SM architecture. Therefore, by tuning the design constants following the rules in [76], the system in (3.5.14) is driven to the origin in a finite time $T_{e_{0_{l_i}}}$. It follows that

$$e_{\theta_i} = e_{\psi_i} = 0, \ \forall i \in \mathcal{L}. \tag{8.2.11}$$

□

Remark 8.1. The proposed third order SM observer scheme in (8.2.1) and the super-twisting observer in (8.2.6) exhibit a distributed structure since they use local voltage phase angles (y_i) and phase angle

measurements gathered by the neighbouring buses ($y_j,\ j \in \mathcal{N}_i$).

Remark 8.2. Fault reconstruction schemes based on sliding mode approaches often require the use of low-pass filters to eliminate the high frequency components and obtain a fault estimation characterised by a good quality [113]. However, such a low-pass filter mechanism is not mandatory for the reconstruction of unknown powers in the present context. This is due to the fact that the signal $\hat{z}_i$ in (8.2.5) and $\hat{\psi}_i$ in (8.2.7) are continuous, because the order of the observers has been increased by one with respect to the order of the system under observation. Specifically, a third order SM observer (8.2.1) has been employed for the second order generator dynamics (8.1.1), and a second order (super twisting) SM observer (8.2.6) for the first order load dynamics (8.1.1). Furthermore, the robust accurate estimation of p_i is achieved in finite time and not asymptotically, as typically happens when a low-pass filter is employed (see, e.g., [114], [67], and [36]).

Assumption 8.3. *There exists a reference-maker which collects all the estimates of unknown power p_i for generators and loads generated by the observers. Therefore, the following column vector can be introduced*

$$\hat{p} \triangleq \mathrm{Col}\left(\hat{p}_1, \ldots, \hat{p}_{|\mathcal{B}|}\right), \tag{8.2.12}$$

where $\hat{p} \in \mathbb{R}^{|\mathcal{B}|}$.

8.3 Controllers Design

The distributed observers, proposed in (8.2.1) and (8.2.6), estimate the unknown power demands, both at generators and load, in finite time. Making use of this estimate, the objective of the controller scheme proposed here is to drive the deviation in frequency asymptotically to zero, while the cost of generators operation is minimised.

Remark 8.3. The proposed control acts on the power grid only after the observers error dynamics (8.2.2) and (8.2.10) convergence to the origin, which takes place in finite time T_{e_0}. Hence, since T_{e_0}, it follows:

$$\hat{\theta} = \theta \tag{8.3.1}$$

$$\Delta\hat{\omega} = \Delta\omega \tag{8.3.2}$$

$$\hat{p} = p \tag{8.3.3}$$

where the estimate vectors $\hat{\theta} \triangleq \mathrm{Col}(\hat{\theta}_1, \ldots, \hat{\theta}_{|\mathcal{B}|}) \in \mathbb{R}^{|\mathcal{B}|}$, and $\Delta\hat{\omega} \triangleq \mathrm{Col}(\Delta\hat{\omega}_1, \ldots, \Delta\hat{\omega}_{|\mathcal{B}|}) \in \mathbb{R}^{|\mathcal{B}|}$. Until T_{e_0}, only the primary frequency control scheme [4] acts on the power grid. This is characterised by the term $-D\Delta\omega \triangleq \mathrm{Col}(-D_{\mathcal{G}}\Delta\omega_{\mathcal{G}}, -D_{\mathcal{L}}\Delta\omega_{\mathcal{L}}) \in \mathbb{R}^{|\mathcal{B}|}$ in (8.1.2). This primary control architecture ensures that, for a given constant power demand $\overline{p}$ in each bus, all the frequencies $\Delta\omega_i$ of the generator buses asymptotically reach the same constant value $\Delta\overline{\omega}$, which is a synchronised frequency deviation, generally different from zero [5], [37].

8.3.1 Economic Dispatch Problem Formulation

The purpose of the Economic Dispatch (ED) problem is to determine the control input P_{m_i} of the generator buses in power systems such that the generator cost is minimised whilst satisfying that the total generation matches the total demand. The ED optimisation problem is formulated as follows [35], [40], [4]:

$$\text{ED} \begin{cases} \min_{P_m,\theta} \; C(P_m) & \triangleq & \frac{1}{2}P_m^T Q P_m = \sum_{i\in\mathcal{G}} \frac{1}{2} Q_i P_{m_i}^2 \\ \text{subject to} & & \\ 0 & = & \underline{1}^T \left(P_m - \nabla_{\mathcal{G}} U(\theta)\right) - \underline{1}^T \nabla_{\mathcal{G}} U(\theta) \\ |\theta_i - \theta_j| & \leq & \alpha_{ij} < \frac{\pi}{2}, \; \forall \, i \in \mathcal{B}, \; j \in \mathcal{N}_i \end{cases} \tag{8.3.4}$$

where $C(P_m)$ is a quadratic cost function, $Q = \text{Diag}(Q_1, \ldots, Q_{|\mathcal{G}|}), \; Q \succ 0, \; Q \in \mathbb{R}^{|\mathcal{G}|\times|\mathcal{G}|}$ is a known positive definite diagonal matrix, the control vector $P_m \in \mathbb{R}^{|\mathcal{G}|} = \text{Col}(P_{m_i})$ has to be designed, and α_{ij} is a positive constant. The single contributions $\frac{1}{2}Q_i P_{m_i}^2$ represents the i-th generator cost.

Assumption 8.4. *Any optimal solution for the ED problem (8.3.4) has the property that the inequality constraint*

$$|\theta_i - \theta_j| < \alpha_{ij} < \frac{\pi}{2}, \quad \forall \, i \in \mathcal{B}, \; j \in \mathcal{N}_i \tag{8.3.5}$$

is strictly satisfied.

Assumption 8.4 is standard in power system analysis [40], [4]). Under Assumption 8.4, the ED problem (8.3.4) can be simplified to a convex quadratic optimisation problem subjected to a linear equality constraint, commonly recognised as Reduced Order Economic Dispatch (RED) [40] [86]:

$$\text{RED} \begin{cases} \min_{u} \; C(u) & \triangleq & \frac{1}{2}P_m^T Q P_m = \sum_{i\in\mathcal{G}} \frac{1}{2} Q_i P_{m_i}^2 \\ \text{subject to} & & \\ 0 & = & \underline{1}^T \hat{p} + \underline{1}^T P_m \end{cases} \tag{8.3.6}$$

Note that the linear constraint in (8.3.6) represents the lossless property of the power network, in which the total power generation matches the total power consumption [5]. The following Lemma holds

Lemma 8.1. *The optimal solution $P_m^\star$ of the RED (8.3.6) is characterised by the identical marginal costs as follows [35]:*

$$Q_i P_{m_i}^\star = Q_j P_{m_j}^\star, \;\; \forall i, j \in \mathcal{G} \tag{8.3.7}$$

Furthermore, any strictly feasible solution of the ED (8.3.4) is optimal solution of the RED (8.3.6) [40]. The vector $\xi^\star \in \mathbb{R}^{|\mathcal{G}|}$ with all equal entries corresponding to the (optimal) identical marginal cost in (8.3.7), which is given by the relation [86]:

$$\xi^\star = \frac{\underline{1}\,\underline{1}^T \hat{p}}{\underline{1}^T Q^{-1} \underline{1}} \tag{8.3.8}$$

In the present paper it is assumed that the optimal value for $\xi^\star$ in (8.3.8) is computed by the same reference maker node in Assumption 8.3. It follows that the reference maker is governed by

the algebraic equation (8.3.8). The optimal control input will be given by [40], [38]:

$$u^\star = Q^{-1}\xi^\star \tag{8.3.9}$$

The underlying idea is to use a SM control architecture which is able to reach the condition (8.3.9) in finite time, by using of both the information coming from the distributed observer scheme and the reference value coming from the reference maker node. It is proven that the frequency deviation asymptotically tends to zero in each generator bus, thus achieving both frequency regulation and RED optimization problem.

Let the vector of deviation in marginal cost be $\Delta\xi \triangleq \xi - \xi^\star$, where ξ is the vector of marginal cost. A variant of dynamic control structure, originally proposed in [38], is proposed in the present chapter to reduce the vector of deviation in marginal cost to zero in finite time, and as a consequence the optimal control input in (8.3.9) is attained in finite time. Compared with existing approaches in [38], [35], [45], the originality of the proposed architecture is represented by the finite time convergence to the optimal control yielding optimal RED.

Proposition 8.2. *Suppose Assumption 8.4 and Lemma 8.1 hold, then, for (8.1.2), the dynamic control scheme*

$$\Delta\dot{\xi} = -W\Delta\xi + \Omega\nu - Q^{-1}\Delta\hat{\omega}_{\mathcal{G}} \tag{8.3.10}$$

$$P_m = Q^{-1}\xi \tag{8.3.11}$$

where $\xi \in \mathbb{R}^{|\mathcal{G}|}$ is the vector of marginal costs, $W = \mathrm{Diag}(W_1, \ldots, W_{|\mathcal{G}|}) \in \mathbb{R}^{|\mathcal{G}|\times|\mathcal{G}|}$, $\Delta\hat{\omega}_{\mathcal{G}} \triangleq \mathrm{Col}(\Delta\hat{\omega}_1, \ldots, \Delta\hat{\omega}_{|\mathcal{G}|})$, and $\Omega \triangleq \mathrm{Diag}(\Omega_1, \ldots, \Omega_{|\mathcal{G}|}) \in \mathbb{R}^{|\mathcal{G}|\times|\mathcal{G}|}$ are positive definite design diagonal matrices, and the discontinuous injection term $\nu = \mathrm{Col}(\mathrm{sign}(\Delta\xi_1), \ldots, \mathrm{sign}(\Delta\xi_{|\mathcal{G}|}))$, $\nu \in \mathbb{R}^{|\mathcal{G}|}$ has to be designed, ensures that:

I) *$\Delta\xi \to 0$ and the RED (8.3.6) are satisfied in a finite time if each scalar component Ω_i of the matrix Ω satisfies*

$$\Omega_i > Q_i^{-1}\Lambda_\omega \tag{8.3.12}$$

Λ_ω is a positive constant.

II) *The frequency regulation is achieved in asymptotic sense.*

I) Note that the dynamics in (8.3.10) are completely decentralised, and consequently each component $\Delta\xi_i$ does not depend on the other ones $\Delta\xi_j,\ j \neq i$. Therefore, it is possible to consider separately each scalar component

$$\Delta\dot{\xi}_i = -W_i\Delta\xi_i - \Omega_i\mathrm{sign}\left(\Delta\xi_i\right) - Q_i^{-1}\Delta\hat{\omega}_i \tag{8.3.13}$$

Note that in equation (8.3.13) the key-novelty is represented by the nonlinear term $\Omega_i\mathrm{sign}\left(\Delta\xi_i\right)$, which was not present in the earlier works [45], [46], [38], [86], where a similar structure for the dynamics in (8.3.13) was proposed. Consider a Lyapunov function

$$V_{c_i} = \frac{1}{2}\Delta\xi_i^2 \tag{8.3.14}$$

Differentiating V_{c_i} along the trajectory of the dynamics in (8.3.13) yields:

$$\begin{aligned} \dot{V}_{c_i} &= -W_i \left|\Delta\xi_i\right|^2 - \Omega_i \left|\Delta\xi_i\right| - \Delta\xi_i Q_i^{-1} \Delta\hat{\omega}_i & (8.3.15) \\ &\leq -\Omega_i \left|\Delta\xi_i\right| + Q_i^{-1} \left|\Delta\hat{\omega}_i\right| \left|\Delta\xi_i\right| & (8.3.16) \end{aligned}$$

In order to guarantee negative definiteness of (8.3.16), one has to verify the following inequality

$$\Omega_i > Q_i^{-1} \left|\Delta\hat{\omega}_i\right| \tag{8.3.17}$$

or, in a more conservative way, it yields

$$\Omega_i > Q_i^{-1} \Lambda_\omega \tag{8.3.18}$$

It follows that $\dot{V}_{c_i} \leq -\eta_i \left|\Delta\xi_i\right|$ for some positive constant η_i. which implies $\Delta\xi_i = 0$ in finite time. Therefore, each component

$$P_{m_i} = Q_i^{-1} \xi_i \tag{8.3.19}$$

of the vector P_m reaches in finite time the optimal value $P_{m_i}^\star$, which proves **I)**.

II) Note that the steady-state solution of (8.1.2) satisfying

$$\begin{aligned} \theta &= \theta^\star \\ \Delta\omega^\star &= \underline{0} \\ P_m^\star &= \nabla U_{\mathcal{G}}(\theta^\star) \end{aligned} \tag{8.3.20}$$

constitutes an optimality condition of equilibrium, as proven in [40]. The aim of the present proof is to show that the trajectories of the closed-loop system asymptotically converge to (8.3.20), by means of a Lyapunov function technique. According to [40] and [45], the closed-loop dynamics can be expanded around steady state:

$$\begin{aligned} \dot{\hat{\theta}} &= \Delta\hat{\omega} & (8.3.21) \\ M_{\mathcal{G}} \Delta\dot{\hat{\omega}}_{\mathcal{G}} &= -D_{\mathcal{G}} \Delta\hat{\omega}_{\mathcal{G}} + Q^{-1} \Delta\xi - \left(\nabla_{\mathcal{G}} U(\hat{\theta}) - \nabla_{\mathcal{G}} U(\theta^\star)\right) \\ 0 &= -D_{\mathcal{L}} \Delta\hat{\omega}_{\mathcal{L}} - \left(\nabla_{\mathcal{L}} U(\hat{\theta}) - \nabla_{\mathcal{L}} U(\theta^\star)\right) & (8.3.22) \\ \Delta\dot{\xi} &= -W \Delta\dot{\xi} + \Omega\nu - Q^{-1} \Delta\hat{\omega}_{\mathcal{G}} & (8.3.23) \end{aligned}$$

Consider the following incremental Lyapunov function:

$$V(\hat{\theta}, \Delta\hat{\omega}_{\mathcal{G}}, \Delta\xi) = \frac{1}{2} \Delta\hat{\omega}_{\mathcal{G}}^T M_{\mathcal{G}} \Delta\hat{\omega}_{\mathcal{G}} + U(\hat{\theta}) - U(\theta^\star) - \nabla U(\theta^\star)^T \left(\hat{\theta} - \theta^\star\right) + \frac{1}{2} \Delta\xi^T \Delta\xi.$$

Under Assumption 8.4, $V(\cdot)$ is strictly convex, which ensures that it is locally positive definite excluding the equilibrium point (8.3.20) [86]. The time derivative of V along the trajectories of the

closed-loop system in (8.3.21)-(8.3.23) yields:

$$\begin{aligned}\dot{V} &= -\Delta\hat{\omega}_{\mathcal{G}}^T D_{\mathcal{G}} \Delta\hat{\omega}_{\mathcal{G}} + \Delta\hat{\omega}_{\mathcal{G}}^T Q^{-1}\Delta\xi - \Delta\hat{\omega}_{\mathcal{G}}^T \nabla_{\mathcal{G}} U(\hat{\theta}) + \Delta\hat{\omega}_{\mathcal{G}}^T \nabla_{\mathcal{G}} U(\theta^\star) \\ &\quad + \Delta\hat{\omega}^T \nabla U(\hat{\theta}) - \nabla U(\theta^\star)^T \Delta\hat{\omega} - \Delta\xi^T W \Delta\xi + \Delta\xi^T \Omega\nu - \Delta\xi^T Q^{-1}\Delta\hat{\omega}_{\mathcal{G}} \quad (8.3.24)\end{aligned}$$

From the developments in part **I)** of Proposition 8.2, the inequality

$$-\Delta\xi^T W \Delta\xi + \Delta\xi^T \Omega\nu < 0, \quad (8.3.25)$$

is satisfied. Given (8.3.25), after straightforward algebraic manipulations, the inequality

$$\dot{V} \leq -\Delta\hat{\omega}_{\mathcal{G}}^T D_{\mathcal{G}} \Delta\hat{\omega}_{\mathcal{G}} - \Delta\hat{\omega}_{\mathcal{G}}^T \nabla_{\mathcal{G}} U(\hat{\theta}) + \Delta\hat{\omega}^T \nabla U(\hat{\theta}) + \Delta\hat{\omega}_{\mathcal{G}}^T \nabla_{\mathcal{G}} U(\theta^\star) - \nabla U(\theta^\star)^T \Delta\hat{\omega} \quad (8.3.26)$$

can be obtained. By exploiting the structure of the right-hand side of (8.3.26), and the substitutions

$$\Delta\hat{\omega}_{\mathcal{L}}^T \nabla_{\mathcal{L}} U(\hat{\theta}) = -\Delta\hat{\omega}_{\mathcal{G}}^T \nabla_{\mathcal{G}} U(\hat{\theta}) + \Delta\hat{\omega}^T \nabla U(\hat{\theta}) \quad (8.3.27)$$

$$-\Delta\hat{\omega}_{\mathcal{L}}^T \nabla_{\mathcal{L}} U(\theta^\star) = \Delta\hat{\omega}_{\mathcal{G}}^T \nabla_{\mathcal{G}} U(\theta^\star) - \nabla U(\theta^\star)^T \Delta\hat{\omega} \quad (8.3.28)$$

are used, thus obtaining

$$\dot{V} \leq -\Delta\hat{\omega}_{\mathcal{G}}^T D_{\mathcal{G}} \Delta\hat{\omega}_{\mathcal{G}} + \Delta\hat{\omega}_{\mathcal{L}}^T \left(\nabla_{\mathcal{L}} U(\hat{\theta}) - \nabla_{\mathcal{L}} U(\theta^\star) \right) \quad (8.3.29)$$

Moreover, given (8.3.22), the vector $\hat{\omega}_{\mathcal{L}}^T$ can be shown to be equal to:

$$\Delta\hat{\omega}_{\mathcal{L}}^T = \left(\nabla_{\mathcal{L}} U(\theta^\star) - \nabla_{\mathcal{L}} U(\hat{\theta}) \right) D_{\mathcal{L}}^{-1} \quad (8.3.30)$$

Note that in (8.3.30) the invertibility property of $D_{\mathcal{L}}$, which is ensured by construction, is used. Substituting for $\Delta\hat{\omega}_{\mathcal{L}}^T$ in (8.3.29), one obtains

$$\dot{V} \leq -\Delta\hat{\omega}_{\mathcal{G}}^T D_{\mathcal{G}} \Delta\hat{\omega}_{\mathcal{G}} - \left(\nabla_{\mathcal{L}} U(\hat{\theta}) - \nabla_{\mathcal{L}} U(\theta^\star) \right)^T D_{\mathcal{L}}^{-1} \left(\nabla_{\mathcal{L}} U(\hat{\theta}) - \nabla_{\mathcal{L}} U(\theta^\star) \right)$$

It follows that

$$\dot{V} < 0. \quad (8.3.31)$$

Therefore, the Lyapunov function is strictly decreasing excluding the equilibrium point (8.3.20). It follows that the closed-loop system trajectories asymptotically converges to (8.3.20), which prove the proposition.

8.4 Simulation Case Study

In this section the performance of the proposed scheme for frequency regulation and ED are evaluated by using the IEEE 39 bus benchmark [96]. This power system, which has been used in other relevant works for assessment purposes (for example in [40], [46], and [45]), and also in Chapter 5 of the present thesis, is composed of an interconnection of 10 generator buses and 29 load buses, as shown

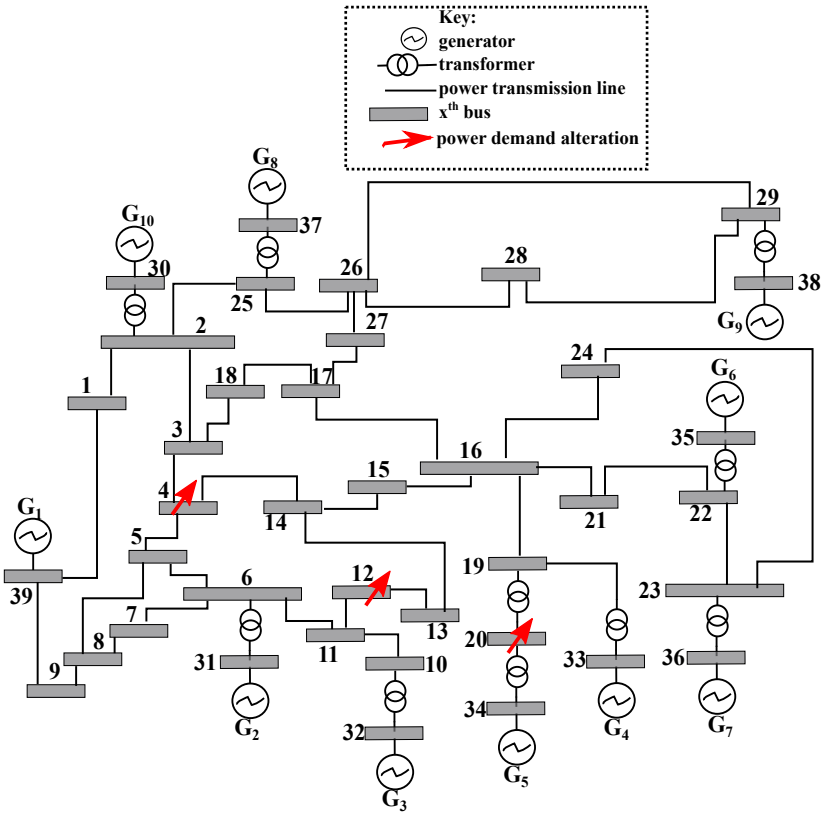

Figure 8.4.1: A schematic of the IEEE 39 bus benchmark. The power demand alterations take place at the 4-th, 12-th, and 20-th load bus.

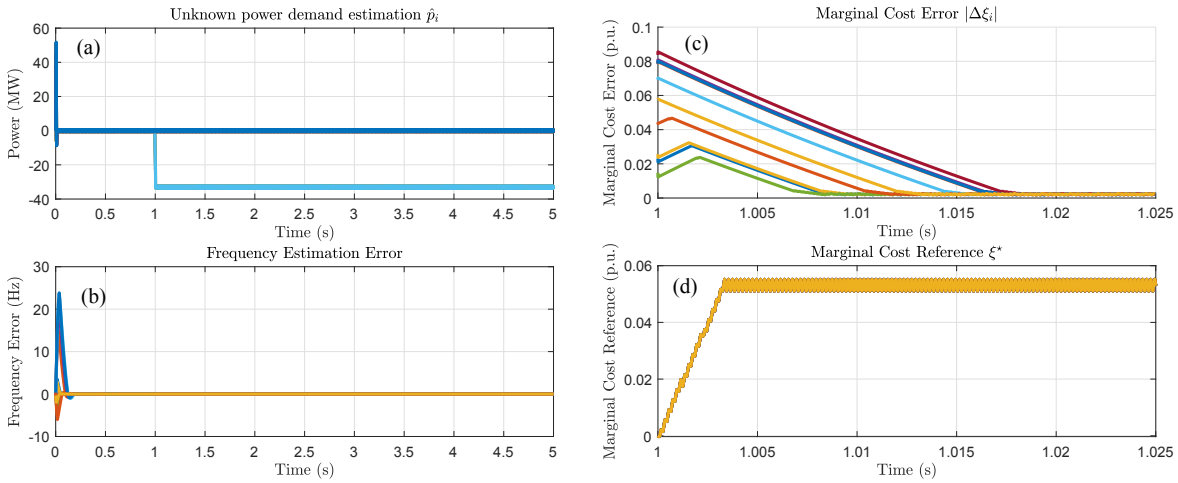

Figure 8.4.2: **(a):** The estimates $\hat{p}_i$ of the unknown power demands; **(b):** The frequency estimation error e_{ω_i}; **(c):** The marginal cost error during the time interval $[1,\ 1.025]$; **(d):** The optimal marginal cost reference during the time interval $[1,\ 1.025]$ seconds.

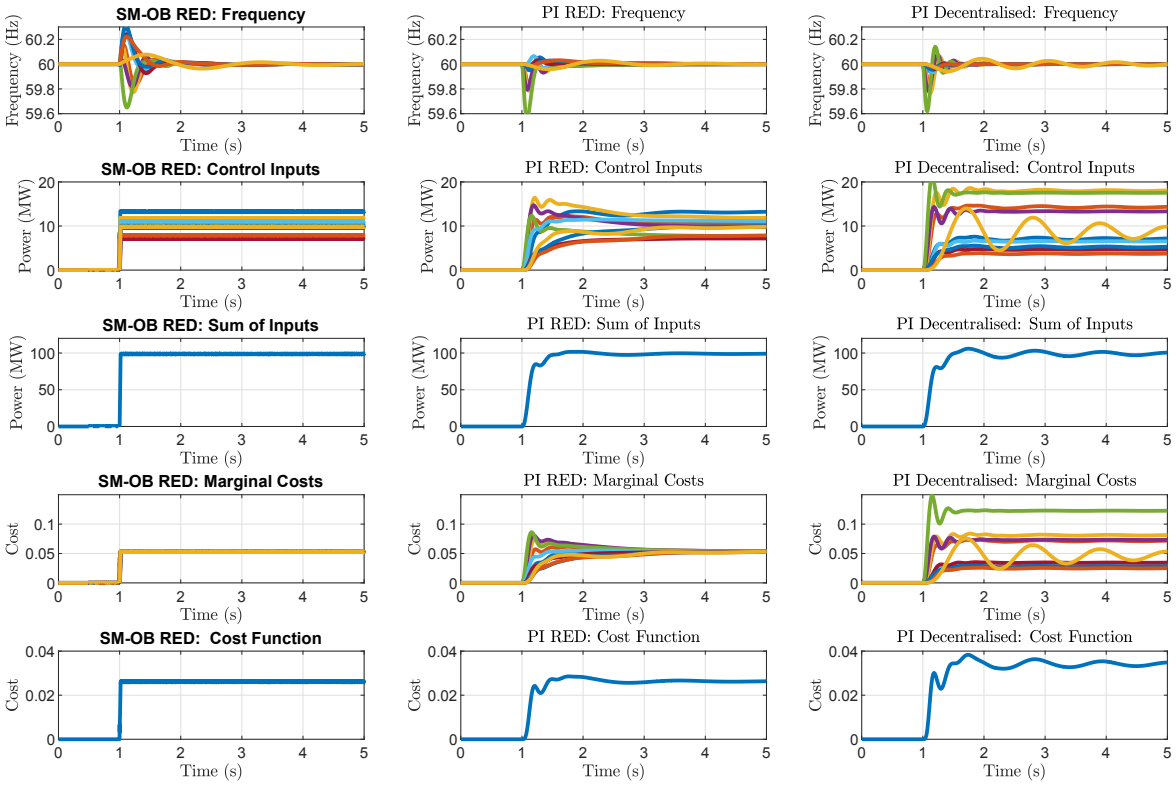

Figure 8.4.3: A comparison of the proposed observer-based control scheme, with the existing ones in the literature. From the top, the following key-indicators are considered: frequency deviations, control inputs, sum of control inputs, marginal costs, cost function.

in the schematic in Figure 8.4.1. The numerical data for this benchmark is reported in [96]. As in [40], [46], and [45], the droop control coefficients are set equal to $D_i = 1\ (p.u.)\ \forall i = 1, \ldots, 39$, and during the simulation, for time $t \geq 1$ seconds, the power demand increases by 33 (MW) at the 4-th, 10-th and 20-th bus.

The generator observer design parameters are $k_{1_{g_i}} = 21$, $k_{2_{g_i}} = 214$, $k_{3_{g_i}} = 250$, $\forall i = 1, \ldots 10$, whilst the load observer gains are $k_{1_{l_i}} = 15$, $k_{2_{l_i}} = 110$, $\forall i = 1, \ldots, 29$. ED design parameters are: $Q = \mathrm{Diag}([0.4,\ 0.0,\ 0.45,\ 0.55,\ 0.7,\ 0.48,\ 0.74,\ 0.53,\ 0.67,\ 0.54])$, and $W = 20I_{(10\times 10)}$. The power network benchmark, together with the proposed observer-based control scheme is implemented in a *Matlab-Simulink R2018a* environment. The fixed integration step size *Ode1* (Euler method) was employed, with an integration step size equal to 50 microseconds. In order to demonstrate the superiority of the proposed scheme with respect to other existing and well-established techniques, a comparison based on this case study is undertaken:

- *SM-OBS RED* denotes the proposed SM observer-based control scheme for frequency regulation and the ED problem;
- *PI-RED* denotes the distributed Proportional Integral (PI) control scheme for the frequency regulation and Reduced Order Economic Dispatch (RED) problem as formulated in [40];
- *PI-Decentralised* denotes a conventional decentralised PI control scheme for frequency regulation.

Figure 8.4.2 shows that the proposed scheme has the ability to estimate in finite time the unknown power demand variation $\hat{p}_i$, which is equal to 33 MW at the 4-th, 10-th and 20-th bus. The negative sign means that the power is associated with an increase of consumption at those buses. Moreover, the frequency estimation errors are steered to zero in finite time. In addition, the marginal cost errors are driven to zero in finite time, thus tracking the marginal cost reference.

Figure 8.4.3 shows an extensive comparison between the proposed scheme and the two well-established control architecture described earlier. From the analysis of this figure, the following comments can be made:

- The frequency is asymptotically steered to zero by all the three control architectures.
- The control inputs counterbalance the growth of power demand. The proposed scheme is characterized by faster controller dynamics, which are able to reach the optimal value in finite time. This results in a perfect counterbalance of 100 MW.
- The marginal costs (which have to be all equal to each other) reach the optimal value in finite time (few seconds) by using the proposed SM-OBS RED, whilst the optimality is asymptotically achieved via PI-RED scheme. In contrast, the decentralised PI architecture is not able to reach the ED requirement.
- The time evolution of the total cost function $C_{(u)}$ in (8.3.4) confirms that the SM-OBS RED achieves in finite time the optimal total generation cost.

From the key-points above, one can conclude that the proposed scheme displays better performance when compared to standard methods. Moreover, by using the observer-estimation techniques it is possible to considerably reduce the number of the sensors required for the implementation of the control scheme.

8.5 Conclusions

In this chapter a novel SM observer-based scheme has been formulated to achieve frequency regulation and ED in structure-preserving power grids composed of an interconnection of generators and load buses. A network of heterogeneous SM observers, connected in a distributed way, has been proposed to estimate the unmeasured frequency deviation in generator buses, and to track the unknown power demand in all the buses in finite time. A SM control architecture was proposed to achieve in finite time the optimal marginal cost for the generator buses. The numerical simulation test case, implemented on the widely used IEEE 39 bus benchmark, has revealed that the proposed scheme displays better performances when compared with existing methods.

Part IV

Identification of the Relative Degree

Chapter 9

Automatic Identification of the Relative Degree of Nonlinear Systems: Application to Sliding Mode Control Design and Experimental Assessment

Abstract In this chapter, a novel approach to identify the relative degree of nonlinear uncertain single-input single-output systems is presented. The proposed approach can be profitably used to design sliding mode controllers even for systems with unknown relative degree. The system is assumed to have an unknown dynamics, and the output is measured in a discrete-time fashion. Provided that a prescribed input signal is applied, it is proven that a set of inequalities holds only for the r-th time derivative of the output, where r denotes the relative degree. A practical algorithm for the relative degree identification is also formulated. Furthermore, a self-configuring sliding mode control architecture is proposed, which automatically selects the controller given the relative degree. The effectiveness of the scheme is demonstrated via a practical set-up composed of a lab-scale overhead crane mechanically coupled with a 12 Volts DC motor. The aim is to identify the relative degree of the position of the crane (the output), with respect to the DC motor armature voltage (the control input). The experimental results reveal high accuracy of the proposed strategy for the identification of the relative degree.

9.1 Introduction

The main contribution of the present chapter is the design and the experimental-based assessment of a method to automatically identify the relative degree of uncertain nonlinear systems affine in the input signal. The method is particularly useful in sliding mode control design, since in that case the relative degree of the input-output mapping between the control input and the sliding variable has to be perfectly known to be able to select the correct "order" of the sliding mode controller [112]. For this reason, in the chapter, the exploitation of the proposed method in a sliding mode control design context is also addressed as a case study. More precisely, a self-configuring sliding mode control

scheme is proposed, which automatically selects the order of the sliding mode controller by using the proposed relative degree identification approach run-time. In the proposed method the identification of the relative degree is performed via a recursive algorithm which is based on analytical criteria. The test input signal is a triangular wave with prescribed maximum value and slope. This particular input signal is able to excite the system in such a way that the relative degree can be automatically identified. Note that the proposed scheme cannot be considered a discrete-time implementation of the practical relative degree concept developed in [59]. In that interesting work a step-input signal was selected to excite the system, and a fixed order Levant's differentiator was used to produce the derivatives of the system output which need to be analysed in order to detect the discontinuity which allow one to conclude about the relative degree. The benefit of Levant's method is the use of a single differentiation, while the limit is that, if the true relative degree of the system exceeds the selected Levant's differentiator fixed order, the identification cannot be done. The difference of the present proposal is the flexibility given by the fact that it is not required to a priori make a decision about the fixed order of the differentiator to use. Through the recursive strategy proposed in the present chapter, any relative degree can be automatically identified since the method, by itself, is capable of selecting the order of the Levant's differentiator which is suitable to perform the identification of the relative degree in any different usage.

9.2 System Descriptions, Assumptions and Facts

Next consider an uncertain nonlinear SISO system in the form of

$$\begin{array}{rcl} \dot{x} & = & a\left(x\right)+b\left(x\right)u \\ y & = & \sigma\left(x\right), \end{array} \tag{9.2.1}$$

where the control input $u \in \mathbb{R}$, $x \in \mathbb{R}^n$ (the knowledge of the dimension of the state variable vectors it is not required in the present framework), whilst $a(\cdot)$, and $b(\cdot)$ are unknown smooth functions.

Definition 9.1 (Relative Degree)**.** Given the dynamical system in (9.2.1), if the input signal u explicitly appears for the first time on the r-th time derivative of the output $\sigma(x)$, then the positive integer number $r \in \mathbb{N}$ is called the relative degree of the output $\sigma(x)$, with respect to the input u. This implies

$$\begin{array}{rcl} L_b L_a^{(i)}\sigma(x) & = & 0\ \forall i = 1,\ldots,r-2 \\ L_b L_a^{(r-2)}\sigma(x) & \neq & 0 \end{array} \tag{9.2.2}$$

Given the system of equation (9.2.2), it can be checked that the relation [47]:

$$\sigma^{(r)}(x) = h(x) + g(x)u. \tag{9.2.3}$$

Definition 9.1 is valid only if the following assumption is imposed:

Assumption 9.1. *Suppose there exists a domain $\mathbb{X} \subseteq \mathbb{R}^n$,. For any $x \in \mathbb{X}$, the smooth uncertain*

functions $h(x)$, $g(x)$ in (9.2.3) are bounded [54]. Specifically, the following inequalities hold

$$-C_h \leq h(x) \leq C_h, \quad \forall x \in \mathbb{X} \tag{9.2.4}$$

$$K_m \leq g(x) \leq K_M, \quad \forall x \in \mathbb{X} \tag{9.2.5}$$

where the positive constants C_h, K_m, K_M are assumed to be known. Furthermore, the relative degree r of the system (9.2.1) is unknown but constant and finite. Therefore, it is upper-bounded as follows

$$r \leq R, \tag{9.2.6}$$

where $R \in \mathbb{N}$ is a known positive integer.

Remark 9.1. Note that (9.2.5) implies that the function $g(\cdot)$ is non-zero uniformly on the domain $\mathbb{X}$. This is standard in sliding mode control theory (see, e.g., [115] [53] [58]), and it is also satisfied in practice, since the operation region of any controlled plant is bounded [115].

Given (9.2.3) and (9.2.4)-(9.2.5), the differential inclusion

$$\sigma^{(r)}(x) \in [-C_h, C_h] + [K_m, K_M]u \tag{9.2.7}$$

can be introduced. Let the output σ be measured in a discrete-time fashion by employing a constant sampling time τ. The time derivatives of the output are not measured, then they must be estimated via discrete-time sliding mode-based differentiation formulated in [116]. The discrete-time architecture for the output measurement is also in accordance with practical implementations, as it will be clarified in Section. It is also assumed that the (unknown) output derivatives $\sigma^{(i)}$ are bounded as [1]

$$\left|\sigma^{(i)}\right| < D_i, \ \forall i = 1, \dots r. \tag{9.2.8}$$

where the positive constants D_i are assumed to be known from an engineering understanding of the system. Following [116], there exists a positive constant μ such that

$$\left|\sigma^{(0)} - \hat{\sigma}^{(0)}\right| \leq \mu\tau^{r+1} \tag{9.2.9}$$

where $\hat{\sigma}^{(0)}$ represents an estimate of $\sigma^{(0)}$. In addition, the following parameters will be considered:

$$\delta_i = \max\left\{\tau^{r-i+1}, \tau D_{i+1}\right\} \ \forall i = 1, \dots, r. \tag{9.2.10}$$

$$\delta = \max\left\{\delta_i\right\}, \tag{9.2.11}$$

The inequality

$$\left|\sigma^{(i)} - \hat{\sigma}^{(i)}\right| \leq \mu\delta, \ \forall i = 1, \dots, r. \tag{9.2.12}$$

[1] The explicit dependence of the signals on the state vector x is omitted from this point of the chapter onwards for the sake of readability.

is satisfied. By making use of (9.2.12), one gets:

$$\sigma^{(r)} - \hat{\sigma}^{(r)} \in [-\mu\delta, \mu\delta]. \tag{9.2.13}$$

It follows that (9.2.7) can be rewritten in the more conservative way:

$$\hat{\sigma}^{(r)}(t_k) \in [-C_h - \mu\delta, C_h + \mu\delta] + [K_m, K_M]u(t_k). \tag{9.2.14}$$

where t_k is a specific time instant. Define

$$C \triangleq C_h + \mu\delta, \tag{9.2.15}$$

then, from (9.2.15) it yields:

$$\hat{\sigma}^{(r)}(t_k) \in [-C, C] + [K_m, K_M]u(t_k). \tag{9.2.16}$$

9.3 Relative Degree Identification Scheme Design

In this section, the proposed relative degree identification scheme is developed. More precisely, for a given test input signal defined in a discrete-time domain, only the discrete-time forward difference of the r-th time derivative of the output σ satisfies a set of inequalities. Suppose that the uncertain SISO system (9.2.1) is excited by the following test input signal, which can be easily implemented on a computer-based scheme:

$$u(t_k) = \begin{cases} 0 & \text{if } t_k \leq t^\star - t_c \\ u(t_{k-1}) + \tau\Delta u & \text{if } t^\star - t_c < t_k \leq t^\star \\ u(t_{k-1}) - \tau\Delta u & \text{if } t^\star < t_k \leq t^\star + t_c \\ 0 & \text{if } t_k > t^\star + t_c \end{cases} \tag{9.3.1}$$

where τ is the same sampling time used for the measurement of the output (it follows that the generic time instant $t_k = k\tau$), $t^\star$ is an arbitrarily chosen time instant (multiple of the sampling time τ) such that the sliding mode differentiator has reached convergences, t_c has to be designed (it is multiple of the sampling time τ as well). The positive incremental constant Δu in is given by

$$\Delta u = \frac{\Omega}{t_c}, \tag{9.3.2}$$

where the positive constant Ω has to be designed also. Exploiting the structure of the input signal in (9.3.1) it is apparent that

$$\begin{aligned} u(t^\star - t_c) &= 0 \\ u(t^\star) &= \Omega \\ u(t^\star + t_c) &= 0. \end{aligned} \tag{9.3.3}$$

Figure 9.3.1 shows a generic example of the adopted test-input signal together with a numerical representation of the introduced design constants.

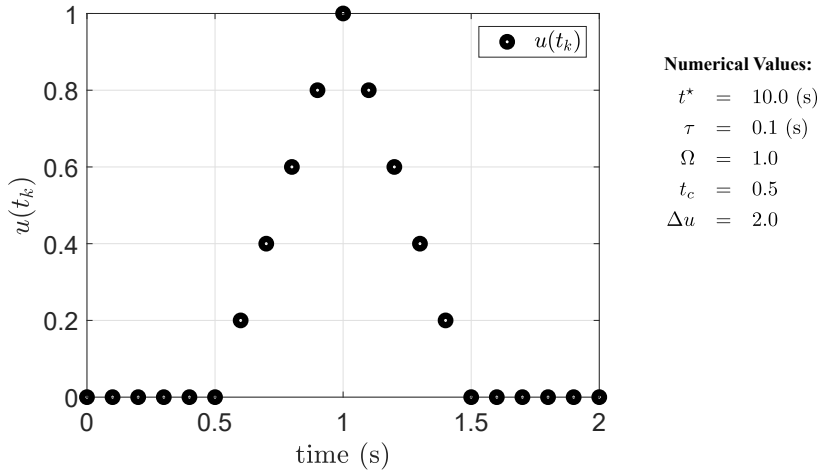

Figure 9.3.1: Time evolution of an example of the test input signal governed by (9.3.1). The numerical representation of the variables is also reported in the figure.

The following proposition will now be proven

Proposition 9.1. *Given the uncertain system (9.2.1), the test input signal (9.3.1), and the differential inclusion (9.2.16), if that the positive constant Ω in (9.3.1) satisfies*

$$\Omega > \frac{4C}{K_m}, \tag{9.3.4}$$

and the time interval t_c satisfies

$$t_c < \frac{2C}{C + K_M \Omega}, \tag{9.3.5}$$

then:

Ia) *If the relative degree of (9.2.1) is equal to r, then:*

$$\Delta_{[t_c]}\hat{\sigma}^{(r)}(t^\star - t_c) \in [-2C, 2C] \tag{9.3.6}$$

$$\Delta_{[t_c]}\hat{\sigma}^{(r)}(t^\star) > 2C \tag{9.3.7}$$

$$\Delta_{[t_c]}\hat{\sigma}^{(r)}(t^\star + t_c) < -2C \tag{9.3.8}$$

$$\Delta_{[t_c]}\hat{\sigma}^{(r)}(t^\star + 2t_c) \in [-2C, 2C]. \tag{9.3.9}$$

where the expression $\Delta_{[t_c]}\hat{\sigma}^{(r)}(t) = \hat{\sigma}^{(r)}(t) - \hat{\sigma}^{(r)}(t - t_c)$ represents the forward difference with fixed spacing t_c, determined at a generic time instant t.

IIa) *The conditions (9.3.6)-(9.3.9) are not satisfied for all the inferior time derivatives, i.e. for $\sigma^{(i)}$ with $i = 1, \ldots, r-1$.*

Proof. Given (9.2.16), (9.3.1), and (9.3.3), it can be shown that:

$$\begin{aligned} \hat{\sigma}^{(r)}(t^\star - t_c) &\in [-C, C] && (9.3.10)\\ \hat{\sigma}^{(r)}(t^\star) &\in [-C, C] + [K_m, K_M]\Omega && (9.3.11)\\ \hat{\sigma}^{(r)}(t^\star + t_c) &\in [-C, C] && (9.3.12)\\ \hat{\sigma}^{(r)}(t^\star + 2t_c) &\in [-C, C] && (9.3.13) \end{aligned}$$

Furthermore, for each generic time time instant t, it is possible to compute the discrete forward difference of $\hat{\sigma}^{(r)}$ with spacing t_c as:

$$\Delta_{[t_c]}\hat{\sigma}^{(r)}(t) = \hat{\sigma}^{(r)}(t) - \hat{\sigma}^{(r)}(t - t_c) \tag{9.3.14}$$

Given the set of differential inclusions in (9.3.10)-(9.3.13), if the design constant Ω satisfies (9.3.4), it can be shown that $\Delta_{[t_c]}\hat{\sigma}^{(r)}$ satisfies (9.3.10)-(9.3.13), which proves **Ia).**

IIa) Following [117], it is possible to determine the expression for the differential inclusions of the $(r-i)$-th estimate derivative of the output σ. These can be shown to be:

$$\begin{aligned} \hat{\sigma}^{(r-i)}(t^\star - t_c) &\in [-C, C]\tfrac{(t^\star - t_c)^i}{i!}\\ \hat{\sigma}^{(r-i)}(t^\star) &\in [-C, C]\tfrac{(t^\star)^i}{i!} + [K_m, K_M]\Omega\tfrac{t_c^i}{i!}\\ \hat{\sigma}_{(r-i)}(t^\star + t_c) &\in [-C, C]\tfrac{(t^\star + t_c)^i}{i!} + [K_m, K_M]\Omega\tfrac{t_c^i}{i!} \end{aligned} \tag{9.3.15}$$

The discrete forward difference of $\hat{\sigma}^{(r-i)}$ with spacing t_c follows:

$$\begin{aligned} \Delta_{[t_c]}\hat{\sigma}^{(r-i)}(t^\star - t_c) &\in [-C, C]\tfrac{(t_c)^i}{i!}\\ \Delta_{[t_c]}\hat{\sigma}^{(r-i)}(t^\star) &\in [-C, C]\tfrac{(t_c)^i}{i!} + [K_m, K_M]\Omega\tfrac{t_c^i}{i!}\\ \Delta_{[t_c]}\hat{\sigma}_{(r-i)}(t^\star + t_c) &\in [-C, C]\tfrac{(t_c)^i}{i!} \end{aligned} \tag{9.3.16}$$

If both the inequalities

$$\begin{aligned} (C + K_M\Omega)\,\tfrac{(t_c)^i}{i!} &< 2C\\ C\tfrac{(t_c)^i}{i!} &< 2C \end{aligned} \tag{9.3.17}$$

are verified, it follows that (9.3.10)-(9.3.13) hold only for the r-th derivative of the output. Solving (9.3.17) for t_c, it yields:

$$\begin{aligned} t_c &< \left(\tfrac{2C}{C + K_M\Omega} i!\right)^{1/i}\\ t_c &< (2i!)^{(1/i)} \end{aligned} \tag{9.3.18}$$

Note that the function $(\alpha i!)^{1/i}$ with $i \in \mathbb{N}$ and α a positive real constant is monotonically increasing. Therefore, the most conservative inequality for t_c can be shown to be:

$$t_c < \frac{2C}{C + K_M\Omega} \tag{9.3.19}$$

which proves **IIa).** □

Remark 9.2. Note that the influence of the initial conditions of $\hat{\sigma}^{(r-i)}$ in (9.3.15) are not considered.

This because the derivatives of the output are estimate via Levant's differentiator, and the initial conditions can be arbitrarily imposed equal to zero. Following [117], in case the initial conditions for the Levant's differentiator estimates differ from zero, the more conservative inequality for the design constant to be satisfied are:

$$t_c < \frac{2C - R\rho_M}{C + K_M\Omega} \tag{9.3.20}$$

where ρ_M represent the maximum value of the magnitude of the initial conditions for$\hat{\sigma}^{(i)}(t=0)$, $i = 1, \ldots, r-1$. Furthermore, in [117] the time interval t_c was set equal to the sampling time τ, i.e. $t_c = \tau$. This can significantly limit the practical applicability of the proposed scheme. More precisely, in experimental set-ups may not be realistic to have a control input with instant jumps with respect to sampling time as happened in [117] :

$$\begin{aligned} u(t^\star - \tau) &= 0 \\ u(t^\star) &= \Omega \\ u(t^\star + \tau) &= 0. \end{aligned} \tag{9.3.21}$$

Differently, in this chapter, it has been shown that the proposed scheme can easily be extended to the case where the design time interval t_c is a multiple of the sampling time τ.

A particular case of Proposition 9.1 will now be considered, which is in accordance with the features of experimental set-up, as it will be clarified in the sequel. Specifically, consider the following modified version of (9.2.4):

$$-C_h \leq h(x) \leq 0 \tag{9.3.22}$$

According to (9.3.22), the sign of the unknown function $h(\cdot)$ is known from a physical understanding of the system. Therefore, the differential inclusion in (9.2.14) can be modified accordingly

$$\hat{\sigma}^{(i)}(t_k) \in [-C, \mu\delta] + [K_m, K_M]u(t_k). \tag{9.3.23}$$

Proposition 9.2. *Given the uncertain system in (9.2.1), the test input signal in (9.3.1), and the differential inclusion in (9.3.23), suppose that the positive constant Ω of the triangular input signal is chosen such that*

$$\Omega > \frac{2C + \mu\delta}{K_m}, \tag{9.3.24}$$

and the time interval t_c is chosen such that

$$t_c < \frac{C}{K_M\Omega + \mu\delta} \tag{9.3.25}$$

***Ib)** If the relative degree of the system (9.2.1) is equal to r, the following relations hold*

$$\Delta_{[t_c]}\hat{\sigma}^{(r)}(t^\star - t_c) \in [-\tilde{C}, \tilde{C}] \tag{9.3.26}$$

$$\Delta_{[t_c]}\hat{\sigma}^{(r)}(t^\star) > \tilde{C} \tag{9.3.27}$$

$$\Delta_{[t_c]}\hat{\sigma}^{(r)}(t^\star + t_c) < \tilde{C} \tag{9.3.28}$$

$$\Delta_{[t_c]}\hat{\sigma}_{(r)}(t^\star + 2t_c) \in [-\tilde{C}, \tilde{C}] \tag{9.3.29}$$

where

$$\tilde{C} \triangleq C + \mu\delta. \tag{9.3.30}$$

IIb) *The conditions in (9.3.27)-(9.3.28) are not satisfied for all the inferior time derivative, i.e. for $\sigma^{(i)}$ with $i = 1, \ldots, r-1$.*

Sketch of the Proof Inspired by [117], and exploiting the proof of Proposition 9.1, the following forward differences hold

$$\begin{aligned} \Delta_{[t_c]}\hat{\sigma}^{(r)}(t^\star - t_c) &\in [-C - \mu\delta, C + \mu\delta] \qquad (9.3.31)\\ \Delta_{[t_c]}\hat{\sigma}^{(r)}(t^\star) &\in [-C - \mu\delta, C + \mu\delta] + [K_m\Omega, K_M\Omega]\\ \Delta_{[t_c]}\hat{\sigma}^{(r)}(t^\star + t_c) &\in [-C - \mu\delta, C + \mu\delta] - [K_m\Omega, K_M\Omega]\\ \Delta_{[t_c]}\hat{\sigma}^{(r)}(t^\star + t_c) &\in [-C - \mu\delta, C + \mu\delta]. \qquad (9.3.32) \end{aligned}$$

Given (9.3.31)-(9.3.32), if (9.3.24) holds, then part **Ib)** of Proposition 9.2 is proven. As for part **IIb)**, the following inclusions yield

$$\begin{aligned} \Delta_{[t_c]}\hat{\sigma}^{(r-i)}(t^\star - t_c) &\in [-C, \mu\delta]\frac{t_c^i}{i!} \qquad (9.3.33)\\ \Delta_{[t_c]}\hat{\sigma}^{(r-i)}(t^\star) &\in [-C, \mu\delta]\frac{t_c^i}{i!} + [K_m, K_M]\Omega\frac{t_c^i}{i!}\\ \Delta_{[t_c]}\hat{\sigma}^{(r-i)}(t^\star + t_c) &\in [-C, C]\frac{t_c^i}{i!}. \qquad (9.3.34) \end{aligned}$$

If the inequality in (9.3.25) is fulfilled, then according to [117] again, also part **IIb)** holds.

Figure 9.3.2 shows a visual interpretation of the proposed identification scheme. Specifically, the aim of the scheme is to make $\Delta_{[t_c]}\hat{\sigma}^{(r)}(t^\star)$ and $\Delta_{[t_c]}\hat{\sigma}^{(r)}(t^\star + t_c)$ go out of the region $[-2C, 2C]$.

In addition, given Proposition 9.1 and Proposition 9.2, it is possible to formulate the (practical) Algorithm 1, which is written in a pseudo-code notation.

Remark 9.3. Note that, under Assumption 9.1, the relative degree is assumed to be unknown, but finite and constant on the domain $(\mathbb{X})$. Assumption 9.1 can be partially relaxed. In particular, for a given i-th iteration index of the **FOR** cycle in Algorithm 1, the relative degree can vary only on the domain of integer numbers $i+1, \ldots, R \in \mathbb{N}$. This can be understood by recalling that the relative degree is identified from the lower to the higher values (to understand this, the reader is referred to the architecture of Algorithm 1). Furthermore, according to the proof of Proposition 9.1, the inequalities (9.3.7)-(9.3.8) are not satisfied for all the inferior time derivatives of the output σ. On the contrary, the proposed scheme fails whenever at the i-th iteration the relative degree changes assuming a value on the interval of integers $1, \ldots, i-1$.

Relative Degree Identification and Self-Configuring Sliding Mode Control The designed identification scheme for the the relative degree can be profitably employed both in an off-line and on-line configuration. For the off-line one, one can excite the system via the proposed identification scheme, thus selecting the correct order for the sliding mode controller, by making reference, for example, to the SM schemes proposed in [112]. Consider now dynamical systems with time-varying relative

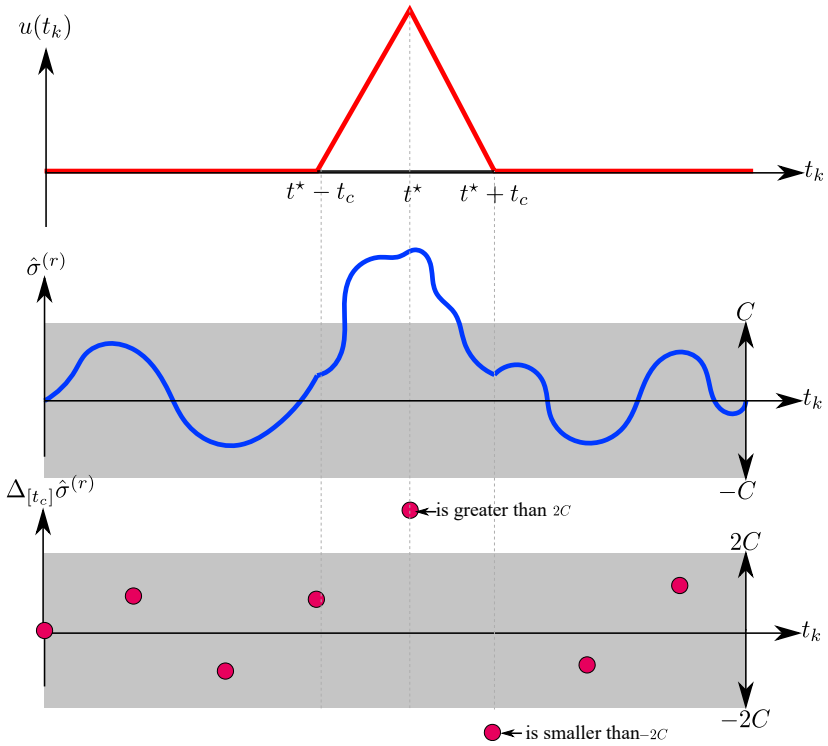

Figure 9.3.2: A visual interpretation of the test input signal, together with the time evolution of the r-th time derivative of the output and the forward difference $\Delta_{[t_c]}\hat{\sigma}^{(r)}$. **Top**: Time evolution of the control input. **Centre**: Time evolution of $\hat{\sigma}^{(r)}$. **Bottom** Time evolution of $\Delta_{[t_c]}\hat{\sigma}^{(r)}$

1. Choose reasonable values for C_h, C, $\tilde{C}$, K_m, K_M, and R from the understating of the system;
2. Choose the constant Ω of the test input signal satisfying (9.3.4) (or the less conservative version (9.3.24));
3. Choose the time interval t_c satisfying (9.3.5) (or (9.3.25));
4. **FOR** $i = 1, \ldots, R$
   (a) Use an i-th order sliding mode differentiator [112] to robustly estimate $\sigma^{(i)}$ in finite time;
   (b) Select a reasonable value for $t^\star$, such that the i-th order sliding mode differentiator has reached convergence before taking the next step;
   (c) Apply the test input signal (9.3.1) and determine the sampled values of $\hat{\sigma}^{(i)}$ at the time instants $t^\star$ and $t^\star + t_c$;
   (d) **IF** $\Delta_{[t_c]}\hat{\sigma}^{(i)}$ satisfies (9.3.7)-(9.3.8) (or (9.3.27)-(9.3.28)) **STOP, the relative degree is equal to** i;
   (e) **ELSE** $i = i + 1$, **RETURN to STEP 4a**);

Algorithm 1: Relative Degree Identification Algorithm

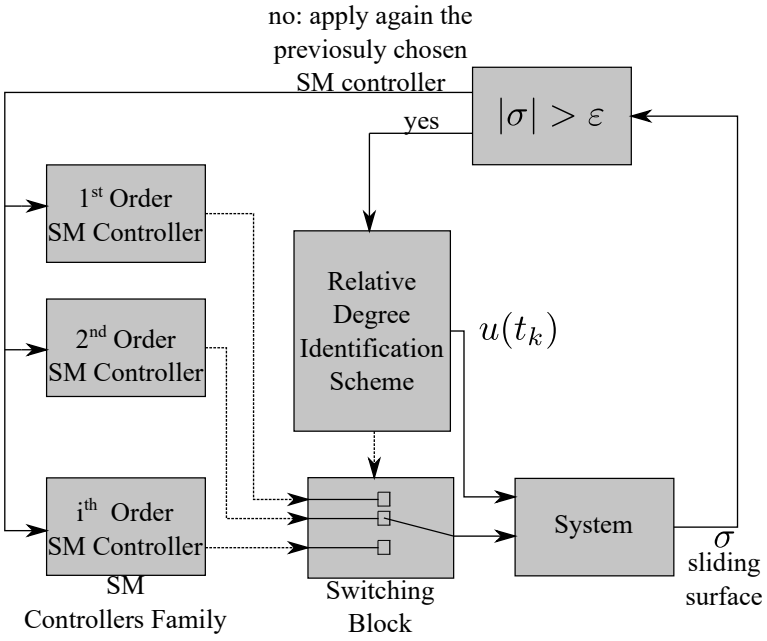

Figure 9.3.3: A block diagram of a self-configuring SM control architecture. Whenever the sliding motion is lost, i.e., the magnitude of the sliding variable passes an arbitrary chosen small threshold ε, the relative degree identification scheme is re-executed in an online configuration, thus selecting another SM controller once the relative degree is identified.

degree. The proposed architecture can be applied in an on-line configuration, implementing a self-configuring control architecture. As proven in [54], the magnitude of the sliding variables remains bounded whenever perturbations make the relative degree of the system fluctuate. If the magnitude of the sliding variable passes an arbitrarily (small) threshold

$$|\sigma| > \varepsilon, \tag{9.3.35}$$

the scheme in Algorithm 1 will be executed, thus selecting the correct controller, as shown in Figure 9.3.3.

Remark 9.4. Note that, from practical perspective, relative degree varies with respect to time due to both changes to working points or to the system configurations. Relevant examples which can be mentioned are micro-grid systems, which exhibit relative degree equal to one in the grid-connected operation mode, whilst relative degree is equal to two in islanded operation mode [118]. Also the kinematic dynamics of vehicle motion exhibit changes in relative degree [54].

9.3.1 Preliminaries and Set-up Description

The lab-scale overhead crane shown in Figure 9.3.4 is adopted to experimentally demonstrate the validity of the relative degree identification scheme. Note that the crane can move in all the three dimensions ($x-y-z$ axis in Figure 9.3.4), only the x-displacement is considered in this framework for the sake of simplicity. It can be shown that the other two displacements display similar features. The experimental set-up is available at Process Control Laboratory of University of Pavia, and it is composed of the following elements: i) the structure of the lab-scale overhead crane; ii) a 12

Volts DC motor, mechanically coupled with the transmission belt in Figure 9.3.4; $iii)$ the encoder (CUI AMT-102V), which is fixed to the belt shaft as shown in Figure 9.3.4. The encoder measures the angular position of the shaft of the belt, which is related to the x- displacement of the crane by making use of basic mechanical relations. The resolution of the encoder is set by default equal to 1 millimetre. The interested reader is referred to [119] for further technical data of the encoder.

The sampling time τ for the measurement and for the test-input signal is chosen equal to $\tau = 0.01$ seconds. The value for the sampling time represents the default setting for the experimental set-up. Furthermore, the resulting discrete-time data acquisition and control architecture result in being acceptably fast to deal with the considered electromechanical system [120]. The armature voltage of the DC motor is considered the control input u, whilst the x- displacement of the crane is the output measurement σ. The objective here is to identify the relative degree of the x-displacement of the crane with respect to the armature voltage of the DC motor.

9.3.2 Simulation Results based on Linear Identified Model

A second order transfer function $G(s)$ in the form of

$$G(s) = \frac{\rho}{s\,(Ts+1)} = \frac{0.002}{s\,(0.175s+1)} \tag{9.3.36}$$

can be adopted to describe the dynamical model of the crane, where ρ represents the dc-gain, and T represents the time constant. Moreover, it follows in the Laplace domain that

$$\sigma(s) = G(s)u(s) \tag{9.3.37}$$

Note that the transfer function in (9.3.36) represents a simplified second order input-output relation in the Laplace domain of the overall mechanical set-up, composed of the DC motor and the crane, mechanically coupled with the DC motor via a transmission belt. The state-space representation of (9.3.36) can be shown to be

$$\begin{aligned} \dot{x}_1 &= \dot{x}_2 && (9.3.38)\\ \dot{x}_2 &= -\frac{1}{T}x_2 + \frac{\rho}{T}u && (9.3.39)\\ \sigma &= x_1. && (9.3.40) \end{aligned}$$

where x_1 represents the x-displacement of the crane, and x_2 represents its speed in the x-direction. By exploiting the structure of (9.3.38)-(9.3.40), it is easy to show that the relative degree of the output $\sigma = x_1$ with respect to the control input u is equal to 2.

Generally, in the literature a more accurate dynamical model is adopted for DC motor simulation

and analysis, which can be shown to be [121]

$$\begin{aligned} \dot{x}_1 &= x_2 && (9.3.41)\\ J\dot{x}_2 &= k_t x_3 - d - Dx_2 && (9.3.42)\\ L\dot{x}_3 &= u - Rx_3 - \lambda_o x_2 && (9.3.43)\\ \sigma &= x_1 && (9.3.44) \end{aligned}$$

where x_1 is the angular position of the DC motor, x_2 is its speed, x_3 is the armature current, u is the armature voltage, and d is the load torque. The introduced model parameters are: J is the inertia, k_t is the torque constant, D is the damping factor, L is the armature inductance, R is the armature resistance, and λ_0 is the electromotive force constant. Therefore, looking at the physical system, i.e. the over-head lab-scale crane, it is not straightforward if it exhibits a relative degree 2 as appears in (9.3.38)-(9.3.40), or relative degree 3, as it appears in (9.3.41)-(9.3.44). For this reason, the relative degree identification method can be profitably applied to the considered mechanical experimental set-up.

Given (9.3.38)-(9.3.40), it is possible to define the (uncertain) function

$$h(x_2) \triangleq -x_2/T \leq 0 \tag{9.3.45}$$

which is always smaller or equal to zero. This is true from a basic understanding of the experimental configuration, in which the speed x_2 of the crane in the actual laboratory configuration is always non-negative.

Note also that the function (9.3.45) is bounded, i.e., by making use of (9.3.22)

$$-C_h \leq h(x_2) \leq 0 \tag{9.3.46}$$

This is always verified if x_2 (the speed of the lab-scale overhead crane) remains bounded. Due to physics of the system, the lab-scale overhead crane exhibits a Bounded-Input Bounded State (BIBS) stability. In particular, given a bounded voltage applied to the armature of the DC motor, the produced speed is also bounded [122]. This property has been generally exploited when sliding mode control has been applied to DC motor drives, as illustrated in [64] and [121], as well as to the design of state observers for mechanical systems, as shown in [75].

The design constants in (9.3.22), (9.2.15), (9.3.30) are chosen as $C_h = 49$ (mm/s^2), $C = C_h + \mu\delta = 50$ (mm/s^2), and $\tilde{C} = C + \mu\delta = 51$ (mm/s^2), respectively. The constants in (9.2.5) are chosen, respectively, equal to $K_m = 10$ (mm^2/s/V), and $K_M = 11$ (mm^2 /s/ V). The numerical representation of the inequality in (9.3.24) ca be shown to be:

$$\Omega > 10.1 \text{ (V)}. \tag{9.3.47}$$

which satisfy the safety constraints prescribed for the DC motor $\Omega \leq 12$ V. The acceptable value $\Omega = 11$ (V) is selected. Moreover, by substituting the values in (9.3.25), one gets

$$t_c < 0.41 \text{ (s)}. \tag{9.3.48}$$

The time interval t_c is set equal to $t_c = 0.40$ (s). In addition, the time interval $t^\star = 1.6$ (s). If the relative degree is equal to r, the numerical representation of the set of inequalities in (9.3.27)-(9.3.28) is given by:

$$\Delta_{[0.4]}\hat{\sigma}^{(r)}(1.6) > 51 \tag{9.3.49}$$

$$\Delta_{[0.4]}\hat{\sigma}^{(r)}(2) < 51. \tag{9.3.50}$$

The system in (9.3.38)-(9.3.40) is simulated in Matlab/Simulink, by making use of the solver *Ode1 (Euler)*, with a fixed integration step time set equal to 10 milliseconds. Figure 9.3.5-(a) shows on the top as a solid (blue) line the time evolution of the simulated output variable σ_{sim}. Following [117], and also according to Algorithm 1, successive higher order sliding mode differentiators are employed to estimate successive time derivatives of the output. In particular the Levant's differentiator

$$\dot{\hat{\sigma}}^{(0)} = -k_{11}\left\lfloor \hat{\sigma}^{(0)} - \sigma^{(0)} \right\rceil^{\frac{1}{2}} + \hat{\sigma}^{(1)} \tag{9.3.51}$$

$$\dot{\hat{\sigma}}^{(1)} = -k_{21}\left\lfloor \hat{\sigma}^{(0)} - \sigma^{(0)} \right\rceil, \tag{9.3.52}$$

can estimate $\sigma^{(1)}$. The positive design constants k_{11} and k_{21} can be tuned according to [112]. The time evolution of $\hat{\sigma}^{(1)}$ for the simulation test case is shown as a solid (blue) line in Figure 9.3.5-(b). According to Figure 9.3.5-(b), the forward difference $\Delta_{[0.4]}\hat{\sigma}^{(1)}$ does not satisfy (9.3.49)-(9.3.50). A third order sliding mode differentiator can be employed to estimate $\hat{\sigma}^{(2)}$

$$\dot{\hat{\sigma}}^{(0)} = -k_{12}\left\lfloor \hat{\sigma}^{(0)} - \sigma^{(0)} \right\rceil^{\frac{2}{3}} + \hat{\sigma}^{(1)} \tag{9.3.53}$$

$$\dot{\hat{\sigma}}^{(1)} = -k_{22}\left\lfloor \hat{\sigma}^{(0)} - \sigma^{(0)} \right\rceil^{\frac{1}{3}} + \hat{\sigma}^{(2)} \tag{9.3.54}$$

$$\dot{\hat{\sigma}}^{(2)} = -k_{32}\left\lfloor \hat{\sigma}^{(0)} - \sigma^{(0)} \right\rceil^{0}, \tag{9.3.55}$$

where the positive design constants k_{12}, k_{22}, k_{32} can be tuned again relying on [112]. According to Figure 9.3.5-(c), the forward difference $\Delta_{[0.4]}\hat{\sigma}^{(2)}$ fulfils (9.3.49)-(9.3.50). Consequently, the relative degree identified via simulation is equal to 2, as expected.

9.3.3 Experimental Results

The numerical representation of the test input signal in (9.3.1) can be shown to be

$$u(t_k) = \begin{cases} 0 & \text{if } t_k \leq 1.2\ (s) \\ u(t_{k-1}) + 0.275\ (V) & \text{if } 1.2\ (s) < t_k \leq 1.6\ (s) \\ u(t_{k-1}) - 0.275\ (V) & \text{if } 1.6\ (s) < t_k \leq 2\ (s) \\ 0 & \text{if } t_k > 2\ (s). \end{cases} \tag{9.3.56}$$

Figure 9.3.5-(d) shows the time evolution of (9.3.56) for the considered experimental set-up. The displacement of the crane measured by the encoder is shown on Figure 9.3.5-(a), labelled as σ_{mis}. The signal is drawn using a (orange) line with circles. Note that the circles represent the actual

displacements measured by the encoder. It is apparent that the output measurement is a discrete-time signal. Once the measurements are acquired, two post-processing strategies are proposed:

1. The output measurement is numerically interpolated via Matlab environment in order to obtain a smooth continuous-time signal to be differentiated at least two times via higher order sliding mode differentiators. To this end, the function *polyfit* was used, with a 5-th order polynomial;

2. Given the discrete-time measurement, its successive derivatives are approximated by the following finite difference:

$$\hat{\sigma}^{(i+1)}(t_k) = \frac{\hat{\sigma}^{(i)}(t_k) - \hat{\sigma}^{(i)}(t_k - T_s)}{T_s}, \tag{9.3.57}$$

   where T_s is a fixed time interval.

The aim here will be to show that two strategies lead to the same conclusion.

9.3.3.1 Interpolated Measurement Analysis

Figure 9.3.5-(a) shows the continuous-time interpolated output measurement as a dashed (red) line. The sliding mode differentiators (9.3.51)-(9.3.52) and (9.3.53)-(9.3.55), can estimate $\hat{\sigma}^{(1)}_{int}$ and $\hat{\sigma}^{(2)}_{int}$, respectively, which are shown on Figure 9.3.5-(b) and on Figure 9.3.5-(c), respectively, using again a dashed (red) line. Then, the forward difference with spacing $t_c = 0.4$ seconds are computed. According to Figure 9.3.5-(bottom), one can conclude that also in this case the identified relative degree reveals to be equal to 2.

9.3.3.2 Discrete-time Measurement Analysis

Figure 9.3.5-(e) and 9.3.5-(f) show the discrete finite differences $\hat{\sigma}^{(1)}_{mis}$, and $\hat{\sigma}^{(2)}_{mis}$, determined by (9.3.57), where $T_s = 0.1$ seconds. Since t_c is an integer multiple of T_s, it is possible to compute $\Delta_{[0.4]}\hat{\sigma}^{(1)}_{mis}$, and $\Delta_{[0.4]}\hat{\sigma}^{(2)}_{mis}$. Also in this framework, the set of inequalities in (9.3.49)-(9.3.50) are satisfied. It follows that also in this approach the identified relative degree is equal to 2.

9.4 Conclusions

In this chapter, an experimental assessment of a recently proposed scheme to identify the relative degree has been undertaken. A lab-scale overhead crane available at the University of Pavia-Process Control Laboratory has been employed. The aim was to identify the relative degree of the x-displacement of the crane (the measured output), with respect to the armature voltage (control input) of a 12 Volts DC Motor. A previously identified second order LTI system has been used as a preliminary knowledge of the mechatronic set-up. A comparison between the simulated and the experimental approaches has been provided, which has lead to the same conclusions regarding the identified value of the relative degree.

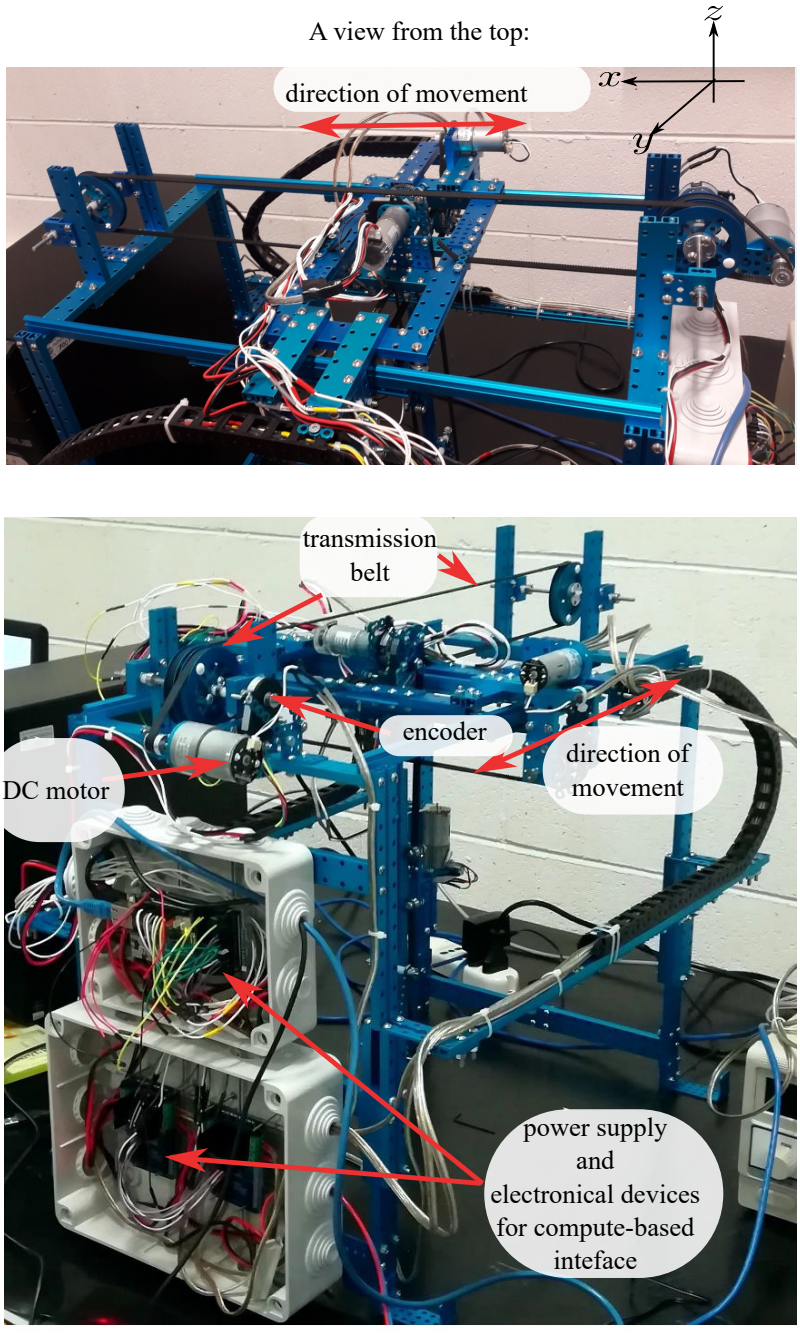

Figure 9.3.4: The lab-scale overhead crane considered in the experimental framework. The relevant components are highlighted in the figure. A view from the top shows the considered direction of movement of the crane.

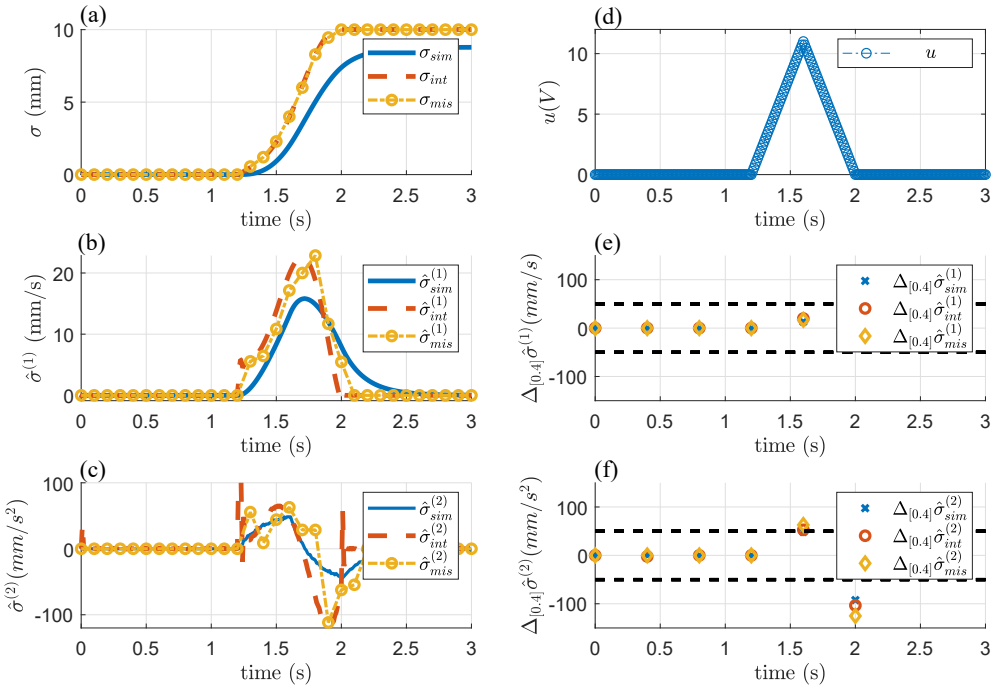

Figure 9.3.5: Time evolution of: **(a):** the simulated output measurement σ_{sim}; the interpolated output measurement σ_{int}; the discrete-time output measured by the encoder σ_{mis}. **(b):** the simulated output first time derivative $\hat{\sigma}^{(1)}_{sim}$; the interpolated output first time derivative $\hat{\sigma}^{(1)}_{int}$; the discrete-time output first finite difference $\hat{\sigma}^{(1)}_{mis}$. **(c)**: the simulated output second time derivative $\hat{\sigma}^{(2)}_{sim}$; the interpolated output second time derivative $\hat{\sigma}^{(2)}_{int}$; the discrete-time output first finite difference $\hat{\sigma}^{(2)}_{mis}$. **(d):** the DC motor armature voltage, which is the control input. **(e):** the simulated output forward difference $\Delta_{[0.4]}\hat{\sigma}^{(1)}_{sim}$; the interpolated output forward difference $\Delta_{[0.4]}\hat{\sigma}^{(1)}_{int}$; the discrete-time output forward difference $\Delta_{[0.4]}\hat{\sigma}^{(1)}_{mis}$. **(f):** the simulated output forward difference $\Delta_{[0.4]}\hat{\sigma}^{(2)}_{sim}$; the interpolated output forward difference $\Delta_{[0.4]}\hat{\sigma}^{(2)}_{int}$; the discrete-time output forward difference $\Delta_{[0.4]}\hat{\sigma}^{(2)}_{mis}$.

Part V

Conclusions, Future Research, and Bibliography

Conclusions

The present thesis has been focused on the design and assessment of novel sliding mode-based estimation and control methodologies with application to modern power systems and electrical engineering components. The first part of the work has been devoted to the presentation of relevant and well-established key-results in the area of both sliding mode theory and power system analysis and modelling.

The first addressed challenge has been the design of robust state estimators which are able to depict in near real time the state of the overall power systems to globally enhance the monitoring of the network. The proposed observers have revealed to be distributed, hence reducing the computational complexity for its practical implementation. Since the proposed observers require minimal measurement information and its exchanges amongst the nodes, it is expected to benefit in reduction of communication load. The real data-based assessment undertaken in Chapter 4 has also represented an element of originality when compared to existing standard approaches. The reader can also note that the super-twisting-like observer originally proposed in Chapter 4 for the robust finite-time frequency estimation in synchronous generators, is applicable to load and inverter components as illustrated in Chapter 5, hence preserving its robustness and stability properties.

The second addressed challenge has been the design of fault detection, reconstruction, and mitigation schemes devoted to enhance the resilience of power networks. A distributed scheme based on an adaptive dual-layer super-twisting sliding mode architecture has been proposed in order to tackle multiple faults and attacks and to perform a compensation strategy still using the standard and well-established PI controller. The exploited adaptation scheme for the observer gains has not generated conservative overestimation of uncertainty. This has helped mitigating chattering and the amplification of noise.

The third addressed challenge has been focused on SM observer-based control methodologies dedicated to achieve both the frequency regulation and the minimisation of the cost associated with the generation of power. The first proposed controller was based on two third-order SM observer for power systems modelled by equivalent turbine-governor dynamics, and on a recently proposed sub-optimal SM control architecture. The second observer-based control scheme has exploited again the third order SM observers in order to estimate the unknown power demand associated with each bus in power systems. The control problem has been addressed in an original two steps approach way. The first step has been focused on the design of a distributed observer scheme, which was able to both estimate in finite time the frequency deviation, and the unknown power demand, both of which were essential for controllers synthesis. The second step has developed the controllers synthesis. A SM control scheme was employed to track in finite time the reference value of the optimal marginal cost, thus achieving in finite time the economic dispatch, and asymptotically steering to zero the frequency deviations.

The fourth addressed challenge has considered an automatic algorithm for the identification of the relative degree with application to electromechanical systems. Specifically, via the recursive strategy proposed in the present thesis, any relative degree can be automatically identified since the method, by itself, has been capable of selecting the order of the Levant's differentiator which is suitable to perform the identification. Furthermore, the experimental-based assessment of the method was

illustrated relying on an set-up composed of a lab-scale overhead crane mechanically coupled with a DC motor.

Future Research

The proposals presented in the thesis can be further developed. In the present section, a brief guideline on possible ideas to be exploited will be presented. The proposed methodologies focused on power systems can be further validated using the advanced professional software such as *DigSilent* in process of procurement, which is considered to be one of the best tools amongst researchers and practitioners for power system simulations and analysis.

Along with this, the exploitation of real-data based assessment can be further undertaken. This original assessment approach is expected to have a stronger impact on researches and practitioners. In addition, the exploited fault mitigation and reconstruction methodologies can be extended to the case of cyber-attacks. In particular, the use of SM approaches can be beneficial for the implementation of cyber-security methodologies.

The proposed methodologies can be also further developed by exploiting the use of adaptive sub-optimal sliding mode observers. These can represent an important theoretical contribution, since adaptive sub-optimal SM techniques have already been used in the existing literature only for the control design area. Furthermore, the adaptive sub-optimal schemes are beneficial also for technological perspective, since they are capable of automatically adjusting the values of the observer gains with respect to the time-varying amount of matched uncertainties affecting their dynamics.

Bibliography

[1] V. V. Quaschning, *Renewable energy and climate change*. Wiley, 2019.

[2] D. Willis, C. Niezrecki, D. Kuchma, E. Hines, S. Arwade, R. Barthelmie, M. DiPaola, P. Drane, C. Hansen, M. Inalpolat *et al.*, "Wind energy research: State-of-the-art and future research directions," *Renewable Energy*, vol. 125, pp. 133–154, 2018.

[3] T. Kerdphol, F. Rahman, and Y. Mitani, "Virtual inertia control application to enhance frequency stability of interconnected power systems with high renewable energy penetration," *Energies*, vol. 11, no. 4, p. 981, 2018.

[4] P. W. Sauer, M. A. Pai, and J. H. Chow, *Power System Dynamics and Stability: With Synchrophasor Measurement and Power System Toolbox*. John Wiley & Sons, 2017.

[5] P. Kundur, N. J. Balu, and M. G. Lauby, *Power system stability and control*. McGraw-hill New York, 1994, vol. 7.

[6] S. A. Boyer, *SCADA: Supervisory Control and Data Acquisition*. International Society of Automation, 2009.

[7] N. P. A. R. T. Force, "A framework for the attributes of PMU data quality and a methodology for examining data quality impacts to synchrophasor applications," *Technical Report*, pp. 1–77, 2017.

[8] Siemens, "SICAM, power quality and measurement," siemens.com/powerquality, Tech. Rep., 2019, accessed: June 2019.

[9] S. Yufei, L. Xuan, L. Zhiyi, M. Shahidehpour, and L. Zuyi, "Intelligent data attacks against power systems using incomplete network information: a review," *Journal of Modern Power Systems and Clean Energy*, vol. 6, no. 4, pp. 630–641, 2018.

[10] A. F. Taha, J. Qi, J. Wang, and J. H. Panchal, "Risk mitigation for dynamic state estimation against cyber attacks and unknown inputs," *IEEE Transactions on Smart Grid*, vol. 9, no. 2, pp. 886–899, 2016.

[11] Y. Wu, Z. Wei, J. Weng, X. Li, and R. H. Deng, "Resonance attacks on load frequency control of smart grids," *IEEE Transactions on Smart Grid*, vol. 9, no. 5, pp. 4490–4502, 2017.

[12] E. Ghahremani and I. Kamwa, "Local and wide-area PMU-based decentralized dynamic state estimation in multi-machine power systems," *IEEE Transactions on Power Systems*, vol. 31, no. 1, pp. 547–562, 2015.

[13] A. Nechifor, M. Albu, R. Hair, and V. Terzija, "An enterprise platform for wide area monitoring of load dynamics using synchronized measurement technology," *IFAC-PapersOnLine*, vol. 49, no. 27, pp. 85–90, 2016.

[14] Z. Huang, P. Du, D. Kosterev, and S. Yang, "Generator dynamic model validation and parameter calibration using phasor measurements at the point of connection," *IEEE Transactions on Power Systems*, vol. 28, no. 2, pp. 1939–1949, 2013.

[15] G. Rinaldi, M. Cucuzzella, and A. Ferrara, "Third order sliding mode observer-based approach for distributed optimal load frequency control," *IEEE Control Systems Letters*, vol. 1, no. 2, pp. 215–220, 2017.

[16] A. A. Hussein, S. S. Salih, and Y. G. Ghasm, "Implementation of proportional-integral-observer techniques for load frequency control of power system," *Procedia Computer Science*, vol. 109, pp. 754–762, 2017.

[17] W. Mielczarski, "Observing the state of a synchronous generator part 2. applications," *International Journal of Control*, vol. 45, no. 3, pp. 1001–1021, 1987.

[18] E. Scholtz and B. C. Lesieutre, "Graphical observer design suitable for large-scale DAE power systems," in *Proc. of 47th IEEE Conference on Decision and Control*, Cancun, Mexico, December 2008, pp. 2955–2960.

[19] E. Ghahremani and I. Kamwa, "Dynamic state estimation in power system by applying the extended Kalman filter with unknown inputs to phasor measurements," *IEEE Transactions on Power Systems*, vol. 26, no. 4, pp. 2556–2566, 2011.

[20] J. Qi, A. F. Taha, and J. Wang, "Comparing kalman filters and observers for power system dynamic state estimation with model uncertainty and malicious cyber attacks," *IEEE Access*, vol. 6, pp. 77 155–77 168, 2018.

[21] G. Anagnostou and B. C. Pal, "Derivative-free Kalman filtering based approaches to dynamic state estimation for power systems with unknown inputs," *IEEE Transactions on Power Systems*, vol. 33, no. 1, pp. 116–130, 2017.

[22] J. Zhao, "Dynamic state estimation with model uncertainties using H_∞ Extended Kalman Filter," *IEEE Transactions on Power Systems*, vol. 33, no. 1, pp. 1099–1100, 2017.

[23] Y. Shtessel, C. Edwards, L. Fridman, and A. Levant, "Conventional sliding mode observers," in *Sliding Mode Control and Observation*. Springer, 2014, pp. 105–141.

[24] C. Mellucci, P. P. Menon, C. Edwards, and A. Ferrara, "Second-order sliding mode observers for fault reconstruction in power networks," *IET Control Theory & Applications*, vol. 11, no. 16, pp. 2772–2782, 2017.

[25] B. Yang, T. Yu, H. Shu, W. Yao, and L. Jiang, "Sliding-mode perturbation observer-based sliding-mode control design for stability enhancement of multi-machine power systems," *Transactions of the Institute of Measurement and Control*, vol. 41, no. 5, pp. 1418–1434, 2019.

[26] A. S. Tummala, R. Inapakurthi, and P. Ramanarao, "Observer based sliding mode frequency control for multi-machine power systems with high renewable energy," *Journal of Modern Power Systems and Clean Energy*, vol. 6, no. 3, pp. 473–481, 2018.

[27] K. Vrdoljak, N. Perić, and I. Petrović, "Sliding mode based load-frequency control in power systems," *Electric Power Systems Research*, vol. 80, no. 5, pp. 514–527, 2010.

[28] F. Pasqualetti, F. Dörfler, and F. Bullo, "Attack detection and identification in cyber-physical systems," *IEEE Transactions on Automatic Control*, vol. 58, no. 11, pp. 2715–2729, 2013.

[29] I.-S. Kim, M.-B. Kim, and M.-J. Youn, "New maximum power point tracker using sliding-mode observer for estimation of solar array current in the grid-connected photovoltaic system," *IEEE Transactions on Industrial Electronics*, vol. 53, no. 4, pp. 1027–1035, 2006.

[30] A. K. Bejestani, A. Annaswamy, and T. Samad, "A hierarchical transactive control architecture for renewables integration in smart grids: Analytical modeling and stability," *IEEE Transactions on Smart Grid*, vol. 5, no. 4, pp. 2054–2065, 2014.

[31] X. Luo, X. Wang, X. Pan, and X. Guan, "Detection and isolation of false data injection attack for smart grids via unknown input observers," *IET Generation, Transmission and Distribution*, vol. 13, no. 8, pp. 1277–1286, 2019.

[32] K. Liao and Y. Xu, "A robust load frequency control scheme for power systems based on second-order sliding mode and extended disturbance observer," *IEEE Transactions on Industrial Informatics*, vol. 14, no. 7, pp. 3076–3086, 2017.

[33] H. H. Alhelou, M. H. Golshan, and J. Askari-Marnani, "Robust sensor fault detection and isolation scheme for interconnected smart power systems in presence of RER and EVs using unknown input observer," *International Journal of Electrical Power & Energy Systems*, vol. 99, pp. 682–694, 2018.

[34] C. Edwards, S. K. Spurgeon, and R. J. Patton, "Sliding mode observers for fault detection and isolation," *Automatica*, vol. 36, no. 4, pp. 541–553, 2000.

[35] S. Trip, M. Cucuzzella, C. De Persis, A. van der Schaft, and A. Ferrara, "Passivity-based design of sliding modes for optimal load frequency control," *IEEE Transactions on Control Systems Technology*, no. 99, pp. 1–14, 2018.

[36] C. Edwards and Y. Shtessel, "Adaptive dual-layer super-twisting control and observation," *International Journal of Control*, vol. 89, no. 9, pp. 1759–1766, 2016.

[37] M. Eremia and M. Shahidehpour, *Handbook of electrical power system dynamics: modeling, stability, and control*. John Wiley & Sons, 2013, vol. 92.

[38] S. Trip, M. Bürger, and C. De Persis, "An internal model approach to (optimal) frequency regulation in power grids with time-varying voltages," *Automatica*, vol. 64, pp. 240–253, 2016.

[39] C. Zhao, U. Topcu, N. Li, and S. Low, "Design and stability of load-side primary frequency control in power systems," *IEEE Transactions on Automatic Control*, vol. 59, no. 5, pp. 1177–1189, 2014.

[40] C. Zhao, E. Mallada, and F. Dörfler, "Distributed frequency control for stability and economic dispatch in power networks," in *Proc. of American Control Conference (ACC)*, Chicago, IL, USA, July 2015, pp. 2359–2364.

[41] C. Zhao, E. Mallada, S. H. Low, and J. Bialek, "Distributed plug-and-play optimal generator and load control for power system frequency regulation," *International Journal of Electrical Power & Energy Systems*, vol. 101, pp. 1–12, 2018.

[42] F. Guo, C. Wen, J. Mao, J. Chen, and Y.-D. Song, "Hierarchical decentralized optimization architecture for economic dispatch: A new approach for large-scale power system," *IEEE Transactions on Industrial Informatics*, vol. 14, no. 2, pp. 523–534, 2017.

[43] X. He, D. W. Ho, T. Huang, J. Yu, H. Abu-Rub, and C. Li, "Second-order continuous-time algorithms for economic power dispatch in smart grids," *IEEE Transactions on Systems, Man, and Cybernetics: Systems*, vol. 48, no. 9, pp. 1482–1492, 2017.

[44] K. Liao and Y. Xu, "A robust load frequency control scheme for power systems based on second-order sliding mode and extended disturbance observer," *IEEE Transactions on Industrial Informatics*, vol. 14, no. 7, pp. 3076–3086, 2018.

[45] F. Dörfler and S. Grammatico, "Gather-and-broadcast frequency control in power systems," *Automatica*, vol. 79, pp. 296–305, 2017.

[46] K. Xi, J. L. Dubbeldam, H. X. Lin, and J. H. van Schuppen, "Power-imbalance allocation control of power systems-secondary frequency control," *Automatica*, vol. 92, pp. 72–85, 2018.

[47] A. Isidori, *Nonlinear control systems*. Springer, 2013.

[48] J. Chen, R. J. Patton, and H.-Y. Zhang, "Design of unknown input observers and robust fault detection filters," *International Journal of control*, vol. 63, no. 1, pp. 85–105, 1996.

[49] M.-S. Chen and C.-C. Chen, "Unknown input observer for linear non-minimum phase systems," *Journal of the Franklin Institute*, vol. 347, no. 2, pp. 577–588, 2010.

[50] G. Rinaldi, M. Cucuzzella, and A. Ferrara, "Sliding mode observers for a network of thermal and hydroelectric power plants," *Automatica*, vol. 98, pp. 51–57, 2018.

[51] C. Zhao and D. Li, "Control design for the SISO system with the unknown order and the unknown relative degree," *ISA transactions*, vol. 53, no. 4, pp. 858–872, 2014.

[52] M. Wang, Y. Liu, and Y. Man, "Global output-feedback stabilization for nonlinear systems with unknown relative degree," *International Journal of Robust and Nonlinear Control*, vol. 28, no. 4, pp. 1425–1439, 2018.

[53] A. Levant and L. M. Fridman, "Accuracy of homogeneous sliding modes in the presence of fast actuators," *IEEE Transactions on Automatic Control*, vol. 55, no. 3, pp. 810–814, 2010.

[54] A. Levant and M. Livne, "Weighted homogeneity and robustness of sliding mode control," *Automatica*, vol. 72, pp. 186–193, 2016.

[55] S.-T. Wu and K. Youcef-Toumi, "On relative degrees and zero dynamics from physical system modeling," *Journal of Dynamic Systems, Measurement, and Control*, vol. 117, no. 2, pp. 205–217, 1995.

[56] A. Delgado, C. Kambhampati, and K. Warwick, "Dynamic recurrent neural network for system identification and control," *IEE Proceedings-Control Theory and Applications*, vol. 142, no. 4, pp. 307–314, 1995.

[57] P. Guo, "Nonlinear predictive functional control based on hopfield network and its application in cstr," in *Proc. of IEEE International Conference on Machine Learning and Cybernetics*, Dalian, China,, 2006, pp. 3036–3039.

[58] A. G. G. Hernandez, L. Fridman, A. Levant, Y. Shtessel, R. Leder, C. R. Monsalve, and S. I. Andrade, "High-order sliding-mode control for blood glucose: Practical relative degree approach," *Control Engineering Practice*, vol. 21, no. 5, pp. 747–758, 2013.

[59] A. Levant, "Practical relative degree approach in sliding-mode control," in *Advances in Sliding Mode Control*. Springer, 2013, pp. 97–115.

[60] A. Barth, C. Weise, and J. Reger, "Application of higher-order sliding-modes to a ball and plate system," in *Proc. of 15-th International Workshop on Variable Structure Systems (VSS)*, Graz, Austria, July 2018, pp. 192–197.

[61] C. Edwards and S. Spurgeon, *Sliding mode control: theory and applications*. CRC Press, 1998.

[62] C. Edwards and S. K. Spurgeon, "On the development of discontinuous observers," *International Journal of control*, vol. 59, no. 5, pp. 1211–1229, 1994.

[63] A. Ferrara, G. P. Incremona, and M. Cucuzzella, *Advanced and Optimization Based Sliding Mode Control Theory and Applications*. Advances in Design and Control Series, SIAM, 2019.

[64] V. Utkin, "Sliding mode control design principles and applications to electric drives," *IEEE Transactions on Industrial Electronics*, vol. 40, no. 1, pp. 23–36, 1993.

[65] C. Edwards, E. F. Colet, and L. Fridman, *Advances in variable structure and sliding mode control*. Springer, 2006.

[66] G. Rinaldi, P. P. Menon, C. Edwards, and A. Ferrara, "Design and validation of a distributedobserver-based estimation scheme for power grids," *IEEE Transactions on Control Systems Technology*, 2018.

[67] L. M. Capisani, A. Ferrara, A. F. de Loza, and L. M. Fridman, "Manipulator fault diagnosis via higher order sliding-mode observers," *IEEE Transactions on Industrial Electronics*, vol. 59, no. 10, pp. 3979–3986, 2012.

[68] N. S. Nise, *Contro Systems Engineering (7-th Ed)*. John Wiley & Sons, 2015.

[69] T. Kailath, *Linear systems*. Prentice-Hall Englewood Cliffs, NJ, 1980, vol. 156.

[70] L. Fridman, A. Levant, and J. Davila, "Observation of linear systems with unknown inputs via high-order sliding-modes," *International Journal of systems science*, vol. 38, no. 10, pp. 773–791, 2007.

[71] Y. Shtessel, C. Edwards, L. Fridman, and A. Levant, *Sliding mode control and observation*. Springer, 2014, vol. 10.

[72] A. Levant, "Robust exact differentiation via sliding mode technique," *Automatica*, vol. 34, no. 3, pp. 379–384, 1998.

[73] E. Cruz-Zavala and J. A. Moreno, "Levant's arbitrary order exact differentiator: A lyapunov approach," *IEEE Transactions on Automatic Control*, 2018.

[74] I. Nagesh and C. Edwards, "A multivariable super-twisting sliding mode approach," *Automatica*, vol. 50, no. 3, pp. 984–988, 2014.

[75] J. Davila, L. Fridman, and A. Levant, "Second-order sliding-mode observer for mechanical systems," *IEEE Transactions on Automatic Control*, vol. 50, no. 11, pp. 1785–1789, 2005.

[76] J. A. Moreno and M. Osorio, "Strict Lyapunov functions for the super-twisting algorithm," *IEEE Transactions on Automatic Control*, vol. 57, no. 4, pp. 1035–1040, 2012.

[77] C. L. Siegel and K. Ramanathan, *Lectures on quadratic forms*. Tata Institute of Fundamental Research, 1955, vol. 7.

[78] X.-G. Yan and C. Edwards, "Robust sliding mode observer-based actuator fault detection and isolation for a class of nonlinear systems," *International Journal of Systems Science*, vol. 39, no. 4, pp. 349–359, 2008.

[79] G. Bartolini, A. Ferrara, and E. Usai, "On boundary layer dimension reduction in sliding mode control of siso uncertain nonlinear systems," in *Proc. IEEE International Conference on Control Applications*, vol. 1, Trieste, Italy, 1998, pp. 242–247.

[80] ——, "Chattering avoidance by second-order sliding mode control," *IEEE Transactions on automatic control*, vol. 43, no. 2, pp. 241–246, 1998.

[81] A. Chalanga, S. Kamal, L. M. Fridman, B. Bandyopadhyay, and J. A. Moreno, "Implementation of super-twisting control: Super-twisting and higher order sliding-mode observer-based approaches," *IEEE Transactions on Industrial Electronics*, vol. 63, no. 6, pp. 3677–3685, 2016.

[82] F. A. Ortiz-Ricardez, T. Sánchez, and J. A. Moreno, "Smooth Lyapunov function and gain design for a second order differentiator," in *Proc. of 54th IEEE Conference on Decision and Control (CDC)*, Osaka, Japan, December 2015, pp. 5402–5407.

[83] F. Aminifar, M. Shahidehpour, M. Fotuhi-Firuzabad, and S. Kamalinia, "Power system dynamic state estimation with synchronized phasor measurements," *IEEE Transactions on Instrumentation and Measurement*, vol. 63, no. 2, pp. 352–363, 2014.

[84] J. Machowski, J. Bialek, and J. Bumby, *Power system dynamics: stability and control*. John Wiley & Sons, 2011.

[85] Q.-C. Zhong and T. Hornik, *Control of power inverters in renewable energy and smart grid integration*. John Wiley & Sons, 2012, vol. 97.

[86] P. Monshizadeh, C. De Persis, T. Stegink, N. Monshizadeh, and A. van der Schaft, "Stability and frequency regulation of inverters with capacitive inertia," in *Proc. of 2017 IEEE 56th Annual Conference on Decision and and Control (CDC)*, Melbourne, Australia, December 2017, pp. 5696–5701.

[87] P. Monshizadeh, C. De Persis, N. Monshizadeh, and A. J. van der Schaft, "Nonlinear analysis of an improved swing equation," in *Proc. 55th IEEE Conference on Decision and Control (CDC)*, Las Vegas, USA, December 2016, pp. 4116–4121.

[88] J. Zhou and Y. Ohsawa, "Improved swing equation and its properties in synchronous generators," *IEEE Transactions on Circuits and Systems I: Regular Papers*, vol. 56, no. 1, pp. 200–209, 2008.

[89] A. R. Bergen and D. J. Hill, "A structure preserving model for power system stability analysis," *IEEE Transactions on Power Apparatus and Systems*, no. 1, pp. 25–35, 1981.

[90] N. Tsolas, A. Arapostathis, and P. Varaiya, "A structure preserving energy function for power system transient stability analysis," *IEEE Transactions on Circuits and Systems*, vol. 32, no. 10, pp. 1041–1049, 1985.

[91] F. Dorfler and F. Bullo, "Kron reduction of graphs with applications to electrical networks," *IEEE Transactions on Circuits and Systems I: Regular Papers*, vol. 60, no. 1, pp. 150–163, 2013.

[92] R. J. Davy and I. A. Hiskens, "Lyapunov functions for multimachine power systems with dynamic loads," *IEEE Transactions on Circuits and Systems I: Fundamental Theory and Applications*, vol. 44, no. 9, pp. 796–812, 1997.

[93] G. Rinaldi, P. P. Menon, A. Ferrara, and C. Edwards, "A super-twisting-like sliding mode observer for frequency reconstruction in power systems: Discussion and real data based assessment," in *Proc. of 15-th International Workshop on Variable Structure Systems (VSS)*, Graz, Austria, July 2018, pp. 444–449.

[94] S. Trip, M. Cucuzzella, A. Ferrara, and C. De Persis, "An energy function based design of second order sliding modes for automatic generation control," in *Proc. 20th IFAC World Congress*, Toulouse, France, July 2017, pp. 11 613–11 618.

[95] A. Delavari, I. Kamwa, and P. Brunelle, "Simscape power systems benchmarks for education and research in power grid dynamics and control," in *Proc. of IEEE Canadian Conference on Electrical & Computer Engineering (CCECE)*, Quebec, Canada, May 2018, pp. 1–5.

[96] I. Hiskens, "IEEE PES task force on benchmark systems for stability controls," *Technical Report*, 2013.

[97] "Fingrid frequency - historical data," https://data.fingrid.fi/en/dataset/frequency-historical-data.

[98] E. Ørum, M. Kuivaniemi, M. Laasonen, A. I. Bruseth, E. A. Jansson, A. Danell, K. Elkington, and N. Modig, "Future system inertia," *ENTSOE, Brussels, Tech. Rep.*, 2015.

[99] Fingrid, "Frequency quality analysis for year 2015," *Report 2015*, pp. 1–91, 2015.

[100] A. Poznyak, "Stochastic output noise effects in sliding mode state estimation," *International Journal of Control*, vol. 76, no. 9-10, pp. 986–999, 2003.

[101] G. Rinaldi, P. P. Menon, C. Edwards, and A. Ferrara, "Sliding mode based dynamic state estimation for synchronous generators in power systems," *IEEE Control Systems Letters*, vol. 2, no. 4, pp. 785–790, 2018.

[102] ——, "Distributed observers for state estimation in power grids," in *Proc. of American Control Conference*, Seattle, WA, USA, May 2017, pp. 5824–5829.

[103] P. Kansal and A. Bose, "Bandwidth and latency requirements for smart transmission grid applications." *IEEE Transactions on Smart Grid*, vol. 3, no. 3, pp. 1344–1352, 2012.

[104] Y. Saad, *Iterative methods for sparse linear systems*. SIAM, 2003.

[105] K. R. James and W. Riha, "Convergence criteria for successive overrelaxation," *SIAM Journal on Numerical Analysis*, vol. 12, pp. 137–143, 1975.

[106] G. F. Franklin, J. D. Powell, M. L. Workman *et al.*, *Digital control of dynamic systems*. Addison-wesley Menlo Park, CA, 1998, vol. 3.

[107] C. Edwards and C. P. Tan, "A comparison of sliding mode and unknown input observers for fault reconstruction," *European Journal of control*, vol. 12, no. 3, pp. 245–260, 2006.

[108] Y. Guan and M. Saif, "A novel approach to the design of unknown input observers," *IEEE Transactions on Automatic Control*, vol. 36, no. 5, pp. 632–635, 1991.

[109] M. Singh and S. Santoso, "Dynamic models for wind turbines and wind power plants," National Renewable Energy Lab.(NREL), Golden, CO (United States), Tech. Rep., 2011.

[110] D. Söffker, T.-J. Yu, and P. C. Müller, "State estimation of dynamical systems with nonlinearities by using proportional-integral observer," *International Journal of Systems Science*, vol. 26, no. 9, pp. 1571–1582, 1995.

[111] D. C. Montgomery, G. C. Runger, and N. F. Hubele, *Engineering statistics*. John Wiley & Sons, 2009.

[112] A. Levant, "Higher-order sliding modes, differentiation and output-feedback control," *International Journal of Control*, vol. 76, no. 9-10, pp. 924–941, 2003.

[113] C. P. Tan and C. Edwards, "Sliding mode observers for robust detection and reconstruction of actuator and sensor faults," *International Journal of Robust and Nonlinear Control: IFAC-Affiliated Journal*, vol. 13, no. 5, pp. 443–463, 2003.

[114] G. Rinaldi and A. Ferrara, "Decentralized integral sliding mode approach for frequency control and unknown demand reconstruction in power systems," in *Proc. of 15th International Workshop on Variable Structure Systems*, Graz, Austria, July 2018, pp. 455–460.

[115] A. Levant, "Robustness of homogeneous sliding modes to relative degree fluctuations," in *Proc. of 6-th IFAC Symposium on Robust Control Design*, Haifa, Israel, June 2009, pp. 167–172.

[116] A. Levant and M. Livne, "Discrete-time sliding-mode-based differentiation," in *Advances in Sliding Mode Control*. Springer, 2013, pp. 299–312.

[117] G. Rinaldi and A. Ferrara, "Relative degree identification for sliding mode controllers design," in *Proc. of 15-th International Workshop on Variable Structure Systems (VSS)*, Graz, Austria, July 2018, pp. 55–60.

[118] M. Cucuzzella, G. P. Incremona, and A. Ferrara, "Design of robust higher order sliding mode control for microgrids," *IEEE Journal on Emerging and Selected Topics in Circuits and Systems*, vol. 5, no. 3, pp. 393–401, 2015.

[119] I. CUI, "Encoders AMT10 series data-sheet," https://www.cui.com/product/resource/amt10.pdf, 2018, accessed: January 2019.

[120] R. Barber, M. Horra, and J. Crespo, "Control practices using Simulink with Arduino as low cost hardware," in *Proc. of 10th IFAC Symposium Advances in Control Education*, Sheffield, UK, August 2013, pp. 250–255.

[121] V. Utkin, J. Guldner, and J. Shi, *Sliding mode control in electro-mechanical systems*. CRC Press, 2009.

[122] R. Kelly, “A linear-state feedback plus adaptive feed-forward control for dc servomotors,” *IEEE Transactions on Industrial Electronics*, no. 2, pp. 153–157, 1987.